Tribochemical Analysis of Si-Doped and Non-Doped Diamond-Like Carbon for Application Within the Internal Combustion Engine

by

Joseph Liam Lanigan

Submitted in accordance with the requirements for the degree of

Doctor of Philosophy

The University of Leeds
School of Mechanical Engineering
Leeds, UK

August, 2015

The candidate confirms that the work submitted is his own, except where work which has formed part of jointly authored publications has been included. The contribution of the candidate and the other authors to this work has been explicitly indicated below. The candidate confirms that appropriate credit has been given within the thesis where reference has been made to the work of others.

Transmission electron microscope sample preparation and operation (including EELS and EDX) was undertaken by Dr Michael Ward. Nano indentation measurements were conducted by Dr Chun Wang.

Fully-fired engine testing was undertaken at Lubrizol Ltd by John Durham as part of 2020 Interface.

Dr Naoko Sono kindly conducted the XPS analysis detailed in this thesis. Dr Sono is part of an ESPRC funded XPS centre called Nexus, based at Newcastle University.

ToF-SIMS experiments were carried out by Dr David Scurr at the School of Pharmacy at Nottingham University.

SS-NMR experiments were conducted by David Apperly at Durham University as part of the ESPRC national service.

Papers Contributing to this Thesis

“Tribochemistry of silicon and oxygen doped, hydrogenated Diamond-Like Carbon in fully-formulated oil against low additive oil” Lanigan, J. Zhao, H. Morina, A. Neville, A. Tribology international 82 Part B. 2015

“DLC-W coatings tested in combustion engine — Frictional and wear analysis” Mutafova, P. Lanigan, J. Neville, A. Cavaleiro, A. Polcar, T. Surface and Coatings Technology Volume 260, 15 December 2014, Pages 284–289

“Repressing oxidative wear within Si doped DLCs” Lanigan, J. Wang, C. Morina, A. Neville, A. Tribology International Available (online 21 November 2014) In Press

Conference presentations

“Synthesis and characterisation of a novel, tri-doped, DLC that exhibits enhanced wear resistance” Lanigan, J. Wang, C. Morina, A. Neville, A. 41st Leeds-Lyon symposium on Tribology. Integrated Tribology. 2nd – 5th September 2014. Leeds, UK.

“Comparing the benefits of a rapidly-formed tribofilm against less tribological active DLCs over time” Lanigan, J. Zhao, H. Morina, A. Neville, A. 40st Leeds-Lyon symposium on Tribology. 4nd – 6th September 2014. Lyon, France.

Acknowledgments

Firstly, I would like to extend my unending gratitude to both of my academic supervisors for their continuous support and guidance throughout my time as a PhD student. My utmost thanks go to Professor Anne Neville for being a constant source of inspiration, enthusiasm and encouragement during my time in iFS. I would also like to thank Professor Ardian Morina who co-supervised my project, providing continuous academic support and extremely helpful advice and direction.

Further thanks go to Dr John Zhao, for his assistance, training and advice on much of the equipment within the tribology lab. I would also like to thank the technical staff within iFS, for without their support I'm not sure how long the labs would last! I would further thank Dr Mike Ward for his help with electron microscopy and numerous entertaining chats.

I would also extend my thanks to Jackie Kidd and Fiona Slade for making sure everything ran smoothly whilst I've been here. I would also like to thank my colleagues and friends at the University of Leeds, for keeping me smiling throughout my studies; Adam Johns for helping me with all things both computer and real-world based, Ben for many reasons (not least of which, introducing me to Anne and Ardian), John Dobson for the numerous pub trips, Karen for helping me hold on to my inner chemist, Louise Austin for all the cackling! Dr Mike Bryant for being ever helpful with XPS and not to mention very entertaining and also Yugal for being the happiest person I've ever met!

Also, I would thank the people who I've had the pleasure of sharing all of my (three!) offices with during my three years in Engineering at Leeds.

Last, but in no means least; I would like to say an eternal thank you to my mother for helping and supporting me in countless ways throughout my time as a student at Leeds. Without her continual support this thesis would probably not have been possible.

Abstract

Due to the ever-increasing global drivers focused on increasing fuel economy in tandem with decreasing the environmental impact of automobile usage; the automotive sector is rapidly embracing widespread use of Diamond-Like Carbon (DLC) coatings. DLC coatings have the potential to reduce the required level of many traditional oil additives that can negatively impact on both the environment and certain parts of the car engine, specifically the catalytic converter. Furthermore DLC shows promise with regards to reducing friction and can be highly efficacious at reducing wear. The field of research into DLC is ever-developing and many examples of doped DLCs exist. Currently, there is no firm consensus on which dopants are best to include in the DLC matrix when it is being employed within the automotive field. Adding to this the lack of a sufficient understanding of how current engine oil additives interact with DLC; the motivation for undertaking an in-depth analysis of both a-C:H and Si-DLC with current engine oils is clear.

This thesis addresses these issues and presents evidence on how both Si-DLCs and a-C:H DLCs interact with current engine oil additives to reduce wear in the engine. The fundamental tribochemistry governing DLC's interactions at the interfaces are explored with specific reference to wearing of Si-DLCs. Tribological experiments are undertaken to emulate certain conditions within an engine using both reciprocating pin-on-plate tribometers and pin-on-disc tribometers. A novel Si-DLC is created and tested to explore the effect of tri-doping on the coating. Advanced surface analysis techniques are used to gain a full understanding of what processes have taken place at the interfaces. This includes use of X-ray Photoelectron Spectroscopy, Secondary Ion Mass Spectrometry and scanning light interferometry. Key findings include the effect that Si doping has on the DLC coating with regards to structure, friction and wear. The fundamental observation that the Si-DLCs examined consistently exhibited wear at higher rates when compared to the a-C:H DLC is explored and tribological mechanisms for this are proposed.

Table of Contents

Table of Figures

List of Tables

Nomenclature

μ	Friction coefficient
a-C:H	Amorphous hydrogenated diamond-like carbon
AW	Anti-wear additive
CI	Cast iron
DLC	Diamond-like Carbon
E	Elastic Modulus (Pa)
EDX	Energy Dispersive X-ray
EELS	Energy Electron Loss Spectroscopy
EP	Extreme pressure additive
H	Hardness (Pa)
hv	Photon Energy (eV)
k	Dimensional wear coefficient (m^3/Nm)
LEMAS	Leeds Electron Microscopy and Spectroscopy Centre
ND	Not detected, species under investigation did not appear in the analysis
NOCH	Nitrogen, Oxygen, Carbon and Hydrogen containing additives
Oil A	Fully formulated oil ‘E6’ with additional

	FM, glycerol mono-oleate added to 1.5 % (w/v %)
Oil B	Fully formulated oil ‘E6’ (from Lubrizol Ltd.) containing SAPS additives including ZDDP. No FM species
Oil C	Fully formulated oil ‘E7’ containing higher SAPS levels, including ZDDP. No FM species
Oil D	Oil D blended to match Oil A in viscosity but only contains low amounts of SAPS. No ZDDP, no FM species present.
PECVD	Plasma Enhanced Chemical Vapor Deposition
P_{max}	Maximum Hertzian Contact Pressure
PVD	Physical Vapor Deposition
Running-in friction	The last phase of friction testing (variable times)
SAPS	Sulphated ash, phosphate and sulphur content
Si,O-DLC	Si-doped DLC whose production process incorporates a substantial amount of oxygen into the coating
Si-DLC	Si-doped DLC with a very low oxygen content
SS-NMR	Solid-state Nuclear Magnetic Resonance
Steady-state friction	The last twenty minutes of friction data from testing (unless otherwise stated)

ToF-SIMS	Time-of-fight Secondary-ion Mass Spectroscopy
XPS	X-ray photoelectron spectroscopy
λ	Lambda ratio

Chapter 1 Introduction

1.1. Background and Theories

1.1.1. Tribology

Tribology and tribochemistry, a sub discipline of the research area, are the key focus of this PhD thesis. Tribology is defined by the Oxford English dictionary (OED) as:

> *"The branch of science and technology concerned with interacting surfaces in relative motion and with associated matters (as friction, wear, lubrication, and the design of bearings)."[1]*

Tribology is not a new subject; there is evidence that in 2400 BC in ancient Egypt water was used as a lubricant to aid the building of the pyramids [2]. However, the real beginning of tribology seems to originate with Leonardo da Vinci (1452–1519) who appears to have drawn a schematic for a tribometer and used this to observe that the resistance of friction is directly proportional to applied load [3, 4]. Before moving on to the crux of the thesis, engine tribology, it must be noted that tribology is not limited to this application but is in fact dealt with every day in the natural world as discussed by Dowson [5]. The area of tribology is ever growing in both scope and importance, as will be addressed further on. The term tribochemistry, as the name suggests (tribo meaning 'rubbing' in Greek), is focused specifically around the chemical reactions that happen at the sliding interfaces [1]. These reactions can be different to the analogous chemical reaction that would be found without tribological influence, in terms of products. This makes the area of tribochemistry a challenging one to

conduct research in, as a variety of disciplines have to be drawn upon to elucidate what happens at the interface.

Despite its widespread prevalence, the area of tribology did not come to full prominence within the academic world until the release of the Jost report in 1996 [6]. The OED definition seen above itself is credited to Peter Jost, who identified the potential within the subject for huge savings if necessary technological advancements were made [6]. When the Jost paper was first published it was expected that if proper research focus was paid to tribology, savings in the GNP of the UK could equate to 1.3 – 1.6 %, which irrefutably represents a valuable goal in terms of cost reduction.

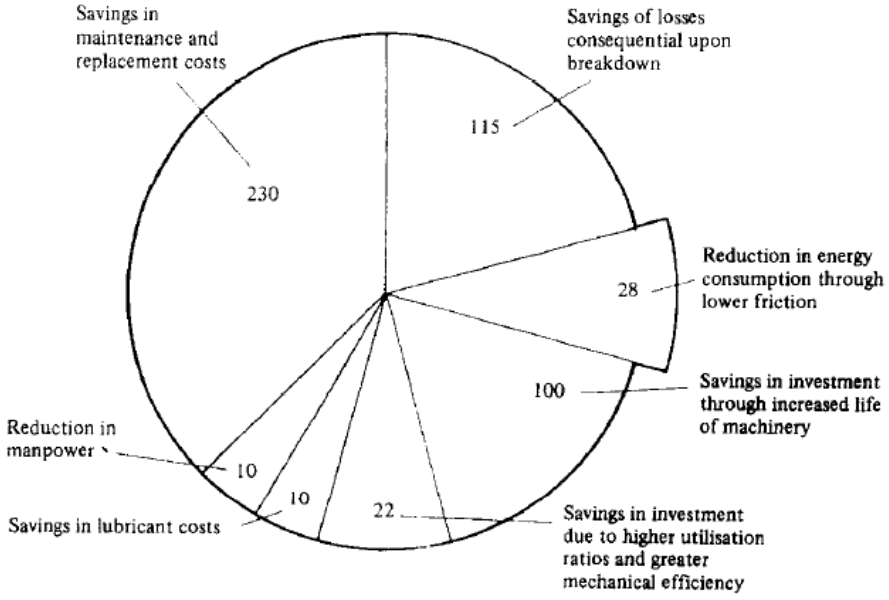

Figure 1-1 Economic savings through tribology, as identified by Jost [6]

The economic impact of effectively understanding tribology is still just as relevant today. Holmberg *et al* [7] identified that even today (paper first published in 2012) the modern internal combustion engine is still incredibly inefficient. Direct frictional losses (with braking friction excluded) equate to 33% of the fuel energy used – this represents a huge area for fiscal savings [7].

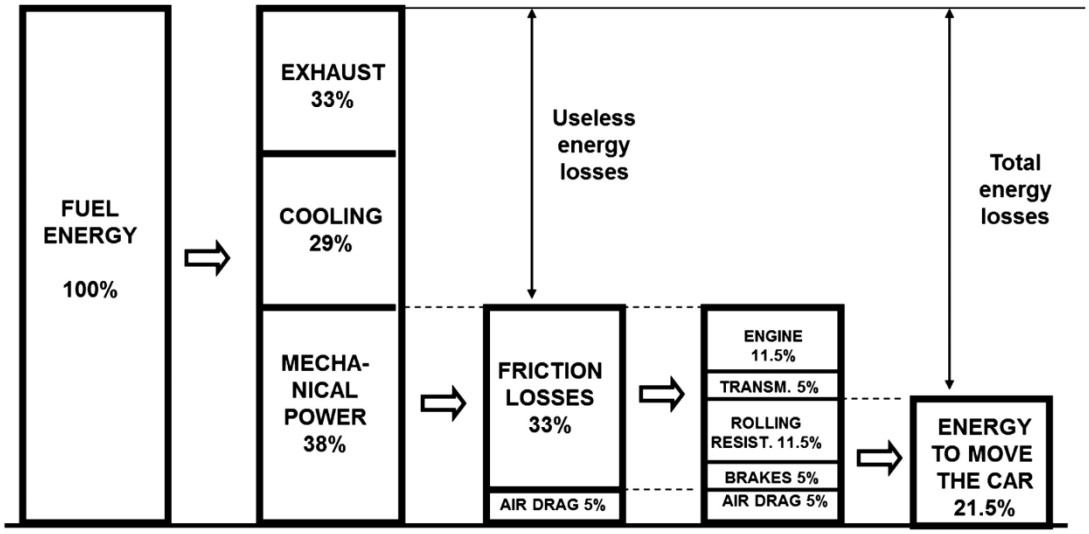

Figure 1-2 Energy losses in an car as identified by Holmberg *et al* [7]

Further modern day drivers in the field of tribochemistry include moving towards greener lubricant chemistry with the goal of reducing reliance on (Sulphated Ash, Phosphate and Sulphur) SAPS-heavy additives, whose emissions and use are known to be detrimental to the environment. These goals have been ratified following new EU legislation on emissions [8]. The overriding driving force herein is to reduce the emission of greenhouse gases from the internal combustion engine, Figure 1-3 . Both CH_4 and N_2O are regarded as greenhouse gases, both of which can be formed from inefficient burning of fuel in an engine [9-11]. This is usually prevented by effective functioning of the catalytic convert in the exhaust where a platinum or palladium catalyst species is located. The catalyst is able to convert carbonaceous species into carbon dioxide, and convert nitrous oxide into di-nitrogen and oxygen [12]. However, sulphated ash, phosphate and sulphur (SAPS) containing additives are known to poison catalytic converters, thus contributing to general noxious emissions and similar environmental issues [13]. The complete burning of fuel is particularly key as CO_2 alone has a much lower Global Warming Potential (GWP of CO_2 = 1, CH_4 = 86 and N_2O = 268) than either methane or nitrous oxide [14]. Furthermore, SAPS-heavy additives also contribute to particulate build up within an engine that can go on to cause huge amounts of wear [13]. As such, a clear goal for lubricant chemistry is to reduce reliance on SAPS type additives and move towards using NOCH additives (containing only Nitrogen, Oxygen, Carbon and Hydrogen) in their place.

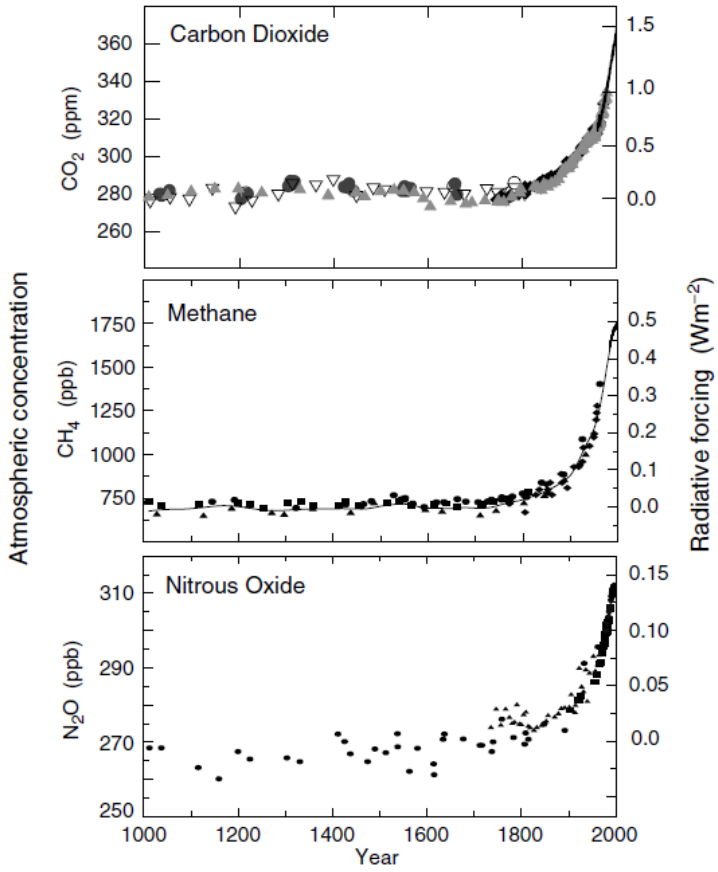

Figure 1-3 Increase in nitrous oxide emissions over time [9]

Obviously there is still much work to be done to reach the goal of further decreasing frictional losses within the engine. This represents a constantly moving goal-post as this directly relates to an increase in fuel economy, a constant driver for change. One approach identified as key is the use of coatings which can provide low friction and wear [7]. This clearly brings the family of coatings known as 'Diamond-Like Carbon' to the forefront of tribological research.

1.1.2. Friction and Lubrication

The principles concerned within this thesis are the friction, wear and lubrication of Diamond-Like Carbon (DLC) coatings when slid against steel. This is of course a vast area of research and much is already understood about the principals involved. Friction is of course defined as the resistance a body meets with moving over a counter body [15]. Lubrication is divided into subsets, or regimes, which are detailed in the next paragraphs.

The hydrodynamic lubrication (HL) regime takes place when a thin layer of fluid is forced through two surfaces due to viscous entrainment. The fluid is then compressed by the bearing surfaces which creates enough pressure to support the load. This lubrication system is often referred to as the ideal lubrication system as very low wear and friction coefficients can be obtained, sometimes as low as 0.001 [16].

A subset of hydrodynamic lubrication is elastohydrodynamic lubrication (EHL). Usually this is associated with a thinner film thickness within the range of 0.5 – 5 mm. In certain areas of the contact, asperities may touch which allows for an increase in pressure that causes a change in the viscosity of the lubricant. Combining this change with the minor elastic deformations that can occur at the contact allows for a good space in which the lubricant can flow though [17].

Mixed lubrication is the transition between HL/EHL and boundary lubrication. In this instance there can be frequent asperity/asperity contacts but there will remain an amount of bearing surface supported by a film [17].

Boundary lubrication is associated with an increase in the coefficient of friction. This is usually due to an increase in load, decrease in speed or a change in the fluid viscosity. Boundary lubrication is the regime in which solid asperity contacts predominate as opposed to the film of lubricant [16]. When in boundary lubrication regimes, friction becomes very high if effective friction modifiers are not employed. Efficacious boundary lubricants such as graphite and MoS_2 form easy-shear films on the two surface that can effectively reduce friction [17].

The Stribeck curve shows the transition between regimes in Figure 1-4. The modified stribeck diagram relates friction to surface roughness. This in turn indicates which regime predominates in which contact of the internal combustion engine, as shown in Figure 1-5. It can be seen that for the applications investigated within this thesis, boundary lubrication is the most relevant. It not only causes the most severe wear but also is the dominant regime at two highly important interfaces.

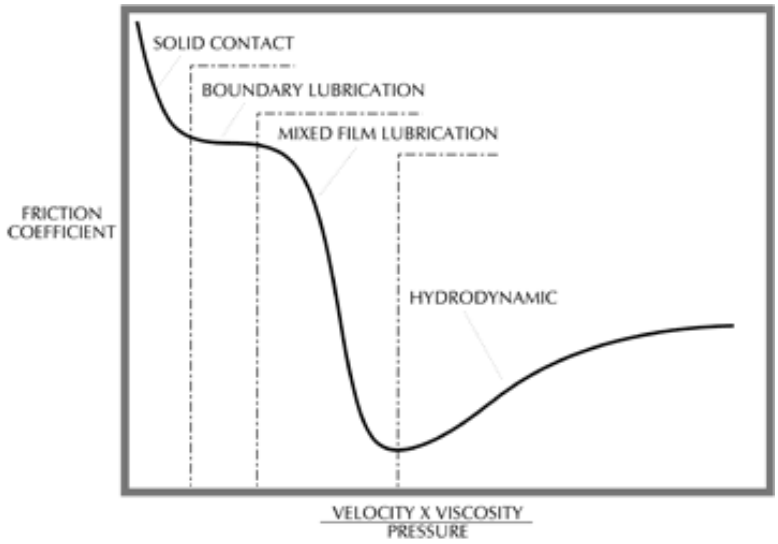

Figure 1-4 Showing the Stribeck curve with the lubrication regimes added to the appropriate area [18]

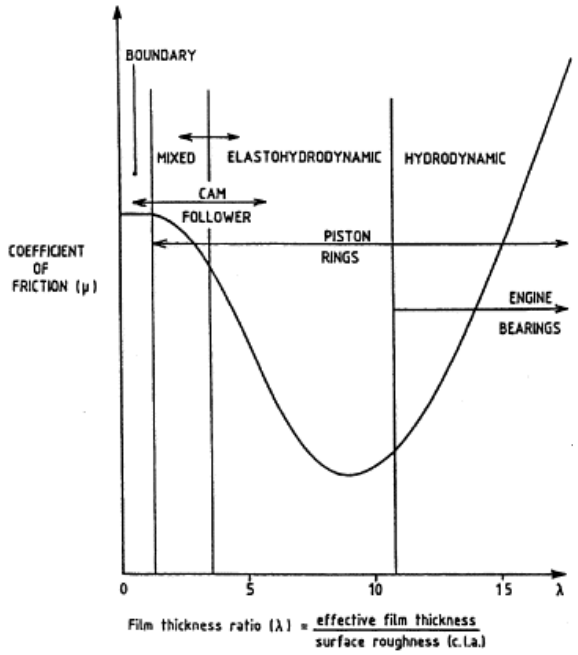

Figure 1-5 Modified Stribeck diagram which shows the regime relevant to certain engine components [19]

To verify that the boundary lubrication regime is indeed the one under investigation some calculations were performed to find the value of λ.

Where film thickness ratio, λ, is given by this equation:

$$\lambda \text{ ratio} = \frac{h_0}{\sigma}$$

Equation 1 give the lambda ratio

Sigma, σ, is the root mean square roughness of the body and counter body in contact, given by:

$$\sigma = \sqrt{\sigma_1^2 + \sigma_2^2}$$

Equation 2 gives sigma.

The minimum film thickness, h_0, is defined as:

$$\frac{h_0}{R'} = 3.63\left(\frac{U\eta_0}{E'R'}\right)^{0.68}(\alpha E')^{0.49}\left(\frac{W}{E'R'^2}\right)^{-0.073}(1 - e^{-0.68k})$$

Equation 3 Minimum film thickness equation [20].

Definition of terms used above: H_0 = minimum film thickness, U = entraining surface velocity [m/s], $Ŋ_0$ = viscosity at atmospheric pressure of the lubricant [Pas], E' = reduced Young's modulus [Pa], R' = reduced radius of curvature [m], α = pressure-viscosity coefficient [m^2/N], W = contact load [N], K = ellipticity parameter defined as: k = a/b, 'a' = semi axis of the contact ellipse in the transverse direction [m] and 'b' is the semi axis in the direction of motion [m].

The equations above were used with known values and standard data available for the system (pressure-viscosity coefficient for mineral oil blends assumed to be 0.0157 mm^2/N. Ellipticity parameter, k, for point contact = 1). The value of lambda was then found using MatLab for the piston-ring and liner contact. The value obtained was λ = 0.0040, as such the modified Stribeck diagram shows that the system is operating under boundary lubrication. This confirms that the friction regime of most relevance to this study is boundary lubrication, as anticipated. This friction regime is the predominant one, occurring in the internal combustion engines at key contacts. Specifically, the piston ring and liner contact as well as at the camshaft interface. These areas are key to an engine's performance as wear at these parts can be very detrimental to the performance of an engine [21, 22]. Low friction in these applications is also highly sought-after to

reduce fuel economy [7]. Both these interfaces can benefit from being coated with DLC as they operate within boundary lubrication. Within boundary lubrication, an important aspect to consider is durability of the contact area where metal-on-metal, or in this case DLC-on-metal, dominates. Here lubricant additives are required to modulate any damage that occurs as a result [23].

Reducing friction in engines has huge potential for reducing fuel consumption globally. It has been shown that only 21.5% of the energy put into an engine is actually translated to moving the vehicle [7]. Reduction in mechanical losses can translate to reduction in fuel consumption [24]. One way to reduce friction in systems like engines is by employing DLC coatings with the aim to reach lower friction, as is sometimes encountered with DLC [25-27].

The rise in demand for non-ferrous coatings has demonstrated the need for optimisation of the lubricant that DLC interacts with. Traditional lubricant formulations are optimised for interactions with ferrous materials and therefore there is an opportunity to improve on this current situation. This is because DLC can be regarded, tribologically, as fundamentally different to steel [28, 29]. This is where room for tribochemical innovation lies, both with respect to the various DLC coatings and oil formulations.

1.1.3. Wear

In order to fully understand wear, first a definition is required:

> *"The process or condition of being worn or gradually reduced in bulk or impaired in quality by continued use, friction, attrition, exposure to atmospheric or other natural destructive agencies; loss or diminution of substance or deterioration of quality due to these causes."[30]*

This definition allows for inclusion not only of mechanical wear as facilitated by friction but also chemical wear as caused by the atmosphere and any reactive species generated through wearing (reactive metal ions, radical species). These factors are far more relevant when looking at DLC contacts

due to the differences in reactivity of steel surfaces and carbonaceous surfaces.

Wear includes changes in surface topography by displacement of material without loss of that material; as well as the more commonly encountered type of wear, involving loss of material to induce change in surface topography. This definition is also wide in scope and further allows for wearing by chemical means to be included. Wear rate is affected by the contact conditions including; materials qualities, pressure, velocity, and lubricant.

Wear rate is a particularly useful parameter, where the influence of time is included to allow for a broader picture of the system's evolution to be obtained. In almost all instances, wear starts at a higher level; this is sometimes termed as the 'running-in' period, after which wear reduces to a steady, lower state. This often coincides with the formation of a protective tribolayer, if and when the correct conditions are met (such as presence of an AW additive).

Wear is broken down into several different mechanisms. The first two of which are most relevant to this study, these are: 'abrasive wear', which can be caused by cutting of bulk surface, and 'adhesive wear' which consists of shear and transfer. 'Flow' and 'fatigue' are also mechanisms of wear [23]. Wear of tribofilms is then further broken down in a similar manner. Tribofilm wear can be caused by delamination, corrosion and shear fracture [31, 32]. Mathematically, wear can be expressed by the Archard equation [23, 33]:

$$Q = \frac{KW}{H}$$

Equation 4 Archard's wear law

Where 'Q' represents the volume of surface removed, 'W' is the normal load applied, 'K' is the wear coefficient. 'H' is the indentation hardness of the surface that is being worn. The involvement of H shows the relevance of DLC coatings with respect to wear inhibition, as DLC films can and do exhibit very high hardness. However, there have been some criticisms of Archard's theory, stating that it ignores the physics and physical metallurgy of the issue as well as having other weak points [34, 35].

It has more recently been theorised that the Archard wear equation does not hold at the nanoscale for materials like DLC under certain conditions [36]. nanoscale wear is proposed to take place as an ‘atom-by-atom attrition’ process and that chemical transition state theory has a role to play in elucidating wear behaviour [37, 38].

In engines and similarly lubricated systems, wear of the surfaces can be reduced by facilitating the formation of a protective film, or tribolayer. In ferrous systems this has been historically reached by using additives such as Zinc dithiophosphate (ZDDP), which is explored in more depth later [17].

The component that potentially undergoes most severe wear within an engine is the piston ring; this is due the complex tribology of the system it is part of. That is to say the piston ring undergoes large and fast variations of: load, speed, temperature and lubricant availability [19]. Priest and Taylor [19] note that in one single stroke of the piston, the piston ring may experience boundary, mixed and full fluid-film lubrication. In fact, cylinder liner wear can set a lifetime on the engine as whole, due to the very-thin films present that lubricate and protect them [39]. Combining this with the knowledge that boundary lubrication is the most destructive in terms of wearing of mechanical parts, the piston ring represents a valuable target for wear protection. Metal-on-metal wear in this context can be very-high, as such a possible solution to this could be coating either surface with an appropriate DLC coating. This represents one area of focus of the thesis research. Camshafts are also an important engine surface that undergoes enhanced wear within an engine. This is most-true in the diesel engine where loads are typically higher [22]. In particular: pitting, polish wear and scuffing are the typical modes of the follower failure in diesel engines [22]. Due to this, camshafts as an application for DLC coatings are also briefly explored within the work in the thesis.

1.2. **Diamond-Like Carbon coatings**

DLC films are a metastable type of amorphous carbon with a large amount of sp^3 bonding incorporated into their structure [40]. There are many attractive properties of DLC from a materials perspective that helped initial

garner interest in research into the coating as a surface treatment. These include its high hardness, chemical inertness and ability to confer very low friction and wear coefficients [41]. The earliest examples of DLC films appear to be those created by Schmellenmeier in 1953, as reported by Erdemir and Donnet [41]. DLC films are currently being used in a wide range of applications including the automotive sector (Formula 1 cars, Nissan Global), as magnetic hard disks and on razor blades [41]. A variety of DLC films now exist including ones made exclusively of carbon and ones with other dopant elements (H, Si, Ti) included [41-43].

Figure 1-6 A selection of DLC coated engine components as produced by Sulzer

1.2.1. Coatings examined within the thesis

The coatings examined in this work were selected with the help of industry experts. The low Si-DLC is currently a commercial sample that is in use within certain automotive companies. As such, this was viewed as an excellent choice for analysis. The same is true for the a-C:H DLC. The high Si-DLC was chosen to assess the influence that increasing Si content would have on the DLC. This DLC was not an industry standard but was made by the sample company who produce the main two DLCs tested, removing any differences to do with interlayers and precursor materials.

1.3. **Aims and objectives**

DLC coatings are no longer in their infancy as a novel research material. However, there is still no accepted consensus on which type of coating to use at which interface, how different dopants affect the tribology of the system and if current oil additives are the most effective they can be, when applied to DLC contacts. The overall aim of this work is to investigate DLC/steel contacts under boundary lubrication at conditions relevant to the internal combustion engine. The goal of this is to gain a better understanding of the friction, wear and tribochemistry of the system. Key objectives of this are:

- A comparison of the tribology of Si doped DLC versus non-doped DLC
- Optimization doping of DLC using tribochemical knowledge gained
- Identifying the precise mechanism by which DLCs react with oil additives using surface analysis methods. For instance, although certain key interactions are already known, such as the role SiO_X oxides play, the mechanism of their formation is not well explored.
- Efficacy with regards to doping of DLCs. If Si doping can activate DLC surfaces toward additives in the oil this could lead to greatly improved friction profiles, however too much activation could be deleterious to overall wear. This complex relationship will be examined.
- Exploring the importance of the role a ferrous body plays when paired with DLC at the contact. Metallic ions may fundamentally alter the tribochemistry of the contact due to their well-known catalytic behavior. This will be explored by comparing self-mated DLC contacts with steel/DLC ones.

These aims were compiled with reference to current industry standards with regards to both coating manufacturers and lubricant manufacturers. As such the knowledge gained here should help to guide the future development of DLC coatings as well as lubricants developed for them.

1.4. **Structure of thesis**

The thesis is split sequentially by key research areas. This is shown in Figure 1-7. Initially a review of the literature on DLCs is given in Chapter 2. Following this Chapter 3 details the materials and experimental methods used throughout the project, giving justifications of the procedures used and specifications of the coatings as well as experimental apparatus. Chapter 4 provides the first experimental chapter of the thesis. In this chapter three coatings are examined with reference to steel to benchmark the coatings efficacy. After this initial work Chapter 5 then goes on to examine two coatings over varied test durations. This work was conducted as there is a distinct absence in the literature of studies on the long duration performance of DLC coatings.

In Chapter 6 the relationship between oil formulations and Si--DLCs tribochemistry is explored, the goal of which is to elucidate whether current oil formulations are working in synergy with the coating. Chapter 7 then fully explores the effect incorporation of Si as a dopant in DLC has on many aspects of the coating. Finally results Chapter 8 then ties together many of the findings of earlier results chapters by addressing one of the key negative aspects of Si doping, the often encountered enhanced wear. Chapter 9 represents the discussion of the results detailed in the earlier chapters and ties together the findings with the aim of tackling key issues. The overarching conclusions of the research are then outlined in the final chapter, Chapter 10.

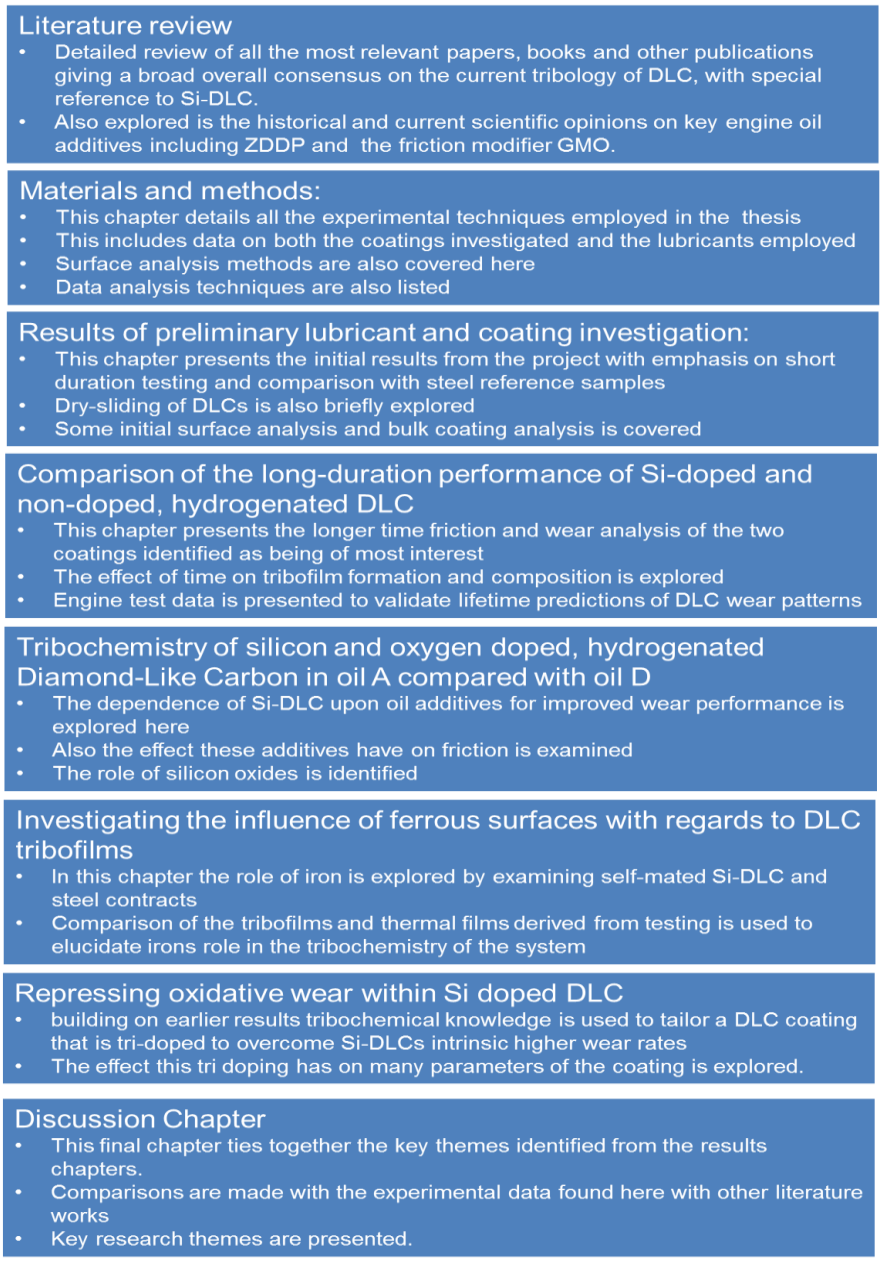

Figure 1-7 Chapter outline shows how the research links together, exploring key areas and culminating in novel findings that helps better the current understanding of lubricated DLC/steel contacts.

Chapter 2 Review of literature on lubrication of DLC coatings

The literature review in this chapter aims to explore key works that help explain the tribological behaviour of DLC coatings, particularly when paired with a metal counter body. It will also closely examine the affect that adding

a doping element can have on a DLC film, with particular reference to the use of silicon. Structurally, the review is split so as to deal with the many aspects of DLC coatings and lubrication in a systematic manner.

Firstly DLC as a whole is addressed with a brief discussion of its inception. This is followed by production methods, which are not explored in depth but must be addressed due to the effect different methods can have on the coatings final structure. Also at this point the first instance of dangling bonds, a highly relevant aspect of DLCs tribology are initially explored.

Following this, both doped and non-doped DLCs are discussed. Particular reference is made to Si doping as this is a major part of the thesis. Other notable dopants are also included.

Friction and wear of non-lubricated DLC contacts are then examined, before moving on to the more relevant area of lubricated friction and wear of DLC contacts. The area of lubricated friction with regards to DLC is well-developed, therefore firm focus was made on the tribology and tribochemistry concerning the contact of ferrous bodies *versus* DLC contacts Finally, surface modification of DLC coatings is addressed. This area of research is relatively novel and as such this section is brief.

The second half of the literature review then focuses on lubrication in general. This includes lubricant additives and their well-known behaviour with steel systems. The tribochemistry of thermal films and tribofilms is then compared. Finally, a summary is presented to bring together the most salient points reported.

2.1. **DLC coatings**

The microstructure of DLCs can vary greatly depending on several factors including: source material (gas, liquid or physical target) chemistry, deposition method and similar parameters. However, broadly speaking hydrogenated DLCs can be visualised as a random network of covalently bonded sp^3/sp^2 carbons with varying degree of C-H bonds included [44]. Although there is no long-range order to the films (hence the name Diamond-like as opposed to diamond, which has long range crystalline

order) it has been observed that there is some medium-range order of about 10 angstroms [44].

2.1.1. Fundamental differences between DLC and steel bodies

DLC films and steel bodies are two very different surfaces. DLC is sometimes considered 'inert' in comparison to steel [45]. This idea can be explained, to some extent, when the electronegativity (χ) of the constituent atoms are examined. DLC is predominately made up of C and H, whose respective electronegative values are $\chi = 2.55$ and $\chi = 2.20$ [46]. Due to the small difference between these values, the surface is comparatively non-polar. When examining a ferrous surface the typical constituent atoms are Fe and O, where Fe $\chi = 1.83$ and O $\chi = 3.44$ [46]. This demonstrates that there is a distinct difference between steel and DLC in terms of surface energy. DLC has a lower surface energy than steel, however this can be manipulated as shown in Table 2-1 [47].

Table 2-1 Surface energies of various DLCs compared to steel [47].

Classification	Polymer	metal	F-DLC	Si-DLC	Si-DLC	Non-doped DLC
Material	**Poly tetra flouro ethylene**	**Steel (1000Cr6)**	**C_2H_2 + C_2F_2**	**C_2H_2 + HDMSO**	**C_2H_2 + TMS**	**C_2H_2**
Surface energy (mN/m)	**18.5**	**>1000**	**19.9**	**24.2**	**31.2**	**41.3**

Surface energy is an important factor when considering interfaces within an engine as many important additives, specifically friction modifiers, have polar head groups with which they interact with the surface [48]. Additives like Glycerol Mono-oleate (GMO) and similar fatty acids have been reported to rely upon tribochemical reactions with metallic surfaces, as reported by Bowden, Gregory and Tabor [49]. As DLCs typically lack metallic components (unless otherwise doped) this could also affect the

tribochemistry of the system. However, this effect does not prevent tribofilm formation [43, 50, 51].

2.2. Production techniques for Diamond-Like Carbon Coatings

A variety of methods exist for producing DLC films. As there are many different production techniques for DLC films, focus is drawn to the technique used to produce the films employed experimentally. The coatings used for this research are produced using the PECVD technique, a subset of PVD.

Currently, PVD is the most common technique encountered with regards to creation of DLC films, having largely superseded CVD (chemical vapour deposition). CVD being a method that relies on more reactive chemical species that are combined in a chamber for film formation, often by reduction or thermal decomposition [52]. CVD has specific disadvantages including the necessity of some highly-reactive precursor chemicals, certain noxious emissions and the use of very high temperatures (up to 1800 °C) [52].

The PVD technique in comparison is a more flexible method allowing for a different range of temperatures (from sub-zero to 400 °C) as well as control over other important variables that can effect film structure, such as bias voltage [41]. Furthermore, PVD is also a faster technique when compared to CVD, offering accelerated deposition rates [53]. PVD can be used to produce DLC films that are almost entirely carbon by using a solid graphite target. This is done using a plasma of an inert gas such as argon. These films, ta-C or a-C typically exhibit very high harnesses' [54].

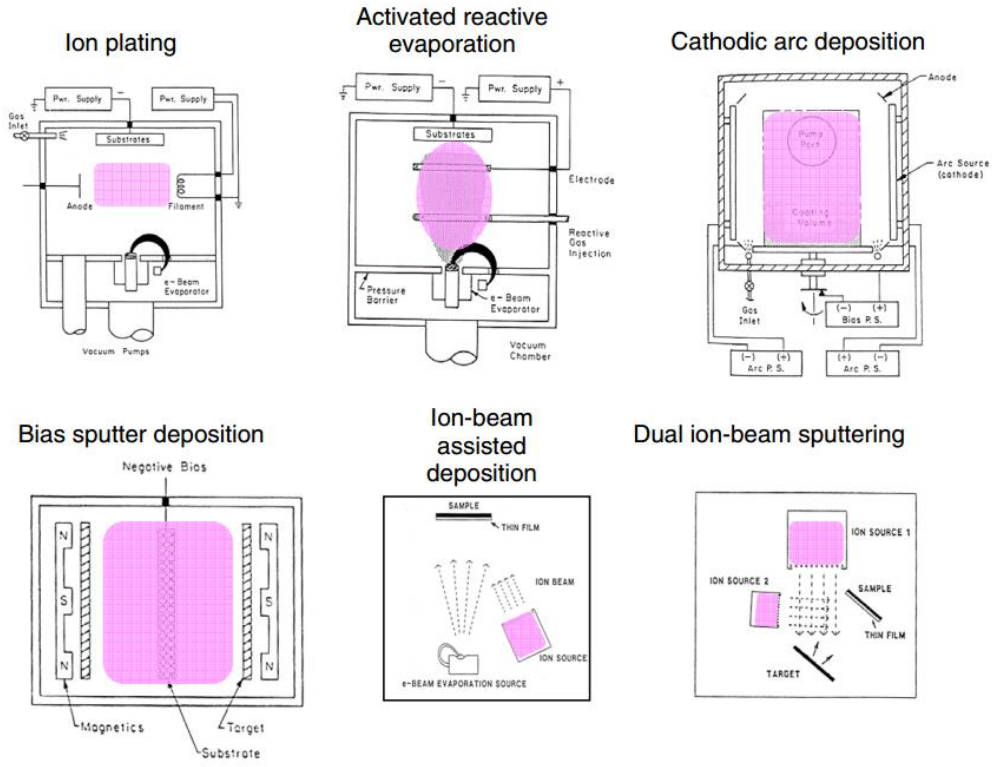

Figure 2-1 A schematic of the various methods used to produce DLC [2].

The PVD technique can be modified to also employ precursor materials (such as acetylene or toluene) thus allowing for manipulation of the final hydrogen content of the film. This modification is typically referred to as PECVD (or in some instances Plasma Assisted CVD) which is a hybrid of PVD and CVD technologies. The plasma used is created from a reactive gas in place of argon. This reduces the need for very high temperatures as the vacuum facilitates the lower temperature deposition process [53]. The PECVD method employed for the synthesis of the DLC coatings used in this project generates a cold plasma with both the chamber and substrate acting as the electrodes.

DLC coatings can be deposited on a wide range of substrates, as a virtue of the lower operating temperatures associated with PVD. To maximise the adhesion of the coating to ferrous substrates, interlayers are often employed, one of which can be Si based. Adhesion is covered in more depth later in the review.

2.2.1. Adhesion of the coating to the substrate

Adhesion can be a problem with regards to DLC coatings on certain substrates. DLC coatings are able to form strongly bonded carbide and silicide layers which then enables enhanced coating adhesion to more commonly encountered materials such as ferrous surfaces or ceramic bodies [41]. The use of this strategy enables the coating to be deposited on a wider range of substrates. As such DLC coatings are often encountered bonded to metallic surfaces via an interlayer of SiC or TiC [41]. One such interlayer is shown in Figure 2-2. Several elements can be used for this purpose: Ti, Si, W and Cr with cost influencing which type to employ within which application. The elements listed are able to form stable compounds with both the metal substrate and the DLC, thus maximising adhesion [41, 55].

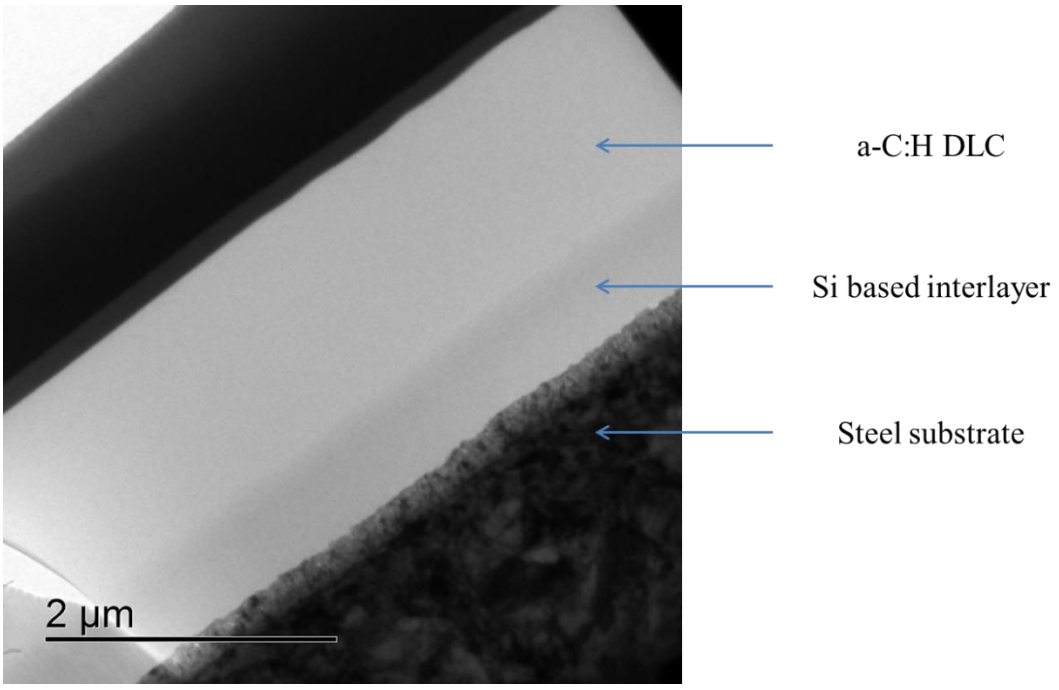

Figure 2-2 Interlayer structure of a-C:H DLC film (courtesy of LEMAS).

The ability of a DLC coating to adhere to its substrate is crucial to the performance of the film. If the coating cannot adhere strongly to the steel (or similar) surface it is deposited on it will very quickly delaminate, which is viewed as coating failure [56]. Poor adhesion is typically caused by weak

bonding between the DLC and the substrate, as addressed previously. It can be caused by the presence of residual stresses in the film post deposition [57].

Si based interlayers are often employed to ensure the DLC is firmly bonded to the substrate. This type of interlayer will be explored in more depth as it can complicate the research on Si-DLCs, as an Si-doped DLC will intrinsically have better coating adhesion than a non-doped DLC without an interlayer present. An example of this is given in the graph in Figure 2-3. SiC incorporation increases critical load (as tested by scratch testing) to in excess of 50 N compared with less than 20 N for the non-SiC coating [58, 59]. The interlayer here is a composite of an initial Si layer followed by a SiC layer which is believed to maximise film adhesion [58].

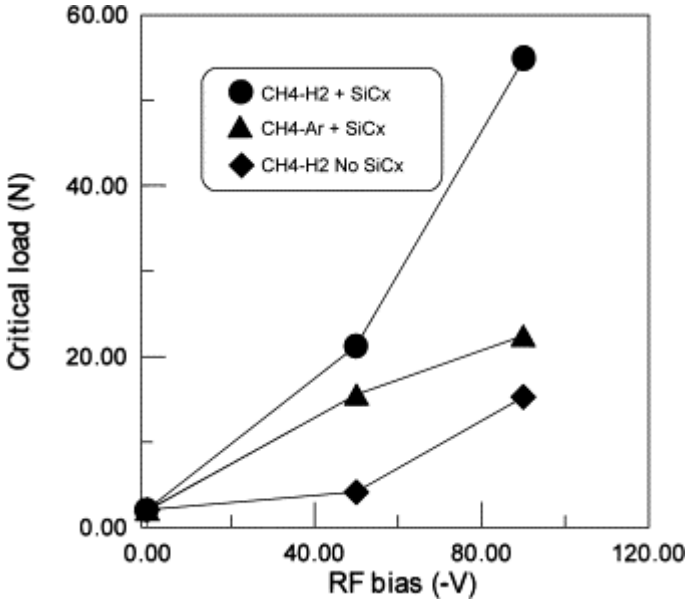

Figure 2-3 Data showing incorporation of SiC increasing coating failure resistance [58]

It is also noted that DLC adhesion is improved when an initial amorphous silicon layer is deposited on another metallic surface, a Ti6Al4V substrate. This effect was independent of surface morphology, with no differences in adhesion being observed over varying surface roughness values [60].

From this it is possible to see that Si-doping is an effective strategy to increase film adhesion. Furthermore, Si adhesion layers can be incorporated using cheaper precursor materials, such as silicon-containing organic reagents. This is opposed to the alternative of expensive, very high purity metals such as Ti and W. However, it must be noted that other approaches exist to combat adhesion problems, such as altering substrate bias to increase critical load [61]. Additionally, other factors exist that negatively affect coating adhesion, such as greatly increased coating thickness [62].

2.3. **Dangling bonds**

Dangling bonds are widely discussed in the literature concerning DLC. Having briefly discussed production methods a review of dangling bonds logically follows on from this. Dangling bonds can form at various stages in the lifetime of DLC coatings.

Primarily however they appear as nascent DLC is removed from the production chamber [63-65]. This nascent DLC is surface-rich in carbon dangling bonds that then are able to react, or be passivated, by molecules in the air. This results in the formation of –OH and –H terminated carbons [65]. These species are known to play a key role in friction [27, 41, 65]. Dangling bonds can be circumvented if a thermal annealing process is employed post production. This suggests a rearrangement of the DLCs microstructure occurs upon heating [64].

A dangling bond is defined as being an immobilised carbon atom whose valance requirements are not fully satisfied. Chemically, the species would be viewed as a radical; these species are known to be highly reactive. If carbon dangling bonds are analogous with those found in similar silicon structures: it can be expected that the electron wave function is largely *p*-like as found in Si [66]. It can also be expected that 50-80% of the electron density is on the central atom, the rest being back bonded to a neighbour.

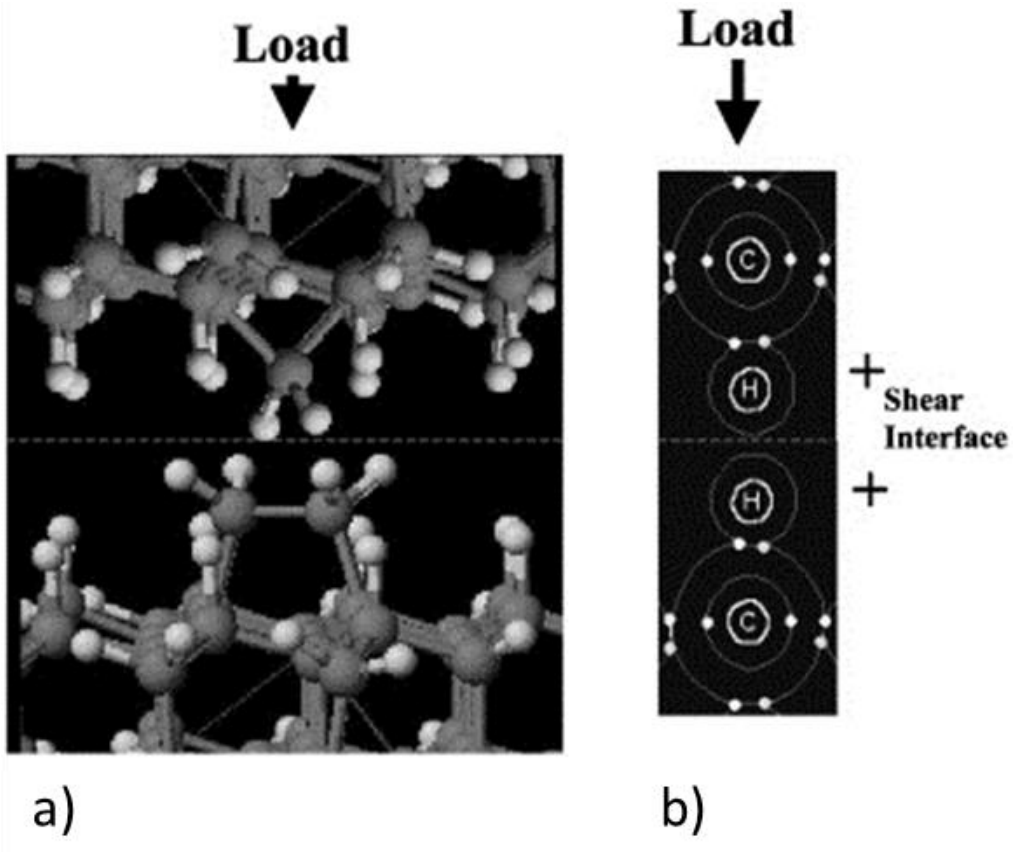

Figure 2-4 Illustration showing how dangling bonds are passivated in H-DLC from [8]. A) shows a super-hydrogenated DLC with di-hydrogenated surface carbons which enable greater chemical inertness. B) Shows the more usual case of mono-hydrogen terminated DLCs.

The presence of dangling bonds has been widely reported in DLC and similar materials [64-70]. One of the key elements affecting friction within self-mated DLC contacts (particularly in vacuum and non-lubricated contacts) is the reactivity of dangling bonds. Erdemir [69] observed that prior to allowing reactive moist air in to a test chamber dangling bonds are able to form strong covalent interactions with the atoms of mated materials. This causes high adhesion and friction. Also noted was that once moist air was allowed into the test chamber these dangling bonds are ‘quenched’ or ‘passivated’ by water molecules or oxygen present in the laboratory air. Erdemir [69] goes on to suggest that DLC surfaces sliding in an inert gas or vacuum have the species that were adsorbed on the dangling bond sites removed, possibly due to mechanical wear or thermal desorption. This re-exposes the sigma bonds and correspondingly raises friction values.

The highly hydrogenated DLC tested by Erdemir [69] has the opposite tribological profile. Super-low friction is observed for the dry sliding of the

DLC and this is attributed to the removal of the possibility of strong covalent and π–π* bonding at the interface as depicted in Figure 2-4. The opposite tribological behaviour is observed when laboratory air is introduced to the test chamber. Super-low friction immediately ceases and μ values rises to 0.06, which the author attributes to the development of capillary forces around the real contact spots. The friction trace of this experiment is shown in Figure 2-5.

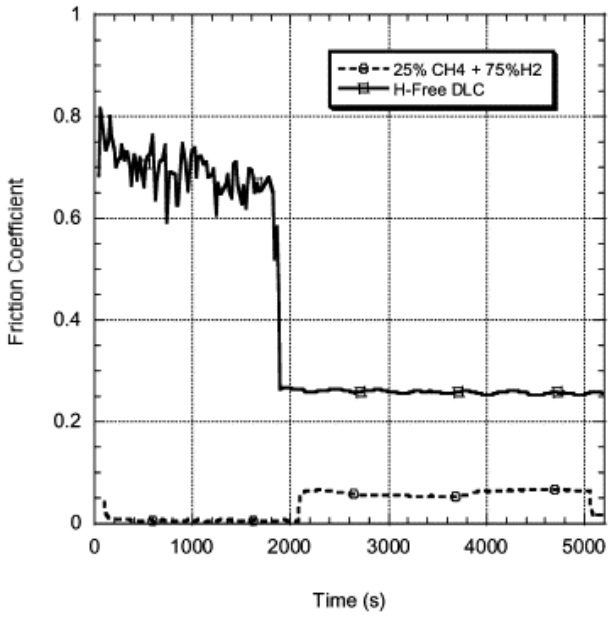

Figure 2-5 Erdemir's comparison of H and H-free DLCs in different environments, with moist air being allowed into the test chamber at just before the 2000 second mark [69].

As yet it is unclear whether, at the sliding interface, passivation becomes a dynamic process; a cycle of bond cleavage and bond forming which affects friction and wear. The alternate case being that passivation could only be relevant during the ‘running in’ period of any sliding contact. The most likely cases being the former as the inevitable consequence of wear is that some additional dangling bond sites will be created, thus ensuring that dangling bonds are always present. Dangling bonds must behave very differently *in lubro* due to the amount of species present that they can react with; this could in fact potentiate the formation of tribofilms on DLC. This is directly opposed to a metallic surface whereby the metallic structure (specifically the presence of delocalized electrons) does not allow for dangling bond formation.

Yamauchi *et al* [65] employed Electron Spin Resonance (ESR), a technique which is only sensitive to unpaired electrons, to follow dangling bond sites (DBS). This showed that in vacuum conditions the DBS are quite stable. They do not decay when held under vacuum at room temperature for several hours. However, they do decay rapidly on exposure to air, a result of passivation [65]. Yamauchi [65] *et al* also looked into the effect of source gas chemistry on the prevalence of DBS in the DLC coatings produced. The results indicated that there is a strong link between unsaturated π bonds in the precursor molecules (e.g. acetylene) which are involved in the formation of DBS when plasma enhanced chemical vapour deposition (PECVD) is used as the production technique. Also the group showed that DBS are highly tenacious as long as they are contained in vacuum conditions. This indicates that all the DBS are immobilised. As, if the sites were not immobilised they could re-combine with each other and thus passivate the dangling bonds. However, upon exposure to air the intensity of DBS markedly drops, due to the reaction with oxygen. Yamauchi's [65] investigations into passivation of DLC draws parallel conclusions to those drawn by Tsu *et al* [67] who looked at a-Si films produced by molecular-beam deposition. Tsu *et al* [67] passivated the DBS of Si using different gas, including fluorine, with success. Yamauchi *et al* [65] go on to suggest there are two types of DBS, classified by their behaviour in oxygen/air. The DBS can be categorised as either 'reactive' or 'non-reactive' DBS, as depicted in Figure 2-6.

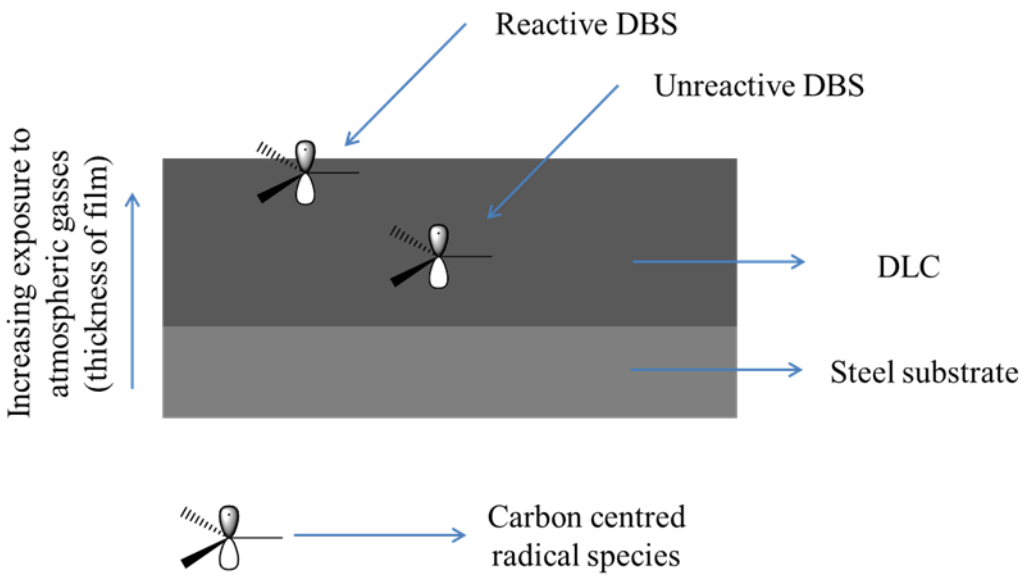

Figure 2-6 Two types of Dangling Bond Sites in DLC films (DBS)

This is also outlined by Tsu *et al* [67] for a-Si films. Yamauchi et al [64] supports the hypothesis with evidence of the DBS intensity decreasing to a limited value in air. The reactive sites are suggested to be reactive due to being close to the surface of the coating. This makes them easily accessible by molecular oxygen, the converse being true for the un-reactive sites which are sterically protected from reactive molecules in the air.

In a later work, Yamauchi *et al* [64] explores the process of heat treating (still under anaerobic conditions, 150 °C for 6 hours) of DLC coatings so as to purposefully decay the DBS. After annealing, the film produced did not include any type of oxygen atoms when analysed by XPS, also the hydrophobicity of the surface was increased [64]. This suggests that the DLC is able to alter its internal microstructure to quench the dangling bonds without the need for external reactants.

Konicek *et al* [70] suggest that the origin of ultralow friction is in fact from the passivation of dangling bonds in DLC type films and coatings. The mechanistic explanation for this is that a cycle occurs whereby: mechanical stress causes bond breakage and passivation follows this as gases like water vapour create –OH and –H terminated species. The low friction and wear observed is attributed to this cycle. The group performed comprehensive analysis using a variety of analytical techniques, including

NEXAFS (Near Edge X-ray Absorption Fine Structure), of ultrananocrystalline diamond as a model for DLC. Intensity of the C=O and C-H bonds in the worn area of tested samples in some cases increased by as much as 205%. It is suggested that this is evidence that dangling bonds were produced and passivated by air. The group also observed that ordered-graphite is not formed in the wear scar; an often proposed mechanism for super lubricity in DLCs. NEXAFS is thought to a more accurate technique than TEM-EELS for detecting graphite [71].

Passivation can also be manipulated to functionalized certain DLCs. Labile molecules can passivate carbon centred dangling bonds on DLC in addition to molecules in the air. This can only occur if the nascent DLC film is protected from air post production and exposed to a different species to oxygen [63, 72]. Tribologically it would be useful to establish if, when the dangling bonds are passivated with either C or H, as opposed to O species, this friction increase is conserved. As O species will typically be polar and increase body/counter-body interactions replacing these with –H terminated surfaces could result in lower friction. Similarly, using F to terminate the dangling bonds could also affect this change. Ideally, passivation could occur with a tribochemically useful element, such as sulphur, could then influence the reactivity of the surface with lubricant additives. This alteration could potentially mitigate some aspects of running-in wear.

2.4. **Non-doped DLC (ta-C, a-C:H)**

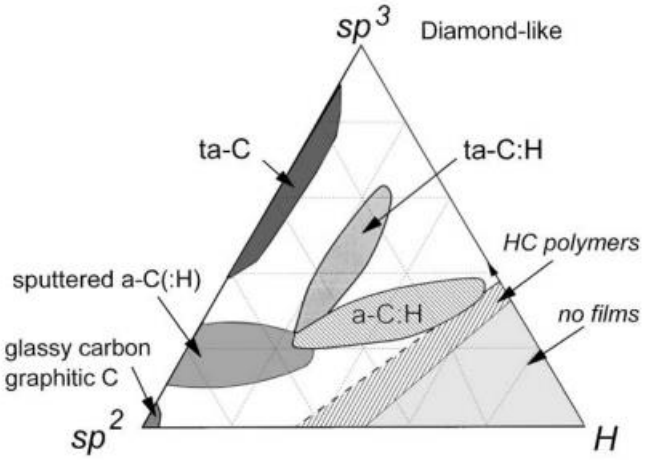

Figure 2-7 Phase diagram of DLC adapted from [73]

Non-doped DLCs would be the classification that applies to the two main types of DLC films; these are; hydrogenated and non-hydrogenated. These would both be regarded as non-doped as dopants in this sense typically refer to other (Ti, Si, W, and F) elements. The degree of hydrogenation within the DLC can affect various qualities of the final coating produced, as shown in the phase diagram above. This will be discussed in more depth later. Although amorphous carbon films are often reported in the literature, these films too must inevitably have a small amount of H and OH within them. This is due to the passivation of dangling bonds swiftly following manufacture of the film [41, 63-65, 69].

The degree of hydrogenation affects the microstructure of the coating and many other properties. ta-C coatings tend to be the hardest of the DLCs produced and show low wear, however they often cause higher wear of counter bodies [55]. Hydrogenated DLCs are softer and typically show lower levels of internal stress [41, 74, 75].

2.5. **Doping with Si**

Doping DLC coatings with silicon or silicon and oxygen is currently an active area of research as summarised in Table 2-2. Many Si-DLCs have been created that consist of varying amount of silicon, often with a co-dopant of oxygen. This has many effects on the coating produced. One of the most explored affects is how Si influences the bonding on the DLC.

2.5.1. Si-DLC *versus* Si, O DLC

There are many examples of doped DLCs, all created with the goal of further enhancing a particular attribute of the DLC coating. One widely explored dopant is Silicon. Silicon-doped DLC has garnered a lot of interest as it can affect the coating in various ways, this includes; sp^3 content of the DLC, affecting better coating adhesion and lowering dry friction coefficients [25, 26, 58, 59, 76-82]. Many examples of differing Si-DLCs exist and there are a

variety of ways to produce these films. Addition of silicon into DLC films can most easily be achieved by using a siloxane compound, a stable silicon and oxygen containing precursor [83]. If siloxanes are employed the film produced will have noticeable oxygen content, due to the Si-O-Si motif, which will further affect the films composition. Si-DLCs can be prepared from silanes, exclusively silicon and hydrogen-containing compounds, if oxygen content is not desirable.

There is also no current consensus on the optimum amount of silicon to incorporate into Si-DLCs for best performance. In one study when various % doping of silicon were tested an optimum of 6.6 at% was found to be best for wear resistance [84]. However, to best reduce internal stresses of the DLC an optimum of 1-2 atomic % was established. This parameter is to be examined experimentally herein by testing two different Si-DLCs.

Author	Deposition method	Precursor	Friction	Wear	Si-O species
Iseki [85]	**PACVD**	**TMS/ Methane/ H_2**	**Not tested**	**Not tested**	**Non detected**
Kato [86]	**PACVD**	**TMS/ H_2**	**Not tested**	**Not tested**	**Silanol (Si-OH)**
Kim [77]	**RF PACVD**	**Benzene/ Silane/ H_2**	**(air) Friction coefficient decrease with increasing silicon content**	**Wear increased with Si content**	**Low friction attributed to silicon-rich oxide debris**
Oguri [26]	**PACVD**	**$SiCl_4$ / Methane / H_2**	**Friction (air) μ = 0.06, (N_2) μ = 0.03**	**Not given**	**Silicon oxide/ silica sol**
Pham [79]	**RF PACVD**	**Composite; Silane upper layer**	**(air) μ = 0.02, 1/3 of un-doped**	**Higher wear rate that un-doped**	**Si-O containing tribofilm**

Moolsradoo [78]	**Plasma based Ion implantation**	**Acetylene/ TMS/ O_2**	**(Air) 34% at. Si μ = 0.04, 25% at. Si exhibited greater μ**	**Wear increases with annealing in argon/air**	**Silicon oxide layer**
Veres [87]	**RF CVD**	**Methane or TMS or HMDSO**	**Not given**	**Not Given**	**O sequesters Si from the coating**

Table 2-2 Overview of current literature on Si-DLC

Due to silicon's typical reactivity, whereby it does not readily form stable double bonds with carbon, Si can influence the sp ratio within a DLC film. It can also affect the coating's surface energy by enhancing wettability [29]. Doping with silicon can be regarded, to some extent, as a double-edged sword. This is because with increasing silicon concentration, the films tend to exhibit lower hardness [82].

2.5.2. Source material affects

There are several strategies by which Si can be incorporated into the DLC matrix. Commonly, the PECVD technique is used with various organosilane compounds. Oguri and Araia [26] produced one of the earlier examples of Si-DLC using silicon tetrachloride ($SiCl_4$) with methane. The tetrachloride was presumably used as it is easier to handle, being a liquid having a history of being used to yield high quality silicon. However, using $SiCl_4$ as a silicon precursor for Si-DLCs inevitably results in a large proportion of chlorine being incorporated into the film. This results in creation of a dually doped system, a factor which was not accounted for in the paper [26]. The film produced was exclusively characterised with Fourier transformed infra-red spectroscopy, a technique which is known to be insensitive to Cl-C bonding. Following this, various other silanes were used to create Si doped DLCs.

Source gas chemistry has been identified as highly influential in terms of the Si-DLC produced. Iseki [85] notes that when Si-DLC is prepared from

silanes exclusively there is a large fraction of both Si-C and Si-H bonding. Also established was that hardness increased as Si content increases, a finding which is at odds with some other research published [28]. Furthermore, increasing Si content resulted in decreased sp^2 clustering within the film. Kato *et al* [86] compares silane based Si-DLC and non-doped DLC, with a range of 4 – 17% Si content. When examined, the Si-DLCs exhibit the presence of silanol on the surface. It was noted that there is no absorbed water on the non-doped DLC's surface, however for all Si-DCLs there is an adsorbed layer present, this shows Si-DLCs affinity towards oxygenated compounds. Additionally, Kim *et al* [77] examined Si-doped DLC created from a silane precursor and tribotested it under ambient conditions. Low and stable friction was observed and was attributed to the formation of silicon-rich oxide debris. Finally, Pham *et al* [79] investigated a silane based DLC and found that when tested in ambient conditions evidence of both Fe and Si oxides were noted and that the Si-DLC had higher wear than non-doped DLC.

When Si, O containing precursors are used a change in the coating structure occurs. FT-IR suggests that the dominant form of Si in the film is as a Si-O network with a smaller fraction coming from Si-C bonds thus affecting the coating's microstructure [78]. This trend was also identified by Veres *et al* [87], in that the presence of oxygen decreased the amount of Si in the carbon matrix.

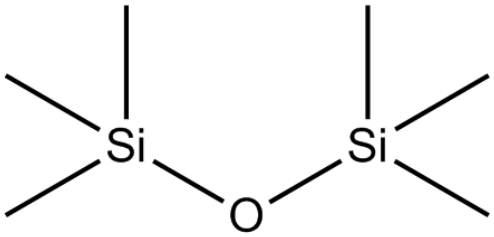

Figure 2-8 HMDSO, a common siloxane used to create Si, O doped DLCs

The inclusion of a large proportion of oxygen must be acknowledged when examining the Si, O-DLCs derived from siloxanes as they can affect the film in a variety of ways. It has been noted that the Si-O backbone can survived

the PECVD process, thus disrupting the DLCs microstructure [78, 87, 88]. Furthermore, inclusion of oxygen with Si will affect the coatings proclivity to react with atmospheric oxygen [43].

2.6. **Other notable dopants (F, Ti, W)**

Silicon is a very-widely used dopant for DLCs. However, other elements are also used prominently within DLC coatings. These include, but are not limited to, fluorine (F), titanium (Ti) and tungsten (W). There are varying motivations for using these elements as dopants. Doping with fluorine is typically performed to reduce surface wettability of the coating [47, 89]. This goal is most likely motivated by the desire to create a surface more like PTFE with its non-stick properties. Some examples in the literature exist where fluorine has been incorporated in a dopant system with other additive elements to create novel DLCs with unique properties, in one instance an a-C:H:Si:O:F DLC was created which was tribotested against an aluminium counter face [25].

It was found that F was able to transfer to the counter body to form AlF_3 and that F species also act in a passivating manner at carbon surfaces. Meanwhile, the Si dopant is able to facilitate low friction. The authors go on to explain a possible mechanism by which low friction is facilitated through F, H and OH, as shown in Figure 2-9.

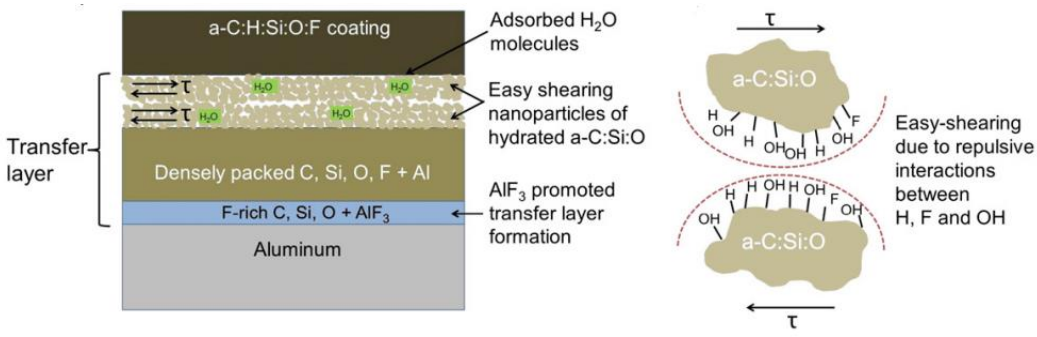

Figure 2-9 Proposed low friction mechanism of novel DLC [25]

However, the proposition that ‘easy-shearing’ is facilitated by repulsive interactions from H, F and OH seems highly unlikely due to the well-known propensity of –OH and –F species to from hydrogen bonds, leading to strong surface-surface interactions, not the ‘repulsive interactions’ postulated by the authors [90]. Therefore it would seem another mechanism is in operation. Doping with metallic elements is typically done with differing outcomes envisaged. Inclusion of Ti in DLCs microstructure has been shown to improve the ability of the DLC to adsorb tribologically relevant elements, particularly P and S [42, 91].

Kalin *et al* hypothesis this enhanced adsorption is due to an increase in surface oxygenation [42]. This theory would explain well the increased affinity for traditional lubricant additives with these specific types of DLCs as they are tailored to work with ferrous surfaces which have inherently oxide rich surfaces.

Doping DLCs with either W or Mo is a goal often pursued within the literature [29, 92]. Mo can influence the DLC film in several way including: lowering internal stress and imparting better coating adhesion [92]. Doping with Mo and W has also been shown to increase the films thermal stability [93]. Interestingly, where Mo/W DLC films are tested in formulated oils containing EP/AW additives no formation of MoS_2 or WS_2 is noted [29, 42]. In fact, even when W-DLCs are tested with MoDTC, the exclusive FM species produced is still MoS_2 [94]. This is noteworthy as MoS_2 and the analogous W species are well known friction modifiers. If a DLC can be created that is able to react with lubricant additives at the surface to produce FM species this would be a hugely useful coating. It would result in a reduction on the dependence of the friction performance on the lubricant additive package.

2.7. **Surface functionalization of Si-DLCs**

One research group has already attempted to exploit the presence of dangling bonds and their inherent reactivity with oxygen. Choi [95] *et al* created self-assembled monolayers (SAMs) on -OH terminated Si-DLC surfaces using a silicon substrate.

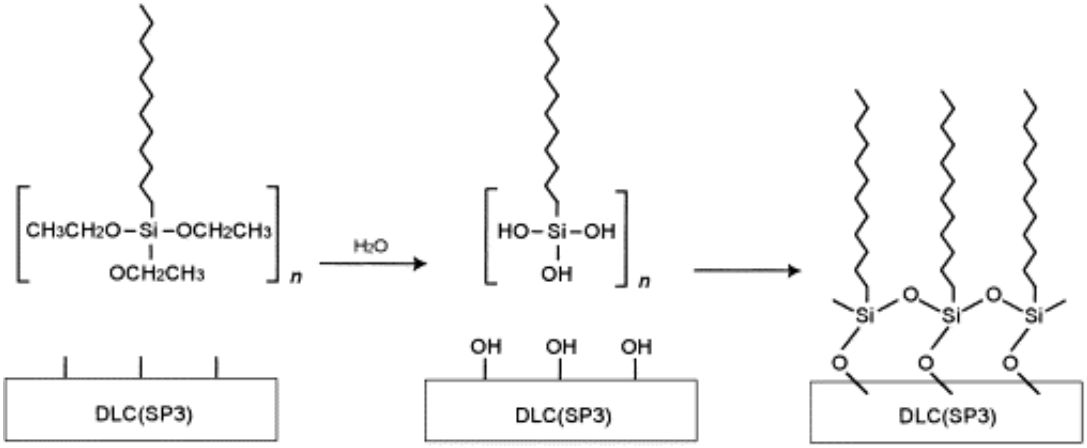

Figure 2-10 SAM layers on DLC [36]

The process was carried out by dip coating of the DLC coupons. The group found that the treated DLC out-performed untreated DLC in un-lubricated conditions. This is presumably as the long chain SAM incorporated onto the DLCs surface can initially act so an immobilised friction modifier, until it is removed by the wear process. A variety of similar self-assembled monolayers have been created on DLCs [96].

2.8. **Friction and wear of DLCs**

2.8.1. Lubricated Friction of DLCs

The role dangling bonds play in the vacuum and dry sliding friction of self-mated DLC films is key to the overall friction profile. However, when sliding against a metal contact or in oil lubricated conditions the friction profiles can change dramatically as dangling bonds have far less of an influence *in lubro*.

In some cases, when lubricated DLC is used in a self-mated contact the enhanced lubricity associated with dry-sliding DLC can be maintained [27, 97, 98]. This is especially true when using lubricants rich in –OH functionalities [97, 99]. However, for most applications, particularly automotive ones, coating both bodies with DLC is an unrealisable goal for many reasons; including cost and the difficult shape/geometries of certain engine parts. As such, self-mated DLC contacts will not be explored in-depth within this review.

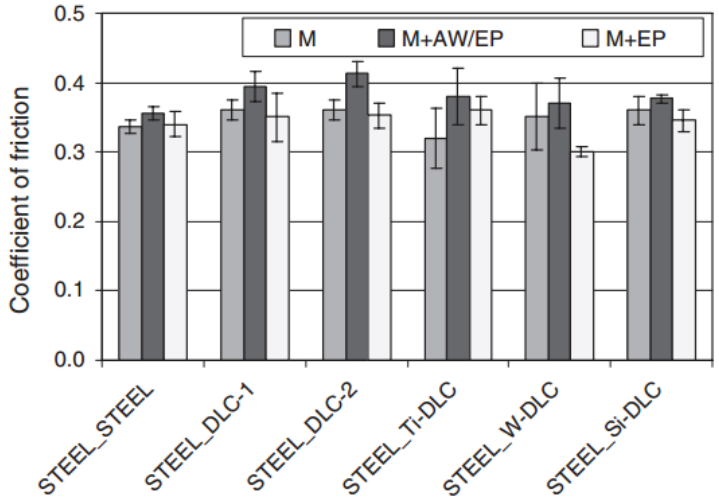

Figure 2-11 Friction behaviour of various DLCs mated with steel counter bodies [29]

Various non-doped and doped DLCs (Ti, W and Si) mated with steel counter bodies do not show the very low friction often associated with self-mated DLCs as given in Figure 2-11. In fact, the coefficients of friction amongst these samples are fairly similar, suggesting a different factor is now dictating the friction of the system. Further to this, when DLCs are tested against steel surface in the presence of ZDDP and MoS_2, as shown in Figure 2-12, the friction performance does not show a large difference from that of steel/steel tribopairs [100].

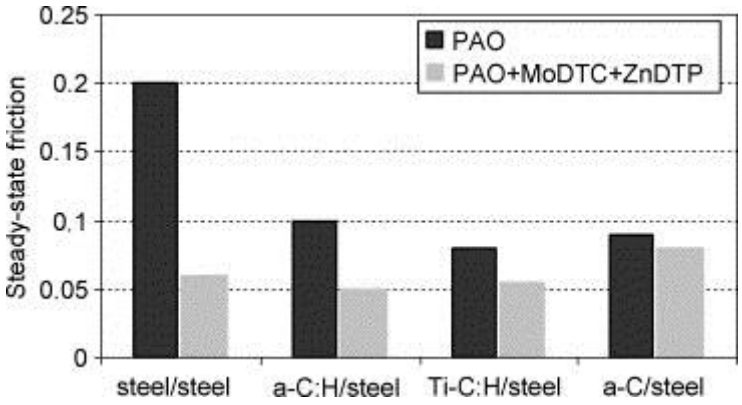

Figure 2-12 Various DLCs against steel in friction modified oil [100]

It can be seen that the MoS_2 friction modifier species is formed and does work with DLC coatings, however the performance of the tribopair does not

offer much of a benefit in terms of friction reduction compared with the steel/steel system [100]. Even when water is used as a lubricant (with a bearing steel ball as a counter a body) both the silicon-doped and non-doped DLCs have higher than may be expected friction coefficients, as shown from research findings in Figure 2-13.

The friction results in Figure 2-13 give a good indication of the values in the literature for lubricated DLC contacts. It can be seen that the DLC coating can exhibit excellent friction profiles but that there is still a need for greater understanding and development of the tribochemistry of the system, especially at DLC/steel contacts.

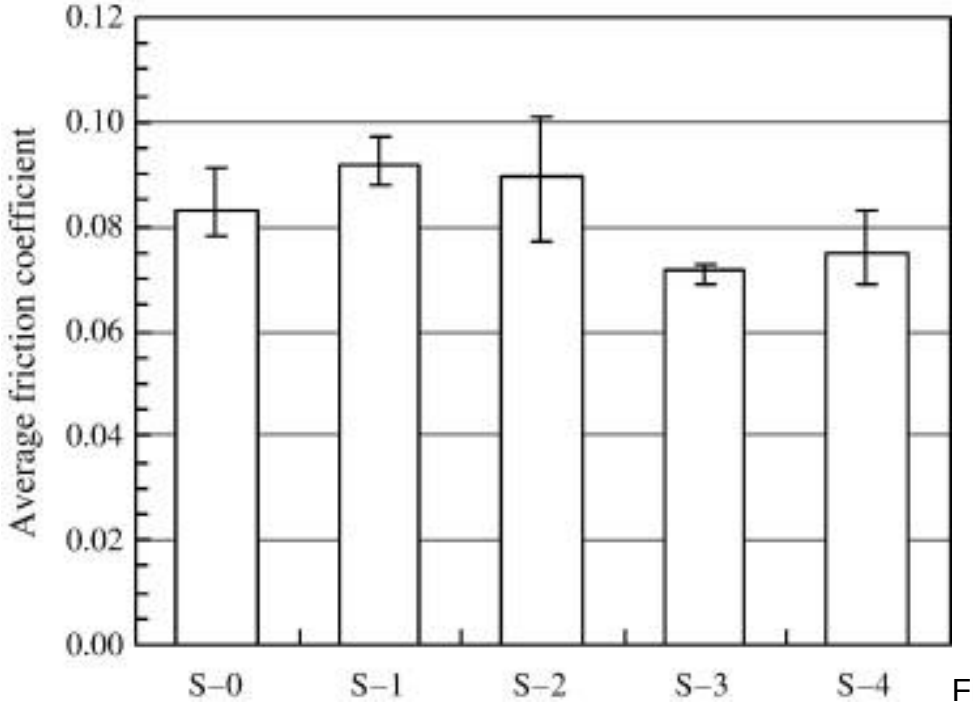

Figure 2-13 Friction performance of Si-doped and non-doped (S-0 represents a-C:H) DLCs in water [17]

Current lubricant blends are not tailored towards the DLC coatings and thus do not work as well as they perhaps could. It appears that, under the conditions explored in the literature, the most influential factor with regards to friction is the lubricant.

Importantly, the boundary lubrication of DLC can be improved by inclusion of certain metallic dopants to the coating [28, 79, 91]. Miyake *et al* [91] tested three metal dopants (Ti, Mo, Fe) and of the three tested Ti showed the lowest friction with MoDTC containing lubricant as well as giving evidence

for a tribochemical reaction at the interface. Certain metals have been shown to mediate the GMO-DLC synergy when considering hydrogen-free, metal doped DLC. It was found that boundary lubrication of DLC films was improved when certain metals (Co, Ce, Mg) were added, in particular Co showed very low friction ($\mu = 0.02$) [101]. It would be useful to know how this low friction was facilitated. Metals are known to interact with certain lubricants, or additives, as explored by Bowden, Tabor and Gregory [49]. Metal ions are can react with fatty acids to form lubricious metal soaps. This affect could be playing a role here. However, the author does not expand on the mechanism.

2.8.2. Dry sliding of Si-DLC contacts

The dry lubricated Si-DLC contact has been widely explored experimentally. Typically, Si-DLCs at non lubricated contacts exhibit friction coefficients far lower than non-doped DLCs [79, 80, 102, 103]. Many mechanistic studies have been centred around finding the cause for the observed low friction; although there is not yet enough evidence to make a firm conclusion on the origin of the enhanced lubricity of the film. It would however appear that the formation of silicon oxides play a key role. Many authors note that when analysing the worn area with a variety of spectroscopic techniques there tend to be a large increase in the amount of various SiO_x type species [26, 77]. These species could affect friction through several mechanisms. One paper explores the low friction mechanism in some depth by comparing the friction obtained from a-C:H:Si:O:F doped DLC (paired with an Al counter body) with that of a silicate glass. The silicate glass gives far higher friction than the DLC in this instance and the authors use this as evidence that the SiO_2 species alone is not what influences the friction but rather the Si and O within a DLC matrix [25].

2.8.3. Lubricated Si-DLC contacts

Although Si-DLCs are known to have excellent friction profiles when in either vacuum or dry sliding conditions, this can change radically when a lubricant is employed with the DLC. As shown above in Figure 2-11, the coefficient of

friction of Si-DLCs when tested in various oils does not show the large reduction in friction associated with dry sliding Si-DLCs.

2.8.4. Wear trends with Si-doped DLCs

As already covered briefly, the wear of silicon doped DLCs tends to be higher than that of non-doped DLCs. The general rule being; increasing the % atomic doping of Si within the coating results in increased wear [76, 77, 79, 84, 104]. Although there is some discourse about this in the literature as inclusion of Si also tends to increase film adhesion, therefore a poorly adhered a-C:H DLC may be outperformed by an analogous DLC with a small inclusion of Si dopant [88, 102]. Several papers have explored the tribological basis of this in varying degrees of depth. Many authors note the presence of silicon rich oxide debris, SiO_x particles or silica-sol type particles [43, 77, 79, 105]. Wear trends as identified in the literature are given in Table 2-4.

2.9. Lubricant additives and oil packages

A problem encountered when lubricating DLC coatings is that, due to the relatively inert nature of DLC when compared to traditionally ferrous materials; knowledge gained on steel/steel tribological contacts cannot be directly applied to DLC [106]. Where metal components can easily adsorb lubricant molecules onto their surface, DLC coatings have a low surface energy which makes this process harder [107]. For metal-lubricant chemistry there is a chemical driving force whereby the polar groups of lubricant additives such as certain –OH, -COOH and –NH groups can make favourable interactions with the polar, metal surface [49].

Certain specific oils have shown promise when their lubricating properties have been tested on DLC coatings. When glycerol is used as a lubricant on hydrogen free ta-C the friction coefficient obtained by Matta *et al* [98] was below 0.01 at steady state. This super-lubricity regime was attributed to ‘easy glide on triboformed OH-terminated surfaces’. The authors go on to

further explain that this could be due to the breakdown of glycerol in to its constituent acids and water.

This then allows for the long organic chain usually associated with these molecules to orientate the fatty chain into the oil, thus satisfying thermodynamic requirements [108]. DLC however is not as polar as its corresponding metal counterparts [48, 63, 109].

Table 2-3 Overview of literature of lubricated Si-DLC contacts

Author	DLC	Counter body	Lubricant	Friction	Wear
Ando [110]	**Si-DLC (CD-PACVD)**	**High-carbon chromium steel bearing ball**	**ATF fluid (Ca, P, B, S containing)**	**Initially lower friction than nitride steel (0.14 – 0.09). Remains steady at Si-DLC 0.11**	**Not quantified**
Ban [104]	**EBEP-CVD Si-DLC**	**Bearing steel**	**ZDDP and base oil**	**ZDDP friction: Si-DLC 0.07, steel 0.08**	**Base oil wear: Si-DLC wears more than steel. ZDDP: no wear reported**
Chapter 6 p.125	**Si,O-DLC PACVD**	**Steel**	**Fully-formulated oil Low additive oil**	**Formulated: 0.09 Low additive: 0.1**	**Wear in low additive Oil higher than in fully-formulated**
Wu [84]	**Si,O-DLC (thermal electron excited plasma CVD)**	**AISI 440C bearing steel**	**Water**	**Lowest value = 0.07, highest value = 0.09**	**Wear increased with silicon content. Less wear for non-doped sample**

Importantly, Kalin *et al* [107] demonstrated that DLC is not as inert as was first thought; it was found that including polar groups and unsaturated fatty acids in the base oil can substantially improve the efficacy of the oil. In fact, the study showed that the non-polar oil had the worst tribological

performance. Several of these relationships have been observed between both glycerol and GMO (glycerol mono-oleate) when lubricating types of DLC, leading Topolovec-Miklozic *et al* to postulate a 'polyol-DLC interaction' [97, 99, 111].

Glycerol monooleate (GMO) also showed a reduction in friction when tested upon two types of DLC coatings. The coatings investigated were; hydrogenated diamond like carbon and Cr-doped, (non-hydrogenated) graphitic DLC. On both the surfaces the additive was shown to remarkably reduce friction at intermediate speeds [111].

Kano *et al* [99] also investigated GMO as an additive in Poly-alpha-Olefin (PAO) and recorded ultralow friction when two ta-C DLC counter faces slid against each other. Spectroscopic techniques (XPS, SIMS) were employed to elucidate a mechanistic explanation for this. It was found that, in the worn areas there were twice as many lower fragment ions of species though to be produced from decomposition of GMO. A suggested explanation is that degradation of GMO produces OH^- species, which may go on to react with dangling bonds on the DLC surface. This is thought to facilitate easy sliding between the two hydroxylated surfaces as shown in Figure 2-14.

Investigations on GMO in PAO have shown that GMO interacts with DLC (author does not specify hydrogen content) via the ester moiety but; that the hydroxyl groups 'play significant roles in the interaction' [112]. ToF-SIMS was used to follow the reaction pathway of the GMO. DLC samples were submerged in solutions of both GMO and a dehydroxy analogue (Butyl oleate). Upon analysis, very little Butyl Oleate was found on the DLC surface; conversely evidence of GMO was found on the surface. The authors go on to note that rubbing the DLC surface did not lead to activation of it. Interestingly a synergism is noted between GMO and PAO.

Table 2-4 Wear trends when examining Si-DLCs

Author	Deposition method	Precursor gas	Si-DLC/ Si,O-DLC	Observed Wear	Si-O species
Gilmore [113]	**PACVD**	**TMS Or TMS/ acetylene**	**Si-DLC**	**Coating wear resistance adversely affected by addition of Si**	**n/a**
Gilmore [76]	**PACVD**	**TMS/ acetylene**	**Si-DLC**	**Addition of Si results in a significant increase in wear rate**	**n/a**
Kim [77]	**RF PACVD**	**Benzene/ Silane/H_2**	**Si-DLC**	**Wear increased with Si content**	**silicon-rich oxide debris detected**
Wu [84]	**CVD**	**Toluene and HMDSO**	**Si,O-DLC**	**Wear increased with the Si content**	**$SiO_x(OH)_y$ gel detected**
Pham [79]	**RF PACVD**	**Composite; Silane upper layer**	**Si-DLC**	**Higher wear rate than un-doped DLC**	**Si-O containing tribofilm detected**
Ban [104]	**electron beam excited plasma**	**CH_4, SiH_4**	**Si-DLC**	**Wear scar diameter of Si- DLC 1.5 times larger than against the DLC film**	**Si-DLCs wear scars contains additional oxygen - SiO_2 detected**
Lubwama [114]	**closed field unbalanced magnetron sputter**	**Ar and C_4H_{10} (solid Si target)**	**Si-DLC**	**Lowest wear depth was observed for DLC films**	**n/a**

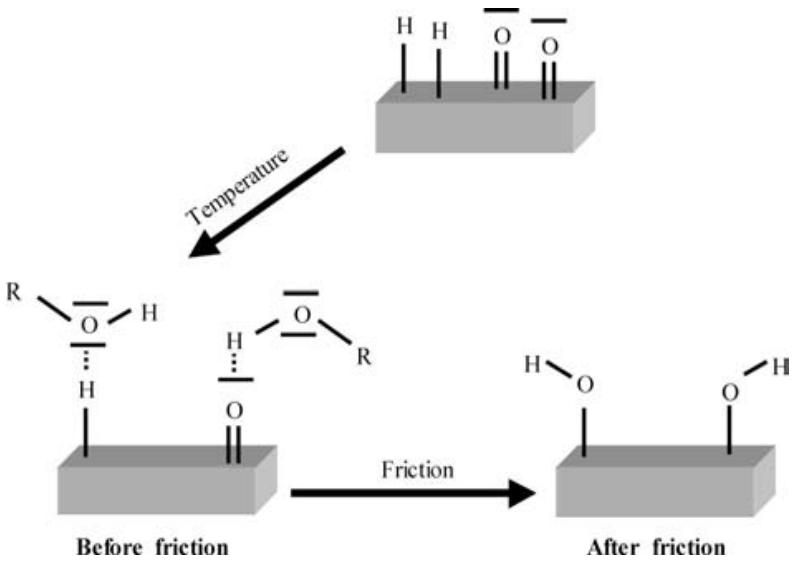

Figure 2-14 Hydroxylation of DLC [112]

When GMO was used as an additive in mineral oil it is far less effective as a lubricant. Minami *et al* suggest this is due to certain alkyl chains of PAO being able to insert themselves into GMO films on the DLC coating [112]. The wealth of literature available on DLC contacts not only shows DLCs can and do react and perform well with traditional lubricant packages; but also that next generation additives, like GMO, are able to work well with them too. This is important as next generation NOCH additives will soon be required to replace older, high-SAPS formulations [8].

2.9.1. The multi-role engine oil additive, ZDDP

The traditional multi-role lubricant additive ZDDP, as shown in Figure 2-15, has been used in the internal combustion engines for many years, it is arguably the most important additive to date in terms of maintaining engine performance. ZDDP was introduced in the early 1930s and is still used currently as it is able to perform many roles within an engine, including oxidation inhibition, wear prevention and corrosion inhibition [115].

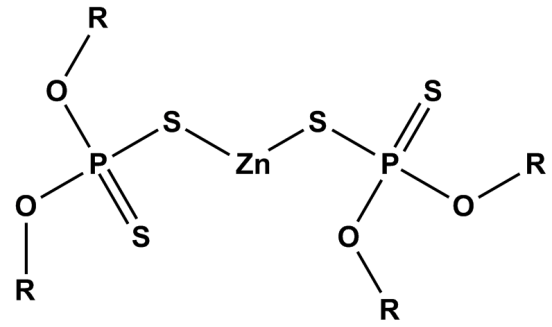

Figure 2-15 One possible structural representation of ZDDP

The efficacy of ZDDP is well-proven in steel-steel systems and is also being validated at the DLC interface, although via different tribochemical mechanisms [51, 100]. The effect of ZDDP on DLC coatings is an active area of research. The focus is typically around comparing the performance of DLCs with that of steel samples, and observing similarities or differences so that knowledge gained can lead to performance improvement.

The ZDDP tribofilm formation mechanism most agreed upon with steel surfaces is that ZDDP is firstly adsorbed on to metallic surfaces, prior to any chemical reaction. This is followed by a chemical reaction at the surface resulting in the formation of phosphates and phosphothionic moieties on the metal [115]. Additional phosphate film precursors are formed from oxidation of ZDDP [116]. Figure 2-16 depicts Willermet *et al's* [116] proposed initiation of a ZDDP film.

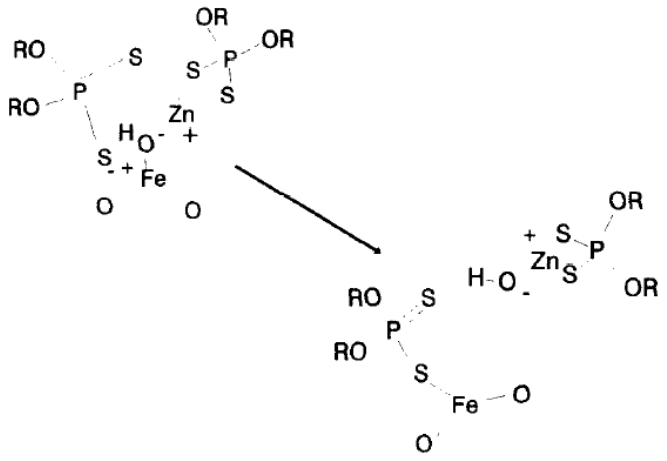

Figure 2-16 Willermet's proposed initial film forming step of ZDDP reacting with a ferrous surface

More recently this mechanistic explanation has been expanded upon, ZDDP is adsorbed onto the steel surface however when temperatures exceed 150 °C Fuller *et al* [117] established that linkage isomers are formed. The linkage isomer then undergoes thermal-oxidation and forms long chain polyphosphates. These can, in some cases, be broken down in the presence of water to create shorter chain polyphosphates.[117, 118]. Spikes [115] further notes the role oxidation plays with regard to the formation of ZDDP films, with comment that in the absence of hyperoxide type species ZDDP thermally degrades at ~ 130 ° C yielding a film, the reaction of which is shown in Figure 2-17.

Haque *et al* [119] elucidated that the mechanism for wear protection of ZDDP must be different on a DLC coated part when compared to the mechanism found on a steel sample. This was established as no Fe or P was detected in the tribofilm. In fact the tribofilm formed on the H-DLC coating was made up of different zinc species including oxides and sulphides [119].

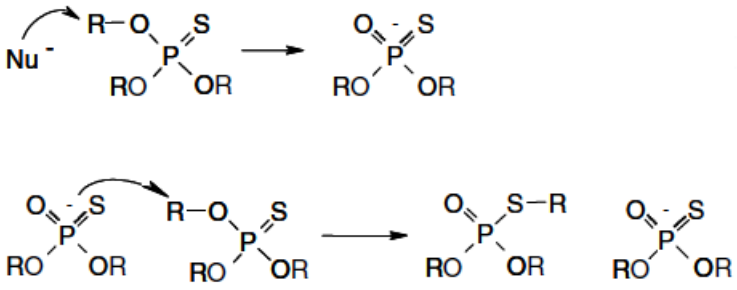

Figure 2-17 Thermal degradation in the presence of oxygen. Nu^- represents nucleophilic species, oxygen based nucleophile [115]

Barros'Bouchet *et al* [51] have observed that MoDTC and ZDDP combined in poly-alpha olefin (PAO) have been shown to react on amorphous DLC coatings. XPS analysis conducted on the coating showed formation of MoS_2 in the wear scar and EDX indicated the presence of Zn and P. The authors suggest the composition of the tribofilm is 'similar' to that obtained from the classic ferrous system - a positive in terms of lubricant DLC interactions [100]. The authors comment that no Fe has been detected in the tribofilm and that no delamination or excessive wear is observed. In a similar

investigation Costa *et al* also established a tribofilm containing MoS_2, ZnO and ZnS is present in the DLC track from MoDTC and ZDDP decomposition [120]. Molybdenum disulphide will not be covered here in depth as this lubricant additive was excluded from all lubricant blends explored within the project.

2.9.2. Organic friction modifiers

There are a few key widely used inorganic friction modifiers, including molybdenum disulphide (and the analogous tungsten disulphide), as well as powdered graphite [121-123]. These compounds are typically classified as dry lubricants as they can lubricate without the presence of oil. MoDTC is the parent additive that creates MoS_2 *in situ* and renders the compound oil soluble [51, 122, 124]. Graphite is not typically used within the engine as it can form soot which negatively affects wear [125]. The dichalcogenides however work extremely well within the internal combustion engine. When examining DLC, molybdenum based friction modifiers are known to increase wear rates, which often prohibits their usage [126]. This necessitates the use of novel, greener FM species to be used with DLC coatings. Certain NOCH additives have been trialled as friction modifiers for DLC interfaces, including amine based additives and fatty acid type-compounds [111]. These additives have a different mechanism to that of the dry lubricants and rely upon interaction with the surface through polar functional groups [49]. One widely investigated friction modifier is GMO [97, 99, 112]. GMO is very effective when used with certain DLCs, and it has been postulated that the presence of the oxygenated head groups interact well with the DLC surface. This behaviour is facilitated by formation of additional –OH species at the contact interface help facilitate this relationship [70, 99]. However, to obtain friction coefficients as low as can be achieved with MoS_2 in fully formulated additive packages there is still much optimisation required. Currently, organic FM species are not as effective when compared to MoDTC type additives which often give friction coefficients as low as 0.05. Whereas, GMO typically gives values of around 0.08 [111, 112].

2.9.3. Detergent additives

Detergents, as well as dispersants, are present in formulated engine oil blends to maintain the proper running of the engine. They do this by trapping insoluble products in suspension which allows for removal by filtration. Further to this, over-basing of the detergent (typically with $CaCO_3$, as shown in Figure 2-18) can also prevent acidification of the lubricant. Acidification is a deleterious phenomenon within the engine as acidic species can corrode steel and cast iron [127]. Some detergents have been shown to have anti wear properties, with $CaCO_3$ films being produced that are mechanically protective [127]. Detergents are also known to form films on DLC surfaces producing a similar protective layer [128].

Once the over-based detergent core has been released the hydrophilic pocket can then begin sequestering particulate debris from the lubricant [127]. Kubo *et al* [128] investigated the anti-wear and friction reducing qualities of calcium sulfonates on DLC/steel interfaces. It was observed that high friction and low wear was facilitated at the steel-DLC contact [128]. This is in line with the behaviour observed at the steel/steel contact [111].The group assessed the tribochemistry of the film using TOF-SIMS and showed that the additive provides a ‘high and stable friction coefficient’ as well as low wear. An Fe rich tribofilm was found on DLC at 30 seconds into the testing.

Detergent additives are able to reduce wear when in contact with DLC surfaces. It appears that forced coalescence plays a key role in detergents tribological behaviour, an effect mediated by mechanical agitation [111]. In contrast, ZDDP has been shown to rely on a variety of affects to accelerate film formation, including: thermal activation and ligand swapping [115].

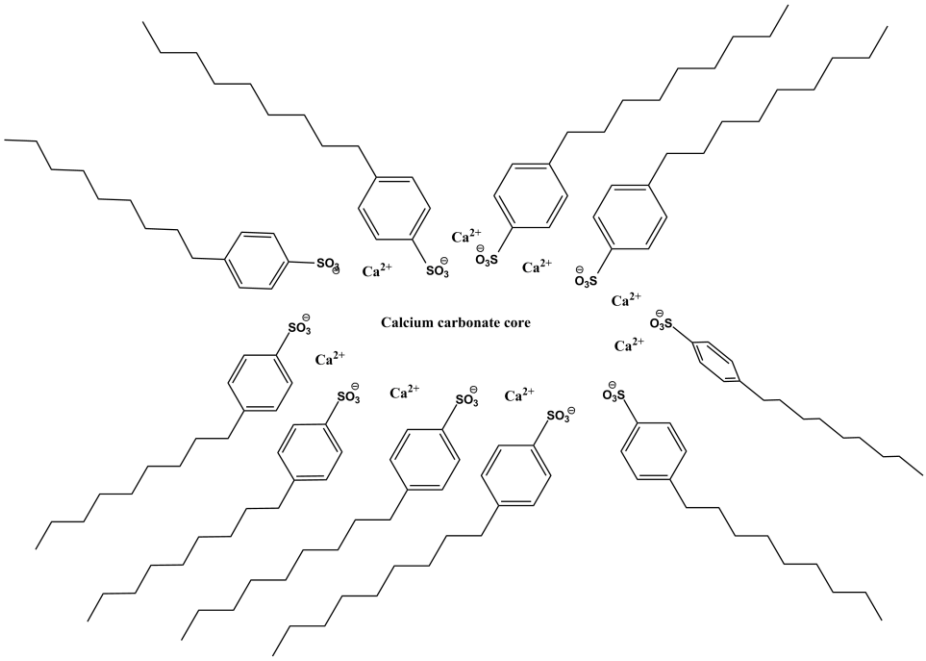

Figure 2-18 Schematic of detergent micelle with over-based core

2.9.4. Dispersant additives

Dispersants play another key role in the lubricant blend; they keep sludge, soot and other deposits from accruing in the system by sequestering them. Dispersants are typically succinimde based and have multiple polar head groups with which they can perform this task [129]. As the dispersant molecules have multiple succinimde head groups on each molecule this differentiates them from detergents and makes them less surface active [130]. That being said, shorter chain succinimide ions (including the head group) have been detected on in the worn area of ATF lubricated, tribotested Si-DLC when examined by ToF-SIMS [110].

2.9.5. Viscosity Index (VI) improvers

Viscosity improvers are inherently surface inactive compounds due their large, polymeric nature that lack polar groups, with which to interact with a surface [131]. VI improvers are far more stable in oil; as such they are not the focus of any major attention herein. However, they are immensely useful engine additives and therefore could not be missed out from the overview. The primary role of VI additives only takes place at higher temperatures, when the engine is fully-fired. VI additives are able to maintain the oil's high

viscosity which is key to reducing wear by maximising interface separation [131].

2.9.6. EP additives

EP, extreme pressure, additives are not limited to the family of ZDDPs.
Many oragno-sulphur based EP additives exist, as shown in Figure 2-19.

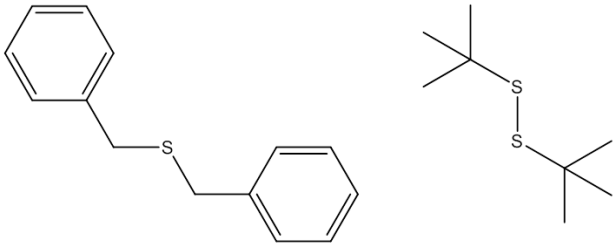

a) b)

Figure 2-19 EP additives a) Dibenzyl disulphide and b) Di-tert butyl disulphide.

As most EP additives depend on sulphur for their efficacy, the traditional requirement of modern engine oils to be rich in SAPS is rationalised [132]. The mechanism by which EP additives are believed to work is dependent on the ease of cleavage of the C-S bonds in the additive molecule. This results in a protective FeS_2 layer being formed [132].

2.10. **Summary**

As explored in this thesis chapter, a large amount of research has already been conducted which establishes key trends and principles associated with the formation of tribofilms, especially with regards to metallic systems. This acts as useful platform from which to explore the tribochemistry that takes place at the, quite different interface of DLC/metal contacts. The differing mechanisms of thermally derived *versus* tribo- films will be all the more important for films on DLC. This is because DLC interfaces have fewer metal ions present. As identified above, metal ions appear to play a key role in the formation of the classical ZDDP film. The literature addressed effectively guides the aims of this research by highlighting areas which need further

study. As DLC is distinctly different from a ferrous surface it quite possibly interacts with oil additives through a variety of different mechanisms. Furthermore, due to DLC's innate ability to reduce wear, this allows for optimisation with regards to oil additives. The main areas that would be most beneficial in terms of further research are:

- Identifying the precise mechanism by which DLCs react with oil additives using surface analysis methods. For instance, although certain key interactions are already known, such as the role SiO_X oxides play, the mechanism of their formation is not well explored.
- Efficacy with regards to doping of DLCs. If Si doping can activate DLC surfaces toward additives in the oil this could lead to greatly improved friction profiles, however too much activation could be deleterious to overall wear. This complex relationship will be examined.
- Exploring the importance of the role a ferrous body plays when paired with DLC at the contact. Metallic ions may fundamentally alter the tribochemistry of the contact due to their well-known catalytic behavior. This will be explored by comparing self-mated DLC contacts with steel/DLC ones.

Chapter 3 Materials and methods

3.1. Introduction

This chapter outlines the main experimental procedures adopted within this project. This includes both mechanical and chemical surface analysis techniques, along with imaging techniques to gauge wear and surface properties.

3.2. Material parameters

3.3. DLC coating specifications

The DLC coatings used in this project were commercial samples produced by Sulzer Sorevi (now a part of Oerlikon) using the PECVD technique. The coatings are produced using lower temperature plasma; the substrate is negatively biased by 500 V with the chamber acting as the electrode. A hot cathode auxiliary system is also employed to enhance plasma generation. The process typically takes place at 10^{-3} mbar. The coatings can be viewed as multi-layered as there are interlayers (Ti, Si), Figure 3-1. The interlayers are employed to improve coating adhesion to the substrate. The substrate is first cleaned by argon ion etching before any deposition commences. Then a titanium layer is deposited, followed by a silicon based interlayer. After interlayer deposition the bulk DLC is deposited.

3.3.1. Manufacturers' ERDA data from the coatings examined

Elastic recoil detection analysis (ERDA) of the coating shows the composition of all elements, including hydrogen, which allows full characterisation of the film. As shown in Table 3-1, the Si-doped coatings also include oxygen (as well as trace amounts of argon) in the coating. For the low Si-DLC there is twice as much silicon within the coating as oxygen when compared with the a-C:H DLC.

As such it can be considered dually doped as it is highly likely that incorporation of additional oxygen into the film will affect the performance. Coating thickness is reported as 2.4 µm for both Si-DLCs. A-C:H DLC has a thickness of 1.4 µm. The manufacturer also supplied coating information including Nano hardness data and Young's modulus values for each coating provided. This information is given in

Table 3-2.

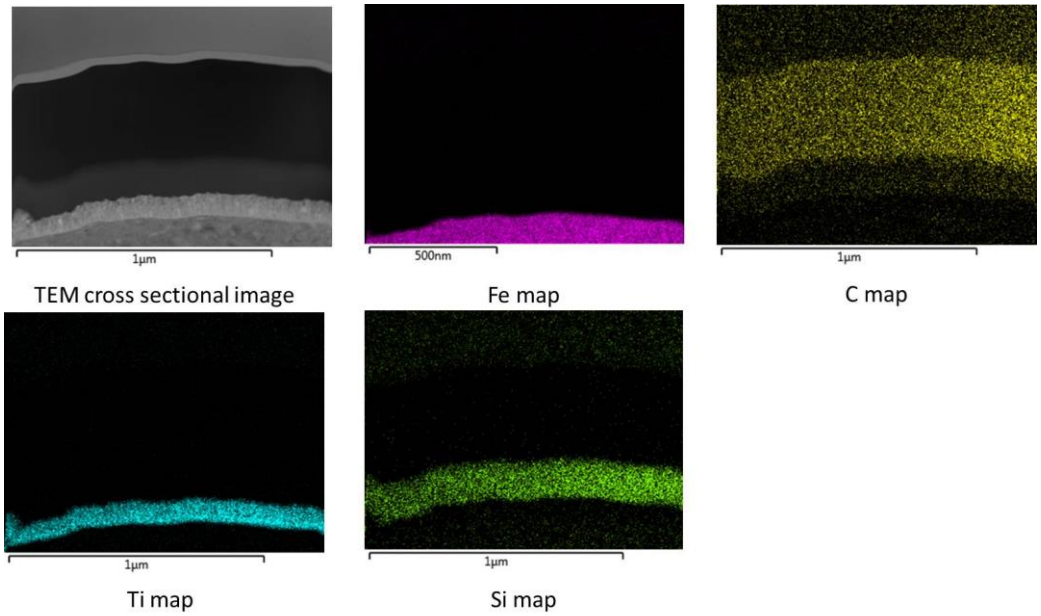

Figure 3-1 TEM cross section with EDX mapping showing inter layer structure of DLCs

Table 3-1 ERDA data from coatings

Coating/ Element %	C	H	O	Si	Ar
High Si-doped	**36**	**30**	**12**	**21**	**1**
a-C:H	**66.5**	**33.5**	**0**	**n/a**	**0.2**
Low Si-doped	**55.6**	**34**	**7**	**14**	**0.4**
Atom accuracy ±	**3**	**2**	**2**	**2**	**0.05**

Table 3-2 Mechanical properties of the coatings

Coating/ Property	Nano hardness (GPa)	St deviation ±	Young's modulus (GPa)	St deviation ±
High Si-doped	**15.4**	**0.9**	**144**	**6.6**
a-C:H	**22**	**1.7**	**191**	**11.6**
Low Si-doped	**17.9**	**1.2**	**150**	**6.1**

3.3.2. Tri-doped DLC

The novel coating was also produced using the Plasma Enhanced Chemical Vapour Deposition (PECVD) technique. These coatings, as per materials section 3.2, where prepared following the set procedure. The coatings can be viewed as multi-layered as there are interlayers employed to improve coating adhesion to the substrate. A titanium layer is deposited, followed by a silicon based interlayer. After interlayer deposition the bulk DLC is deposited. This layer is ~ 1.2 µm thick and is made from a precursor that is highly sp^2 hybridised. The silicon containing component cannot be revealed due to commercial sensitivity. The fluorine component is introduced into the DLC exclusively by use of Fluoroform whose chemical structure is shown in Figure 8-1.

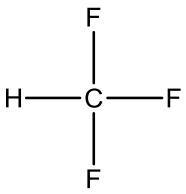

Figure 3-2 F-doping agent, Fluoroform (Trifluoromethane)

The specific protocol for production of a composite DLC with a Si,O,F doped top-layer, is as follows:

- Layer 1 of Si,O doped DLC (undisclosed organometallic precursor material)
- Layer 2 : Short transition of a mix of (organometallic precursor material) + C_xH_y + Argon
- Layer 3 : Additional Si,O doped DLC
- Layer 4: (top surface) Combination of the organometallic precursor and Fluoroform. Followed by venting with Fluoroform.

The doped coatings were analysed by XPS as shown in Table 8-1, to ascertain the % atomic dopant levels.

Table 3-3 %Atomic concentration of dopants in doped samples. Nd = not detected

Sample	Si	O	F
Si,O,F Doped	**3%**	**11%**	**1%**

The novel coatings hardness, prior to wear testing is given below in Table 8-2.

Table 3-4 Coating hardness values

Sample	Hardness (GPa)	St deviation ±
Si,O,F Doped	**13.9**	**3.8**

3.3.3. Coating Substrates and counter bodies

For the pin on plate tribotesting, the DLCs were deposited on AISI 52100 steel plates of dimensions 7x 7x 3 mm with a maximum roughness of (R_a) 0.08 µm. Two pins were employed over the course of this project. These were:

- AISI 52100 steel with semi spherical end with a radius of 120-150mm, 58-60 HRC and a maximum roughness (R_a) of 0.3 µm. This pin is used to simulate the lower pressure piston-ring/liner contact.
- BS1452 cast iron pins with a semi spherical end with a radius of 10 mm at the head were the second pin type used. The pin has a hardness of 44 – 46 HRC, a maximum roughness (R_a) of 0.2 – 0.3 µm was used to simulate the cam/follower conditions needed for the experiment.

For pin-on-disc testing, highly polished AISI 52100 chrome steel was used as a substrates for both body and counter bodies. Both contact surfaces were coated in low Si-DLC. The steel ball is of these parameters: (6.35 mm/0.25 inch diameter) AISI 52100, a maximum roughness (R_a) = 12 nm. The steel disc has a 25 mm inner diameter/ 42 mm outer diameter, it is 1 mm thick, and had a maximum roughness (R_a) of 112 nm.

3.3.4. Lubricants used for the research programme

There are four lubricants used within this work, they are summarized in Table 3-5. These include a commercially available diesel engine oil, 10w40 viscosity grade (Oil B). A bespoke lubricant which is a version of the same also blended with GMO (Oil A). A heavy duty diesel engine oil (Oil C) and a low additive oil (Oil D). The lubricants are commercial samples and as such their exact composition cannot be disclosed however ICP analysis was provided and this data is given in Table 3-6.

The fully-formulated oil also contains Ca, P, S and Zn elements. ZDDP is known to be blended into the lubricant. The oil also contains anti-oxidants, detergents and dispersants. The friction modified oil differs only by inclusion of 1.5% (w/v) Glycerol Mono Oleate (GMO) as a friction modifier, which is depicted in Figure 3-3.

The final, low-additive oil was viscosity matched to the formulated oil and contains minimal additives. No corresponding ICP analysis is available for the oil D, as it has minimal additives contained in it. However, the oil does contain detergent molecules and viscosity modifiers to eliminate any difference caused by potential changes in viscosity between oils.

Table 3-5 Oils used within the project

Oil	Type	FM
Oil A	**Fully-formulated**	**GMO**
Oil B	**Fully-formulated**	**None**
Oil C	**Heavy-duty (extra S based EP)**	**None**

Oil D	**Low-additive oil (no ZDDP, viscosity matched to other oils)**	**None**

Table 3-6 ICP analysis of the oils A and B used throughout the project, with A having additional GMO.

ICP analysis	Ca	Mg	P	S	Si	Zn
PPM	**2391**	**81**	**761**	**2064**	**4**	**833**

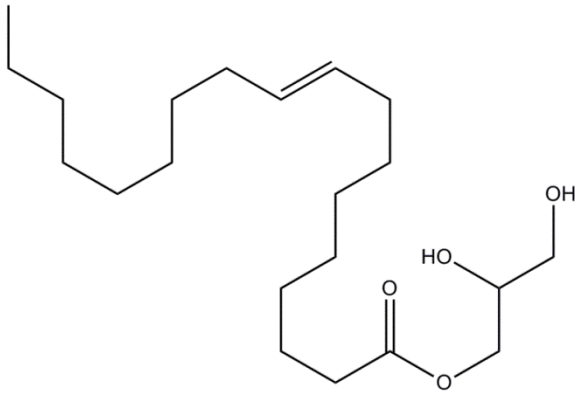

Figure 3-3 Skeletal formula of GMO, a well-known friction modifier species.

3.4. Experimental methods for surface analysis preparation/bulk analysis preparation

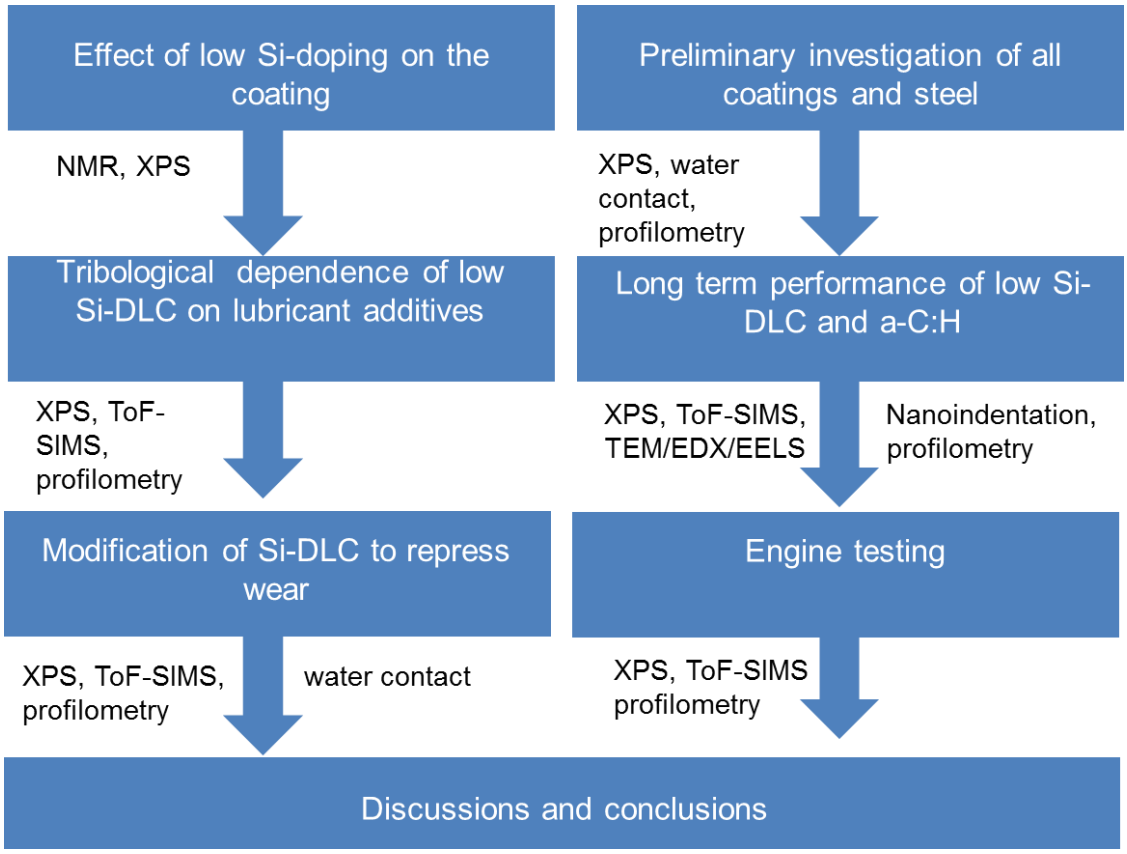

Figure 3-4 Diagram of experimental work flow with analytical techniques included

3.4.1. Assessing the tendency of low Si-DLC to oxidise under controlled environments

In order to assess to what extent Si-DLCs oxidises without tribological influence, a test was devised. Low Si-DLC samples were submerged in Oil D and placed in flasks. One flask was flushed through with nitrogen for twenty minutes and then sealed; the other was kept open to laboratory air via a needle through a rubber bung. Both samples were heated at 80 °C for 600 hours. 600 hours was an extended time period selected to fully assess how the DLC would behave not only in the initial stage of its life but over longer periods. The samples were then washed in heptane and analysed by XPS, along with an un-heated sample.

3.4.2. Thermal film forming capabilities of low Si-DLC

In order to fully understand the differences between tribofilms and thermally derived films, it was necessary to prepare a thermal film on the low Si-DLC. This thermal study involved a low Si-DLC coated plate being heated at 80 ºC for seven hours in an open-beaker submerged in Oil A. This time period was chosen to allow full formation of any thermal film that may develop; in preliminary experimental work it had been observed that seven hours allows enough time for full formation of a tribofilm even on less reactive (a-C:H) DLCs. As such, this indicates that seven hours should allow for at least partial formation of a thermal film. Thermal films from fully formulated oils on steel coupons are able to form in short time periods [117, 133, 134].

3.4.3. Surface functionalization to explore influence of altering surface chemistry

Within published works examining Si-DLCs, there is a key focus around the influence SiO_x type species play with regards to friction and wear. To explore this further, it was deemed necessary to create a low Si-DLC surface that had the Si-OH type groups capped, using a dip-procedure. To form silyl ethers on low Si-DLC surfaces a modified preparation was adapted from a published work [95]. The surface –OH groups of the Si-DLCs are key to the modified silanization reaction employed (Figure 3-5). The low Si-DLC coated components were submerged in chloroform (50 ml), the solution was then made up to a dilution of 1% (v/v) chlorotrimethylsilane by slow addition of the silane. The solution and submerged parts were then allowed to react at room temperature for two hours with occasional stirring. After this period the components were removed, rinsed with chloroform and then stored in chloroform until used. The reaction follows this general scheme:

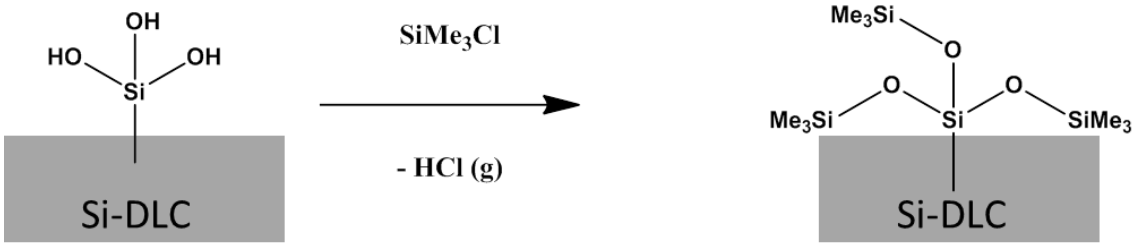

Figure 3-5 Skeletal formula of surface functionalization reaction. Me = methyl group, CH_3.

3.4.4. Preparation of Samples for Solid-State Nuclear Magnetic Resonance (NMR) Analysis

NMR is a very useful technique for probing carbon chemical state environments; however it is not surface sensitive. It instead examines a bulk of material. NMR works by interacting with non-spin paired nuclei, as found in hydrogen. In the case of carbon, the isotope that is most abundant is not NMR active. However ^{13}C is NMR active and as this isotope represents approximately 1% of all total carbon atoms; if a sample of enough mass is prepared, NMR can yield very useful data. NMR probes the spin environment and returns chemical shift values of the species investigated. This is immensely useful for DLCs as carbon NMR chemical shift values can then be used to establish the sp^3:sp^2 ratio of carbons in a sample [85].

The silicon-doped and a-C:H DLC samples were converted to powder, prior to any tribological testing, to allow for NMR analysis. The powders were prepared using a modified literature procedure [85]. A large coated aluminium substrate (~ 200 cm^2 and 10 µm thick) was soaked in 15% hydrochloric acid solution for two hours with external cooling. The DLC remained intact. The metal substrate, including the interlayers, were sequestered by the acid resulting in black, flake-like products that were filtered from the solution, washed with purified water and heptane and then finally dried at 40 ºC overnight. Between 50–100 mg (50 mg a-C:H, 100 mg silicon doped) of the DLC powders from each sample was obtained and sent for analysis. A greater amount of both the Si-DLCs were required in order to obtain carbon signals from the sample, as incorporation of silicon reduces

carbon content of the overall coating. It is expected that the Ti interlayers were completely removed by exposure to acid, however if this is not the case, metallic Ti would not affect or appear in a C NMR spectrum and thus is not viewed as a pertinent issue.

3.5. **Tribometer testing methods**

3.5.1. Pin-on-plate tribometer testing procedures

The ‘TE77’ reciprocating pin on plate tribometer platform allows for tribological investigations under different temperatures and loads to simulate various conditions. In this case boundary lubrication is characterised by the as the lambda value for the piston ring and liner type system (with pin of radius 120 - 150mm) was calculated to be λ= 0.0040. Before experimental set-up, all mechanical parts are sonically cleaned in acetone for twenty minutes and dried thoroughly. Heating is controlled by a thermo couple that regulates the oil temperature according to a user defined value. The heater plate is positioned below the sample holder. The load cell is able to measure the frictional force and converts this to a digital signal, using an analogue to digital converter. Figure 3-6 shows a schematic of the TE77 tribometer.

The frictional force is the average measurement read at five minute intervals for a set number of hours, all these variables are controlled through LabView. Friction data is then processed by the Labview software suite.

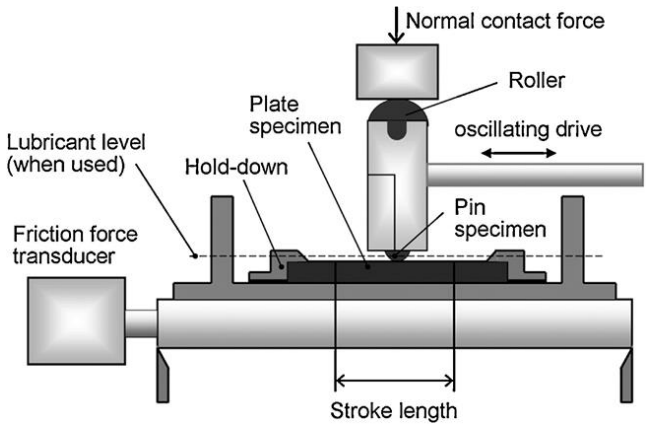

Figure 3-6 Schematic of a TE77 tribometer [135]

An initial Hertzian contact pressure is given to emulate the conditions of a piston ring contact or a cam shaft and follower. DLC coatings can and are being used in both of these interfaces within the internal combustion engine which is why these pressures are the ones investigated [136]. Once finished, the pin and plate are rinsed in heptane to remove excess oil and stored in aluminium foil to avoid contamination. Differing experimental set-ups are detailed in Table 3-7. Dry sliding experimental conditions were altered from the above to prevent catastropic wear, as detailed in Table 3-8.

Table 3-7 TE77 running conditions

Running Conditions	Piston ring conditions	Cam follower conditions
Load	**28 N**	**25 N**
Maximum Hertzian Pressure	**0.15 GPa**	**0.81 GPa**
Running Speed	**0.2 m/s**	**0.2 m/s**
Temperature	**100 °C**	**100 °C**
Frequency	**20 Hz**	**20 Hz**
Roughness (R_a)	**0.08 µm**	**0.08 µm**
Volume of oil	**4 mls**	**4 mls**
Pin radius	**120 - 150 mm**	**6 mm**

3.5.2. Pin-on-disc tribometer setup

For the self-mated DLC contact study, a pin-on-disc tribometer was chosen as the highly polished ball bearing counterpart was ideal for coating with DLC, which requires a surface to be below a specified roughness in order to ensure coating adhesion to the substrate. The pin-on-disc tribometer has the added benefit that it can be run in unidirectional mode, thus allowing for lower wear but higher pressure regimes. For all experiments at least two repeats were obtained to allow for calculation of standard deviation.

Table 3-8 Dry sliding pin-on-plate conditions

Running Conditions	Dry sliding
Load	**6.9 N**
Maximum Hertzian Pressure	**0.09 GPa**
Running Speed	**0.2 m/s**
Temperature	**100 °C**
Frequency	**20 Hz**
Roughness (Ra)	**0.08 µm**
Pin radius	**150 mm**

This factor is of high importance as it was necessary to produce a clearly identifiable tribofilm without exposing the steel substrate on either the plate or the pin. For the tribometer testing procedure a pressure of 1.5 GPa was selected following a brief optimisation study that found this pressure was able to create a visible wear track on both DLC bodies without overly-severe wear. The initial pressure of 1.5 GPa is a higher pressure than typically associated with engine lubrication. However, for this study it was deemed appropriate. This type of non-destructive wear is key herein so as to ensure that non-ferrous surfaces were present for the whole test duration. Thirty minutes was an adequate time frame to ensure the DLC coated pin did not wear through but the worn areas were clearly visible. Following tribotesting all samples were rinsed in heptane to remove excess lubricant and stored in aluminium foil. Only one lubricant was used for this experimental setup, this was Oil B with friction modifiers being left out of the lubricant blend. This allows for easier assessment of the friction profile as surface modification was explored using this setup. Experimental set-up is detailed in Table 3-9.

Table 3-9 Pin-on-disc tribometer setup

Running conditions	Setting
Load	**14.7 N**

Maximum Hertzian Pressure	**1.5 GPa**
Running Speed	**5 m/s**
Temperature	**90 °C**
Lubricant	**Oil B**

3.6. **Analytical techniques**

Certain analytical techniques were selected for use with the coatings both prior to and post testing. Nuclear Magnetic Resonance (NMR) and Electron Energy Loss Spectroscopy (EELS) were both used to gauge sp^2/sp^3 content of the films. X-ray photoelectron spectroscopy (XPS) and Secondary Ion Mass Spectroscopy (SIMS) were used to asses the tribofilms, as was Energy-dispersive X-ray (EDX) mapping of the cross section. Water contact angle was used to asses surface energy of the DLCs and steel surfaces. Interferometry and contact profilometry were used to analyse wear results. Nanoindentation was used to give establish if a thick, mechanically hard tribofilm was formed at any point.

3.6.1. X-ray Photoelectron Spectroscopy (XPS)

XPS is a surface sensitive analytical technique that relies upon the interaction of X-rays with the surface on interest. Upon interaction with the surface, the x-ray provokes ejection of electrons that are characterised in terms of their kinetic energy, in electron volts (eV), by an electron detector. This technique takes place under high vacuum.

XPS was primarily employed to completely assess any tribochemical interactions that may have occurred at the surface. XPS was carried out using a VG ESCALAB 250 X-ray Photoelectron Spectrometer which uses monochromatized X-rays from an aluminium K alpha source. The system also employs high transmission electron optics and a multi-channel detector. An approximate area of 500 μm^2 was analysed in the worn area.

XPS is surface specific in that it can only penetrate the upper few nanometres (typically 5-10 nm) of the sample [137, 138]. A short survey

scan was carried out at first to determine which elements were present. This was done with the settings of 200eV pass energy, 1eV for energy step size and a 50ms dwell time. Longer (high resolution) scans of selected element peak regions were carried out to allow for full resolution of the peak components present. The settings for high-resolution scans were: 40eV for pass energy, 0.1eV for energy step size and 100 ms for dwell time. CASA XPS software was used to analyse the data. Reported literature precedents for C1s calibrations for various DLC and Si-DLC samples were in agreement on the calibration reference value of 284.4 eV for the main C-H peak [87, 139-141]. Evaluation of Si 2p position was also verified using literature values [87, 142-144]. For cases where steel surfaces were examined either the known eV value for iron oxide was used to calibrate the spectra or, in cases with thicker tribofilms, adventitious carbon was used as reference [143, 145, 146]. Steel counter parts were analysed at the seven hour mark using XPS to confirm presence of a tribofilm. Counter bodies were also tribochemically assessed for low Si-DLC in Oils A and D at the seven hour mark. This was again to show a tribofilm had formed and exhibited oil dependency.

When profiling of samples was needed, an etching gun of mono atomic Ar gas ions with an energy of 4000 eV was employed. A raster size of 1 mm x 2 mm was used. Etching allows removal of species when surface contamination is suspected or there is a need to spatially explore a film in the z axis.

In certain instances XPS cannot definitively attribute how an element is incorporated into a film. Two prominent examples of this are calcium carbonate versus calcium phosphate which appear at very similar eV values (347 eV for both compounds) and zinc oxide versus zinc sulphide (1021 – 1022 eV) [143, 146, 147]. In these instances other analytical techniques and fundamental chemical knowledge are invoked to fully attribute species present. A schematic showing the theory behind XPS analysis is given in Figure 3-7.

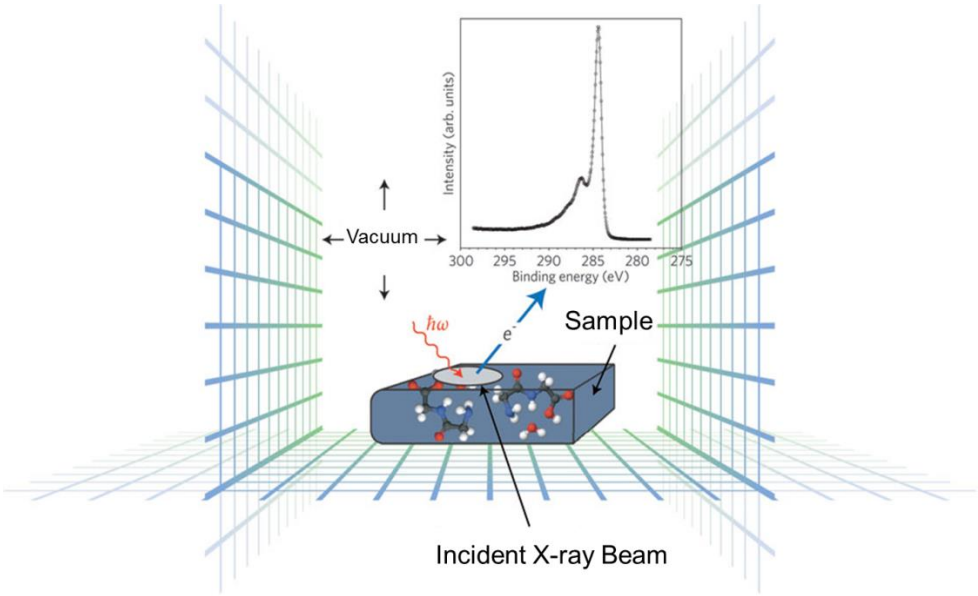

Figure 3-7 Schematic of how XPS analysis takes place, adapted from [148]

3.6.2. Time-of-Flight Secondary Ion Mass Spectroscopy (ToF-SIMS)

Static Time-of-Flight Secondary Ion Mass Spectrometry (ToF-SIMS) is a highly surface-sensitive technique that outperforms XPS in terms of sensitivity and again requires high vacuum. ToF-SIMS can be sensitive down to 1-2 nm [138]. The ToF-SIMS technique used employs a primary ion beam source of bismuth, in the form of a liquid metal ion gun. The primary ions are fired at the worn area and impact the surface provoking ejection of secondary ions from the surface of interest. The cluster ion beam used was Bi^{3+} with an energy of 2 KeV for static SIMS. The target current was 1 Pico Amp (or within the range 0.1-3 Pico Amps), from the flood gun to compensate for charge build up. A random scanning pattern, as opposed to raster scanning, was employed to further prevent charge build up on the sample. Depth profiles were undertaken using a C_{60} source to allow for slower profiling with a maximum time of 800 seconds. Figure 3-8 shows the typical interaction that takes place when the primary ion beam encounters the surface on interest.

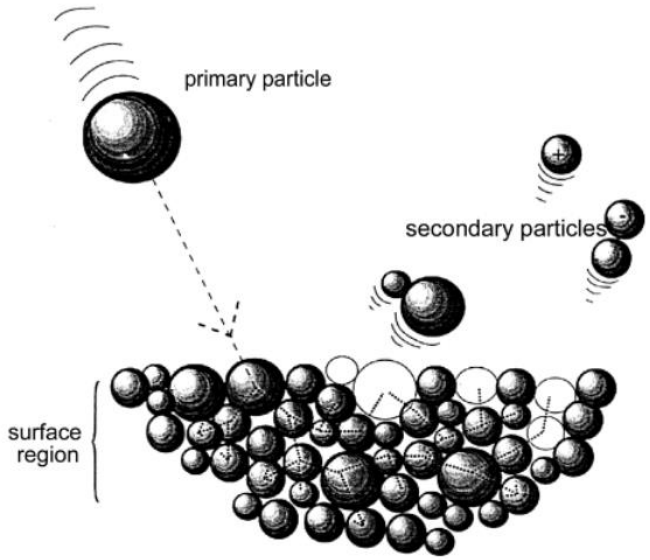

Figure 3-8 Schematic of how ToF-SIMS analysis takes place [149]

All sample spectra were examined for the presence of: P, S, and O species along with various C, H, and (where applicable) Si species. Spectra obtained were analysed using ION-TOF software. Individual spectra were calibrated to the H, C, CH, O and OH signals for the negative spectra and a deviation limit of 70 ppm was used to ensure accuracy.

3.6.3. Solid State Nuclear Magnetic Resonance (SS NMR)

Solid state NMR was also used to analyse the DLC films. For this particular investigation, cross-polarisation was used, a technique that transfers radio frequency energy from hydrogen nuclei to carbon nuclei. This is useful for two reasons. It has been previously detailed in the literature on DLC and it increases the response from the carbon nuclei and focuses the spectral data to carbons directly bonded to hydrogen atoms [85]. A frequency of 100 MHz was used to excite the target nuclei, with an acquisition time of 10.0 ms.

A typical NMR spectrum of DLC will be composed of few peaks, depending on dopant level. Typically the C sp^2 peak appears around 125-130 ppm and the C sp^3 peak appears around 20-35 ppm. This may shift depending on, in the case of DLC, incorporation of O or Si [85].

Solid-state NMR data is produced without repeats due to the difficulty in synthesis the large amount of DLC necessary. As such NMR was compared with EELS data to validate the outcome. The techniques show good agreement, NMR indicates the low Si-DLC has a sp^2 fraction of 46.9% and that the a-C:H DLC has a higher sp^2 fraction of 61.8. EELS data of an unworn sample of a-C:H DLC is in good agreement with the SS-NMR data, as EELS indicates the sp^2 fraction is 59.1 ± 6.3%.

3.6.4. Water contact angle measurements

The instrument used to measure water contact angles in this case was a 'FTA4000' video drop shape analysis system [150]. To ensure accurate results, 'Mili-Q' high purity, deionised water is used this is pumped via a 'Nano Dispense' electronic pump to aid accurate dispensing. Two microscopes are fitted to the equipment: an analytical microscope to capture the drop shape image and a look-down alignment microscope. The analytical microscope has a zoomed horizontal field of view from 2 mm down to 200 µm. The viewing angle is adjustable to 0° or 3° with respect to the specimen surface. The apparatus is housed within a dark room and is enclosed to protect from local fluctuations in heat. The stage is back-lit by a high intensity LED source. Image capturing is dynamic with variable resolutions. A schematic of a typical water drop experiment is giving below in Figure 3-9 where Θ represents the contact angle. L,S and V refer to the interfaces of liquid, solid and vapour phases, respectively. Lambda is the interfacial tension between the phases.

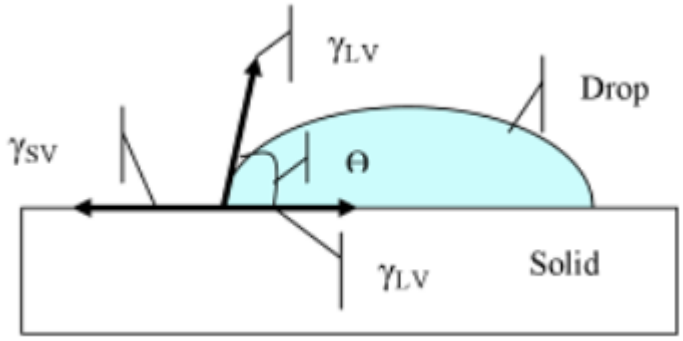

Figure 3-9 Schematic of water contact angle experiment adapted from [151].

The software associated with the machine provides static contact angle analysis from the images captured. The contact angle of three water droplets were analysed for each sample, ensuring accuracy and allowing for standard deviation to be calculated. Surface wettability is highly relevant to DLCs within engines as many oil additives are surface active, polar molecules. As such a lower water contact angle should favour interactions of the DLC with the additives. A water contact angle of below 90º corresponds to a high wettability, whereas angles above 90° correspond to a low wettability [152].

3.6.5. Focused Ion Beam (FIB)

A focused ion beam was coupled with scanning electron microscopy to enable the creation of cross sections from the worn area. Cross sections of the worn area are particularly useful as, with use of appropriate optical imagining techniques, accurate measurements of tribofilms can be obtained. To this end, a FEI Nova200 Nanolab dual beam SEM/FIB system was employed to image and etch into samples. In order to protect the area of interest an initial layer of platinum is laid down, using an electron beam, on top of the worn area. This prevents damage to the surface from the more destructive ion beam. Once a protective layer is formed a bulk layer of Pt is laid down using the ion beam to an approximate thickness of 1.5 µm. Once this was complete, material either side of the deposited Pt layer was milled away to an approximate depth of 10 µm using the ion beam at 30kV. Following this, trenches on all four sides of the area of interest are milled using the ion beam. Once the trenches are milled the cross section is thinned and cut away from the bulk material. The sample is then attached to a copper TEM grid using a micromanipulator; the attachment is achieved by bonding with Pt in a similar fashion to the protective layer deposition. Finally, in order to produce a cross section that is below a specific thickness (5 nm) further sample milling is conducted [153].

Figure 3-10 shows how a TEM cross section is prepared in a stepwise fashion. A) Area of interest identified and protected with an electron beam deposited layer of platinum. b) Areas around the cross section are milled away, c) the sides of the cross section are milled away d) the cross section is removed by attaching it to the micro-manipulator with a Pt layer e) the

cross section is attached a copper TEM grim and the manipulator is detached with ion etching. f) The cross section is thinned to the desired thickness appropriate for TEM.

3.6.6. Transmission Electron Microscopy (TEM)

Transmission Electron Microscopy (TEM) was employed to image any tribolayers present, as well as being used to examine the microstructure of the coating. TEM uses the interaction between a beam of electrons (at 200 kV) fired through the surface in question to form an image of the material. Energy-dispersive X-ray analysis was used to identify elements within the film. A Philips CM200 FEGTEM Field emission gun TEM/STEM with Supertwin Objective lens and cryoshielding, was used to obtain the TEM images. Oxford Instruments INCA EDX system and Gatan Imaging Filter were used to produce high resolution TEM images, microanalysis and mapping.

3.6.7. Energy Dispersive X-ray analysis(EDX)

EDX spectra were obtained using both ‘spot’ analysis modes and ‘mapping’ modes. Mapping modes were predominately used to verifying coating composition and interlayer structure. Spot analysis was employed to verify the presence of certain elements in the tribolayer and compare this with background spot analysis.

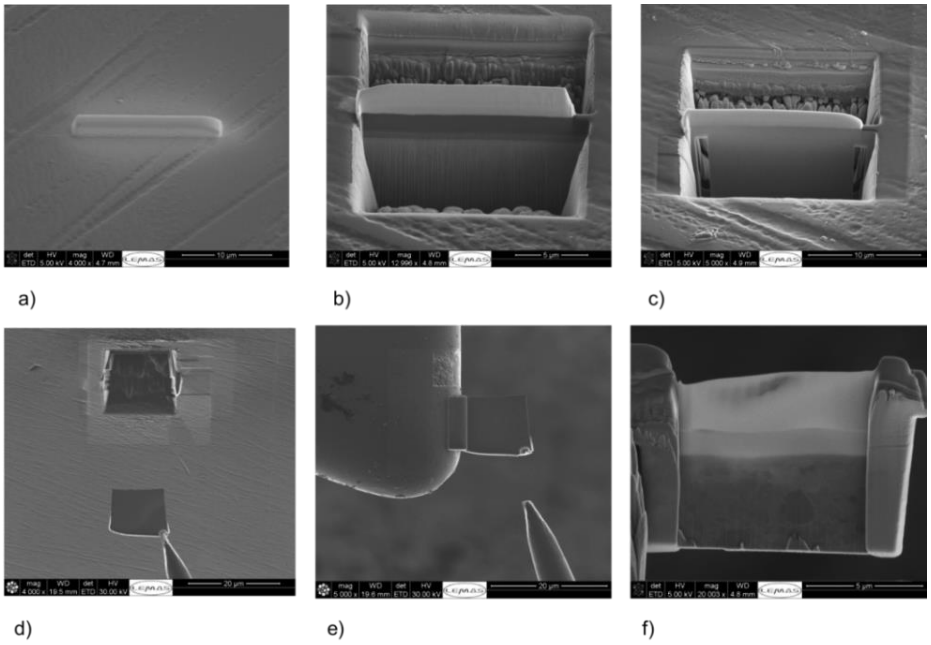

Figure 3-10 Annotated schematic of the production of a TEM cross section using the FIB.

3.6.8. Electron Energy Loss Spectra (EELS)

Electron Energy Loss Spectra (EELS) were obtained for certain films to investigate the carbon hybridisation in the worn area. The carbon peaks of these spectra can be analysed to yield useful sp^2 data which gives information on the microstructure of the coating and how it chances with wear. EELS spectra were recorded using a Gatan imaging filter and both were processed using the Gatan digital micrograph software suite. Initially, the thickness of the TEM cross section is computed using the software to ensure the slice is thin enough for accurate data. Then the data is calibrated to the zero loss peak ensuring the peak is centred at 0.0 eV. The sp^2 fraction from the sample are then obtained using Gaussian peak fitting around the well-established π* peak at 285.0 eV [154]. C–H bonds are observed only in DLC films at energy positions around 287.5 eV. The C–C bonds are observed above 290 eV depending on the specimens and the dose [155]. Three total contributions make up part of the 20 eV window, leaving a small residual signal that is representative of certain strained carbon bonds, Figure 3-11. These peaks then represent the whole carbon signal of the sample. This allows for comparison of the obtained sp^2 value to value of a known a

100% sp^2 (highly ordered pyrolytic graphite) sample obtained from the literature [154].

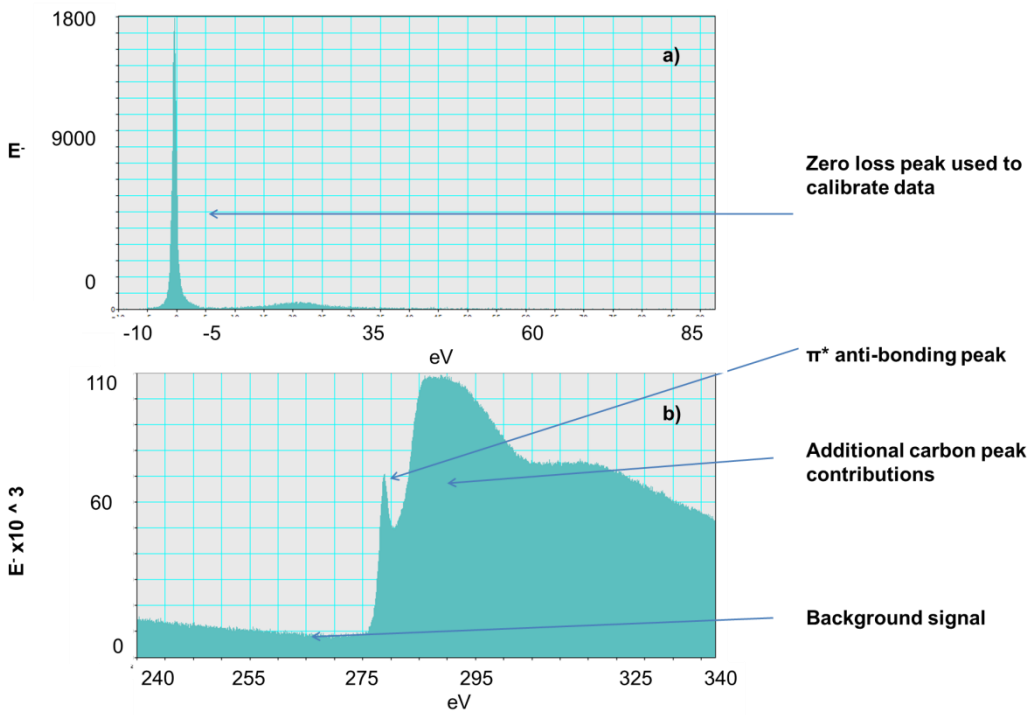

Figure 3-11 Annotated EELS zero loss and core loss spectra. A) shows the zero loss peak, b) shows additional carbon peaks.

3.6.9. Nano-hardness measurements

Surface hardness values were obtained using a Nanotest™ Nano indenter produced by Micro Materials Ltd Wrexham, UK. The test apparatus is in an enclosed, temperature regulated box to ensure no fluctuations due to heating or cooling processes. The Nanotest platform software suite and micro capture camera were used to obtain, analyse and interpret the data. Following the experimental method devised by Oliver and Pharr [156] a diamond tipped probe with a Berkovich indenter of 130 ° was employed for testing. All samples were mounted to the holder using a high strength adhesive. The maximum penetration depth employed was 51.3 nm or a penetration depth of 4% into the coating. Eight measurements were made either within or outside of the worn area to allow for good levels of accuracy, standard deviation is provided with the data.

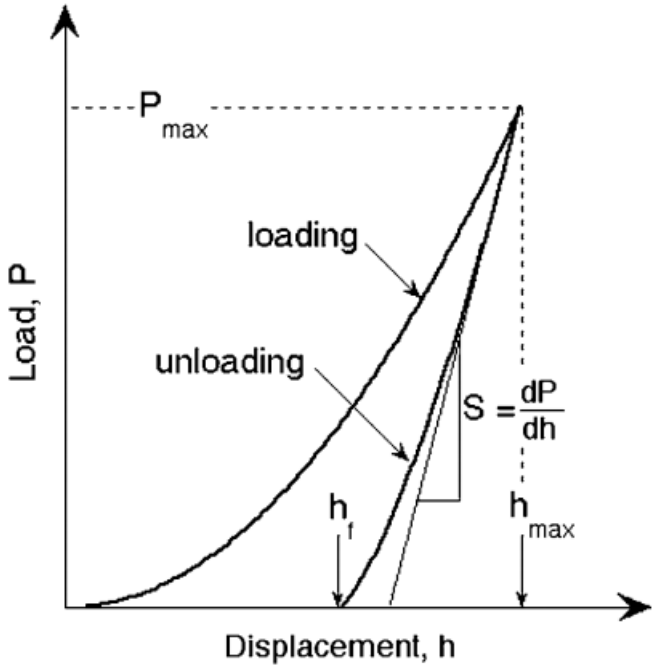

Figure 3-12 Schematic of the indentation data as typically obtained from the experiment. Adapted from [157]. P represents load, h represents displacement and S represents the elastic unloading stiffness.

3.7. **Wear measurements**

3.7.1. Non-contact profilometry

A variety of post wear analyses were conducted to fully characterise topographical, mechanical and chemical changes in the surface. For gauging wear, this includes scanning white light interferometry which was conducted using scanning white light interferometry on a Bruker NP FLEX™ interferometer. The interferometer is able to move in 3-dimensions to accurately use non-contact methods to produce an image of the surface examined. The 'Vision64' software suite is then used to analyse the data obtained. This data is then interpreted by the software suite which is able to remove surface bias like curvature and tilt and then give information on volume lost, roughness and other useful surface parameters. All measurements were taken using vertical scanning interferometry mode, scan speed of x3, magnification of x2.5. Light interferometry is a highly precise technique for measuring small displacements and surface irregularities [158]. The technique works by directing a wave, typically from a

light or laser source, at a beam splitter which divides the beam into two. One beam encounters a reference surface whilst the other encounters the sample being examined. Both of these beams are reflected back to a detector. When being reflected back to the detector waves of the same frequency combine or undergo ‘constructive interference‘, and waves not of the same frequency destructively interfere. The points where the interference difference pattern is visible is the contour line for a given height [158].

Wear can be calculated from profilometry data and then can be converted into dimensional wear coefficients. These values are useful as they allow comparisons of wear over different testing parameters. The dimensional wear coefficient is the volume worn (m^3) divided by the sliding distance (m) multiplied by the unit of load (N). Wear of the coating can also be measured as the point of maximum depth loss to gauge loss of coating thickness.

3.7.2. Contact Profilometry

In cases where interferometry did not provide a high enough level of accuracy contact profilometry measurements were obtained. This is because contact profilometry is known to be more accurate than interferometry in certain circumstances [159-161]. Contact profilometry measurements were obtained using a Taylor Hobson Form Taly surf 120 L. Prior to measurements the stylus is calibrated with a standard to ensure accuracy. Measurements were interpreted using the ‘µltra 5.23.87’ software suite to produce visual images and obtain numerical data. Four data sets were obtained for each measurement and these values were averaged. The standard deviation of each set was found. Worn volumes can be calculated from profilometry data and this then can be converted into a dimensional wear coefficient. Profilometry data yields wear scar width and depth measurements, length of the wear scar was already known as it is part of the experimental setup. This allows calculation of worn volumes.

3.7.3. Leica optical microscope

For certain tribopairs, optical images were necessary to establish the nature of wear and if a transfer/tribofilm is present. Optical images were obtained

for selections of both DLC coated plates and metal counter bodies. The Leica DM6000 optical microscope and accompanying software suite allows for accurate measurements to be made of wear scar length and width as well as wear scar radius on pins. Filters can be employed to better differentiate between worn and unworn areas, also specific illumination levels can be set to maximise visibility. Typically, a magnification of x2.5 was employed for imaging wear scar tracks and x10 for imaging counter bodies. LAS viewer, the software associated with the machine, then enables accurate measurements to be taken from the images produced.

Chapter 4 Results of preliminary lubricant and coating investigation

4.1. Introduction

This chapter gives the initial experimental work associated with the project, the goals of which were to verify literature trends and gain early stage data on the coatings examined. Three DLC coatings were selected for initial testing, two of which were doped with amounts of silicon. The other was a hydrogenated DLC. In addition to this, two lubricants were also examined. The aim of this was to find the optimum coating/lubricant tribopair that would give the lowest friction and wear within an engine. To fully understand the tribology of the system, several different techniques were used to analyse and characterise the coatings both pre and post wearing. This includes NMR and XPS analysis as well as scanning light interferometry.

4.2. Results

4.2.1. Pre-wear coating characterisation

4.2.2. Solid-state NMR analysis (pre wear)

To validate literature findings on the effect that silicon (and oxygen) inclusion has on the film, solid-state NMR data was obtained. The coatings examined are all deposited using the same process, although changes in precursor materials and amounts is required to alter the amount of Si in the coating. Solid-state NMR (SS NMR) data can give information on the coatings sp^2/sp^3 ratio as well as information about other aspects of bonding. This ratio is highly influential with respect to the performance of the DLC coating as increasing the sp^3 content forces the coating to be more ‘diamond-like’ in structure, in accordance with the DLC phase diagram shown previously in

Figure 2-7 [40]. It is widely reported that incorporating silicon into the DLC microstructure as a dopant is able to increase the sp^3 content [85, 88]. This is due to the unstable nature of Si π systems, or double bonds, which Si does not readily take part in sp^2 bonding with carbon [162, 163]. Pre-wear solid-state NMR data, shown in Figure 4-1, identifies an unusual relationship between the Si incorporation in the films examined here and the sp^3 bonding fractions. The low Si-DLC has a greater ratio of sp^3 bonded carbons when compared to the a-C:H film. However, the high Si-doped sample has a lower amount of sp^3 bonded carbons. In depth analysis of the high Si-doped DLC is not pursued although it seems that differing atomic concentrations of Si affects the DLC in different ways. The move from a mix of C_xH_y gas with the Si organometallic precursor (molecule comprised of CHSiO) as in the low Si-DLC, to the high-Si doped coating, which is made exclusively from the organometallic precursor could also be causing a shift in sp^2 ratios as this will inevitably also effect the coating microstructure.

In one instance, high Si doping has been shown to inhibit sp^2 clustering formation [85]. It has also been shown that the parameters under which the Si-DLC coating is created can affect the sp^2/sp^3 ratio [88]. Both these factors could explain why the high-Si DLC has a lower than expected amount of sp^3 bonded carbons.

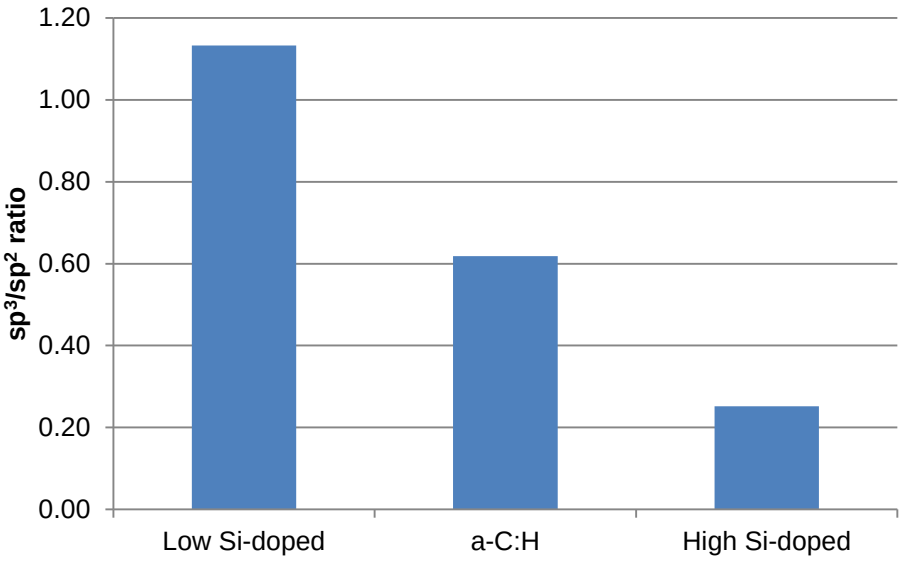

Figure 4-1 sp^2 quantification by solid-state NMR analysis. Due to the nature of NMR measurements, whereby the technique requires a large amount of material to perform, repeats were not obtained.

NMR data, despite lacking standard deviation as no repetitions were possible, is later compared to EELS sp^2 data. This allows validation as the sp^2 content of the unworn, a-C:H film is found to be 59.6 ± 6.3 %.

When the a-C:H and high-Si doped coatings are compared the carbon spectra appear quite similar, Figure 4-2 & Table 4-1. The main difference is the presence of an additional shoulder to the spectra of the high Si-DLC at around 200 ppm, indicative of additional C-O type compounds [164]. This suggests there are a variety of different bonding modes within the microstructure for this DLC.

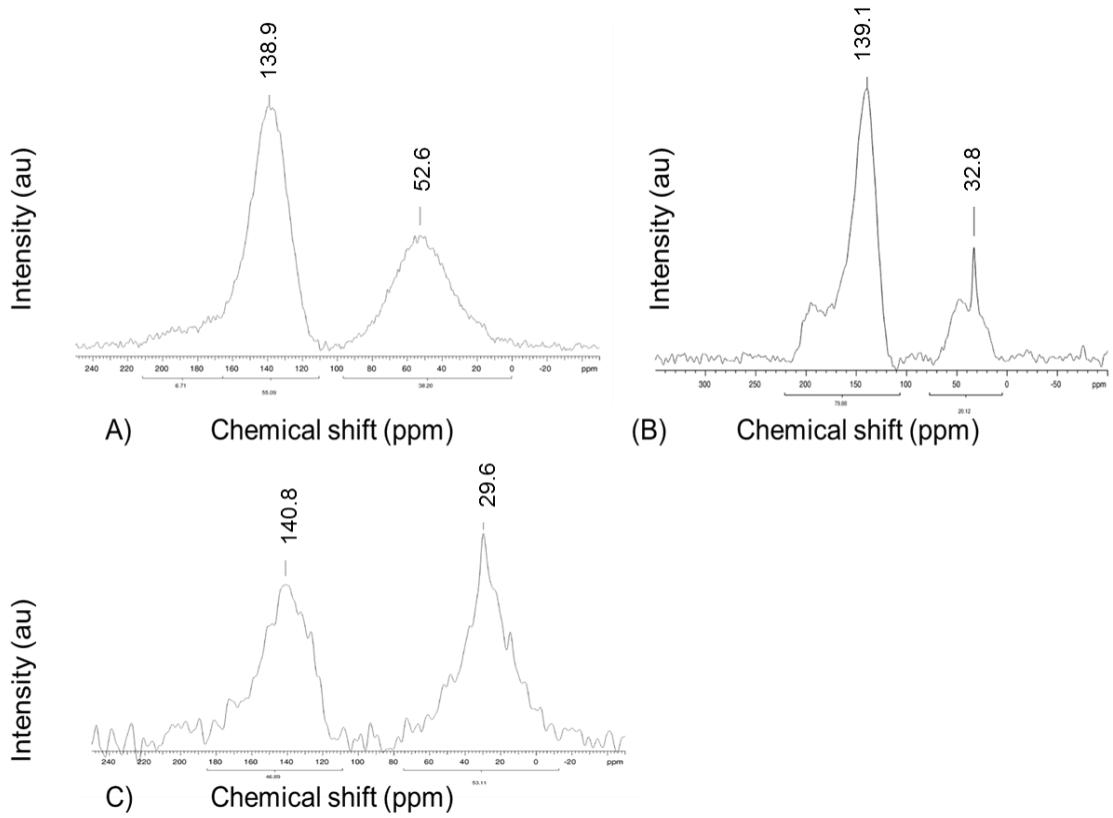

Figure 4-2 Solid-state NMR results of (A) a-C:H DLC (B) Highly Si-doped DLC (C) Low Si-doped DLC. Intensity in arbitrary units (au)

Table 4-1 Tabulated carbon NMR data of the three coatings

Attribution of NMR peaks	A-C:H (%)	Low-Si (%)	High-Si (%)
Sp^3	**38.2**	**53.11**	**20.12**
Sp^2	**55.09**	**46.89**	**79.88**
C-O type	**6.71**		

Solid-state NMR spectra for the higher % Si coating was also able to yield useful data and is shown in Figure 4-3. It shows how Si is incorporated into the film. Similar data for the lower % Si coating is not available as it did not contain a high enough Si content to produce a significant response to the technique.

The main peak is the large peak centred around 0 ppm [85, 164]. This is indicative of a tetravalent sp^3 coordinated $Si-(C)_3$ or similar Si-O-C species [85]. The three other peaks present in the spectra are all indicative of silanes and silicates, a combination of Si-H and SiO_x networks [165, 166]. The data in Figure 4-3 confirms that Si is not only present in the film in a Si-C bonding motif. As a large proportion of the Si in the film is chemically bonded to oxygen this could explain the observed increased in sp^3 fraction as the SiOx backbone could maximise C-C bonding.

Table 4-2 Tabulated SS-NMR data. ppm range directly correlates to chemical species present [165, 166].

ppm range:	% amount:	Attribution:
60 to 0 ppm	**40**	**SiC**
0 to -50 ppm	**40**	**C-Si-O**
-50 to -80 ppm	**7.8**	**Silane (Si-H)**
-80 to -125 ppm	**7.5**	**Silicate (SiO_x)**

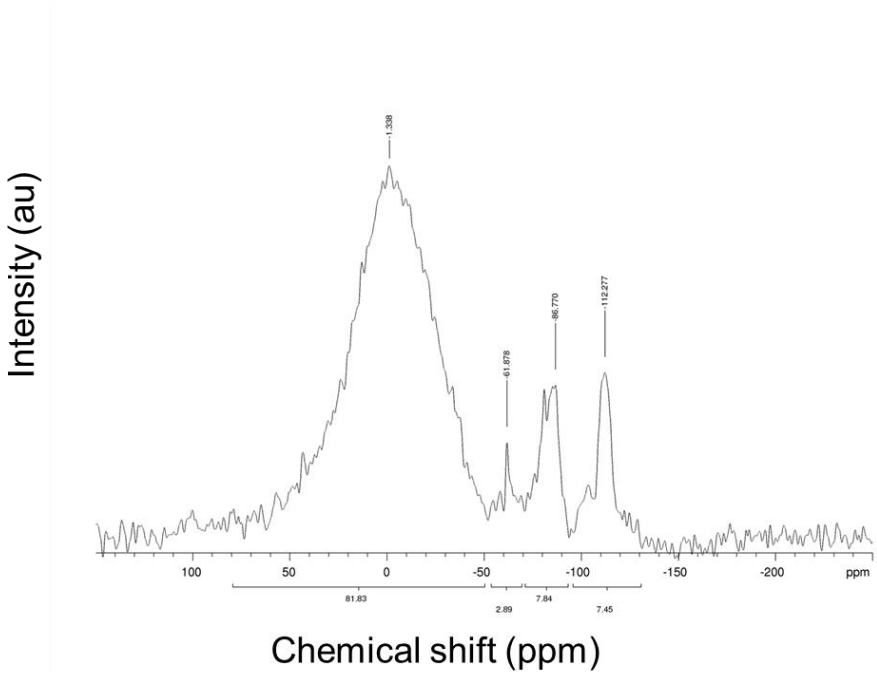

Figure 4-3 Silicon solid-state NMR spectrum of high Si DLC showing varying Si environments.

4.2.3. Surface Wettability (pre-wear)

Water contact angles were obtained for the Si and a-C:H coating and are given in Figure 4-4. Water contact angles give good indication of the affinity of a surface for a certain polar molecule. In this instance the values should give a picture of how active the surfaces are towards polar lubricant additives, like detergent species. A higher affinity for such additives can affect friction and wear. This is because detergent species have shown film forming and friction affecting behaviour in certain systems [127]. For reference the water contact angle of steel is recorded as 44 º [167]. This data suggests the low Si-DLC should have a higher affinity for certain polar additives.

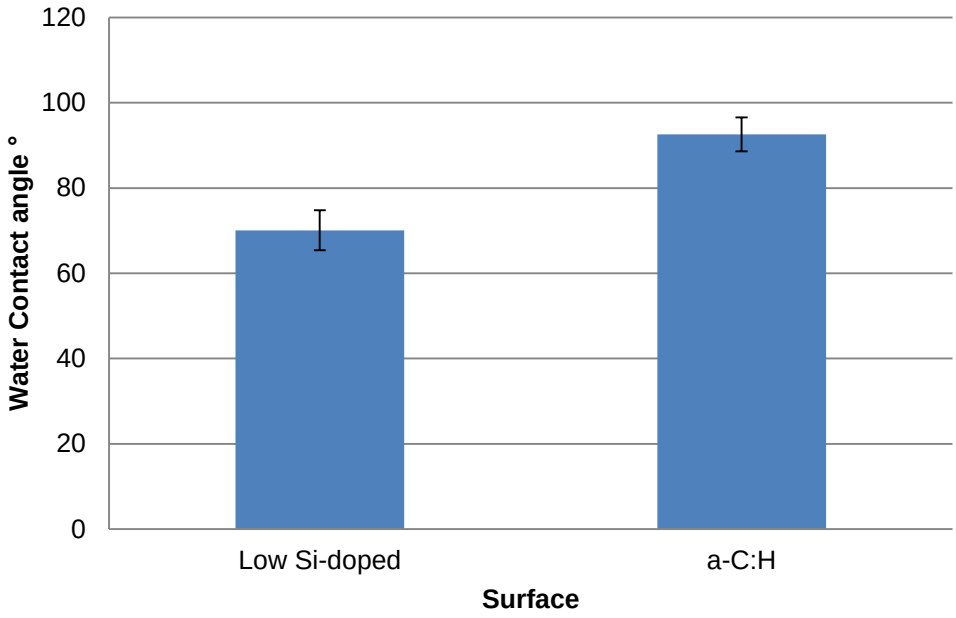

Figure 4-4 Water contact angle of the coatings tested. Si-doped sample relates to low Si-DLC

4.2.4. High-resolution XPS analysis of Si 2p peak from virgin, low % Si-DLC

High-resolution XPS was obtained of the Si 2p peak at the low Si-DLC's surface. The spectrum was first calibrated to the main C 1s peak at 284.4 eV. This is in line with other works in the literature whereby the spectra of DLC films are calibrated to the hydrocarbon (CH_x) peak [87, 144, 168, 169]. Following this, the Si 2p peak window was fitted with the functional groups known to be pertinent to Si-DLC films, as confirmed by the eV position and their corresponding FWHM values, listed in Table 4-3 [144]. The value of FWHM of XPS peaks herein is a convolution of analyser resolution and of natural FWHM of the selected chemical species peaks.

The most likely chemical species were determined using a variety of sources. ERDA data of the coating given earlier in Table 3-1 proves that Si, C, H and O are all incorporated in the coating, as expected with this type of DLC. As Si-H species are highly pyrophoric and unstable, if any were present within the upper 10 nm (as per XPS' penetration depth) they would instantaneously oxidise to Si-O species upon reaction with atmospheric

oxygen [83]. This means the species being detected must be only composed of Si, C and O. The prevalence of Si-O species within Si-DLCs is well known and thermodynamically, oxides of Si are to be expected at the surface. This leads to the firm conclusion that the peaks fitted in Figure 4-5 not only make sense chemically but also experimentally, as confirmed by agreement with FWHM values and binding energies.

The data confirms the survival (or reformation) of the C-Si-O backbone through the PECVD process as previously noted [87]. Also noted is the presence of the SiO_x species in agreement with the results shown in Figure 4-3. This species is likely only present in large quantities at the upper-surface and is evidence of ambient oxidation of the coating. This conclusion can be drawn as ERDA data of the coating is provided by the manufacturer. This indicates a lower amount of oxygen in the coating as a whole than the amount found at the surface by XPS.

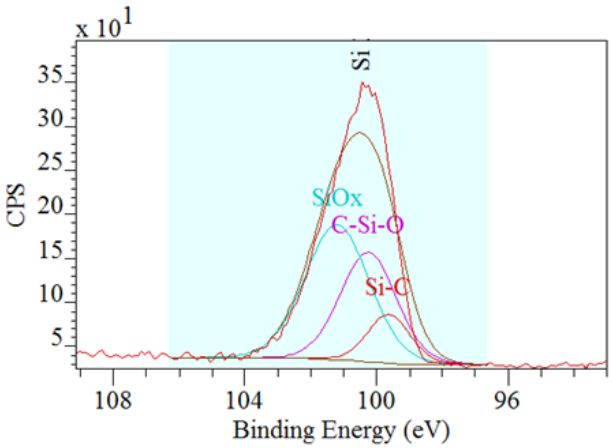

Figure 4-5 High-resolution spectra of Si peak in low Si-DLC with peak attributions.

Table 4-3 Si 2p peak data from the low Si-DLC

Attribution	Position (eV)	FWHM	% Concentration
C-Si-O	**100.3**	**2.0**	**36.3**
SiO_x	**101.2**	**2.3**	**51.4**
Si-C	**99.6**	**1.5**	**12.3**

4.2.5. Dry sliding results

4.2.6. Friction

The non-lubricated tribological behaviour of Si-doped DLCs is what generated first interest around the coating [26, 77-80]. This is because Si-DLCs typically exhibit far lower coefficients of friction when compared to a-C:H DLCs in unlubricated contacts when mated against a steel counterbody. This behaviour is typically attributed to the formation of silicon oxide species [26, 77, 79, 80, 102]. As such, the dry sliding of the two coatings (a-C:H and low Si-doped) was investigated to confirm this is true for the two specific coatings under anlaysis herein. Results from the dry sliding experiment, shown in Figure 4-6, confirms that the low Si-doped DLC outperforms the a-C:H DLC in this nonlubricated contact. The high Si-doped coating was not explored with regards to dry sliding after the two initial dry sliding experiments were conducted. This was because the low Si DLC underwent very high wear and it is known that increasing Si % dopants correspondingly increases wear rates [76, 77, 79, 84, 104, 113, 114].

Literature works conducted on a-C:H DLC/steel contacts do tend to show high friction when tested in dry air. This is also seen in the experiments conducted and presented here, as shown in Figure 4-6. Typically, the coefficients of friction are bettween 0.1 – 0.45 [170, 171]. This high friction behaviour of a-C:H DLCs has also been noted by Erdemir [69] which is given for comparison in Figure 4-7. When a-C:H DLC films were tested in air they show significantly increased coefficients of friction in comparison to the sliding experiment conducted in nitrogen [69].

4.2.7. Wear

In terms of wear, the low Si-DLC exhibits far higher volume loss than the a-C:H sample; this trend is expected. This is because, consistently in the literature, doping DLCs with any amount of Si results in higher wear of the coating, when compared with a a-C:H analogous coating [76, 77, 79, 84, 104, 113, 114].

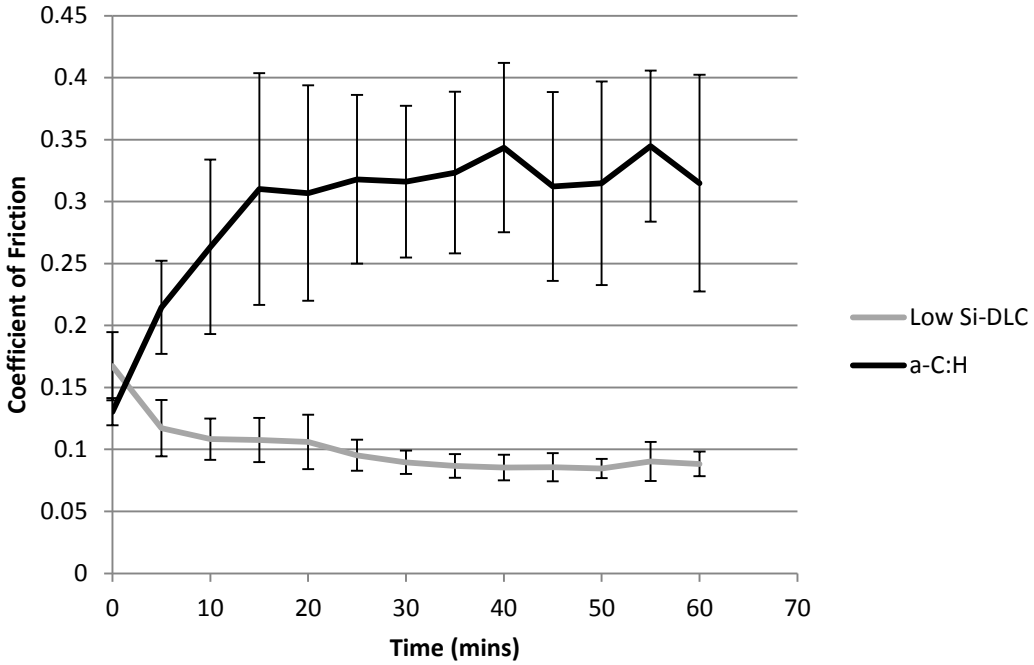

Figure 4-6 Friction plots of dry sliding low Si-DLC/a-C:H DLC against steel counter body. Running conditions as per experimental section on dry sliding, section 3.5.1.

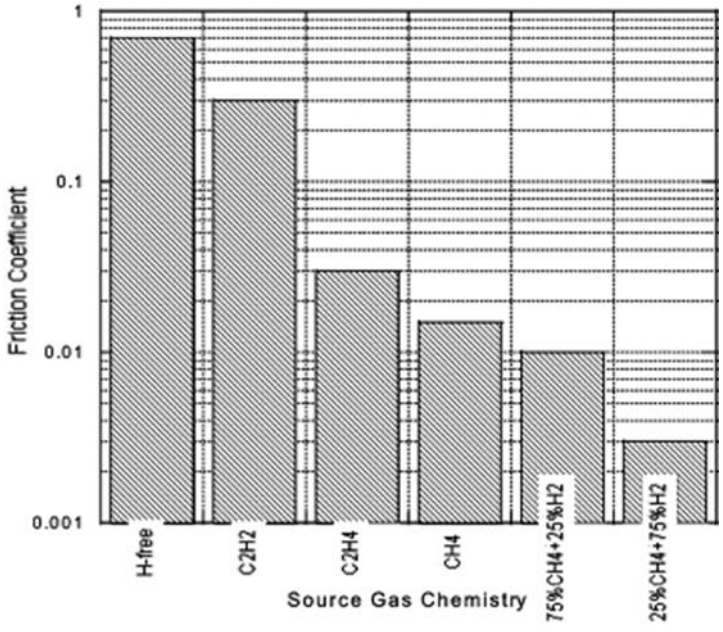

Figure 4-7 Literature results from Erdemir's work with a-C and a-C:H DLCs dry sliding showing the high friction values associated with these experiments [69].

The worn volumes were used to calculate specific wear rates for both coatings as given in Figure 4-8. The enhanced wear of Si-DLC is expected as it is known that silicon oxides play a role in reducing the friction and these species are representative of systematic oxidative-destruction of the silicon within the DLC. These results are in line with findings in the literature of wear of Si-DLCs when compared with a-C:H DLCs [76, 77, 79, 84, 104, 113, 114].

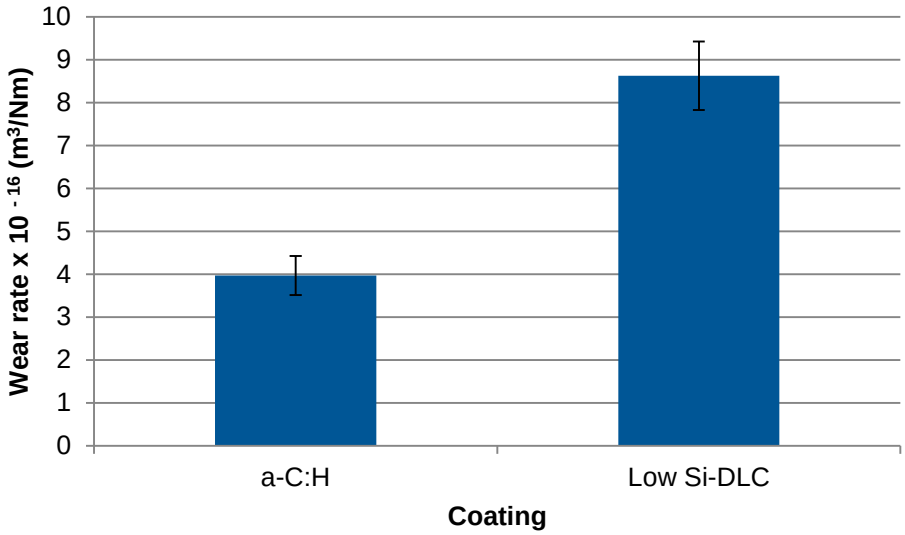

Figure 4-8 Specific wear rate of DLC plates when tested against steel counter body without lubricant. Experimental details different to lubricated contacts to prevent catastrophic wear. Running conditions given in Table 3-8.

4.3. **Tribological performance of lubricated tests (oil A)**

4.3.1. Friction profiles

To assess the friction values for a range of DLCs under the boundary lubrication regime, a test matrix was devised. The high Si-DLC is included in this test matrix as the presence of fully formulated oil will reduce wear, which could allow the high Si-DLC to be a viable coating in this instance. The test duration was set for two hours, as per the experimental section. The results are detailed in Figure 4-9 and Figure 4-10. With respect to friction performance, the steel/steel tribopair slightly outperforms the DLCs tested. The coefficient of friction of the steel/steel system is lower than the DLCs but

somewhat unstable. Both the doped and a-C:H DLCs show very similar friction values in this oil. It is notable that the friction of both Si systems is not markedly lower than that of the a-C:H DLC, as is often the case in dry sliding. The values obtained for both Si-DLCs are within those found in the literature for lubricated sliding [43, 104, 110, 172]. Friction values for a-C:H DLC/steel contacts are found to be within the range μ = 0.05- 0.1 with improved performance depending on inclusion of inorganic FM species [100, 173]. However, higher friction values (μ = 0.3 – 0.4) have been recorded for a-C:H DLC/steel systems at higher (1GPa) contact pressures [29]. As such the friction values reported below are in-line with similar experiments in the literature.

4.3.1. Wear results

All samples were analysed with respect to wear. Optical examination of the a-C:H coating tested in Oil A confirmed that there was only very minor wear. For the a-C:H coating the wear was immeasurable with scanning light interferometry. The remaining three samples (high Si, low Si and steel) were examined using this technique to ascertain which pair gives overall lowest wear, Figure 4-11. Interferometry confirms that all DLCs are able to reduce wear when compared to steel.

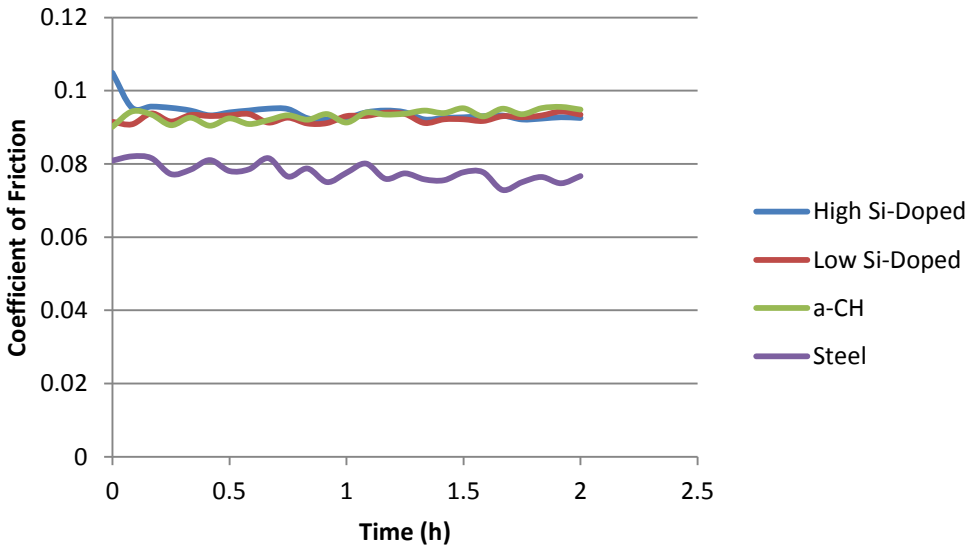

Figure 4-9 Friction traces of coated and uncoated surfaces in Oil A. Error bars excluded for clarity. Conditions as per experimental for piston ring contact setup which are given in Table 3-7.

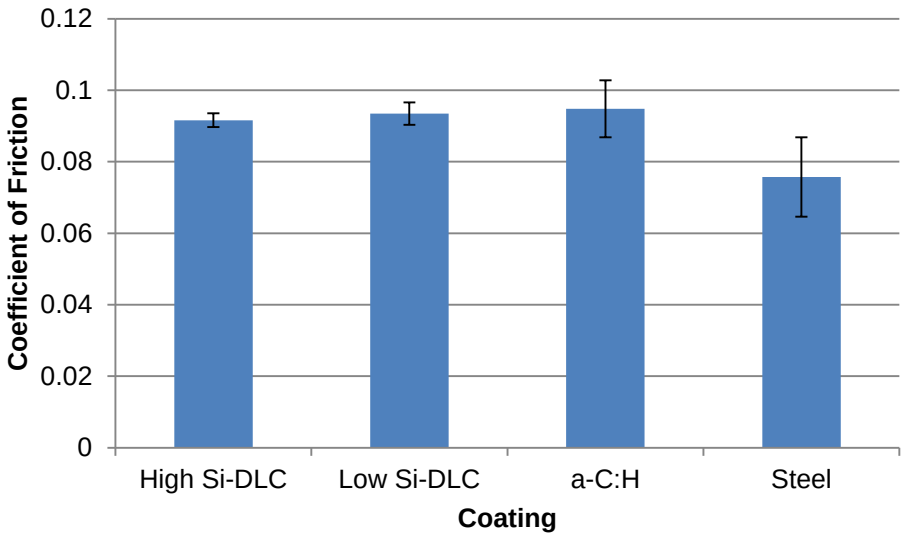

Figure 4-10 Steady-state friction (last 20 minutes of testing) of all coatings tested in oil A.

The low Si-DLC shows on average a 55% reduction in wear when compared with the steel surface. The high Si-DLC reduces wear when compared with steel but not as markedly as the other DLCs. It is well reported in the literature that incorporation of Si within DLC causes aggravated wear rates when compared to a-C:H DLC, as such the findings here agree with this trend [76, 77, 79, 84, 104, 113, 114].

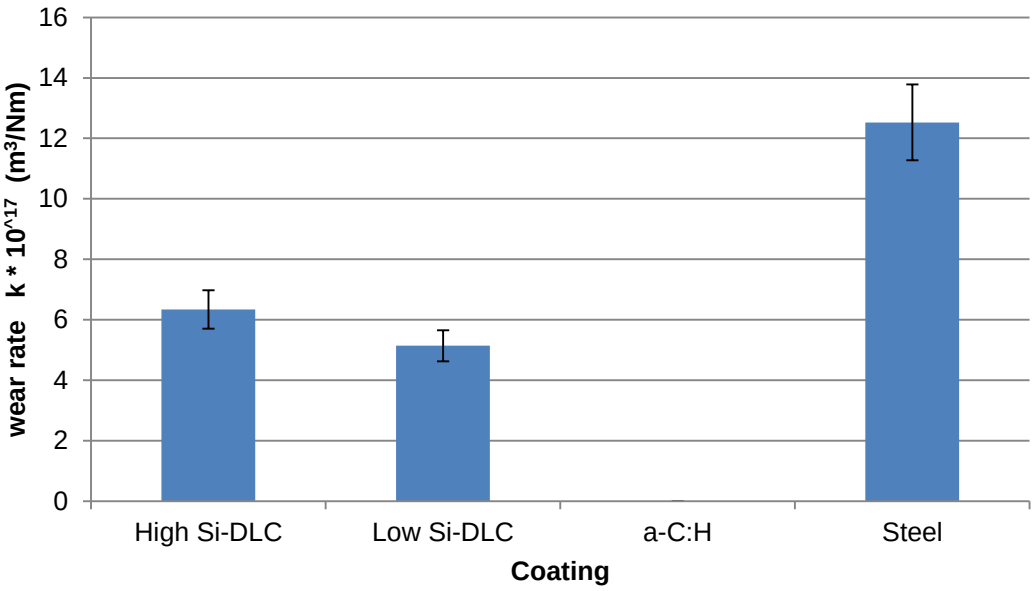

Figure 4-11 Specific wear rate of coated and un-coated surfaces in oil A.

4.3.2. Effect of friction modifier species

In order to establish if inclusion of an organic friction modifier species in the lubricant blend for a DLC/steel tribopair affords an appreciable drop in friction, a non-FM containing oil (Oil B) was also tested against the various tribopairs, Figure 4-12. Steady state friction values, shown in Figure 4-12 suggests that the organic friction modifier species appear to exert no effects on the a-C:H coating as the friction values for both oils are within experimental deviation of each other.

The friction modifier MoS_2 has been shown to positively affect the friction values of a-C:H/steel contacts [100, 174]. However, in an a-CH/CI system this friction reduction was not noted, with both fully formulated oils (one containing MoS_2) giving a coefficient of friction of $\mu \sim 0.1$ [175]. Work has been conducted on DLCs with organic friction modifiers but these are confined to ta-C and a-C DLCs. In some cases ultra-low friction is observed $\mu = 0.03$ [98, 99]. The reported lubricated friction values of Si-DLCs are typically around $\mu \sim 0.1$, depending on lubricant composition [43, 104, 110, 172].

The high Si-DLC shows better friction values with Oil A. It can be seen that at steady state the low Si-doped DLC shows a slight friction reduction when compared to the a-C:H DLC.

4.3.3. Wear of low Si-DLC plates in the lubricated contacts

Of the two Si doped DLCs, the low doped Si outperforms the high-doped coating with respect to wear. This is in agreement with findings in the literature, increasing Si content typically results in higher wear rates [77, 84]. In order to assess to what extent surface active species like GMO affect wear rates, wear of the Si plates at the two hour interval in oils A & B were compared, Figure 4-13. Comparable data for the a-C:H sample is not available as the wear was immeasurable in either oil at that point. There is no significant change in wear rate between the two oils for the low Si-DLC.

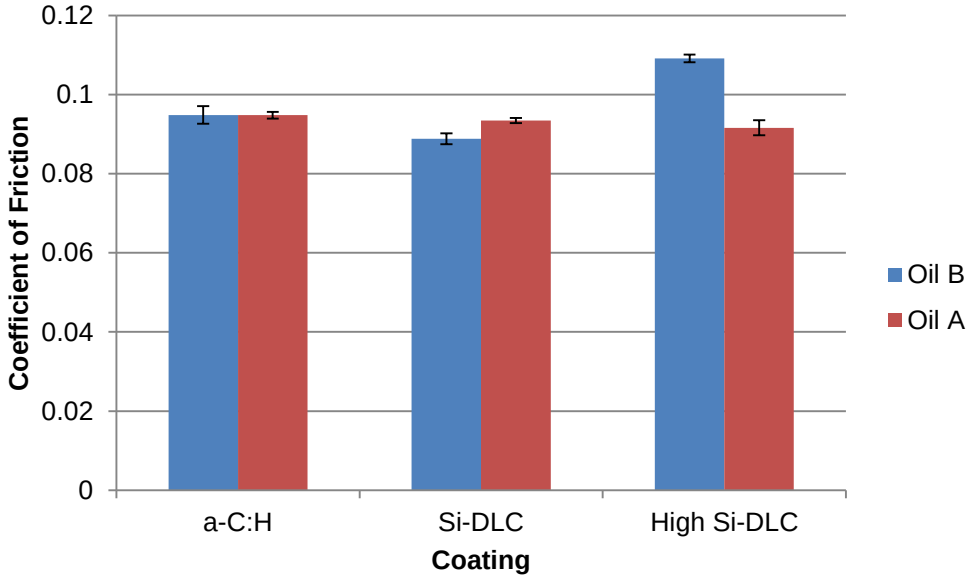

Figure 4-12 Steady state friction values compared for various tribopairs in oils A and B

The same is true for the a-C:H DLC which shows no wear at two hours in either oil. The high Si-DLC showed higher wear in both oils. This is most likely due to the tendency of Si within the DLC to oxidise and degrade the coating [43, 105]. Thus it follows that a greater incorporation of Si in the coating equates to a great wear rate. This mechanism of wear is discussed in depth later. This combined with it not imparting any advantage on friction

meant that it was excluded from the test matrix as the low Si-DLC showed an overall better friction profile.

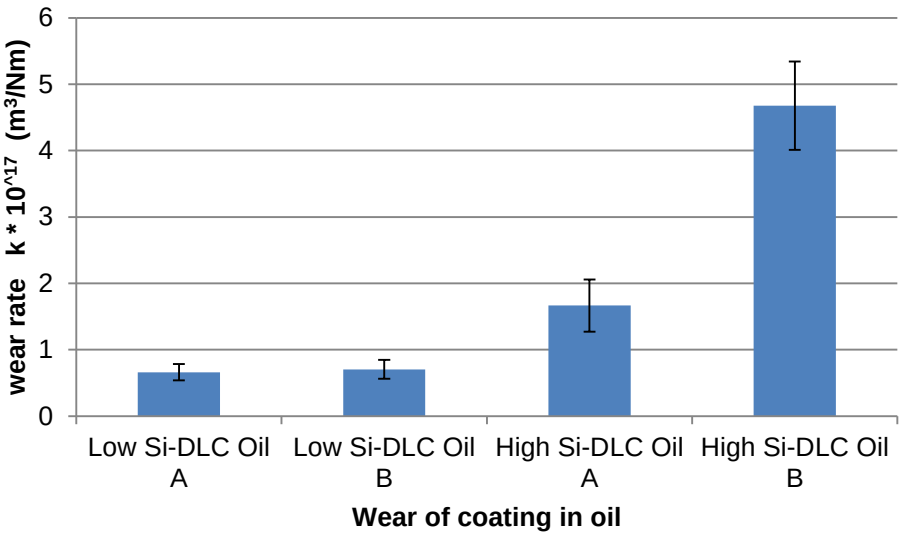

Figure 4-13 Low Si-DLC specific wear rate by oil. Inclusion of GMO as FM does not affect wear as the values are not outside error of each other.

4.4. **Surface analysis**

4.4.1. Surface analysis (XPS) of the steel tribopair

To characterise surface interactions of the DLC/steel tribopair it is first necessary to understand the tribochemical reactions that take place at the steel/steel interface. Figure 4-14 and Table 4-4 show the XPS data obtained from both the pin and plate.

XPS analysis confirms the presence of a tribofilm on both the plate and the pin. Carbon (omitted for scaling) makes up the bulk of this material which is likely from various sources including GMO and detergent species, which contain carbonate cores and similar carbonaceous additives. XPS indicates the presence of a calcium phosphate type film with trace amounts of zinc phosphate and zinc oxide within this film. Also noted is zinc sulphide. It is notable that Fe is not detected on the plate (however it is on the pin). This suggests a tribofilm thicker than 10 nm has formed. Otherwise, Fe would be detectable from the steel plate below as the penetration depth of XPS is well established [137].

The attributions made above cannot, at this stage be conclusive, although a calcium phosphate based tribofilm is indicated, there is difficulty in attributing the Ca and P peak as there are several molecules that would come at this eV point in the spectrum. The Ca peak at 347-348 eV coincides with both calcium carbonate and calcium phosphate [143, 147]. Both species are likely to be present in varying proportions. The formation of calcium phosphate based films, derived from ZDDP and detergents, at steel/steel interfaces in the literature are well reported [147, 176, 177]. As such, these results are in agreement with these findings, a calcium phosphate type film with partial inclusion of zinc phosphate and zinc oxide does represent a viable tribofilm. Calcium phosphate is well-known to act in an anti-wear capacity [176, 177].

The sulphur peak also leaves room for multiple compounds to be present on the surface. This is because the eV position for sulphides ranges from 160 – 163.5 eV [143, 146]. Furthermore, the zinc $2p_{3/2}$ peak is also difficult to deconvolute with the oxide and sulphide peaks overlapping at ~ 1022 eV [143, 146]. Fortunately knowing the stoichiometry of ZDDP, whereby the ratio of Zn:S is 1:4, it is possible to conclude that there is more reactive sulphur available than zinc, therefore formation of FeS_2 is not only viable but also likely. It then follows that the presence of ZnS_2, ZnO and FeS_2 are all probable in this system. It would be possible to gain more certain knowledge of the species present with further surface analysis. However, as the ZDDP at a ferrous/ferrous interface is well documented and commented on in the literature further analysis was not pursued.

4.4.2. Surface analysis (XPS) of the DLC plates

XPS spectra were obtained of the two DLCs that performed best. Specifically a-C:H DLC, for its low wear and the low Si-doped DLC, for its potential to alter the surface energy without the high wear seen with the high Si-DLC . This was to ascertain what tribochemical processes were taking place at the surface.

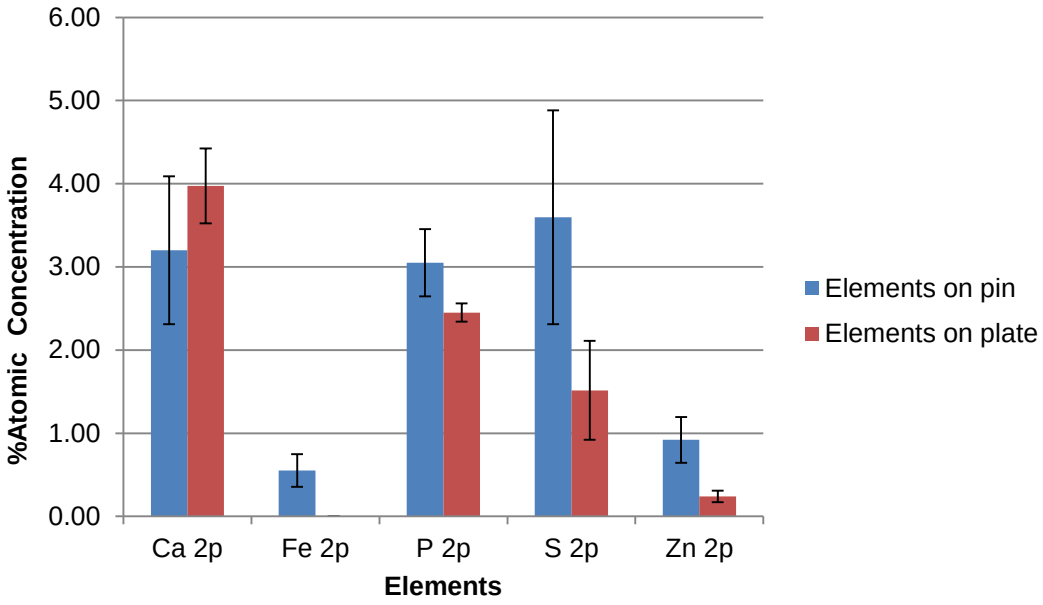

Figure 4-14 XPS data from steel/steel tribo-contact post testing. C and O left out for scaling. Error is measured as standard deviation over three anaylsis points.

Table 4-4 XPS attribution of steel plate and steel pin post testing. nd = not detected.

Element	Pin (eV)	Attribution	Plate (eV)	Attribution
Ca 2p	**347.1**	**Calcium carbonate/ calcium phosphate**	**348.1**	**Calcium carbonate**
Fe 2p	**710.1**	**Iron (III) oxide**	**nd**	
P 2p	**133.1**	**Phosphate**	**133.6**	**Phosphate**
S 2p	**161.1**	**ZnS/FeS**	**162.1**	**ZnS**
Zn 2p	**1022.1**	**Zinc oxide/ Zinc sulphide**	**1022.1**	**Zinc oxide/ Zinc sulphide**

XPS shows Ca adsorption from both DLCs tested and is given in Table 4-5. Where the a-C:H sample only shows inclusion of Ca in its tribofilm, the low Si-DLC appears to be more tribologically active at the two hour interval with inclusion of P and Zn. XPS results suggest the presence of calcium phosphate and zinc oxides within the film at the low Si-DLC.

Table 4-5 XPS data comparison of low Si-DLC and a-C:H DLC in Oil A. Nd = not detected

Element	% At Concentration low Si-DLC	Attribution (eV)	% At Concentration a-C:H	Attribution (eV)
C 1s	**79.5**	**284.40**	**90.31**	**285.08**
Ca 2p	**1.2**	**Ca phosphate/ $CaCO_3$ (347.40)**	**1.0**	**$CaCO_3$ (347.08)**
O 1s	**12.8**	**531.30**	**8.9**	**532.08**
P 2p	**0.3**	**Pyrophosphate /Pyrophosphate (133.00)**	**Nd**	**-**
Si 2p	**6.2**	**SiC (100.00)**	**Nd**	**-**
Zn 2p	**0.1**	**ZnO (1021.50)**	**Nd**	**-**

To elucidate the effect the inclusion of the surface active friction modifier GMO has on the friction performance XPS analysis was also obtained for low Si-DLC tested in Oil B, as shown in Figure 4-16. When comparing XPS data for the two samples of low Si-DLC, an interesting trend appears. The sample tested in the Oil A contains less calcium, phosphate and zinc.

However, the film shows a greater inclusion of carbon. To attribute this finding solely to the presence of the friction modifier would require further experimental work. However, friction data combined with the XPS findings do firmly indicate that the FM species is playing a key role in tribofilm formation. It would seem that inclusion of GMO decreases the amount of elements other than carbon at the surface and that this slightly lowers the friction profile for the low Si-DLC.

4.5. **Initial long-duration test**

With the clear goal of assessing life-time performance of the DLCs examined, an initial long-duration study was carried out with the low Si-DLC; as it was shown to be the most tribologically active at two hours. The test was carried out within a specifically selected oil, Oil C (heavy duty, high

SAPS, engine oil) to ensure full tribofilm formation. The overall friction profile is given in Figure 4-15. The steady state friction value for this system was μ = 0.096. The coating gave no observable wear at seven hours in oil C, which had a high additive level.

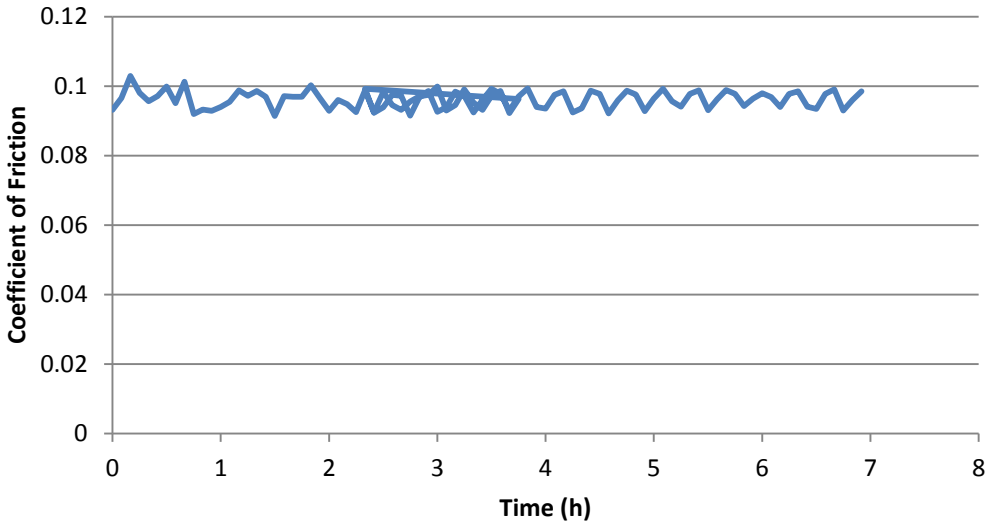

Figure 4-15 Initial long-duration test of low Si-DLC in oil C

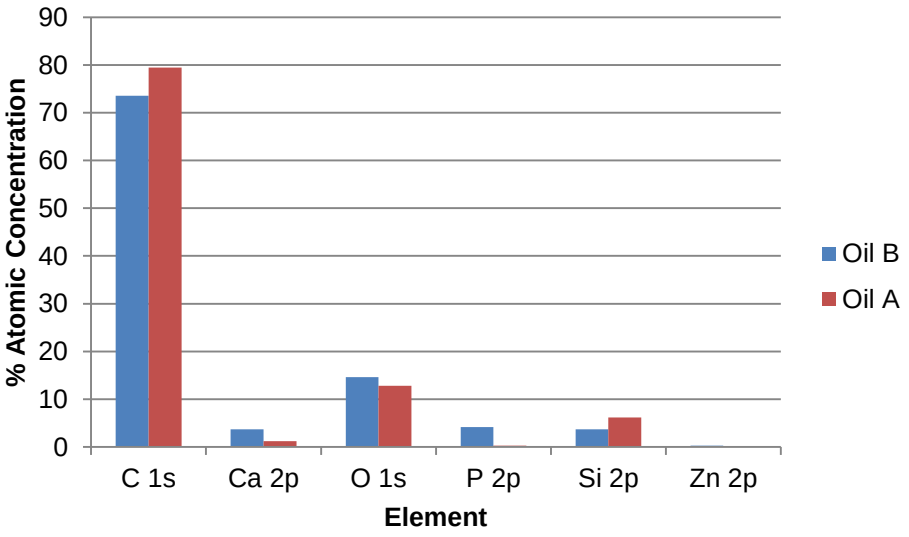

Figure 4-16 low Si-DLC surface %atomic concentration, separated by oil. NB P (0.29% for oil A) and Zn (0.28% for oil B, 0.04% for FM A) are present in both samples.

Oil C is similar to Oil B, ICP analysis (available from the manufacturer) confirms it has a higher amount of sulphur based additives incorporated in the lubricant package. Oil B contains 2064 ppm S whereas Oil C contains

8309 ppm S. This is highly indicative of sulphur based EP additives being included [132]. The objective of using Oil C was to verify that the DLCs can and do form thick tribofilms that dictate their wear and friction profile.

TEM and EDX were used in this instance to characterise a cross-section of the worn area of the film as it was essential to observe if a tribofilm was formed. Low Si-DLC, tribotested for fourteen hours, did yield interesting results shown in Figure 4-17. TEM/EDX analysis confirms the presence of a thick tribofilm (15.2 ± 1.2 nm), present consistently across the surface of the DLC comprising Ca, P, Si, S and trace Fe.

However, this oil was not taken forward for further testing as the wear rate was far too low for the a-C:H DLC (no well-defined wear scar visible at the 14 hour interval) that it would have made further experimentation difficult. Further to this, the oil would be classified as high SAPS and in general lubricants are moving away from such high SAPS formulations [8].

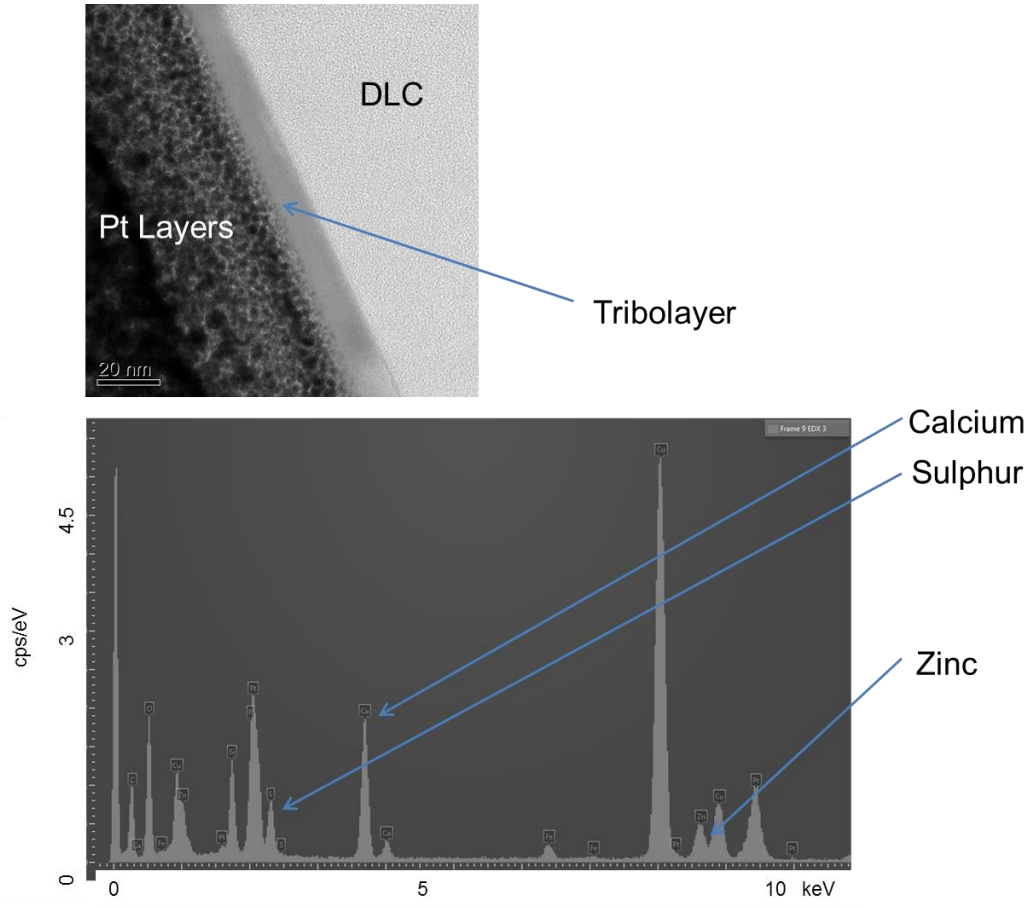

Figure 4-17 TEM cross sectional image of the tribofilm formed on low Si-DLC in Oil C. Inset of EDX spectra from the interface of the tribocontact showing Ca, P, S. Cu and Pt are artefacts from the creation of the cross section.

4.6. **Summary**

To fully understand the tribochemical process taking place at both the a-C:H and the low Si-doped DLCs it is necessary to test the samples for longer time periods. This allows for full tribofilm formation and an accurate time wear/tribofilm relationship to be elucidated. Due to the immeasurable wear of the a-C:H sample it can therefore be identified as low wear. Whether this is due to the DLCs mechanical characteristics or tribological properties is unclear at this specific time interval but is investigated in more depth later in Chapter 5. As Si-DLCs are typically supposed to have a better friction profile than the one obtained and shown in Figure 4-9, longer duration experiments were sought with both the a-C:H and Si-doped DLCs to investigate whether either the friction or wear profiles change with lifetime.

Currently, there are not many published papers on the long duration performance of DLCs, as such it seems highly relevant to explore the DLCs further, with longer term testing. Factors that could come into effect at longer durations include: enhanced polishing-wear, time dependence of tribochemistry and the move from running-in to steady-state friction and wear regimes. The a-C:H sample gave immeasurable wear in both oils A and B at the two hour interval.

The three coatings exhibit very similar friction at the two hour interval. As such, the decision on which coatings to take forward to next stage of testing was based on the wear results. The a-C:H coating exhibits ultra-low wear, therefore this coating was taken forward, along with the low Si-DLC coating. Due to the similarities in the friction between the coatings, the need to optimize the lubricant becomes apparent. The coatings are both able to reduce wear very effectively; the remaining issue is reduction of friction. As friction is the prominent factor, Oil A was chosen for longer duration testing. Oil A contains GMO which is purported to work well with certain DLC coatings with respect to friction, as such this oil was taken forward [97, 99, 112]. The main findings from the initial, short term testing are as follows:

- Inclusion of Si into the DLC's matrix affects the DLC's microstructure and sp^x ratio, a phenomena consistent with findings in the literature [81, 82].
- Both the Si-DLC's showed friction performance in lubricated contacts with steel that is not superior to that of a-C:H DLC. This is the opposite of the behavior observed at the non-lubricated contact. The most likely mechanism of this is that the relevant SiO_X species are removed from the contact area and further production is inhibiting by the tribofilm, a mechanism explored in more depth in the discussion.
- Inclusion of Si increases overall wear of the DLC coating, when compared to the a-C:H coating. Further to this, Si-DLCs wear increases with increasing Si content.
- The low Si-DLC forms thick (nm scale) tribofilms that protect them from wear.

- a-C:H DLCs appear to be less tribologically active than Si-DLCs at the two hour interval.
- Si-doping affects the coatings' ability to interact with lubricant additives. A more polar surface favors reactions with more polar additives.

Chapter 5 Results: Comparison of the long-duration performance of low Si-doped and a-C:H, hydrogenated DLC

5.1. Introduction

Chapter 4 deals with the shorter duration testing of DLCs. In this chapter the lack of literature focusing on the long duration performance of DLCs is addressed. This study was motivated by the need to have a fuller comprehension of how DLCs perform over a longer testing duration. One main theme under investigation is to establish if there is an initial trade-of to be made, whereby Si-doped DLC's higher running-in wear is facilitated by a higher reactivity of the coating. This higher reactivity could actually be beneficial over the long duration in terms of tribofilm formation.

The DLCs brought forward from the previous stage (a-C:H DLC and the low Si-DLC) were examined in Oil A at various time intervals up until thirty five hours. It must be noted that friction values are only given up until 14 hours, whereas wear data is available until 35 hours. This was due to employing two tribometers, one of which does not provide friction data. The thirty five hour time frame was chosen to give insight into lifetime performance of the DLCs whilst still being practical in terms of experimental work-load.

5.2. Results

5.2.1. Friction results

Figure 5-1 shows the friction results obtained for both the coatings up to the thirty five hour mark as tested in Oil A. Steady state friction data was compiled from the last twenty minutes of testing and these are summarised in Figure 5-2. From the friction data it appears that the silicon-doped and the

a-C:H DLCs are comparable, with low Si-DLC showing a slightly reduced friction profile toward the end of testing. These results are in-line with literature precedents of Si-DLCs tested in formulated oil, in that the inherent improved lubricity is lost when tested *in lubro* [104, 110, 172].

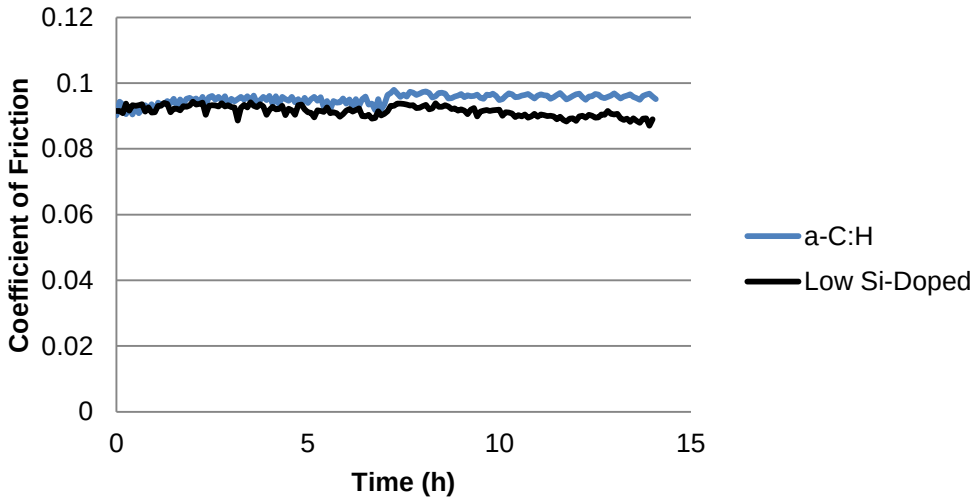

Figure 5-1 Long duration friction of the DLCs (error bars excluded for clarity) Conditions as reported in the experimental section for the piston ring contact profile.

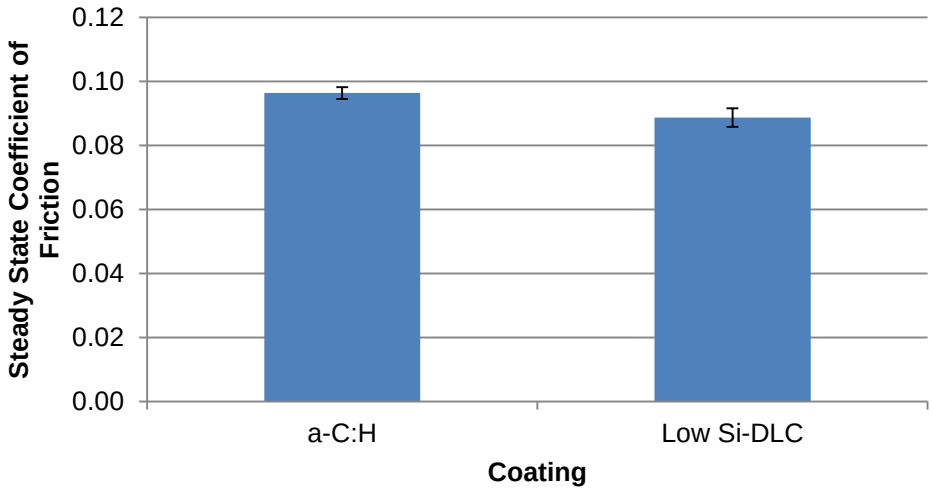

Figure 5-2 Steady-state friction profiles (last twenty minutes of testing) of the DLCs, included to show error associated with either value.

5.2.2. Wear

Wear analysis was undertaken at each time interval shown, including an additional time interval of thirty five hours to allow for a fuller picture of the wear-time relationship. This was done as it would be useful to know how the running-in period, in terms of wear performance, would affect the DLC coatings. If the running-in process is too severe it could compromise the entire coating and negate the benefits imparted. It was assumed that this process would have finished by thirty five hours, at which point the system would be at a steady state. For the first time interval, two hours, wear was immeasurable for the a-C:H sample. Worn volumes shown in Figure 5-3 were converted into dimensional wear coefficients, shown in Figure 5-4. This allows for comparisons to be made with similar coatings/materials. These values are calculated from profilometry data. The dimensional wear coefficient is the volume worn (m^3) divided by the sliding distance (m) multiplied by the unit of load (N). It must be noted that despite the low Si-DLC having a higher wear rate than the a-C:H DLC, both DLCs appear to be undergoing only polishing wear, rather than a more severe type of wear.

The initial wear profiles of the two samples share some similarities. Both DLCs have higher initial wear rates when compared with longer-testing. This is associated with the running-in period; however the wear rate of the low Si-DLC is far higher than that of the a-C:H DLC and occurs for a longer time (starting at two hours).

Furthermore, there is a clear change present when examining the specific wear rate trace of both the DLCs between the seven and fourteen hour marks. This is indicative of an efficacious protective tribofilm forming.

Optical microscope images taken of the thirty-five hour wear scar shows the differences in the two plate’s wear behaviour, images are shown in Figure 5-6.

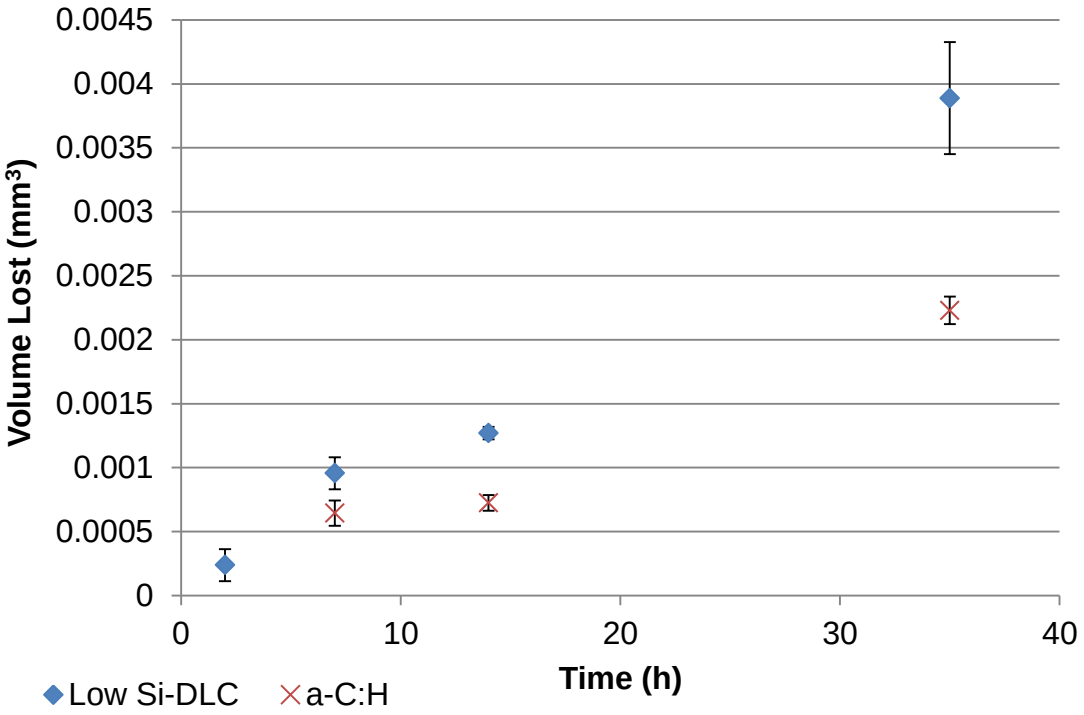

Figure 5-3 Volume loss of each coating plotted against time. Initial wear value of a-C:H DLC is not given as it was immeasurable.

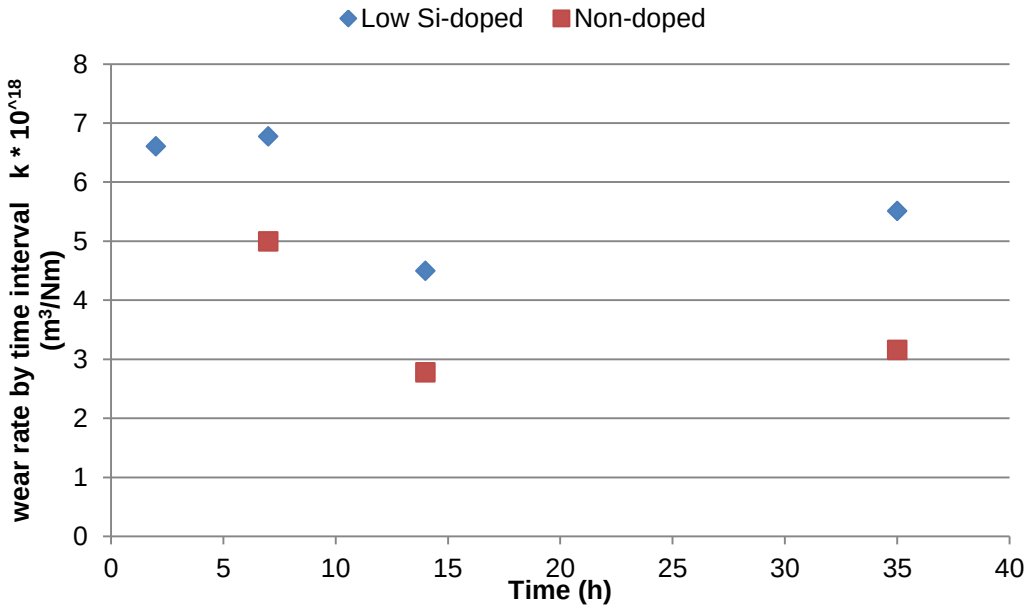

Figure 5-4 Wear coefficients of the low Si and a-C:H DLC. Again, no initial two hour wear value is available for the a-C:H coating as wear was immeasurable at this time interval. Each point is the wear rate of the coating at that time interval.

At the thirty five hour point, total coating depth loss was gauged as this is the standard by which coatings are assessed for overall wear performance. This

is given in Figure 5-5. As shown, the a-C:H coating outperforms the low Si-doped DLC. The original coating thickness was 2.4 µm for the low Si-DLC, giving an overall reduction of thickness of 25% of the coating. For the a-C:H coating, the initial thickness is 1.4 µm, giving a loss of only 10% of the total thickness.

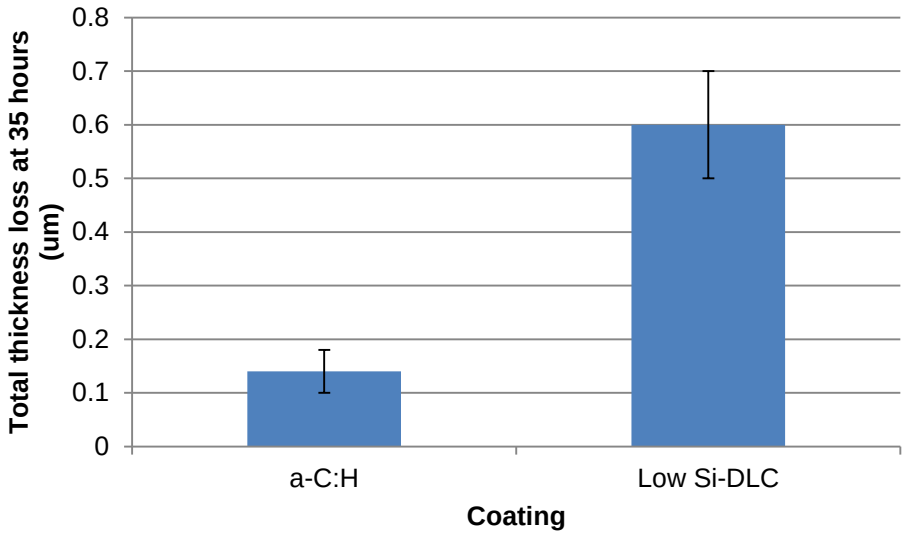

Figure 5-5 Total coating depth loss at the end of testing

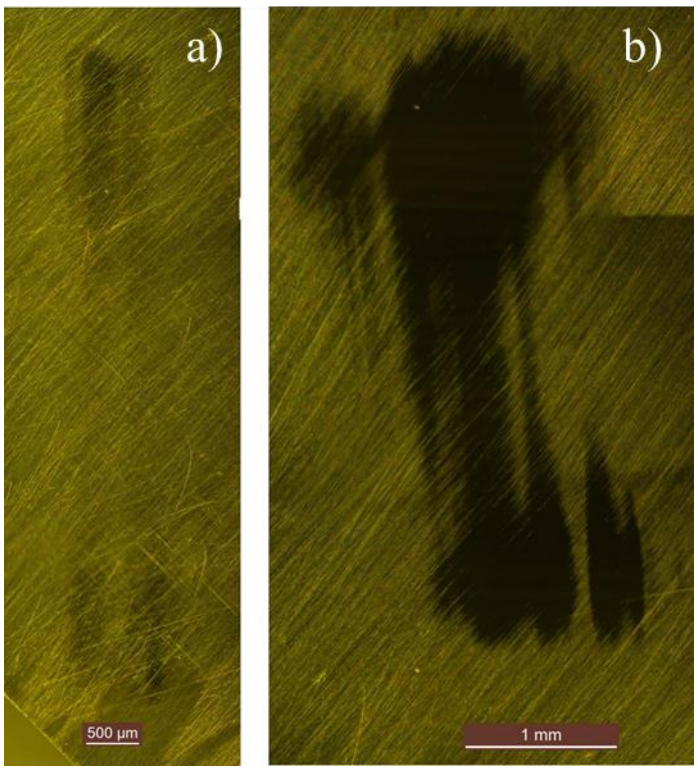

Figure 5-6 Wear at 35 hours of a-C:H DLC a) and low Si-DLC b)

5.2.3. Surface analysis

As there is clear evidence of a tribofilm forming, due to the reduction in wear, a range of different surface analysis techniques were employed to assess the tribochemistry at the interface. XPS analysis was sought for each time interval to get an overview of the composition of the tribofilm and how it developed as a function of time. Other techniques were employed at different, set time intervals for a more comprehensive picture and to validate conclusions made based on XPS data.

5.2.4. XPS analysis of the low Si-DLC

Time resolved XPS analysis of the low Si-DLC coupons were compiled to give an overall picture of tribofilm formation as shown in Figure 5-7.This gives an overview of the elemental composition of the film at various intervals. This data was then further interrogated to get information on how each element is present and how this evolves with time. It is crucial to know the type of species present when looking at wear impeding films. XPS data was tabulated as shown in Table 5-1, and attributed to show the most appropriate chemical species for the system. These attributions were set using XPS databases, reference books and fundamental tribochemical knowledge as well as from the literature [87, 143, 146, 178-180]. As mentioned earlier, the Ca peak at 347-348 eV coincides with both calcium carbonate and calcium phosphate [143, 147]. Both species are likely to be present. Zn peaks at 1022 eV coincide for either ZnS or ZnO, both are viable species [143].

The main section of the XPS signal (excluding coating constituents) from the tribofilm on the Si-DLC at the two hour interval is from the Ca and P components of the spectrum. Comparison with eV values from the NIST database indicates that calcium phosphate type species are present in the worn area with P incorporated as pyrophosphate [146]. Formation of calcium phosphate is viable within this lubricated system and is encountered when steel/steel contacts are lubricated in fully formulated oil [147, 176, 177]. The tribofilm does appear to change in character with regards to time, this is thought to be partly due to the detection limits of XPS. This change

involves the evolution of a new peak on the C1s spectrum showing far greater incorporation of Ca. The novel C1s peak is in the correct binding energy for calcium carbonate, as shown in Figure 5-8. This peak appears to occlude other elements of the tribofilm from being detected.

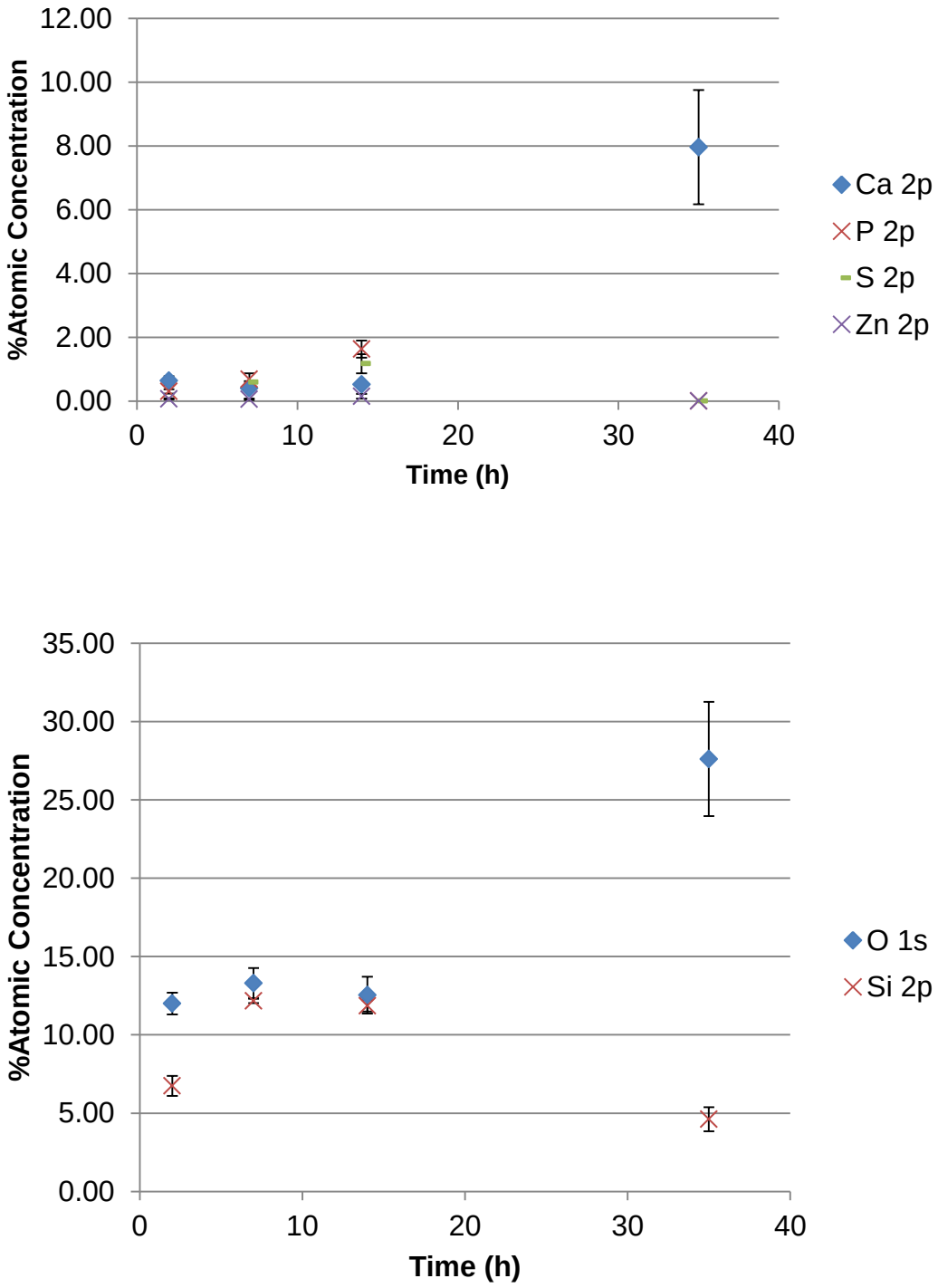

Figure 5-7 XPS of low Si-doped DLC plotted against time. Separated by into tribofilm elements and coating constituents. Average is of 3 spot analysis.

Table 5-1 XPS key-peak breakdown of low Si-DLC. Nd = not detected

Element/ Time	Ca (eV)	P (eV)	S (eV)	Zn (eV)
2	**347.4 calcium phosphate**	**133.0 calcium phosphate (pyrophosphate)**	**nd**	**1021.5 zinc oxide**
7	**347.2 calcium phosphate**	**133.5 calcium phosphate (pyrophosphate)**	**162 Zinc sulphide**	**1022 zinc oxide/ sulphide**
14	**347.5 calcium phosphate**	**133.5 calcium phosphate (pyrophosphate)**	**162 zinc sulphide**	**1022 zinc oxide/ sulphide**
35	**347.15 calcium carbonate rich layer**	**nd**	**nd**	**nd**

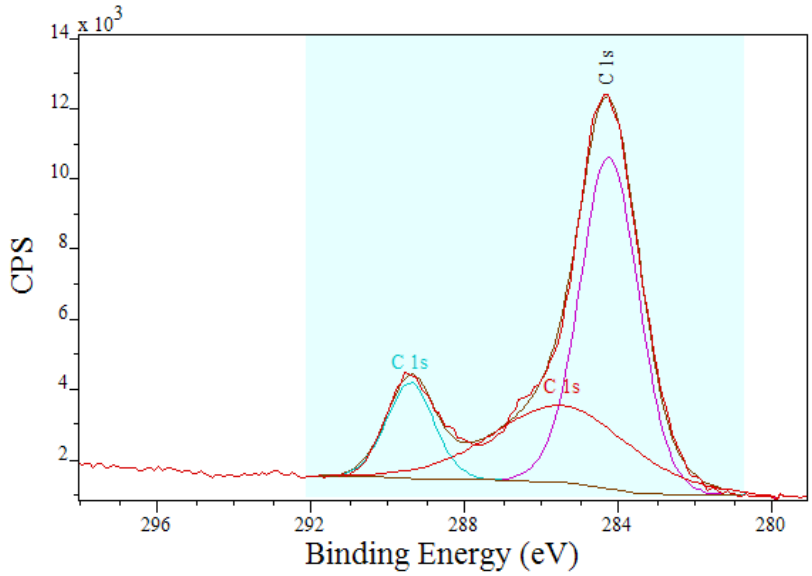

Figure 5-8 C 1s peaks at 35h for low Si-DLC. Clear evolution of second peak.

5.2.5. ToF-SIMS chemical maps of the low Si-DLC

To verify the effect XPS sensitivities were having on detection of key species, ToF-SIMS chemical maps were also sought for certain species. Specifically to verify the presence of phosphate groups which are one of the most relevant species when exploring anti-wear films. Negative ion spectra chemical maps were compiled from a plate at the seven hour interval shown in Figure 5-9. ToF-SIMS chemical maps validate many of the XPS findings and show that even though certain species were undetectable by XPS they were still present in the film. S, HS and PO^3 anion fragments are in good agreement with the species detected. Metal ions are not detected as negative spectra were obtained and metal ions occur in the positive side of the spectrum, as Ca and Zn showed good response to XPS this data was not obtained.

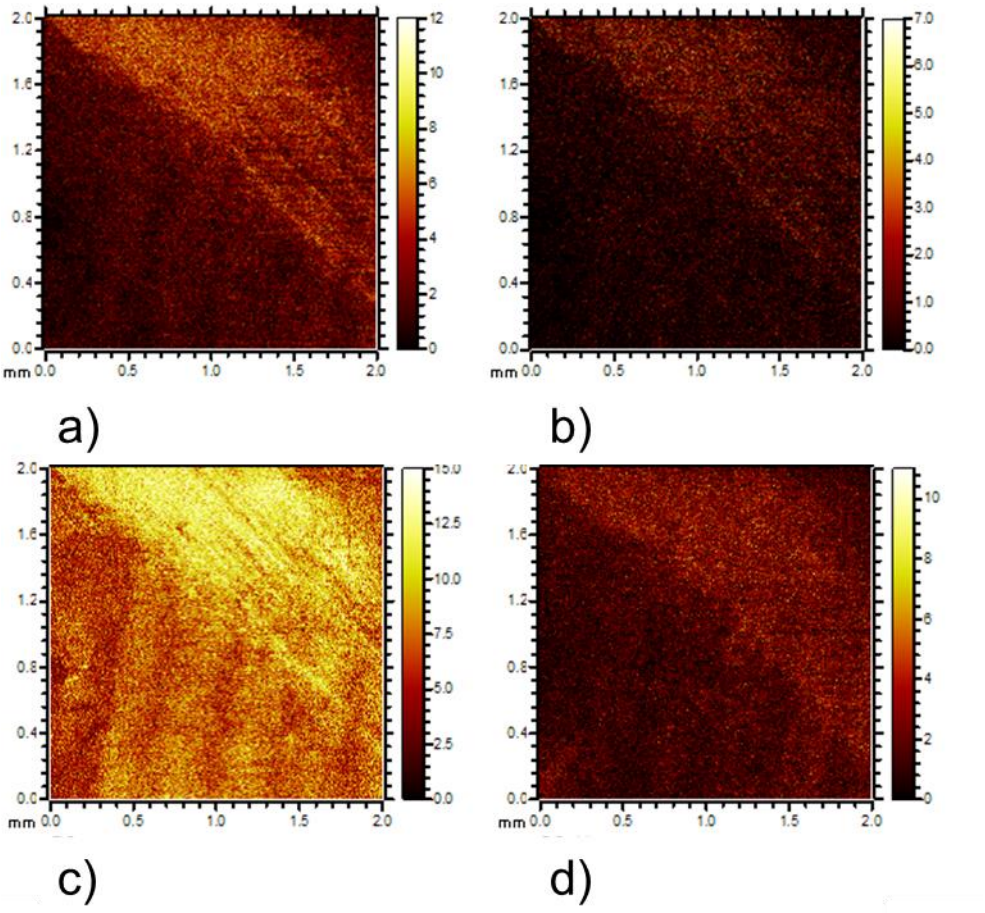

Figure 5-9 ToF-SIMS negative ion chemical map of the low Si-DLC at 7 hours, showing the presence of a) HS, b) S, c) PO_3 and d) SO_3H.

5.2.6. XPS analysis of a-C:H DLC

Time-resoled XPS analysis of the a-C:H DLC coupons were compiled to give an overall picture of tribofilm formation as shown Figure 5-10. XPS data was tabulated in Table 5-2 and attributed to show the most appropriate chemical species for the system. These attributions were set using XPS databases, spectra reference books and fundamental tribochemical knowledge as well as literature precedents [143, 146]. The a-C:H DLC shows some similarities with the silicon doped sample. The first element identified is calcium as the carbonate or oxide. At the later stages of testing, greater amounts of certain elements and species appear in the worn area. This is indicative of the large-scale build-up of a wear impeding tribofilm. The species identified are very similar with those on the Si-DLC including a calcium phosphate species and varying Zn and S compounds.

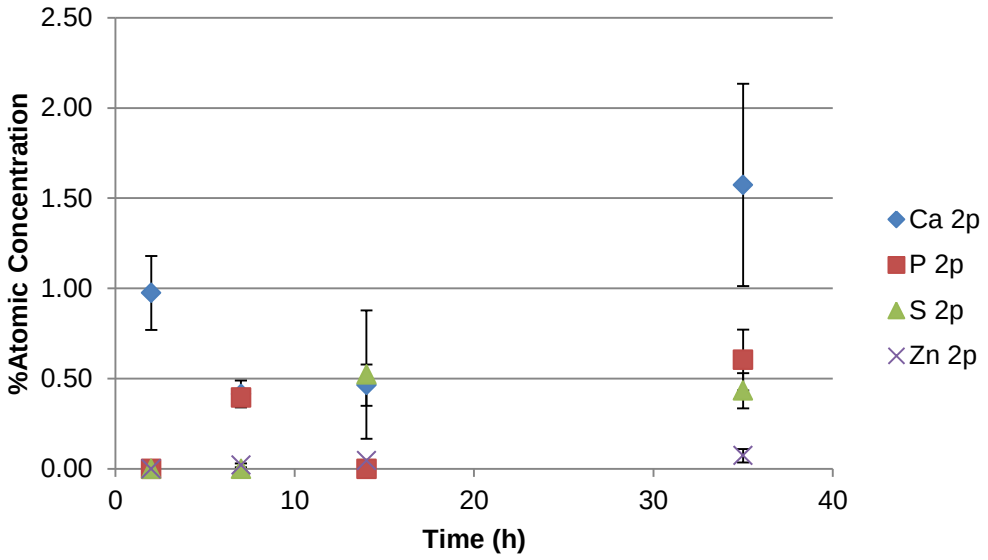

Figure 5-10 XPS of a-C:H DLC plotted against time

Again, ToF-SIMS chemical mapping was employed to confirm the chemical species from the XPS data which is shown in Figure 5-11 and to assess how the sensitivity of XPS could effect tribofilm analysis. ToF-SIMS analysis is in good agreement with the general findings from the XPS data. This provides a good level of confidence in the identification of the species made thus far. However, it also shows XPS is not as good a technique for thin films as SIMS as XPS cannot detect S at the seven hour time interval.

Table 5-2 XPS attributions on a-C:H DLC at seven hours. Nd = not detected

Time/ Element	Ca (eV)	P (eV)	S (eV)	Zn (eV)
2	**346.0 calcium carbonate/ calcium oxide**	**nd**	**nd**	**nd**
7	**347.8 calcium phosphate**	**133.5 pyrophosphate**	**nd**	**1022.8 zinc oxide**
14	**347.1 calcium carbonate**	**nd**	**169.1 calcium /zinc sulphate**	**1022.8 zinc oxide/sulphide**
35	**347.1 calcium phosphate**	**133.1 pyrophosphate**	**164.1 organic sulphur**	**1022.1 Zinc oxide/ sulphide**

5.2.6.1. ToF-SIMS chemical maps of a-C:H –DLC

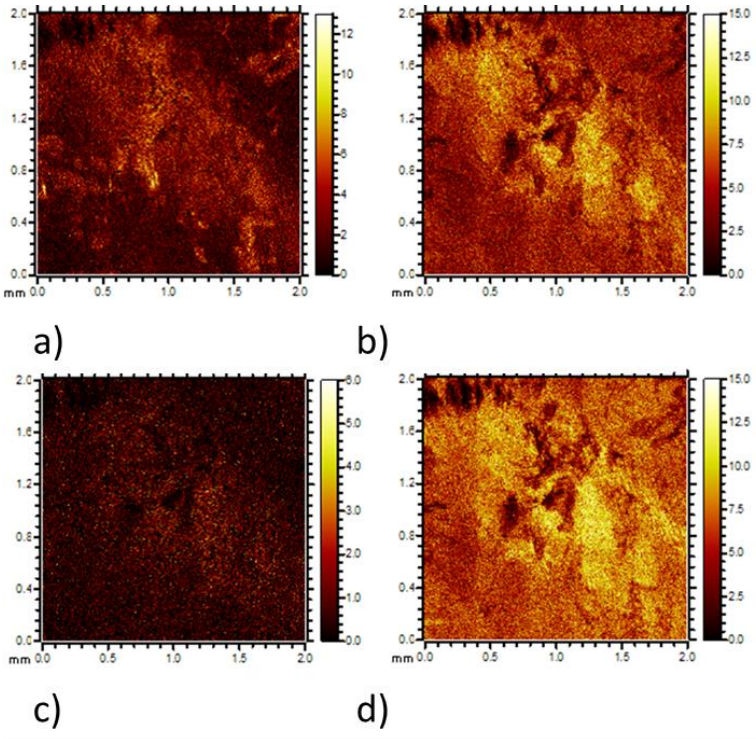

Figure 5-11 ToF-SIMS mapping of the a-C:H DLC at the seven hour interval showing a) SO_2, b) PO_2, c) S and d) PO_3.

5.2.7. Dynamic SIMS profiles

Dynamic SIMS profiles were also obtained in order to help estimate the thickness of the tribofilms on either sample. Although the dynamic SIMS experiments are not, in this case, calibrated against depth (as no reference is available for this type of tribofilm) comparing either profile will give an indication of tribofilm thickness that can be validated with other experimental techniques. For this purpose two species were picked, PO_2 and SO_3 as both of these groups are present in both tribofilms – the PO_2 unit being particularly relevant as it could be involved in phosphate glass type compounds. Profiles are shown in Figure 5-12. SIMS depth profiling uses a C_{60} source which profiles through the tribofilm relatively quickly.

The fact that the dynamic SIMS data herein is not calibrated against depth is not a major issue. This is because combination with additional data allows for more conclusive film-depth gauging later. The difference in depth profiles is indicative of a thicker tribofilm being present on the Si-DLC sample. This is because the time taken to reach baseline for important species (SO_3, PO_3) is greater for Si-DLC. When compared with the a-C:H DLC (t = 2 s) it takes a longer amount of time (t = 12 s) for the signals to reduce to baseline on the Si-DLC. Combining this information with TEM images, shown in Figure 5-14, offers firm evidence of a thicker tribofilm being formed on the Si-doped sample.

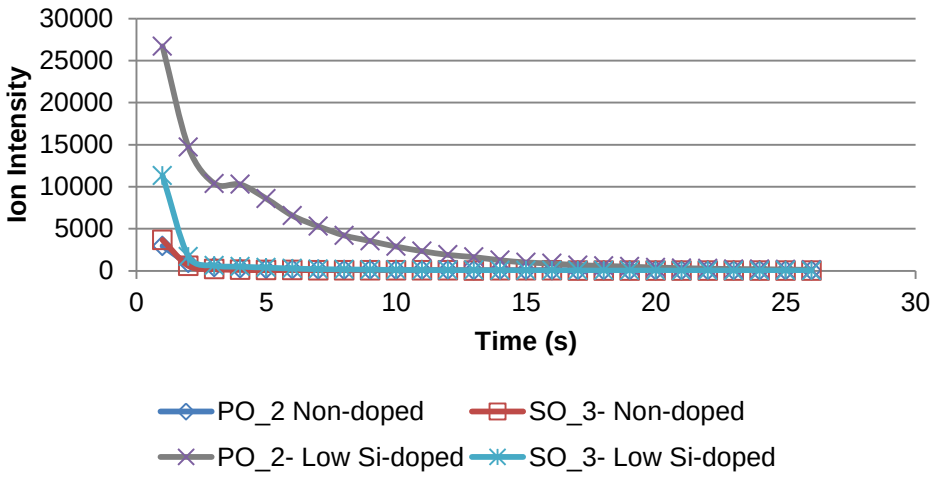

Figure 5-12 Dynamic SIMS profile of both the DLCs tribofilms

5.2.8. XPS of steel counter bodies

The steel counter bodies were analysed using XPS at the seven hour interval to gain insight into whether the films on the opposing bodies are analogous to the films on the DLCs. This data is given in Figure 5-13 and Table 5-3. XPS data of steel pins were used without further charge corrections as the steel counter body is conductive and does not allow for charge build up as the DLC coating does.

The Fe peak (which is known to be Fe_2O_3 in steel materials as opposed to Fe in stainless steel where there is a mix of oxides) was used to validate the spectra [181]. There are slight differences on the film from the steel counter body in terms of composition when compared with the DLC film. There is clear evidence of a calcium phosphate type anti-wear film being generated on either pin.

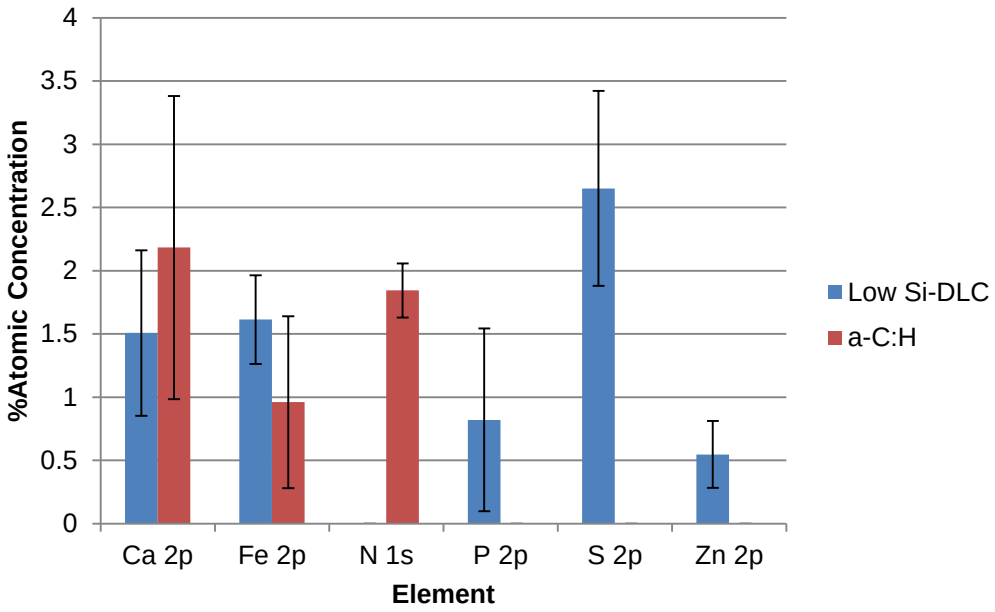

Figure 5-13 XPS of the steel counter bodies tested against DLC coated components, at the seven hour interval is shown. Zn was only recorded in one of the spots analysed for the a-C:H mated pin.

Table 5-3 Attributions of counter body XPS data. Nd = not detected

	Low Si-Doped (eV)	Attribution	a-C:H (eV)	Attribution
Ca 2p	**347**	**Calcium phosphate**	**346**	**Calcium carbonate**
Fe 2p	**711**	**Fe_2O_3**	**711**	**Fe_2O_3**
N 1s	**400**		**nd**	**N in organic matrix**
P 2p	**133**	**pyrophosphate**	**132**	**Nd**
S 2p	**162**	**zinc sulphide**	**nd**	**nd**
Zn 2p	**1022**	**zinc sulphide/ zinc oxide**	**1022**	**Zinc oxide**

5.2.9. TEM images of cross sections from the worn area

TEM images were obtained of the samples at the fourteen hour interval shown in Figure 5-14. This time interval was chosen to ensure as thick as possible a tribofilm would be present on the a-C:H DLC, as spectral characterisation indicated that it was less active toward building a tribolayer. At the seven hour interval, for the a-C:H DLC it is very difficult to distinguish the tribofilm from the Pt layer. As such, the fourteen hour time interval is the best choice for characterisation.

Si-DLC a) shows a thicker (15.5 nm ± 1.3), uneven tribofilm present. The a-C:H DLC indicates the presence of a (2.8 nm ± 0.3) tribolayer present on the sample. Spot-EDX was conducted to confirm the thin film is indeed a present. EDX, as given in Figure 5-15, confirms presence of calcium and oxygen, neither of which are present in the background EDX spectrum, further verifying the presence of a tribofilm.

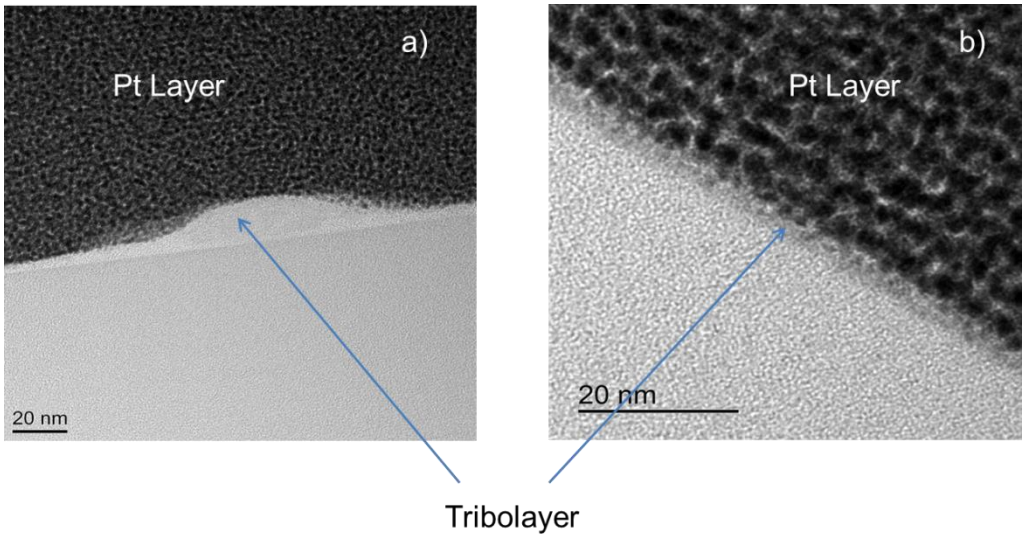

Figure 5-14 A) low Si-DLC showing thicker tribofilm. B) a-C:H DLC showing very thin tribolayer.

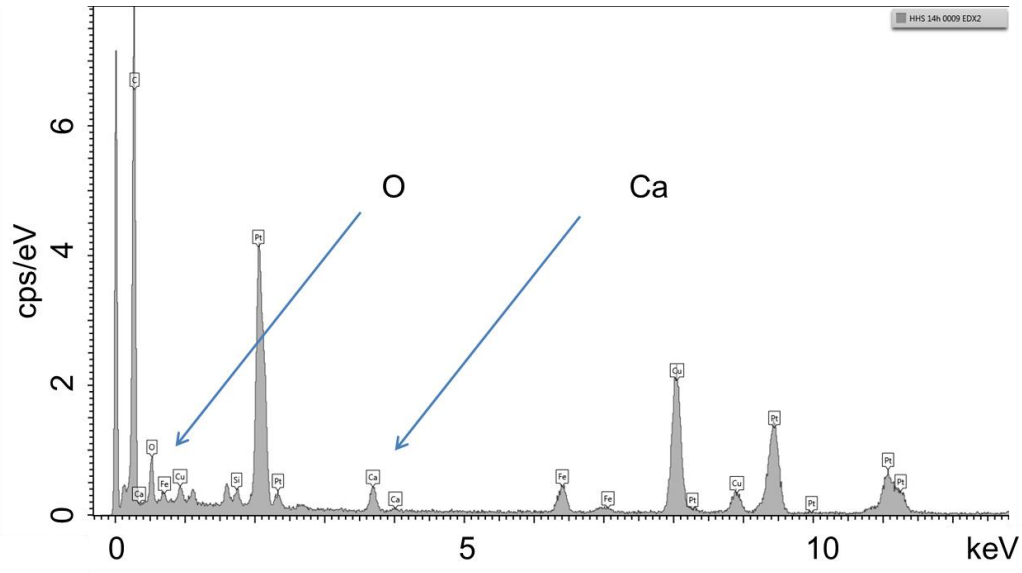

Figure 5-15 Spot EDX of the a-C:H DLC at 14 hours confirming presence of Ca and O

5.2.10. Nano-mechanical analysis

Nanoindentation data was obtained for the samples at two time intervals to ascertain what, if any role hardness plays within the wear profile. Hardness values are shown in Figure 5-16. At both the fourteen hour interval and the thirty five hour interval there appears to be no change, outside of deviation, in hardness when comparing either coating's worn area to the unworn area's

value. To allow for accurate values, eight measurements were taken in a line along the wear scar, or outside of it for the unworn values).The a-C:H coating remains the hardest of the two coatings throughout the times tested and the error associated with the measurement decreases with time, this suggest the surface is undergoing polishing wear; removing some surface asperities. The error associated with the measurements appears to decrease with wear. This behaviour is again indicative of the surface becoming smoother through wearing and yielding more accurate nanoindentation results. This has been seen before in the literature where rough films give lower nanohardness values than the same smooth films [182].

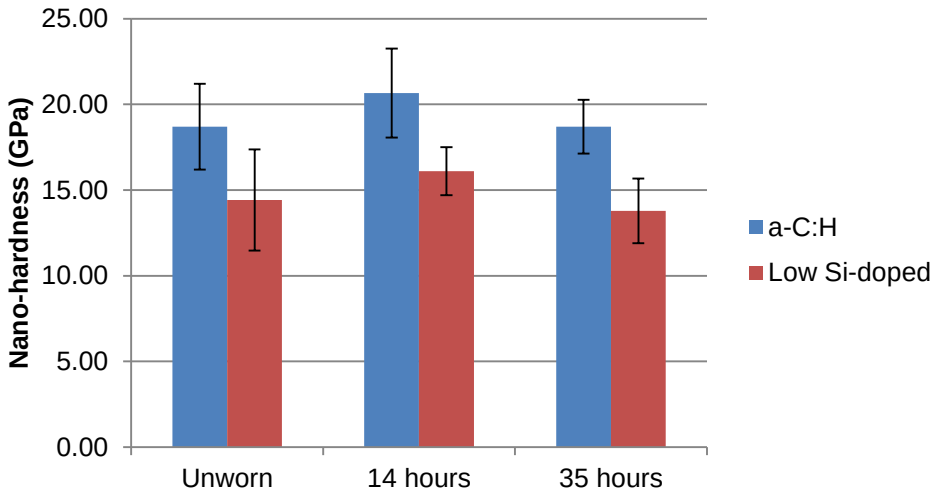

Figure 5-16 Nanoindentation data, carried out as per experimental section 3.6.9. Indent depth was set to 50 nm, the values obtained will therefore be a convolution of tribofilm hardness and DLC hardness.

5.2.11. sp^2 signal evolution as a function of time

Carbon hybridisation, or sp ratios of DLC films often garner much interest as this type of bonding can influence the hardness of the DLC films produced. Furthermore, there is much discourse in the literature surrounding the relevance of graphitisation when examining DLC components. EELS can effectively address this issue. As such, the sp ratio was established for each film and its evolution with time followed at certain intervals. In order to get an accurate sp ratio value, for each sample examined three spots were picked for EELS analysis which is demonstrated in Figure 5-17.

For the three a-C:H samples examined, each cross-section exhibited local fluctuation in sp^2 values dependant on analysis point. There was no continuous trend with which EELS spot (i.e. EELS 1, 2 or 3) would have the highest or lowest sp^2 content. As such, average values for each cross-section are used to give accurate sp ratios. These values are given in Table 5-4.

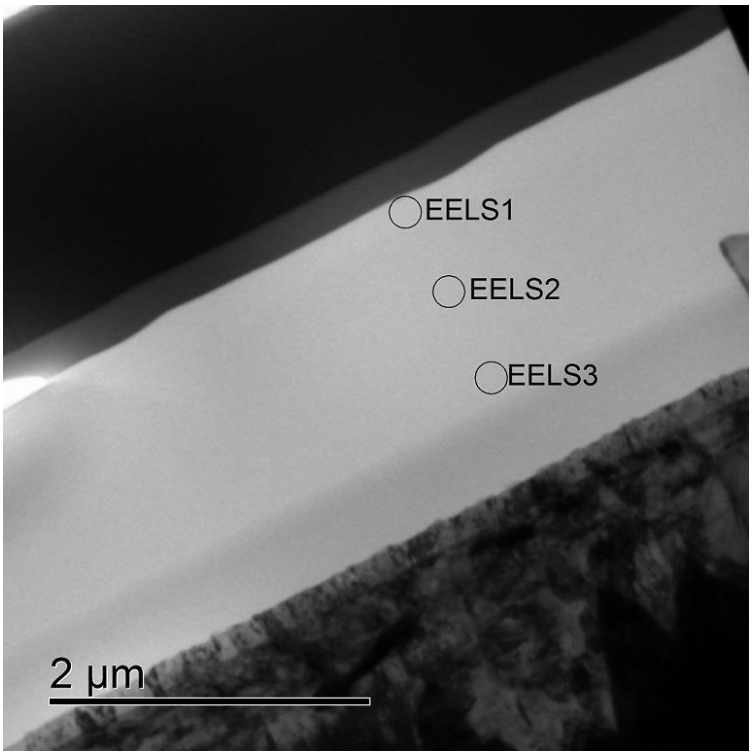

Figure 5-17 DLC cross-section with EELS analysis spots shown, purposefully avoiding shaded interlayer area.

Table 5-4 showing sp^2 evolution as function of time worn.

Coating	EELS unworn	EELS seven hours	EELS fourteen hours	Total change
a-C:H	59.63 (± 6.3)	75.45 (± 5.9)	82.07 (± 4.4)	20.27
Low Si-Doped	38.39 (± 1.5)	not obtained	40.97(± 4.2)	n/a

Due to the difficult and time-consuming nature of producing cross sections of the worn area, EELS analysis was not undertaken for the seven hour tested low Si-DLC sample. This decision was made as Si is known to stabilise the

coatings sp^3 ratio and it was suspected that this would not change much with time.

At the seven hour interval EELS indicates a sp^2 fraction of 75.4% ± 5.9 , showing an increase from the initial value. The sp^2 fraction increases further by the fourteen hour point to 82.07 ± 4.4%. This continual increase in sp^2 fraction suggests a change in the coatings microstructure is occurring for the a-C:H DLC. EELS data was not obtained for the a-C:H nor the low Si-doped sample at thirty-five hours.

EELS data from the low Si-DLC at the fourteen hour mark in the experimental matrix shows that the sp^2 fraction is now 40.97 ± 4.2%. This does not show a change outside of standard deviation from the unworn coating. Comparison of unworn EELS data and NMR data does indicate a good level of correlation, adding further validity to the results. In addition to EELS data, TEM images were also obtained of the cross sections. These were obtained as graphite appears very distinctly in TEM images due to its long-range order as demonstrated by the TEM image in Figure 5-18 from [154].

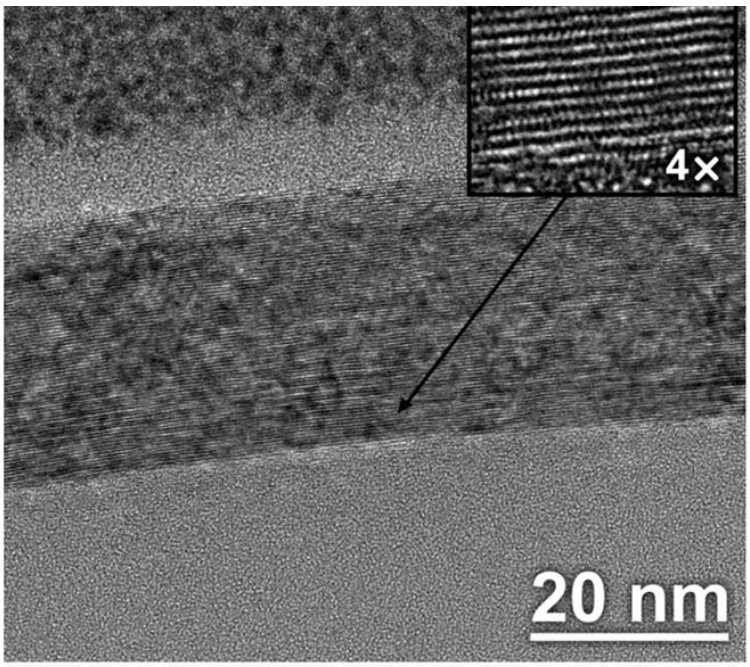

Figure 5-18 TEM image of a graphite film on silica, showing highly ordered basal planes taken from Colby et al [183]

As such, graphitic regions should be easily identifiable in the images shown in Figure 5-19. However this is not the case; suggesting no bulk graphitisation has occurred.

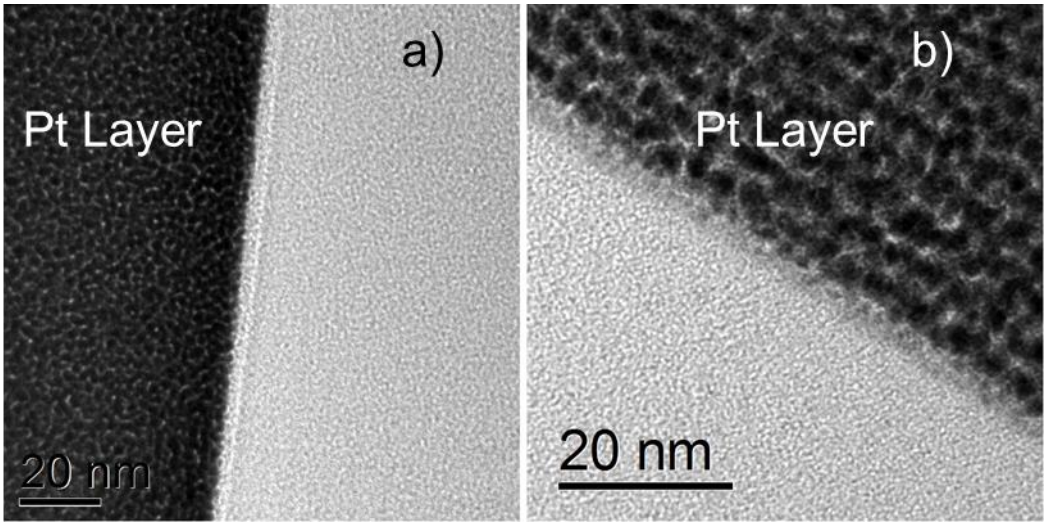

Figure 5-19 TEM images of a-C:H DLCs at 7 hours a) and 14 hours b) showing no evidence of graphitic planes in the carbonaceous area (light grey).

5.3. **Results: tribochemical analysis of engine tested, diamond-like carbon coated tappets**

5.3.1. DLC in Engines

There are many reasons as to why DLC coatings are employed within the automotive industry and currently there are several factors driving forward research and development of DLCs. The on-going drive to reduce friction and improve fuel economy can be more easily reached by using DLC coatings which are known to exhibit low friction [7, 99]. In addition to this, the need to comply with EU legislation equates to reducing the allowed levels of certain car emissions. This limits Sulphated Ash, Phosphorous and Sulphur (SAPS) levels in oils which could be redressed using DLC with its intrinsic wear resistance [8, 184]. Finally the continuing move towards more compact engines can also be eased by employing these coatings, which are designed to withstand far harsher conditions [19]. DLC has the added benefit that only

one surface of the tribo-pair needs to be coated to affect the reduction in friction and impart other beneficial factors [45].

Within this section the testing of DLC coated tappets (of the type already explored experimentally on the bench-top) will be presented. The aim of which is to give insight into the effect actual working conditions of an engine will have in terms of the wear performance of the DLCs.

5.3.2. Engine Testing

Engine testing of coatings is an excellent way to validate the performance of any novel coating or oil as it accounts for conditions and circumstances that may not occur during bench-top tribotesting. The differing factors within an engine that affect the tribology are mainly due to the various physical and chemical processes occurring. This includes formation of combustion products and alkyl radicals [185]. Various other gases that are not accounted for during bench tests could also influence the tribology of the system including highly-reactive gases that have not yet reached the catalytic converter: carbon monoxide, un-burnt hydrocarbons and NO_x. Other non-gaseous species such as fuel and trace water contaminants will also be present within the engine. Having these present will account for any affect they may have on the coating. There are different working pressures associated within an engine that may not be effectively accounted for during bench-top testing. Finally the length of an engine test, 300 hours, also helps further validate the lifetime performance of DLCs more fully as an engine test duration exceeds most standard lab test times in a tribometer.

There are however major downsides associated with engine testing. This includes the large costs associated with running a fully-fired engine for a long period, the special test areas required for the running of them and the need for them to be supervised for the entire running cycle, in this case 300 hours. Therefore, augmenting bench-top testing with engine testing data allows for a fuller picture of the tribology of the system.

5.3.3. Additional test methods

Engine testing was undertaken in house by Lubrizol. Following engine testing, the tappets were analysed using various methods at the University of Leeds. As such, some of the experimental methods of this chapter are different to previous ones.

5.3.4. Engine Testing at Lubrizol

Wear testing was conducted at Lubrizol Limited using the CEC-L-099-08 test procedure which utilises a four cylinder, Mercedes-Benz OM646LA 2.2L diesel engine. This procedure is an industry standard and is an Association des Constructeurs Européens Del Automobile [Association of European automotive manufacturers] (ACEA) requirement for all categories of the A/B, C and E sequence for service-fill oils which defines the minimum acceptable oil quality level [186]. Engine details are shown in Table 5-4.

Table 5-4 Engine test details as conducted in house at Lubrizol Ltd.

Manufacturer	Daimler
Displacement	**2148cc**
Fuel	**Common Rail Diesel Direct Injection**
Induction	**Turbocharged**
Cylinders	**In-line-4**
Valves	**16**
Valve Actuation	**Direct Follower**
Exhaust After Treatment	**Oxy-Cat / DPF**
Emissions Compliance Level	**Euro IV**

The engine has eight inlet valves and eight exhaust valves, two of each per cylinder. In this work pairs of the standard steel tappets were replaced by tappets coated with different DLCs. These were the silicon-doped and a-C:H DLC as investigated above. Two tappets of each type were inserted into the inlet side of the engine and two tappets of each type were inserted into the exhaust side.

5.3.5. Engine Test Procedure

The engine test consists of several phases; there is a short break-in period (~75 minutes) followed by a power curve (~ 65 minutes) and a short oil consumption run. The oil used for testing was Oil B. The main test repeats a one hour multi-stage speed and load profile for 300 hours. At the end of the test the engine is dismantled.

5.3.6. Wear results – Cam

Wear analysis of the cams was undertaken in-house at Lubrizol, cam wear data is given in Figure 5-20. Cam wear data clearly shows that DLC greatly enhances wear resistance when compared to steel alone. Both types of DLC have a significant impact on cam lobe wear. On the steel reference, the cam outlet wear level is higher compared to the inlet. This remains true for the a-C:H DLC; The Si-doped DLC exhibits similar very low wear levels on both sides of the engine (inlet & outlet).

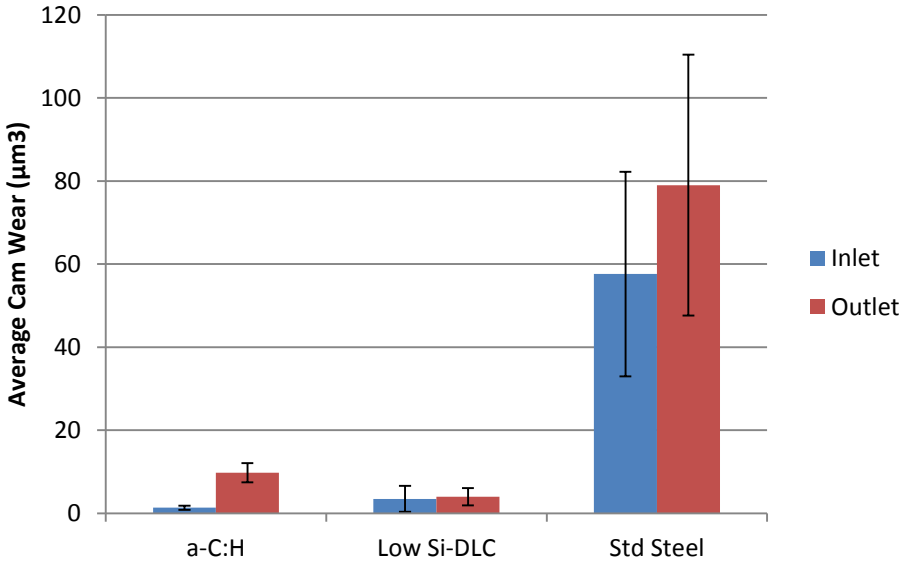

Figure 5-20 Shows wear of cam lobe being sharply reduced by the presence of a DLC counter body

5.3.7. Wear results - Tappets

Examination by eye shows the clear difference in performance between the two samples. The low silicon-doped DLC which shows a large circular patch

of exposed steel (7 mm in diameter) where the most severe wear has taken place, at the centre of the tappet. In comparison the a-C:H DLC shows no such severe wear. Scanning light interferometry was employed on a representative central section of each tappet, shown in Table 5-5 and Figure 5-21.

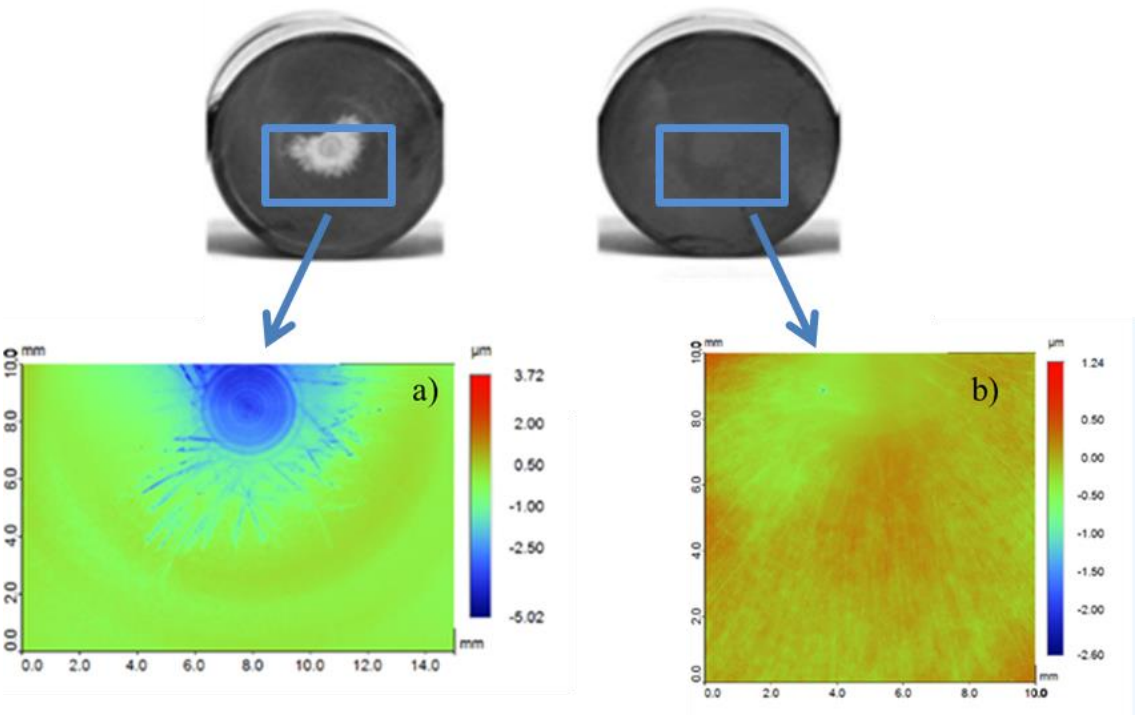

Figure 5-21 Scanning light interferometry maps of sections of the worn areas of the tappets. a) shows the severely worn areas (given in blue) of the low Si-DLC tappet, b) shows the very mild wear of the a-C:H tappet.

A maximum depth loss of 3 µm was recorded at the most severe point for the Si-doped tappet. For the a-C:H coated tappet, very minor wear is observed. A maximum loss in depth is recorded as 0.3 µm. When examined using the interferometer the coating appears polished, rather than destructively worn. This suggests the a-C:H has good anti-wear stability at all points in its lifetime.

Table 5-5 DLC wear measurements

	a-C:H	Low Si-DLC
Maximum recorded depth loss (µm)	**0.3**	**3.0**

5.3.8. Tribofilm analysis - XPS results

XPS profiles were conducted on the central area of the tappets and are given in Figure 5-22. Fewer than expected tribologically relevant elements were identified using this technique. Only one of the three test spots showed Ca on the Si-doped sample, as such it is not given in the graph.

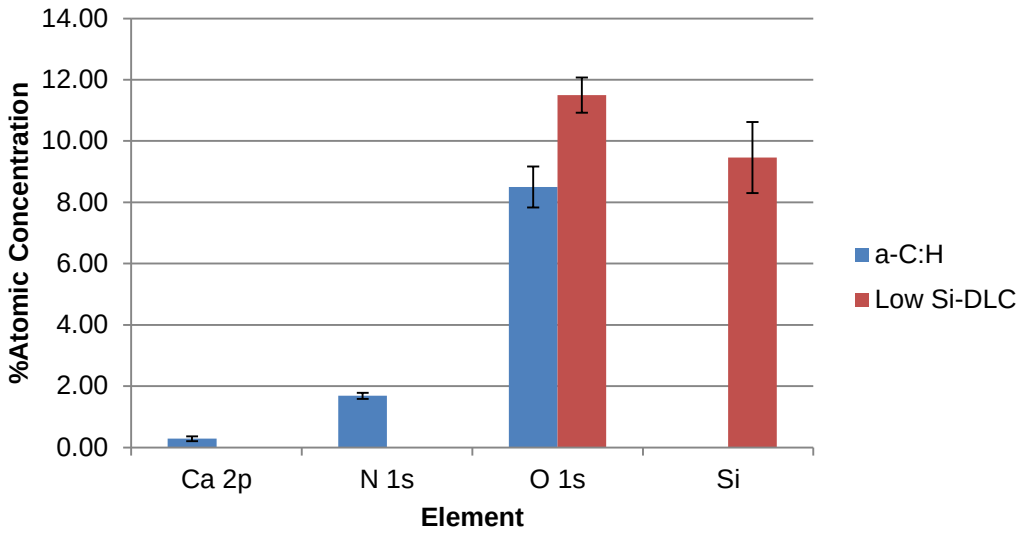

Figure 5-22 XPS analysis of engine-tested, worn tappets. Carbon omitted for scaling

Trace calcium is detected in both samples. However, the lack of other tribologically important species warranted further investigation as the engine was lubricated with fully formulated oil containing ZDDP and other additives. It is notable that the a-C:H sample has a slightly higher % atomic concentration of Ca on the surface. In previous testing, the low Si-doped sample usually accrues more species in the film than the a-C:H sample. To gain further insight into what tribological processes were taking place at the surface, an argon gas cluster ion beam (GCIB) was employed to etch into the tappet shown in Figure 5-23 and Table 5-6. GCIB was selected in this case, as opposed to other etching techniques, as it is known to be a slower, less aggressive profiling technique.

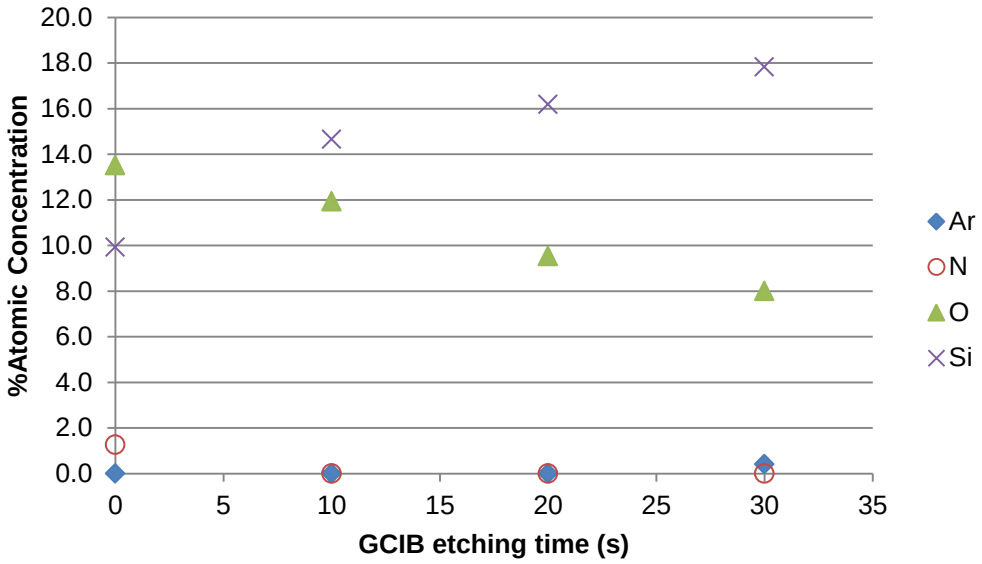

Figure 5-23 XPS GCIB profile of the low Si-DLC coated tappet. Area selected was intact DLC, away from completely worn area. Carbon, omitted for scaling, remains fairly constant around 73 – 65 % atomic concentration.

Table 5-6 Data from gas cluster ion beam profiling of the low Si-DLC tappet

Element	Surface (% atomic conc.)	After 30 s profiling (%atomic conc.)	Change on profiling
Ar 2p	**nd**	**0.4**	**Argon revealed**
C 1s	**75.3**	**73.8**	
N 1s	**1.3**	**nd**	**Surface nitrogen removed**
O 1s	**13.5**	**8.0**	**Surface oxides removed**
Si 2p	**9.9**	**17.8**	**Far greater amount of Si in bulk**

The argon GCIB results show some changes that take place as the beam penetrates into the surface. Due the time consuming nature of GCIB profiling, no high-resolution spectra were obtained. As such no Ca is detected; Ca was previously only detected after high-resolution scans were employed.

Although no new elements are uncovered, changes do take place in the spectra. C1s % atomic concentration (omitted from spectra for scaling) stays stable throughout the progress. Argon is revealed, nitrogen disappears, the oxygen signal decreases and the silicon signal increases. This again

underlines the propensity of the low Si-DLC tappet to oxidise at the surface. It also shows that the tribofilm is very thin as profiling with GCIB, typically a less destructive profiling technique (when compared to Ar ion etching), removes all traces of the film with no new elements being identified [187]. ToF-SIMS results were sought, as this technique is known to be far more sensitive than XPS to surface layers [137, 188]. When examining certain surfaces ToF-SIMS has been shown to have a detection limit of 0.1 ng/cm^2 compared to that of XPS, 10 ng/cm^2 [188].

5.3.9. ToF-SIMS mapping

Chemical maps were obtained of each of the engine tested tappets to fully characterise the surface. As XPS data did not show the expected elements it could be the case that a film too thin for the detection limits of XPS is present. These are shown in

Figure 5-24 and Figure 5-25 Several functional groups were identified on the tappets and are given in Table 5-7 and Table 5-8. These species include P, S, Ca and Zn on both tappets. This confirms a thin tribofilm to be present.

Table 5-7 ToF SIMS negative ion analysis

Tappet/Element:	O	CNO	P	S	Ca	Si
A-C:H	**OH**	**CHNO**	**PO_3**	**SO_3, SO_4, HS**	**nd**	**nd**
Si-doped	**OH**	**CHNO**	**PO_3**	**SO_2, SO_3, HS**	**$Ca(OH)_2$**	**SiO_2, $SiHO_2$**

nd = not detected

Table 5-8 ToF SIMS positive ion analysis

Tappet/Element:	Zn	Fe	P	S	Ca	Si
A-C:H	**Zn**	**n/a**	**ZnP**	**$CaSO_4$**	**$CaSO_4$**	**nd**
Si-doped	**Zn**	**FeO_2**	**nd**	**nd**	**nd**	**Si_2O**

nd = not detected

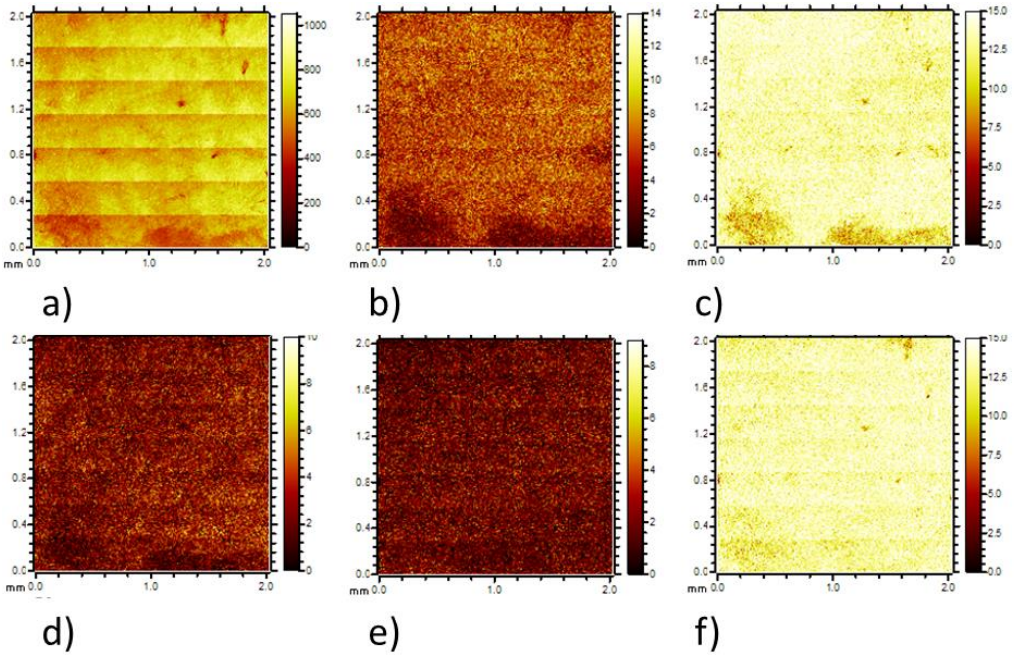

Figure 5-24 Shows ToF- SIMS mapping with of the a-C:H tappet with a) total ions, b) OH, c) CHNO, d) PO_3, e) HS and f) SO_3 anions.

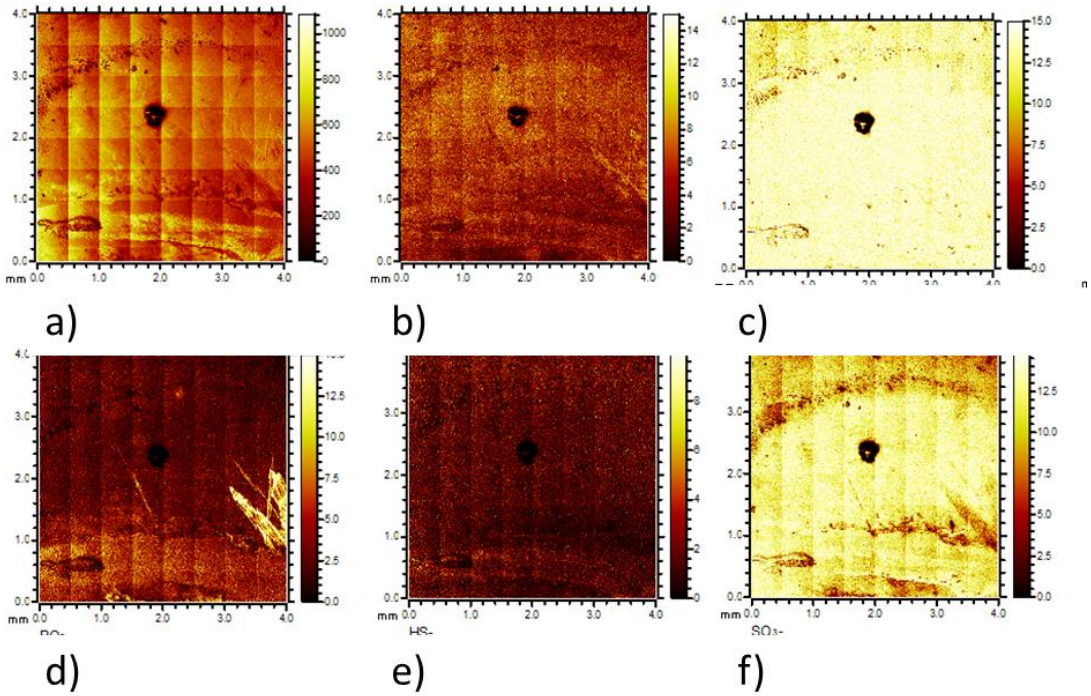

Figure 5-25 shows ToF- SIMS mapping of the low Si-DLC tappet with a) total ions, b) OH, c) CHNO, d) PO_3, e) HS and f) SO_3 anions.

5.4. **Summary**

- In terms of wear performance the a-C:H film outperforms the low Si-DLC which has higher wear particularly at the initial stages (running-in) of experiment, as expected. This suggests Si-DLC shows higher dependence on tribofilm formation than the a-C:H DLC. A-C:H DLC shows lower running in-wear.
- Effective nanometer tribofilms are present that confer enhanced wear resistance. DLCs' inherent hardness as a coating appears to greatly reduce the need for a ~100 nanometer scale, thicker tribofilm as encountered on ferrous surfaces.
- The low Si-DLC's tribofilm is thicker than the a-C:H film (by a factor of 5); however neither tribofilm appears to increase the hardness in the worn area, suggesting wear reduction is facilitated by a chemical anti-wear mechanism.
- An sp^2 signal increase with time is noted for the a-C:H sample but it appears that inclusion of Si prevents this occurring in the low Si-DLC. The change in sp ratio does not appear to affect coating hardness.
- Fired-engine tested tappets analyzed herein demonstrate a-C:H DLC outperforms the low Si-doped DLC in terms of wear reduction on both the tappet and cam. This is in line with similar bench top tests conducted at the University of Leeds, with the a-C:H DLC outperforming in terms of wear.
- It is noted that DLCs should be considered an improvement on the standard steel/steel tribo-couple in terms of wear protection.
- The low Si-DLC appears to give lower counter body wear.
- It is most probable that the harsher conditions associated with fired-engine testing accelerate the wear of the low Si-DLC as there are more oxidative processes taking place within the engine.
- There may be room to further optimize oil formulations for use with Si-doped DLCs by inclusion of additional anti-oxidant species. The

current oil formulation does however appear to work well with the a-C:H DLC.

- Tribofilms are present on both tappets. The comparison of XPS data with SIMS data suggests that the tribofilm present is in fact very thin, potentially on the scale of 1-2 nms
- There are large amounts of similarity between the two tribofilms formed on either tappet. SIMS data suggests a variety of tribologically relevant elements present. In terms of wear the a-C:H DLC appears to be already activated towards lubricant additives, perhaps further doping for the purpose of wear protection is not necessary.

Chapter 6 Results: tribochemistry of low Si-doped DLC in oil A compared with oil D

6.1. Introduction

In this chapter, the tribological dependence on oil formulation of the low Si-DLC examined in this project is explored. To fully assess to what extent wear protection depends on the highly effective and well known oil additive ZDDP, comparisons are made between a ZDDP containing oil (A) and low additive oil (D). The low Si-DLC is the focus of this study as it shows greater wear than a-C:H DLC so has the most potential to benefit from effective lubrication. It also shows enhanced activity towards tribofilm formation, as established previously. Oxygen is known to play a key role in the tribological behaviour of Si-DLCs, thus ZDDP could be a highly relevant additive when examining its performance within an engine. As such, an extensive analysis is carried out prior to and after tribotesting.

6.2. Coating characterisation pre-wear

6.2.1. Dynamic SIMS data of unworn sample

Dynamic profile data was obtained of the low Si-DLC to investigated the relationship between surface rich compounds and compounds present in the bulk and allows for comparison after testing. Dynamic profile data (Figure 6-1 a, b) confirms an inverse relationship of certain species within the DLC. It appears that hydrated carbon, silicon oxide and hydroxyl groups are at greatest concentration at the surface.

However, with profiling deeper into the surface these species deplete. In comparison the unsaturated carbon chains and less oxidised silicon species appear to increase in concentration with etching; the main fragments being Si:O 1:1, compared with the surface. This shows that there is indeed a rich oxide layer at the upper surface of the DLC and that this is not maintained in the bulk of the material.

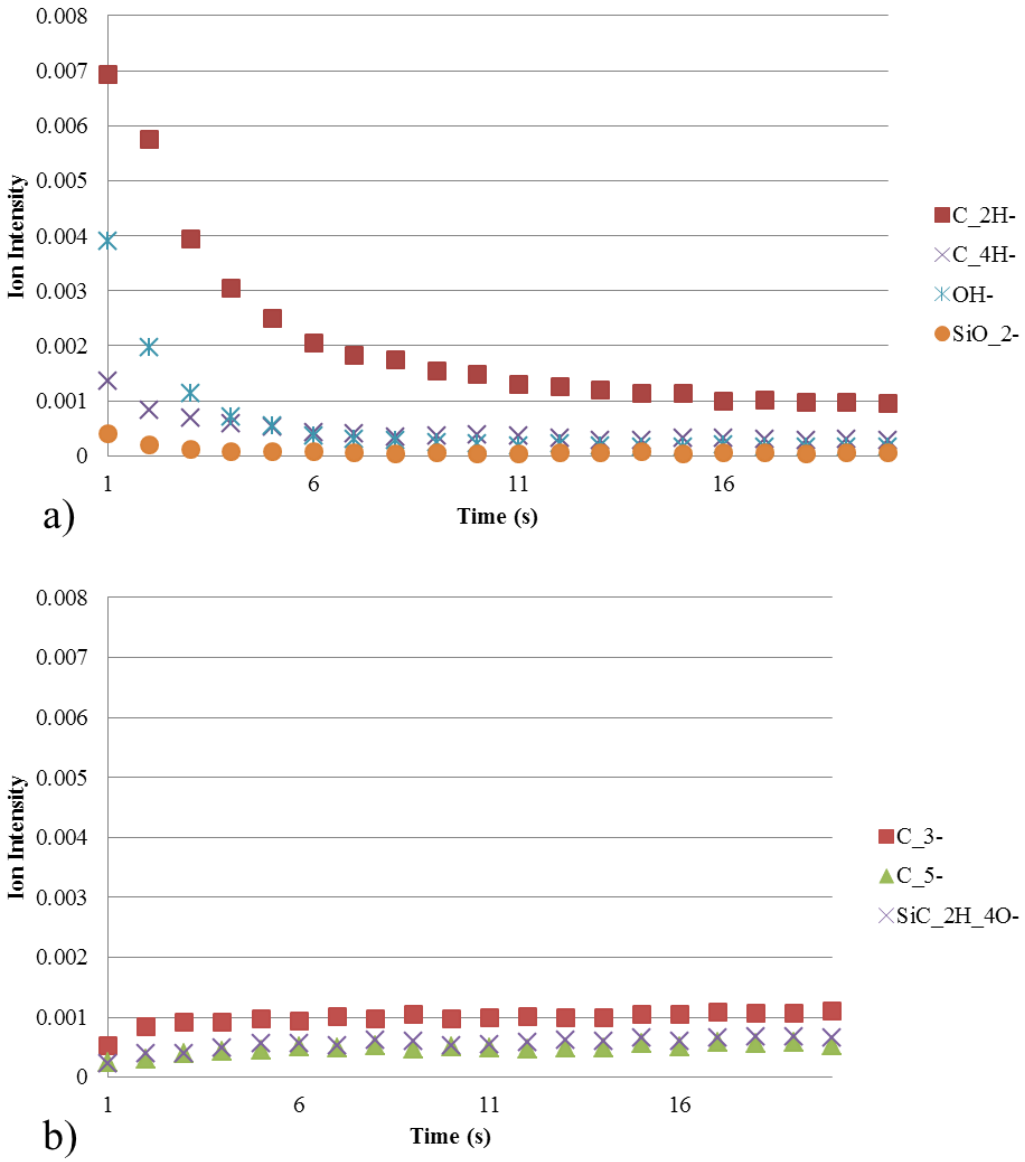

Figure 6-1 a) ToF-SIMS dynamic profile of unworn low Si-DLC, separated to include only surface rich components. b) ToF-SIMS dynamic profile of unworn low Si-DLC, separated to show bulk DLC constituent ions.

The dynamic profile is not directly calibrated to depth; however combining the SIMS data with XPS data, an approximate depth of the presence of the Si oxide layer would suggest a minimum of 10 nm if not greater based on XPS penetration depth.

6.2.2. XPS pre-wear

XPS analysis of the coating prior to wear gives insight into the surface rich species. XPS profile of the coating surface as shown in Figure 6-2

demonstrates that oxygen makes up 12% of the spectrum and silicon makes up 15%. ERDA data as given in section 3.3.1. Table 3-1 suggests there should be approximately twice as much silicon compared to oxygen when the coating is analysed as a whole.

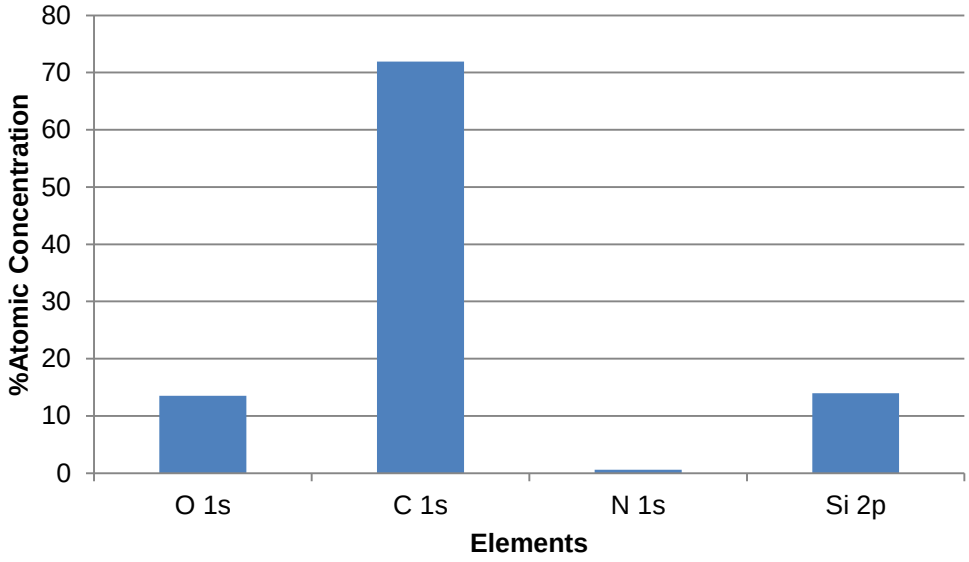

Figure 6-2 XPS of unworn low Si-DLC coupon

6.3. Friction results from the low Si-DLC tested over seven hours

Friction data has been presented in two graphs for clarity. Initial friction is given in Figure 6-3 and shows up to the two hour time interval with error bars included. This shows oil A giving a slight reduction in friction when compared to oil D, outside of error. However, the reduction observed is small being recorded as a maximum reduction of 10%. With the full friction profile error bars have been omitted for clarity, as toward the end of the experiment the values become close together, Figure 6-4.

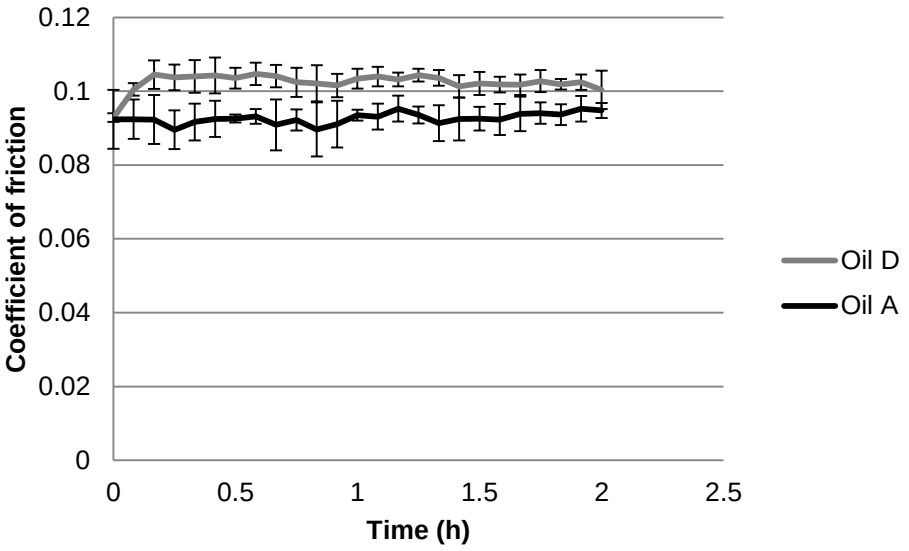

Figure 6-3 Early stage friction with error bars included. This shows the different tribological profile, as dependant on oil.

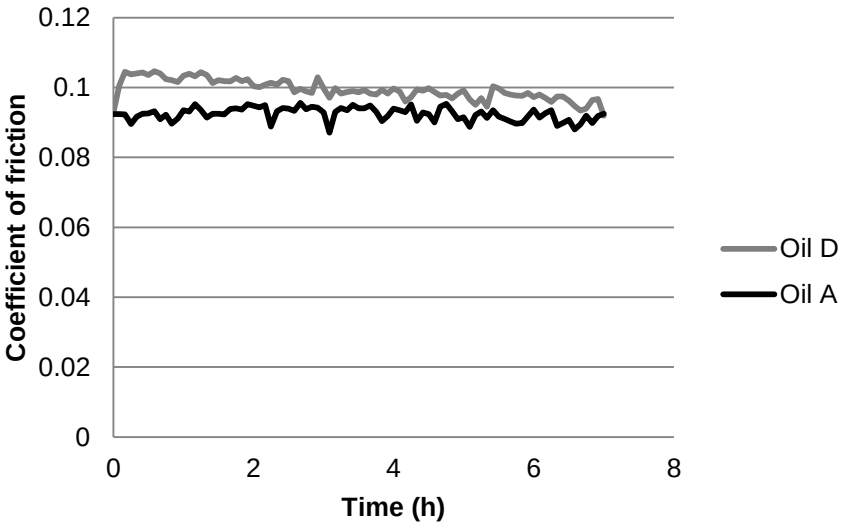

Figure 6-4 Full duration friction graph by oil, error bars omitted for clarity due to the closeness of values towards the end of testing. This shows the friction values merging toward the end of testing.

The respective coefficients of friction appear to merge as shown in the with friction traces given in Figure 6-4. These tests show that the friction coefficient of the sample tested in oil D continues to reduce, whereas oil A affects no such gradual decline in friction.

6.4. **Pin and plate microscope analysis**

Optical images of the pin are shown in Figure 6-5. The sample tested in oil D shows a black layer on the pin. Optical images show a clear difference between the two tribopairs. The pair tested in oil D have higher wear and clear formation of a transfer film on the steel pin is seen.

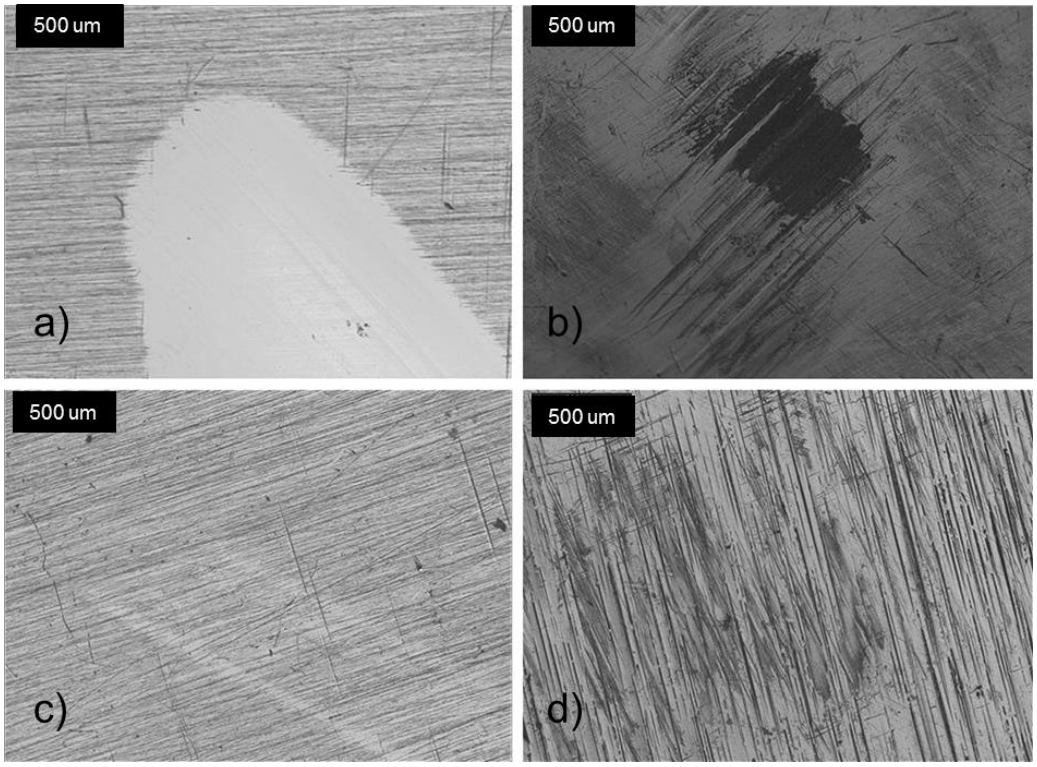

Figure 6-5 Optical images of the worn areas on the plate and pin tested in oil D are labelled a and b, respectively. The worn areas as tested in oil A are given in c) and d).

6.5. **Wear results**

Wear of coatings are shown in Table 6-1. Wear is recorded after seven hours of testing and shows greater total wear of the low Si-DLC when tested in oil D, as predicted. Dimensional wear coefficients (k) were used to compare wear of the samples in the different oils. For the samples tested in oil A, k is recorded as $3.7E^{-18} \pm 1.4E^{-18}$ m^3/Nm. The sample tested in oil D has a k value of $9.0E^{-17} \pm 6.2E^{-18}$ m^3/Nm. This clearly indicates fully-formulated oil (oil A) works synergistically with the coating to reduce wear.

Wear of the coating was also measured at the point of maximum depth loss to gauge loss of coating thickness. The depth lost (2.2 μm ± 0.16 μm) when tested in the oil D suggests the coating, total thickness 2.4 μm, has been completely removed by wear in certain places. This can be further validated by inspection by eye as the steel substrate has been clearly revealed in specific sections of the sample. Following the wear progress it would appear that some of the more severe wear, where steel is revealed, takes place earlier on (~ 2 hours) into testing. However, the coating is not completely removed by the end of the test. This is not the case for oil A which only facilitates a loss in coating thickness of only 0.6 μm ± 0.09 μm.

Table 6-1 Quantified plate wear

	Wear of plate (m^3/Nm)	Max. Thickness lost (μm)
Oil D	**9.0E-17 ± 6.2E-18**	**2.2 ± 0.16**
Oil A	**3.7E-18 ± 1.4E-18**	**0.6 ± 0.09**

6.6. **Thermal effects of gas absorption upon the coating**

The importance of oxides on the surface of Si-DLC is made obvious from the literature. It is important to establish the mechanism by which silicon in the coating oxidises and whether this depends on tribological effects. XPS spectra of the samples were obtained after different treatments as shown in Figure 6-6.

Heating the sample, as XPS data shows in Figure 6-6b, in an atmosphere of nitrogen induces a change in the coating. An additional peak appears that is indicative of more oxidised forms of Si being present. The sample heated in air as shown in Figure 6-6c produces an even more defined change, with a clearly visible shoulder to the Si 2p region. The emerging peak at 102.4 eV is indicative of silicon bonded to, proportionally more oxygen

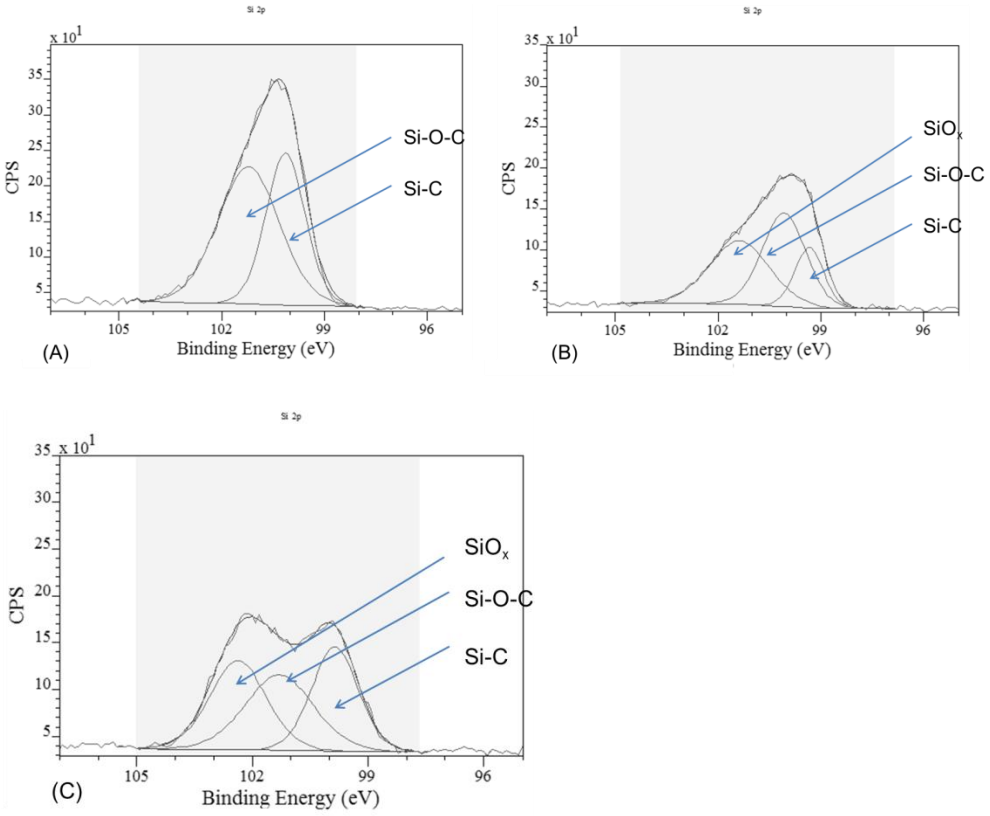

Figure 6-6 XPS analysis of Si 2p peaks from the low Si-DLC heated under different conditions. a) low Si-DLC untreated, b) low Si-DLC heated under N_2, and c) low Si-DLC heated under O_2.

The inclusion of additional oxygen atoms raises the eV for the environment at silicon 2p [144]. The oxygen signal for the sample heated in air is 533.34 eV again confirming the presence of SiO_2 type species. Therefore it can be observed that silicon doped DLC does oxidise when heated in air, without the need for any tribological influence.

6.7. **Wear scar analysis results**

6.7.1. XPS results for low Si-DLC in Oil D

The upper surface of the sample tested in Oil D, as examined by XPS are given in Figure 6-7. The data shows the presence of O, C and Si, all of which are constituents of the DLC. XPS peak component break-down at Si is shown in Figure 6-8. Here, two distinct peaks are identifiable. One is at

102.8 eV, which is again indicative of Si at a higher oxidation state [144]. Oxygen peak components are in agreement with this.

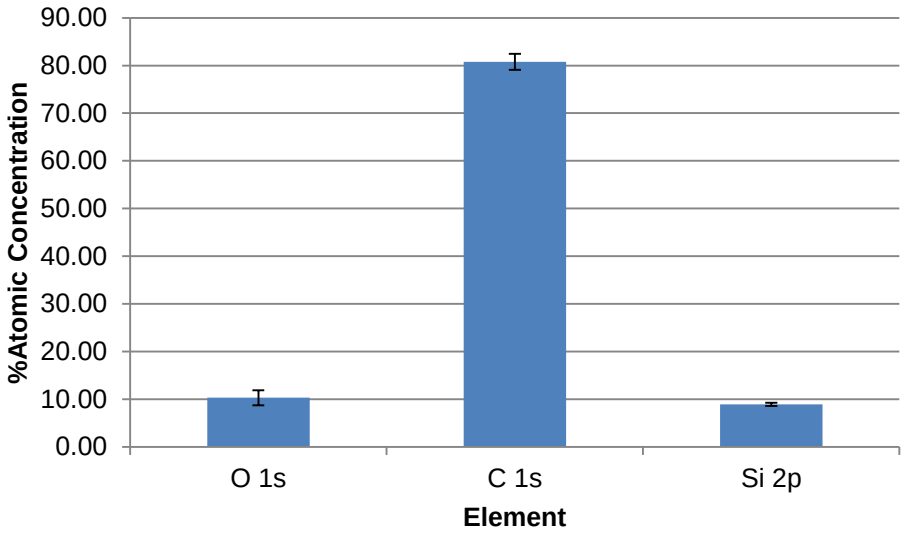

Figure 6-7 XPS analysis showing % atomic concentration of elements on low Si-DLC after testing in Oil D.

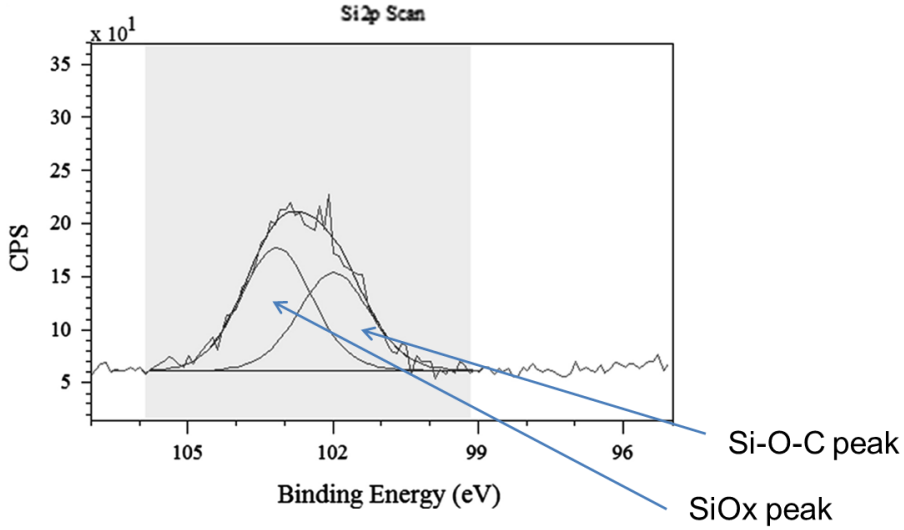

Figure 6-8 High resolution Si 2p peak window as obtained in oil D, showing oxidation of Si.

This shows that the silicon in the coating is being severely worn and exposed to oxygen. The rise in eV value of the Si 2p peak echoes the spectra of the sample that was heated in air. Both samples appear to be

oxidised quite severely. However, the tribo-tested sample shows complete loss of the Si-C signal, indicating enhanced oxidation at the tribocontact.

6.7.2. XPS results for low Si-DLC in Oil A

Unlike in the oil D, oil A appears to suppress the emergence of a peak at a higher eV value in the low Si-DLC spectrum as shown in Figure 6-9. The two components of the peak are at 100.4 eV and 101.4 eV, indicating C-Si and Si-O-C respectively. The sole presence of these two components for the Si 2p peak suggests that the coating resists most wear-based changes to its microstructure. In addition to this calcium, zinc and phosphorous peaks are present in the spectrum (Figure 6-10); evidence of the formation of a tribofilm.

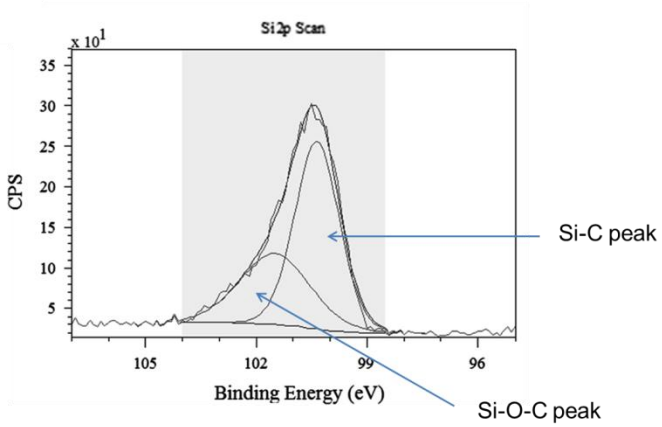

Figure 6-9 XPS analysis of Si 2p peak window when tested in Oil A, showing less oxidation of Si.

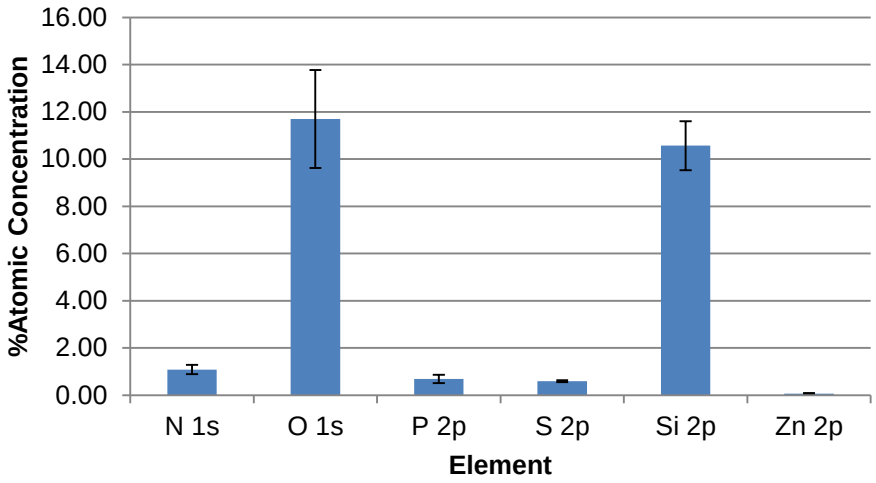

Figure 6-10 Elements in the tribofilm (carbon omitted for scaling) of oil A. The presence of nitrogen is noted as contamination.

Table 6-2 Peak attributions of XPS data from the tribofilm composed from Oil A.

Element	Position (eV)	Attribution [143, 146, 147]
P 2p	**133.8**	**Pyrophosphate**
S 2p	**163.9**	**Sulphide**
O 1s	**532.1**	**Phosphate**
Ca 2p	**348.1**	**Calcium carbonate/phosphate**
Zn 2p	**1023.1**	**Zinc sulphide**

6.7.3. XPS results for counter bodies

XPS analysis of the pins reveals a tribofilm on the counter bodies as given in Table 6-3. XPS analysis identifies Zn, S and P present on the pin tested in formulated oil but not on the pin tested in oil D, suggesting formation of a Zn based protective tribofilm.

Table 6-3 XPS analysis of counter bodies. Nd = not detected

Element (% atomic concentration)	Oil A	Oil D
O	**25.5**	**23.8**
C	**54**	**63.1**
N	**1.5**	**2.4**
Zn	**0.3**	**0.0**
Fe	**1.1**	**0.8**
Ca	**1.5**	**0.6**
Mg	**12.5**	**7.3**
S	**2.0**	**Nd**
P	**1.6**	**Nd**
Cr	**Nd**	**0.3**
Si	**Nd**	**1.7**

Peak attribution for the Zn peak (1022.1 eV) and S peak (162.1 eV) suggests the presence of zinc sulphide. A calcium phosphate species is also indicated (Ca = 347.1 eV) as is pyrophosphate (P = 133.1 eV).The pin tested in oil D shows the presence of Si and Cr that are not observed in oil A. This is indicative of increased wear as both Si and Cr are components of the tribopairs. The Si signal appears at 102 eV and is indicative of an Si-O type compound [146]. It is notable that Si is lacking from the spectrum from oil A.

6.7.4. TEM/EDX data from the low Si-DLC in oil A

A Transmission Electron Microscope image (TEM) was obtained of a cross section of the worn area. Figure 6-11 shows the cross sectional area which was prepared using a focused ion beam. A tribofilm is evident for the low Si-DLC when tested in oil A.

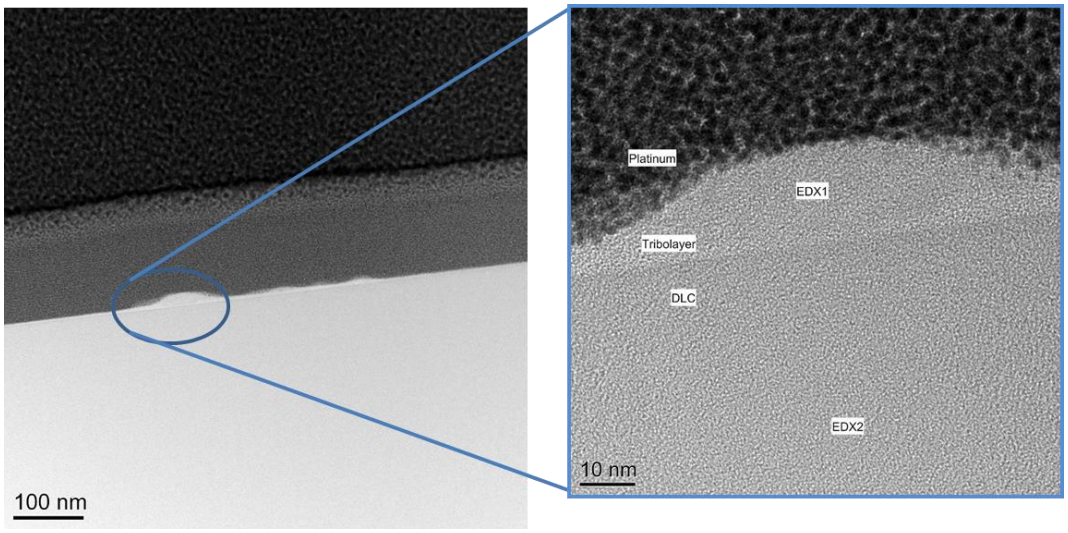

Figure 6-11 TEM image showing the uneven nature of the tribofilm. Area for analysis was selected as it contained the thickest section of the film.

The tribofilm pictured appears to be unevenly distributed and thicker in certain areas. Maximum film thickness was recorded as 15.0 nm. EDX spectra shown in Figure 6-12 were obtained of the DLC, as background, and the tribolayer. Zinc, sulphur and calcium are all identified to be present in the tribofilm. The silicon signal appears to be far less intense in the tribolayer than in the DLC, in contrast the carbon peak intensity does not appear to change between the two.

6.7.5. SIMS chemical map data from the sample tested in oil D

Secondary-ion mass spectrometry was conducted on both samples post-wear. Chemical maps were obtained. Silicon species, as shown in Figure 6-13, are present on the plate but they are now present as oxides and no longer appear to be fragments of a carbon chain. Silicon is now mainly present as smaller ion fragments including $SiHO_2$ and SiO_2.

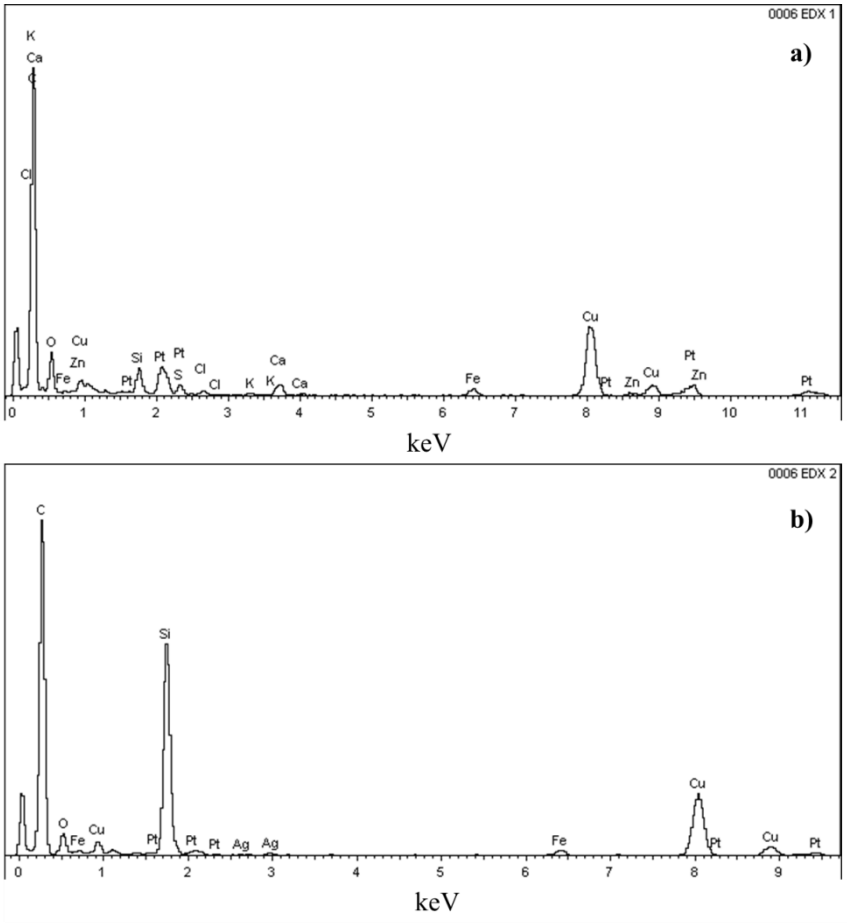

Figure 6-12 EDX spectra showing a) the tribolayer confirming presence of Ca, Zn O and S. The background signal is shown on b). Cu, Pt are artefacts from the production process. Other trace elements noted as contaminants from manufacture of the cross-section.

The lack of ions where silicon is within a carbon matrix is evidence of the severe wear the coating has undergone, suggesting that silicon has been actively sequestered from the coating during the wear process. The full mechanism of this is explored in the discussion section. However, it appears that sequential oxidation of silicon within the coating, as part of the wear process then goes on to accelerate overall wear of the coating. Preventing this oxidation is key to extending the lifetime of Si-DLCs.

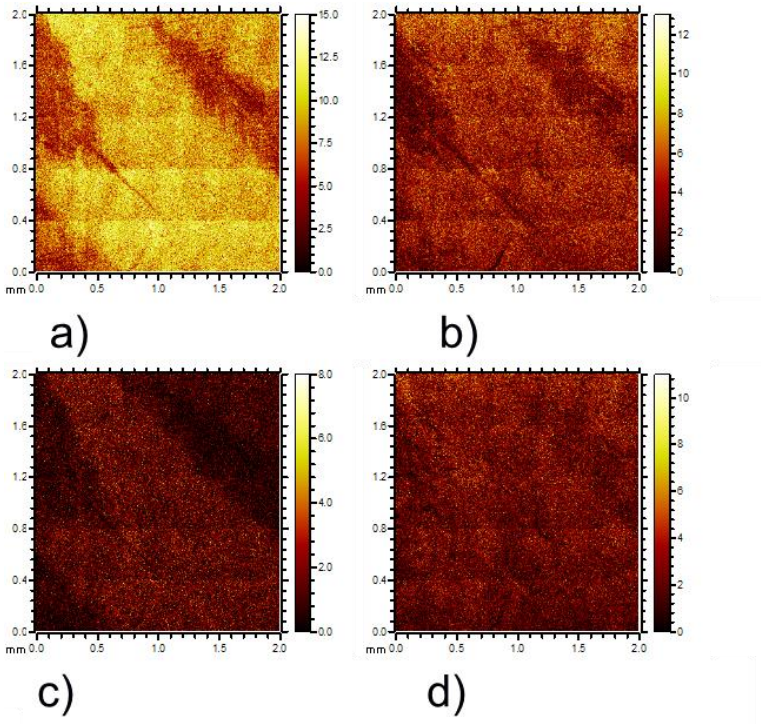

Figure 6-13 SIMS chemical map of sample in oil D showing widespread oxidation of coating constituents. Negative ion ToF-SIMS map of low Si-DLC tribotested in oil D. (a) C_4H, (b) $SiHO_2$, (c) C_6, and (d) SiO_2. Lighter areas indicating greater concentration of ions

6.7.6. SIMS chemical map data from oil A tested sample

Chemical map data, shown in Figure 6-14, of the sample tested in oil A shows a well-defined, constrained wear track in which several trends are apparent. There is a pronounced difference from within the wear track when compared with the unworn section of the film. The worn area shows depletion of oxygen anions when compared to the whole plate. As well as loss of the higher oxides of silicon, where silicon: oxygen ratio is 1:2 or higher. An opposite trend is observed with sulphur and phosphorous species. The worn area contains a far larger amount of anions: PO_3, PO_2 and SO_2 are noted. In addition to this there appears to be great concentration of silicon maintained in a carbon matrix, in that the signal for Si-C type compounds appear richer in the worn area.

It would appear that build-up of P and S compounds, most likely originating from Zn-type additive molecules, in the worn area are able to reduce oxygen concentration in the worn area. They also appear to help maintain the DLCs

microstructure; with more silicon incorporated with carbon. This is demonstrated by the ToF-SIMS map of SiC_2H_5O in Figure 6-14, which is clearly richer in the worn area following protection from oxidation by the tribofilm that has formed.

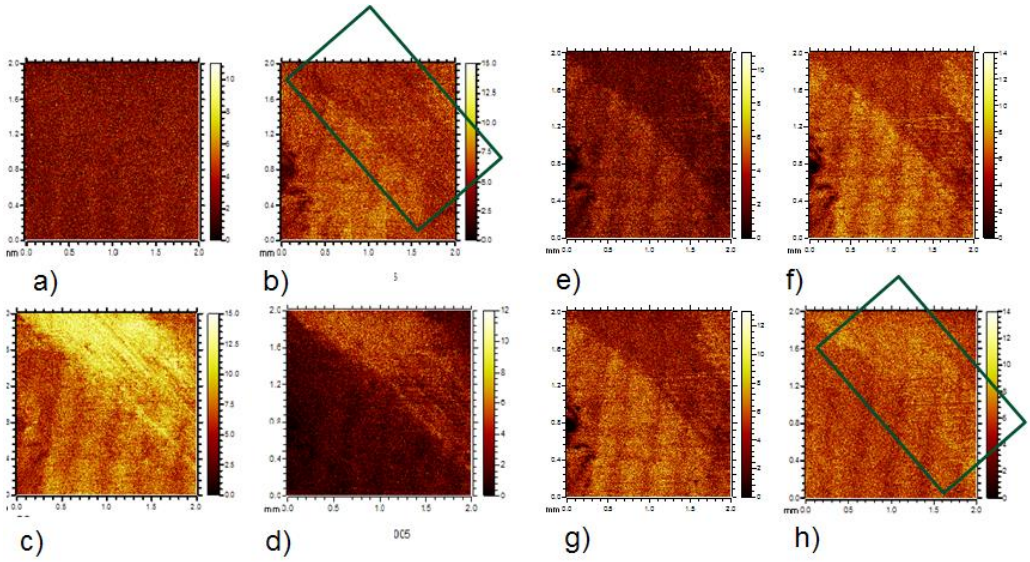

Figure 6-14 SIMS maps of samples tested in Oil A oil showing reduction in oxygen content within the worn area. Negative ion ToF-SIMS map of low Si-DLC tribotested in Oil A. (a) CH_2, (b) O, (c) PO_3, (d) HS, (e) SiO_2, (f) $SiHO_3$, (g) $SiHO_2$ and (h) SiC_2H_5O. Boxed area showing increases in amount of SiC_2H_5O and reduction in amount of O in wear scar. Lighter areas indicating greater concentration of ions.

6.7.7. Dynamic SIMS profile data

Dynamic SIMS profile data as given in Figure 6-15 a, b and c was obtained for the sample tested in oil A. This was sought to help investigate the relationship of P and S ions with the Si-C type species. A C_{60} source was used to etch into the samples.

The profile obtained shows a definite pattern emerging whereby the immediate surface layer is markedly different to the bulk material, further in. Present at the immediate surface are oxygenated species including hydroxides and oxides of sulphur and phosphorous. In addition to this there are also trace amounts of highly oxidised silicon type species at the surface, however these tail off very steeply; unlike the signal for both P and S which is prominent for longer. Presence of these species at the upper surface is

clearly indicative of tribofilm formation. Once these species are uncovered by profiling, new signals emerge that account for the further bulk of the DLC.

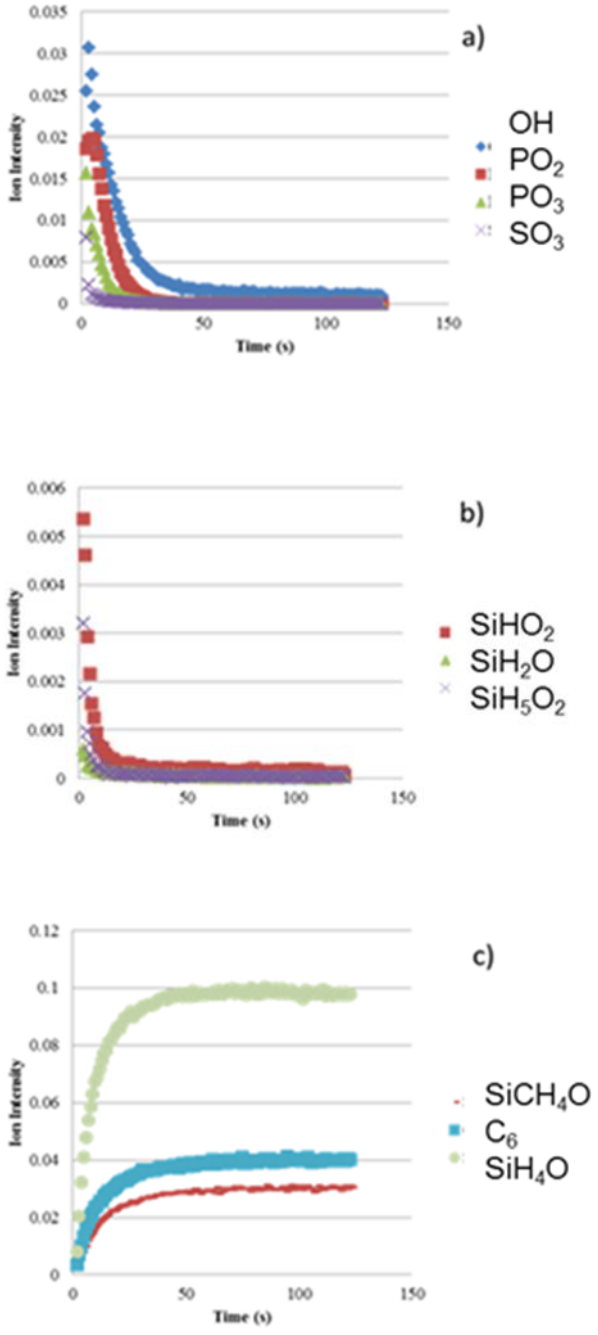

Figure 6-15 Dynamic SIMS data from Oil A tested sample.

These include carbon chains, and species including silicon bonded to hydrogen and carbon as well as some oxygen, as expected. Si within the bulk of the film appears largely to be present as the hydride or bonded to carbon, along with some oxygen. Profiling data appears to confirm that presence of P and S at the upper surface reduces the amount of silicon oxides formed. Dynamic profiles of the samples tested in oil D were not obtained.

6.8. **Summary**

Characterisation of Si, O containing Diamond-like Carbon has been achieved both prior to and following wear testing. Chemical composition of the film can be seen to alter upon wear, depending on conditions. Chemical states of silicon show the most discernible change upon either exposure to oxygen or wear-processes.

Si, O –doped, hydrogenated DLC has been tested in two different oils and analysed in terms of friction and wear profiles. Using a variety of spectral techniques elements important to wear protection were identified in the worn area including P, S, Zn and Ca species.

- The role of oxygen in the wear of the coating is shown.
- The low Si-DLC shows high dependence on oil formulation for improved-wear performance when tested over seven hours.
- A mechanism is proposed whereby sequential oxidation of silicon within the coating accelerates degradation of the DLC.
- Inclusion of anti-oxidant species within fully-formulated oils are proposed as the major factor limiting the wear of Si,O-DLC.

In future, additional organic additives could be incorporated in to oil formulations to further guard against oxidative damage of Si,O-doped DLCs. DLCs doped solely with silicon, omitting oxygen, may behave differently to

those with both Si and O. However, the tendency of silicon within the coating to oxidize will be maintained and could be potentiated by the lack of oxygen in the bulk coating.

Chapter 7 Results: Investigating the influence of ferrous surfaces with respect to DLC tribofilms

7.1. Introduction

In order to fully characterise surface interactions and tribological dependencies of Si-DLC, a study involving self-mated DLC contacts was undertaken. This also extends to exploring interactions that Si-DLC has with a lubricant when heated to observe formation of a thermal film. Investigating the tribocontact in absence of a ferrous body is the main motivation for this study to establish how tribologically reactive Si-DCLs are without influence from a ferrous counter body. This will also serve to help answer the question often posed in the literature; what role do Fe ions play within DLC/steel contacts in development of the tribofilm. Finally, a surface modification is carried out to further clarify the role of very-top surface functionalities on friction.

7.2. Results

7.2.1. Thermal film investigation

To first confirm if Si-DLC coatings are able to form films without any influence from steel counter bodies or indeed Fe ions, a thermal dependency investigation was carried out. The DLC coupon was fully-submerged in Oil A at 80 °C and heated for seven hours. This time frame was chosen as it is noted as sufficient for tribofilm formation. The samples were then rinsed with heptane and allowed to dry. XPS analysis was then conducted on the surface, this data is presented in Table 7-1. This can be compared with previously obtained XPS data of an unworn low Si-DLC surface. Both sets of XPS data were calibrated to the 284.4 eV C 1s peak component associated with DLC bonding, specifically the C-H bond [87, 139]. As such the broader

C 1s parent peak does not exactly match the calibration point. The procedure is employed to ensure that any oxidation of carbon that may take place during thermal film formation does not skew the dataset.

Table 7-1 Tabulated data from XPS analysis of the unworn low Si-DLC and the thermal film grown on the same DLC

	Thermal Film		Unworn low Si-DLC	
Element	**Position (eV)**	**%At Conc.**	**Position (eV)**	**%At Conc.**
C 1s	**285.8**	**74.0**	**284.3**	**71.9**
N 1s	**400.8**	**1.1**	**400.3**	**0.6**
O 1s	**532.8**	**10.6**	**532.3**	**13.4**
Si 2p	**101.8**	**14.1**	**101.3**	**13.9**
Zn 2p	**1022.8**	**0.1**	**nd**	**nd**

Nd = not detected

There is only one major chemical difference between the two surfaces analysed. Zn is present on the thermally treated sample with a Zn 2p peak at 1022.8 eV. High-resolution scans were also conducted for Ca, P and S however none of these elements were detected. The Zn 2p peak cannot be definitively attributed without additional analytical techniques.

However literature sources suggest a variety of species could account for this including various Zn oxides, hydroxides, silicates or carbonates [143, 146]. Despite Zn only being present in 0.1 % this result can be relied upon as, Zn is both present in the survey scan and high-resolution scan. Furthermore, three XPS high-resolution spot analyses were conducted on the sample, all confirming the presence of Zn. The Zn 2p peak window is shown in Figure 7-1.

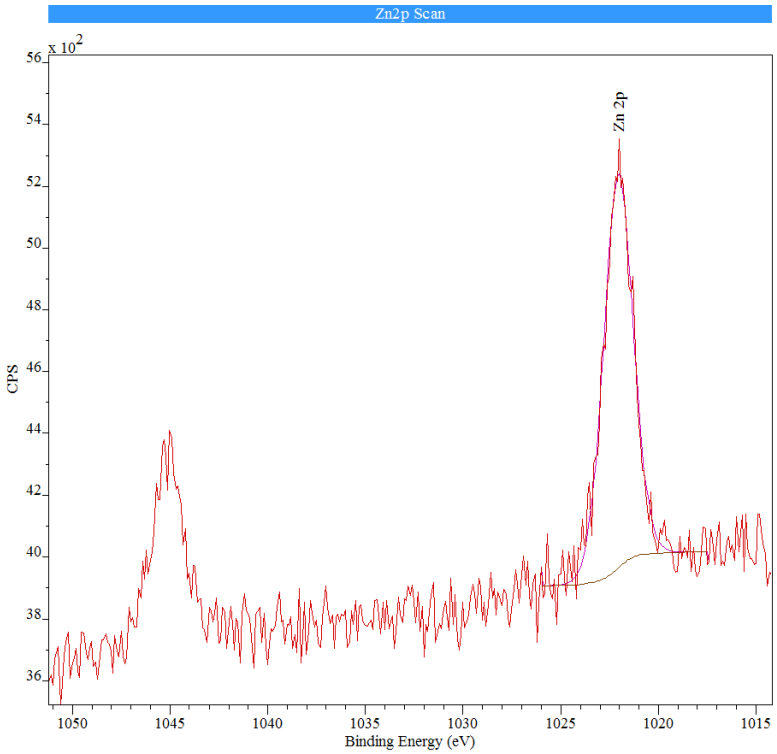

Figure 7-1 High-resolution Zn 2p peak window from XPS spectrum

7.2.2. Friction of self-mated low Si-DLC *versus* self-mated steel

The friction profiles of the self-mated steel and self-mated low Si-DLC contacts are shown in Figure 7-2 and Figure 7-3. The steel/steel contact shows constantly higher friction values when compared with the low Si-DLC tribopair. In the friction profile it can clearly be seen that both the coated and metal surface reach steady state friction in the testing period.

7.2.1. Wear overview

Optical micrographs were obtained of both the pin and plate worn areas. The pin shows clear evidence of formation of a tribofilm or transfer layer at the point of contact, as a dark pad is observed. This is shown in Figure 7-4 The wear track is difficult to distinguish due to the low-wear nature of the contact with the plate. Wear track width is measured as: 169.75 ± 6.03 μm and a darkening is observed within this area.

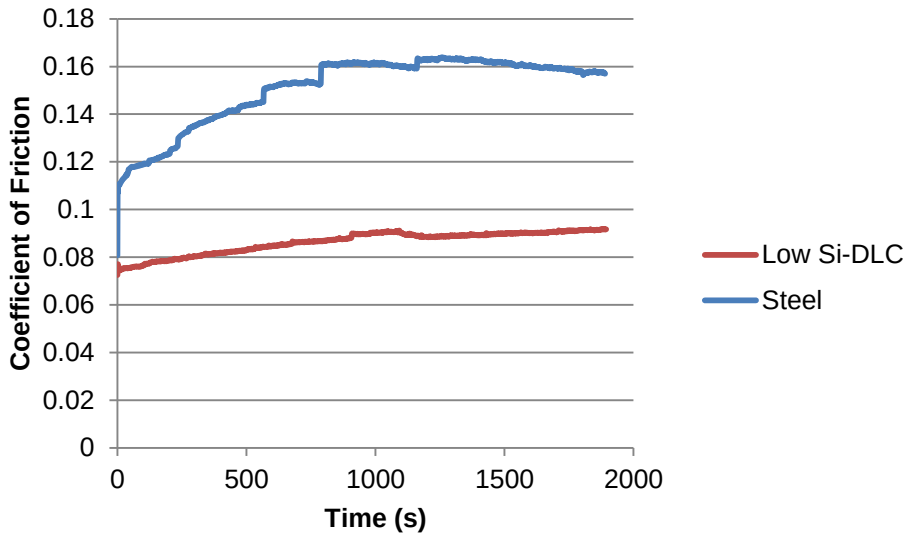

Figure 7-2 friction profile of self-mated steel and low Si-DLC contacts. Conditions as per experimental setup in section 3.5.2. Error bars omitted for clarity.

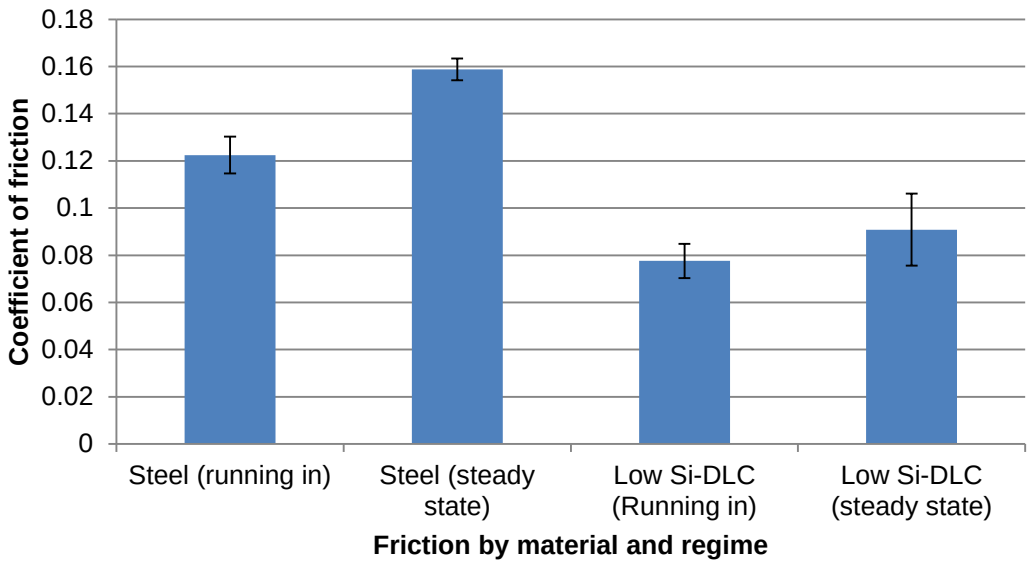

Figure 7-3 Steady-state and running-in friction (first and last five minutes of testing) of both tribopoairs

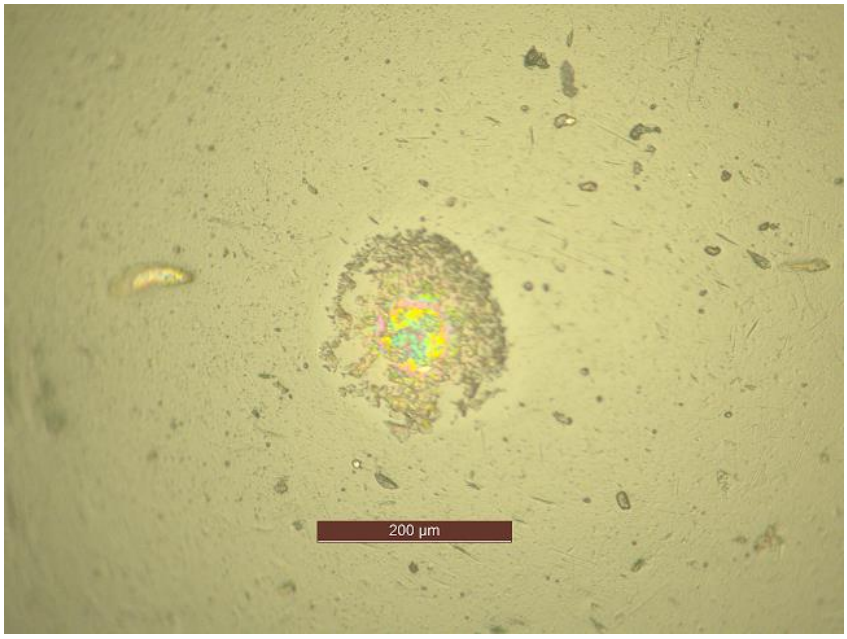

Figure 7-4 Optical image of the self-mated DLC pin post-tribotesting, showing a dark pad or transfer/tribo film where contact occurred. The coating appears intact, with no steel being revealed XPS confirms no Fe is present.

Optical imaging of a section of the wear track on the low Si-DLC disc is also imaged, as given in Figure 7-5.

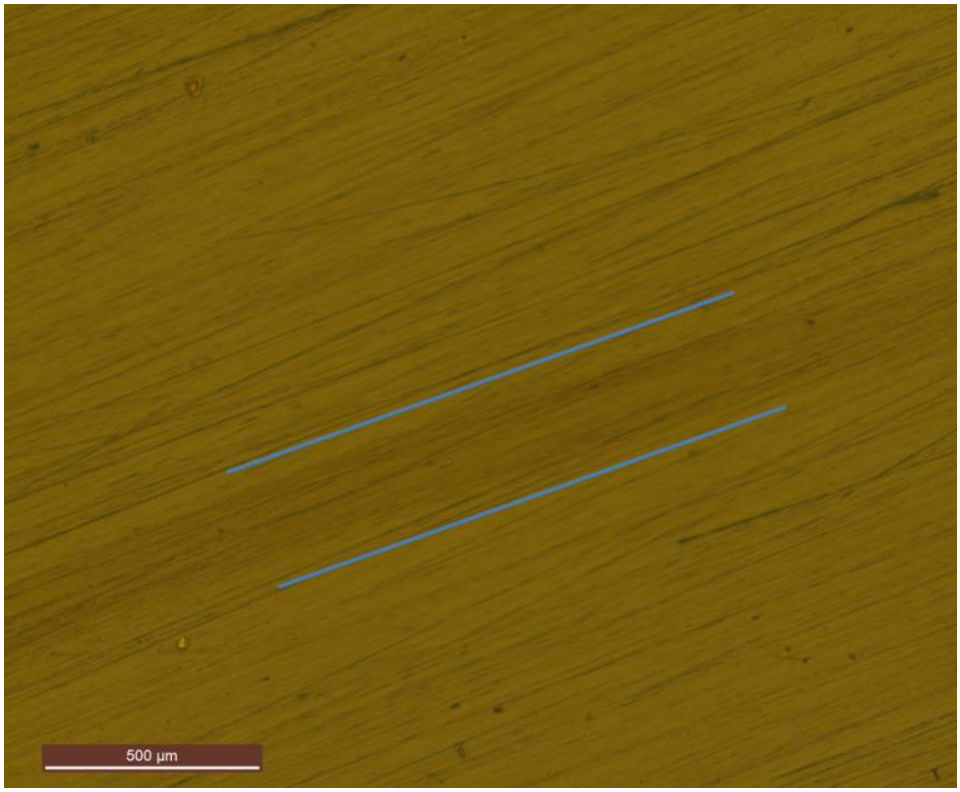

Figure 7-5 Optical image of the plate post-tribotesting, showing a faint wear track contact occurred

7.2.2. Surface analysis

XPS spectra were obtained for both parts of all the tribocouples to fully-characterise surface interactions. XPS analysis of the steel/steel tribopair shows evidence of a Ca-ZDDP type tribofilm being produced on the plate as given in Table 7-2. All peaks were calibrated to the presence of adventitious carbon on the steel sample, which comes higher in the spectra than any DLC associated peaks [189].

Table 7-2 XPS analysis of tribofilm on steel plate

Element	Position (eV)	%Atomic Concentration	Attribution
C 1s	**285.2**	**50.6**	**adventitious**
Ca 2p	**347.4**	**2.7**	**$CaCO_3$**
P 2p	**133.5**	**7.2**	**pyrophosphate**
S 2p	**161.8**	**1.2**	**sulphide**
O 1s	**530.7**	**36.1**	**phosphate/iron oxide**

Fe 2p	**710.7**	**1.3**	**iron oxide**
Zn 2p	**1022.4**	**1**	**zinc phosphate/ oxide**

When analysing the pin less species than expected were found, typically a classical ZDDP-ferrous system should leave a phosphate film [115]. As shown in the spectra shown in Figure 7-6 no P was detected. To ensure that surface contamination was not occluding the tribofilm proper, argon ion etching was conducted on the sample. An etch using mono atomic Ar gas ions with an energy of 4000 eV was employed for this purpose. A raster size of 1 mm x 2 mm was used.

As shown below, no sulphur or phosphorous is detected on the worn area of the steel pin despite high-resolution scans being employed. Notable species in the worn area are limited to Zn (eV = 1022.4, indicative of ZnO) and Ca (eV = 347.8, indicative of $CaCO_3$).

This could be accounted for two different explanations. It is possible that:

- different mechanisms govern the formation of tribofilm on the pin
- or that the film on the pin is very thin (<10 nms) and XPS analysis is not sensitive enough for examining this film.

This will be explored in the discussion chapter.

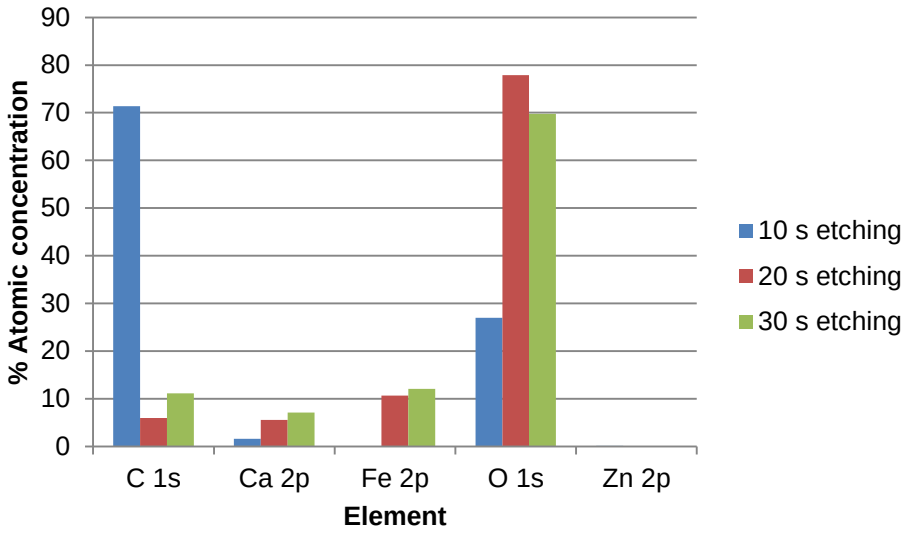

Figure 7-6 XPS results from the pin of the steel/steel contact. Results showing etching data. The presence of Zn is noted at the 10s mark as 0.1 % atomic concentration.

XPS analysis was also undertaken of the DLC/DLC pin-on-disc contact. Importantly, no Fe was detected when high-resolution scans were employed on either worn surface. This ensures any tribofilms identified were the product of low Si-DLC/low Si-DLC interactions and produced without any influence of Fe. XPS peaks values were used to attribute chemical species using literature values as shown in Table 7-3 [143, 146].

XPS analysis of the tribopair indicates the presence of a Zn, P, Ca, O species. Also noted are the presence of trace metal sulphides and sulphates. Again, three spot tests were used to ensure accuracy of results. There is a distinct difference between the body and counter-body makeup in terms of tribochemistry.

Table 7-3 XPS breakdown of DLC plate and pin tribofilms. Nd = not detected.

	Plate			Pin		
Element	**Position (eV)**	**%At Conc.**	**Attribution**	**Position (eV)**	**%At Conc.**	**Attribution**
C 1s	**284.7**	**61.9**	**DLC**	**284.5**	**78.8**	**DLC**

Ca 2p	**348.7**	**1.8**	**Calcium phosphate**	**347.5**	**1.7**	**Calcium sulphate/ carbonate**
N 1s	**400.7**	**1.1**		**399.5**	**1.0**	
O 1s	**532.7**	**20.1**	**SiO_2 /SiC**	**531.5**	**12.4**	**SiO_2 /SiC**
P 2p	**134.7**	**1.0**	**Meta phosphate**	**Nd**	**Nd**	
S 2p	**162.8**	**0.1**	**ZnS**	**168.5**	**1.0**	**sulphate**
Si 2p	**100.7**	**13.7**	**SiC**	**100.5**	**5.6**	**SiC**
Zn 2p	**1022.7**	**0.1**	**ZnO, ZnS**	**1021.5**	**0.4**	**ZnO**

Tribochemically the pin contains different sulphur groups when compared to the plate, with sulphur at a higher eV value. This confirms the harsher oxidative conditions, sulphide is oxidised to the sulphate. XPS analysis of the pin reveals slightly different species in the worn area. Notably, no phosphorous is detected and the oxide of zinc is the predominant form. Comparing the Si peak regions on the plate and the pin again shows differences.

High resolution spectra show that on the plate, as shown in Figure 7-7, there is a third peak contribution to the Si signal, this contribution appears to be from an SiO_2 species as verified by the binding energy; the higher eV the more oxygen, proportionally, is bonded to the Si [144, 146]. The corresponding peak window of the pin, shown in Figure 7-7 lacks the SiOx species.

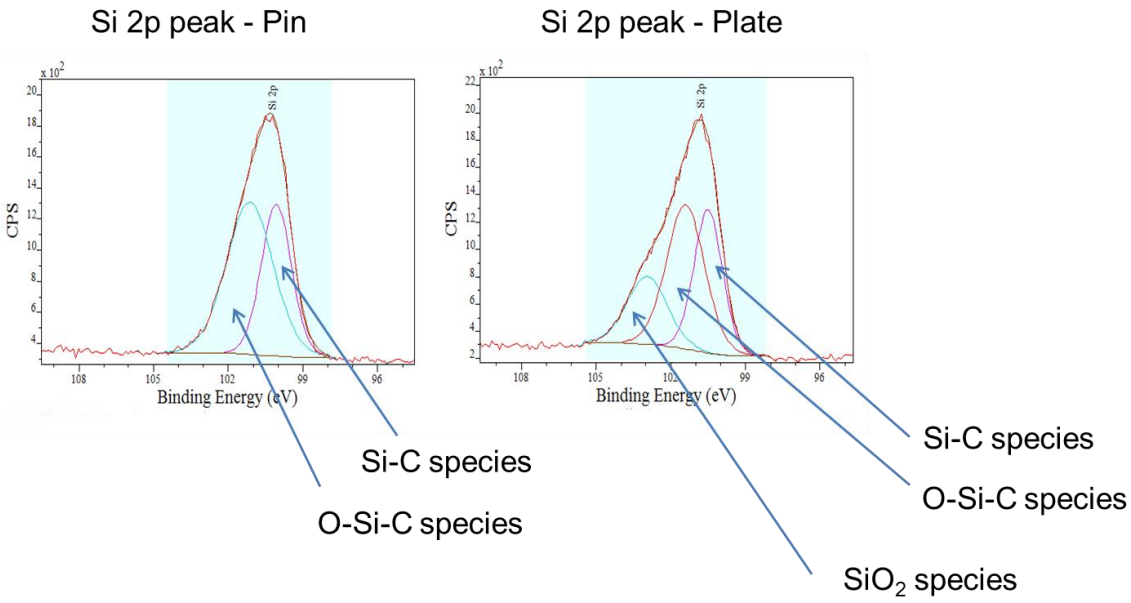

Figure 7-7 Showing the pin Si peak and the plate Si peak. FWHM values constrained to those of Si-C (100 eV), C-Si-O (101.5 eV) and (plate only) SiO_2 (103 eV)

7.2.3. Atomic Force Microscopy (AFM)

AFM traces of the thermally treated sample and the tribo-tested samples were obtained to gain further insight into the differences and similarities between the two films produced. These traces are shown in Figure 7-8. It is clear that the two films have a distinctly different surface topography, with the tribofilm shown in Figure 7-8 a showing a smoother surface finish. It appears that the thermal film is not as thick as the tribofilm, and that because of this surface asperities are still visible. This is further evidence for the distinction between the thermal and tribological films.

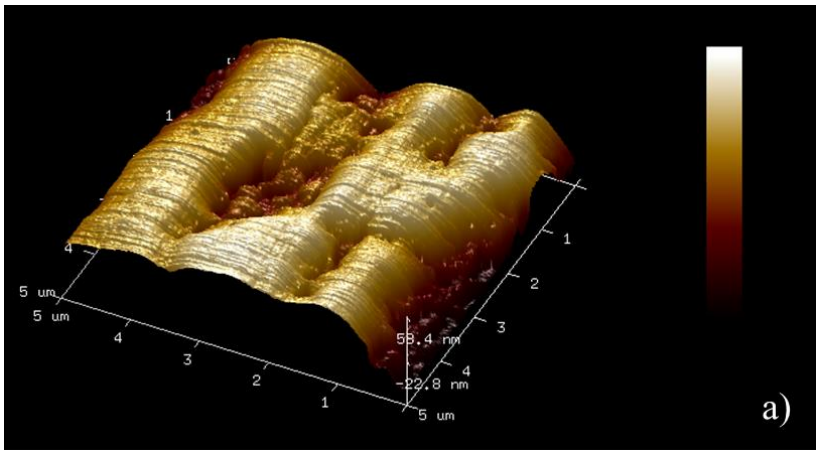

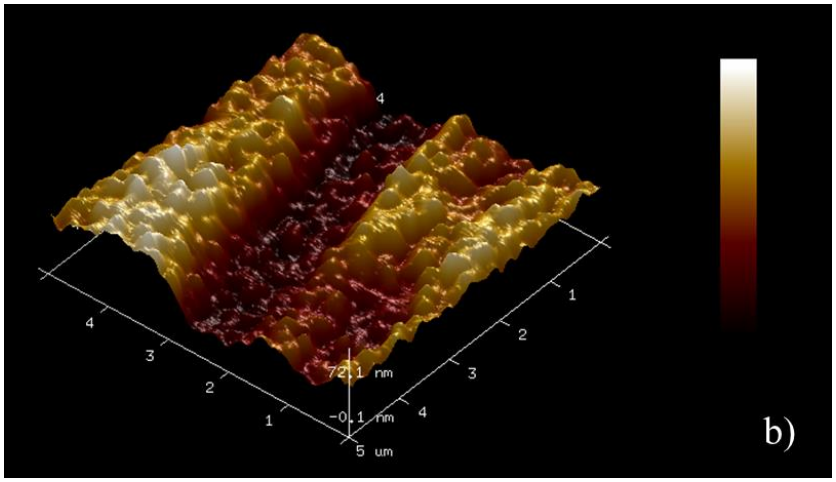

Figure 7-8 AFM images of the tribofilm a) with a smoother surface, and the thermal film b) with a far rougher surface.

7.2.4. Surface functionalization

The surface functionalization reaction was carried out (as detailed in page 56 section 3.4.3) and the silanized tribopairs were tested. The surface functionalization, in this instance, was not envisaged as a long-term friction reducing method. Rather, as a technique to establish how influential SiOx groups are in dictating the friction profile and how converting these to Si-O-R affects friction. Due to the nature of the functionalization, the functionalization would not penetrate deeply (maximal depth of a few atomic layers) into the DLCs microstructure and is thus expected to be lost even when there is minimal wear. Figure 7-9 shows the effect the surface functionalization has on the friction.

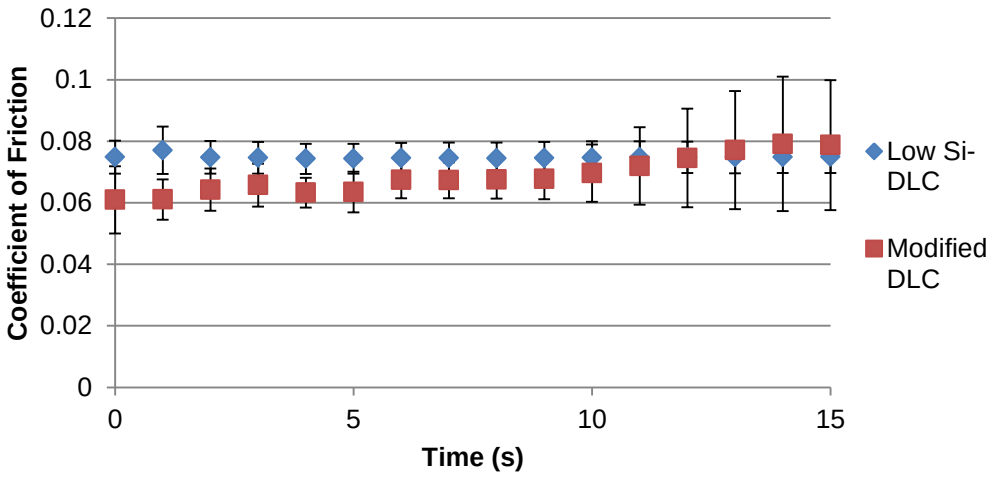

Figure 7-9 Effect on friction of the surface functionalization. Both contacts are the low Si-DLC/Si-DLC interfaces in oil b at 1.5 GPa.

The modified DLC does exhibit slightly lower initial coefficients of friction than the non-modified DLC. However, the values do remain close together at the start of the test. By the end of the testing the friction for the modified DLC is much higher than that of the low Si-DLC, suggesting the salinization process (which is known to release acid) damaged the coating which negatively impacted friction.

7.2.5. Summary

This chapter explores the role iron plays with regards to DLC. By removing iron it is possible to see how dependant tribofilm formation is upon this reactive element. Iron's role is well known and defined with respect to ZDDP [115]. However, it would seem that even without a ferrous surface, tribofilms do form at the low Si-DLC/Si-DLC contacts.

- Silicon-doped DLC contacts are able to make tribofilms independently of any ferrous body
- These tribofilms are chemically different to thermal films observed and thus are definitively tribofilms
- The self-mated low Si-DLC contacts show similar behavior to that observed with the steel/ low Si-DLC tribopair in that Si is sequestered from the coating with wear.
- Si cannot be considered analogous to Fe in terms of tribochemistry as the thermal film observed is not similar to a ZDDP thermal film on a steel surface.
- SiO_x groups are not key to the lubricated friction performance of Si-DLC as demonstrated by removing them from the surface
- Ca plays a key role in the tribofilm formation at the low Si-DLC/ low Si-DLC interface investigated.

Chapter 8 Results: Repressing oxidative wear within Si doped DLCs

8.1. Introduction

The mechanism of accelerated wear within Si-DLCs was explored extensively with XPS and ToF-SIMS in an earlier chapter[43]. It is widely accepted that the formation of silicon oxides play an integral role in the wear processes of Si-DLCs, Table 2-2- Table 2-4. In order to stabilise Si-DLCs with respect to wear the coating needs to have greater oxidative stability as silicon within a carbon matrix has a propensity to oxidise. This is because there is a strong thermodynamic driving force for this reaction [46]. Whether the Si-DLC is produced from solely a silane or a combination of hydrocarbon and siloxane, the wear is typically far higher for the Si-DLC, or Si,O –DLC than that of the a-C:H DLC.

To fully explore the wear behaviour of Si-DLCs a novel doped DLC was produced and tested in formulated oil. Advanced surface analysis techniques were then conducted to explore the mechanisms underlying the frequently observed higher friction or wear with these types of DLC coatings.

8.2. Coatings

The DLC coatings used in this section include two commercially available DLCs, as well as a novel, DLC. All were produced using the Plasma Enhanced Chemical Vapour Deposition (PECVD) technique. These coatings, as per materials section 3.2, where prepared following a set procedure: using lower temperature plasma, the substrate is negatively biased by 500 V with the chamber acting as the electrode. A hot cathode auxiliary system is also employed to enhance plasma generation. The

process typically takes place at 10^{-3} mbar. The coatings can be viewed as multi-layered as there are interlayers employed to improve coating adhesion to the substrate. The substrate is first cleaned with argon ion etching before any deposition commences. Then a titanium layer is deposited, followed by a silicon based interlayer. After interlayer deposition the bulk DLC is deposited. This layer is ~ 1.2 µm thick and is made from a precursor that is highly sp^2 hybridised. The silicon containing component cannot be revealed due to commercial sensitivity. The fluorine component is introduced into the DLC exclusively by use of Fluoroform whose chemical structure is shown in Figure 8-1.

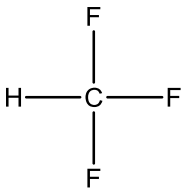

Figure 8-1 F-doping agent, Fluoroform (Trifluoromethane)

The specific protocol for production of a composite DLC with a Si,O,F doped top-layer, is as follows:

- Layer 1 of Si,O doped DLC (undisclosed organometallic precursor material)
- Layer 2 : Short transition of a mix of (organometallic precursor material) + C_xH_y + Argon
- Layer 3 : Additional Si,O doped DLC
- Layer 4: (top surface) Combination of the organometallic precursor and Fluoroform. Followed by venting with Fluoroform.

The doped coatings were analysed by XPS as shown in Table 8-1, to ascertain the % atomic dopant levels.

Table 8-1 %Atomic concentration of dopants in doped samples. Nd = not detected

Sample	Si	O	F
Si,O,F Doped	**3%**	**11%**	**1%**
Si,O Doped	**18%**	**14%**	**Nd**

It is noted that the %Si content of the two DLCs is different. Due to the nature of one DLC being a commercial sample and the difficulty of incorporating three dopants into the DLCs, this could not easily be altered. The potential affect this could have upon results is discussed later. Each coating's hardness prior to wear testing is given below in Table 8-2.

Table 8-2 Coating hardness values

Sample	Hardness (GPa)	St deviation ±
Si,O,F Doped	**13.9**	**3.8**
a-C:H	**18.0**	**2.1**
Si,O Doped	**14.4**	**3.0**

Thus, prior to testing, it can be seen that inclusion of Si does appear to reduce coating hardness. The dual combination of Si and F appears to reduce hardness further. This could be due to a variety of factors, most likely of which is the disruption of C-C bonding networks within the coating. This behaviour has been observed in the literature previously, with increasing fluorine content resulting in increased sp^2 bonding [190, 191].

8.3. Preliminary optimisation of the surface modification process

Initially the process modification envisaged was based around the manipulation of dangling bonds at the DLCs upper surface. These bonds are an artefact of the PVD/PECVD process and are always present at any

nascent DLCs surface post production, in a chamber under vacuum [63-65]. Previous work in the literature has shown that dangling bonds can be selectively modified using certain reagents [63]. This knowledge coupled with fundamental tribochemistry resulted in the selection of the gas trifluoromethane as a good candidate for surface reaction.

Initial results, whereby the traditional a-C:H DLC was deposited and then held in the chamber whilst being exposed to trifluoromethane without any plasma activation were not as successful as hoped. This resulted in only a 0.15 % atomic concentration of fluorine being incorporated on to the DLCs surface, ascertained by XPS analysis. This low amount would not be enough to affect the tribology of the system. From this unsuccessful modification attempt it was deduced that trifluoromethane was not active enough towards radical termination reactions; the reaction required to 'cap' dangling bonds.

To enable the fluorine containing reagent to fully react with the DLCs surface, the next experimental step was to use the plasma source available in the PVD rig. The process was run again with the plasma source left on whilst trifluoromethane was allowed into the chamber. XPS analysis revels that this yields a 4.69 % atomic concentration of fluorine on the DLCs surface. This represented a useful level of doping that, it was expected, would affect the tribology of the system.

8.4. **Results**

8.4.1. ºSurface wettability of the coatings

Water contact angle measurements were obtained for the three coatings examined which are given in Figure 8-2. Contact angle results suggest that the inclusion of both F and Si simultaneously does not affect the surface wettability when compared with a-C:H a-C:H DLC. The Si,O doped sample however does have improved wettability when compared to the a-C:H sample. Thus it can be expected that of the three coatings, the Si,O DLC should have greater affinities for any surface-active lubricant additives; such as detergent species. This concept is explored more thoroughly in the discussion section.

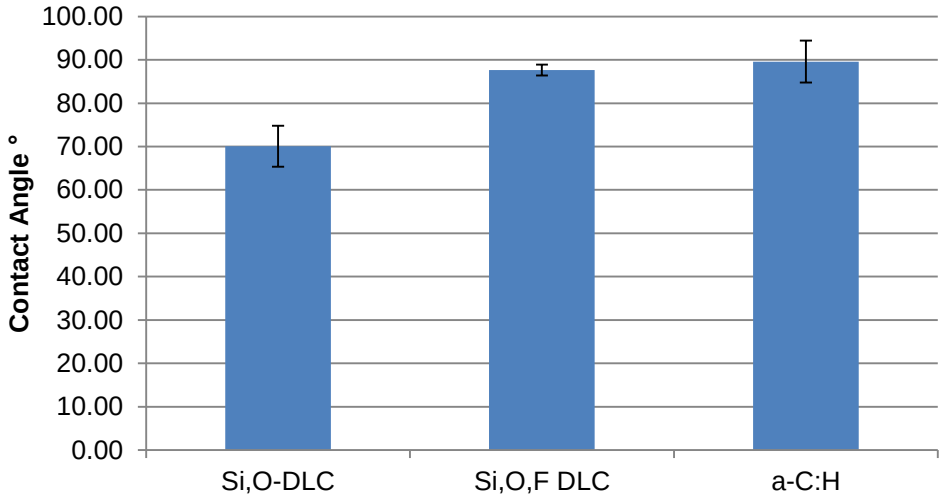

Figure 8-2 Water contact angle of the DLCs examined

8.4.2. Friction profiles of the samples

The friction profiles, as given in Figure 8-3 for the Si,O and a-C:H DLCs are, for the majority, within error of each other; suggesting there is no real difference between the friction performance of the two. However, the Si,O,F DLC shows a distinct rise in friction towards the end of testing.

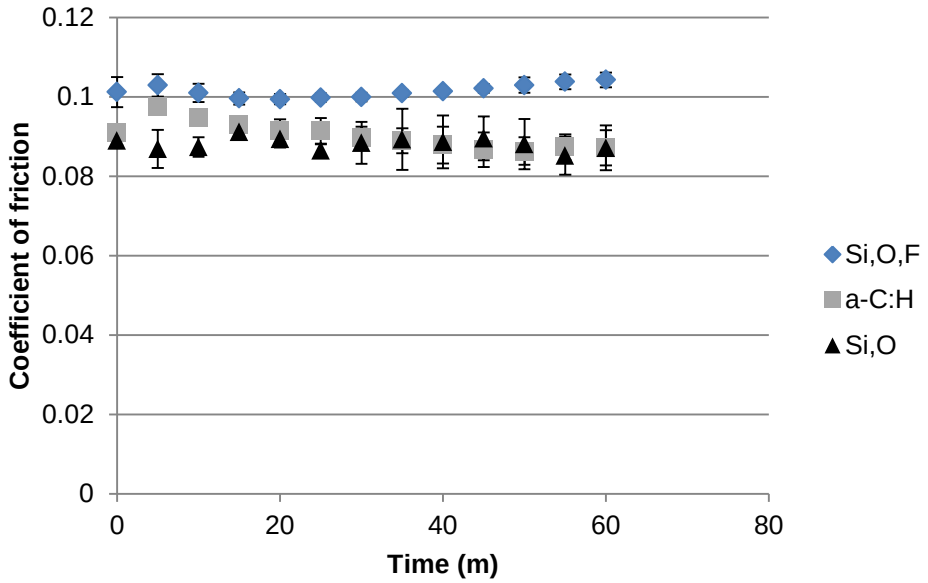

Figure 8-3 Overall friction profiles of novel DLCs in oil. Conditions: as per experimental for camshaft contacts. Coatings tested in Oil D.

Friction values from the literature of lubricated Si-DLC, as summarised in the discussion chapter, show similar friction profiles to the ones obtained herein. Initial friction data for the samples tested start at a similar value. However, by the end of the test duration Si,O,F-DLC actually has the higher friction of the three DLCs tested.

8.4.3. Wear of the coatings

8.4.4. Optical microscope images of wear scars

Optical microscope images, shown in Figure 8-4, identifies the nature of the wear within the scars on the plate. For the Si,O,F doped DLC the worn area undergoes only very minor polishing, made clear by the preservation of the scratches in the DLC surface; these are artefacts from the steel substrate. The a-C:H sample shows more severe wear than the Si,O,F doped sample, there is clear evidence of polishing wear on the plate. The Si,O-DLC shows the highest level of wear with the widest wear track.

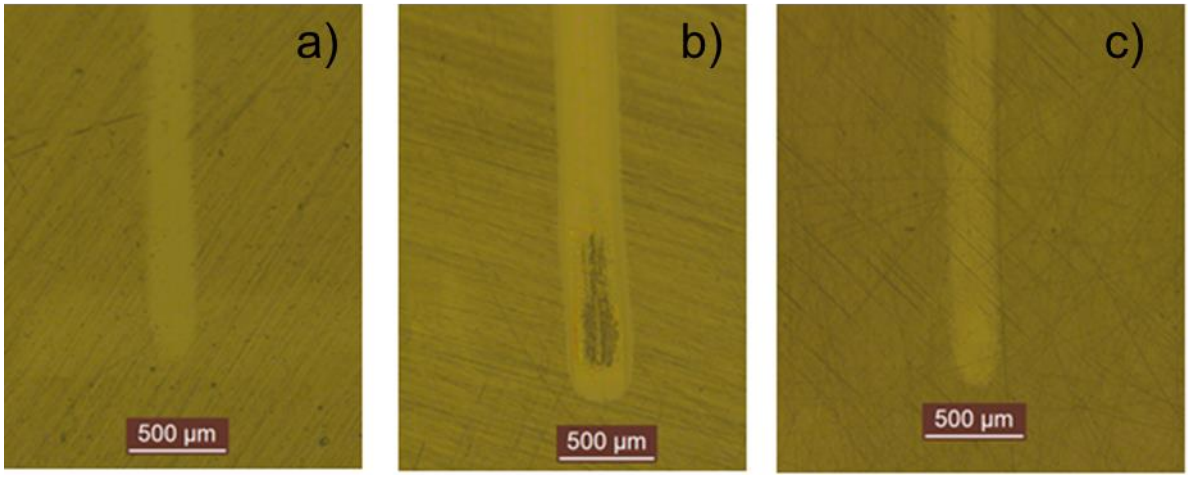

Figure 8-4 Optical microscopy from the worn area a) a-C:H, b) Si,O-DLC, c) Si,O,F-DLC.

8.4.5. Wear of counter bodies

Counter body wear was measured and is given in Figure 8-5 for the cast iron pin and was comparable for the Si,O,F and a-C:H samples. Far greater wear was noticed on the pin mated with the Si,O-DLC. Optical microscope based measurements show that the Si,O,F doped DLC appears to have the better wear profile of the set tested as the Si,O,F-DLC's wear is lower than the a-C:H DLC in terms of plate wear.

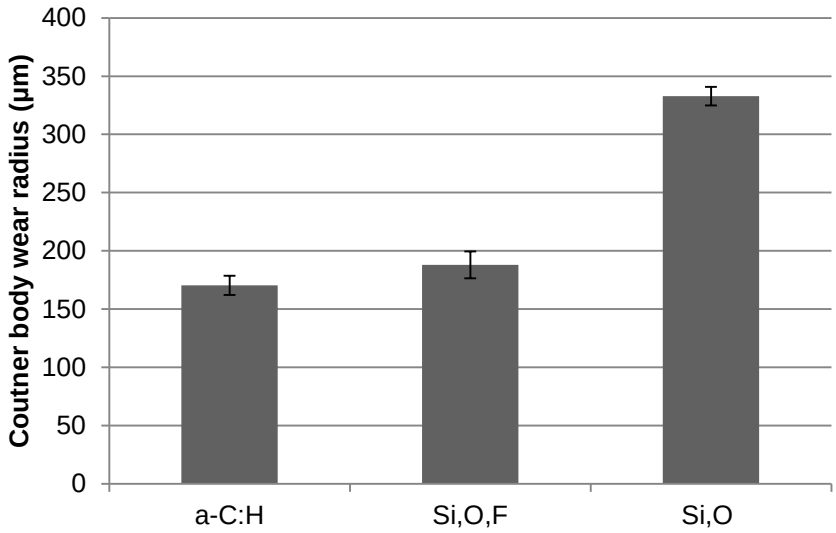

Figure 8-5 Wear of counter body

8.4.6. Contact profilometry measurements

To verify the results obtained via optical microscopy, that the Si,O,F DLC outperformed the a-C:H DLC, contact profilometry measurements were also obtained of the worn areas and are given in Figure 8-6 and converted into wear coefficients in Figure 8-7.

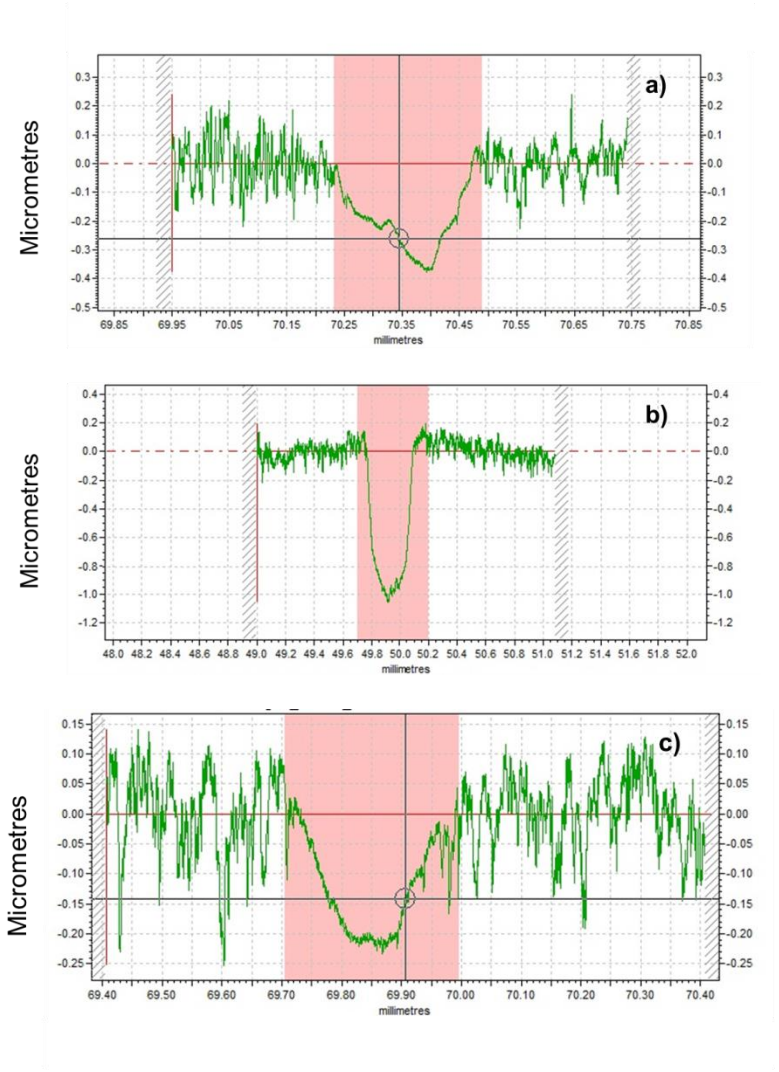

Figure 8-6 Contact profilometry results of the coatings, a-C:H (a), Si,O (b) and Si,O,F (c) confirming the lower wear track depth of the SiOF doped sample (0.2 µm).

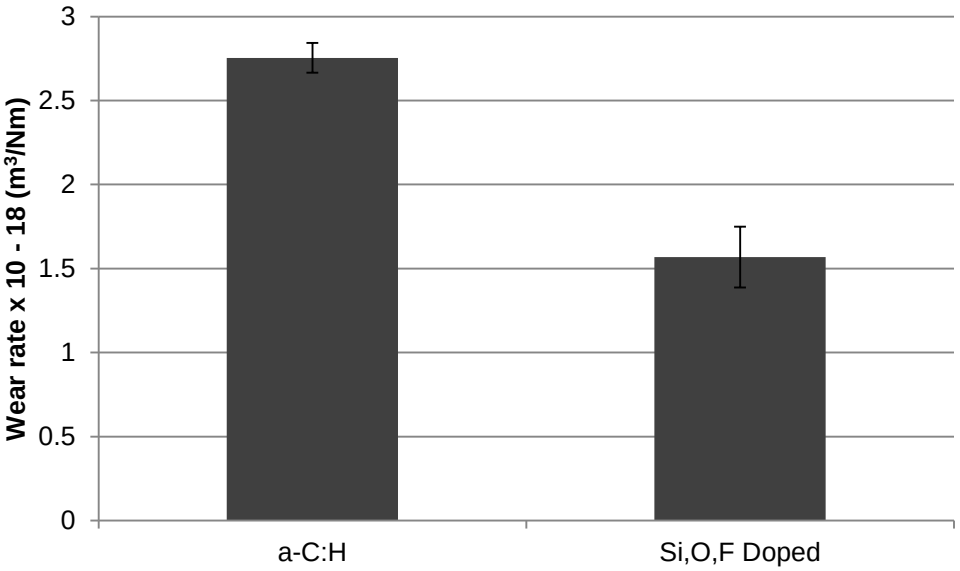

Figure 8-7 Dimensional wear coefficients of the coatings. Conditions of testing, as before: 25 N, 2 hours, 0.81 GPa , 0.2 m/s, 100 °C

Wear as listed in Figure 8-6 and Figure 8-7 of the modified surface is reduced on average by 43 % when compared to the a-C:H sample, showing a clear reduction in plate wear. The results here show that when Si is incorporated into the DLC with O and F, creating a tri-doped system, the wear is sharply reduced.

8.4.7. Coating hardness

The hardness of the novel and a-C:H coatings within the worn area were obtained to ascertain whether hardness was playing a key role in wear performance and if it changed with wear, hardness values are shown in Figure 8-8.

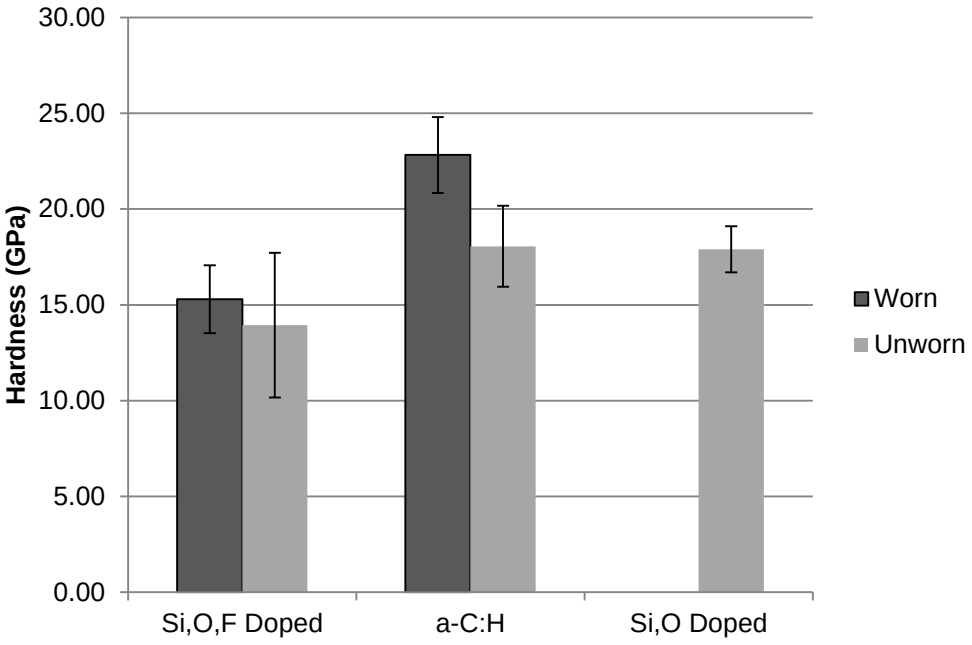

Figure 8-8 Coating hardness prior to wear testing and post- wear testing. Si,O doped DLC's hardness not examined within the wear scar following poor wear performance.

Prior to tribotesting the DLCs are all within a similar range of each other in terms of coating hardness. This suggests that mechanical hardness is not the key issue in this case, with respect to wear reduction. Roughness values of the worn and unworn areas were obtained to check whether this factor was skewing the nano hardness data as given in Figure 8-9.

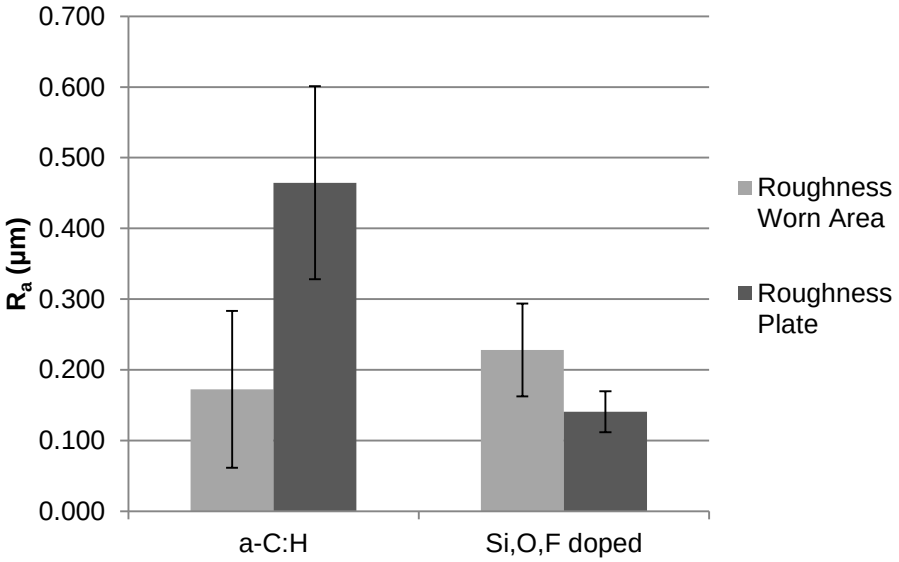

Figure 8-9 R_a values for the coatings within and outside of the wear track

Roughness remains unchanged for the tri-doped system. Whereas, the a-C:H system shows an increase of surface roughness within the worn area. As such, nanoindenation of the worn area of the tri-doped system should be more reliable, as the surface is smoother.

8.4.8. Surface analysis – XPS results

XPS analysis of the Si,O,F plate are given in Figure 8-10. The data comes from within the worn area confirms the presence, and therefore preservation, of doping elements as well as a trace amount of sulphur.

High-resolution scans were conducted for the Si peak region to verify peak components, which is shown in Figure 8-11. There appear to be three main peak contributions to the Si 2p peak window. These peaks have been constrained to the natural FWHM values given in Table 8-4, associated with the species expected. The peaks have been attributed as: Si-F, C-Si-O and Si-C.

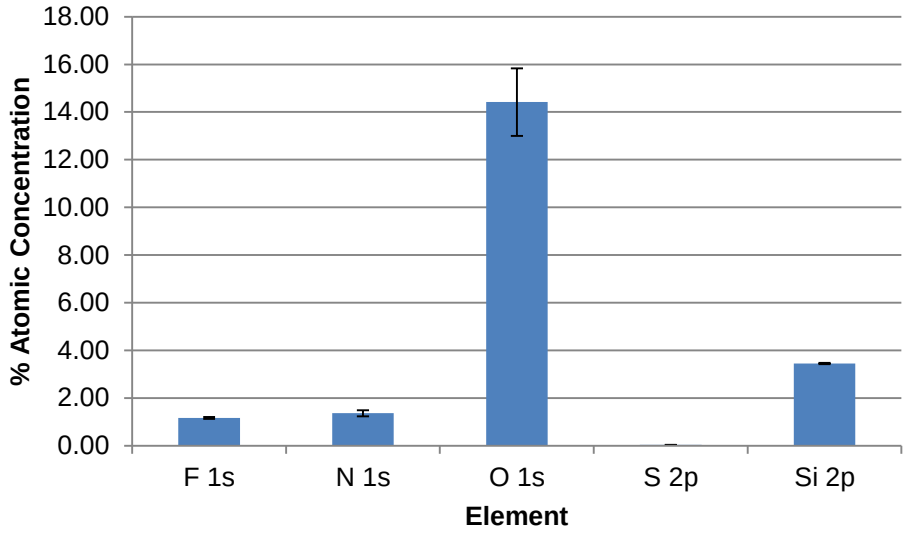

Figure 8-10 XPS data from the Si,O,F doped DLC. Carbon excluded for scaling.

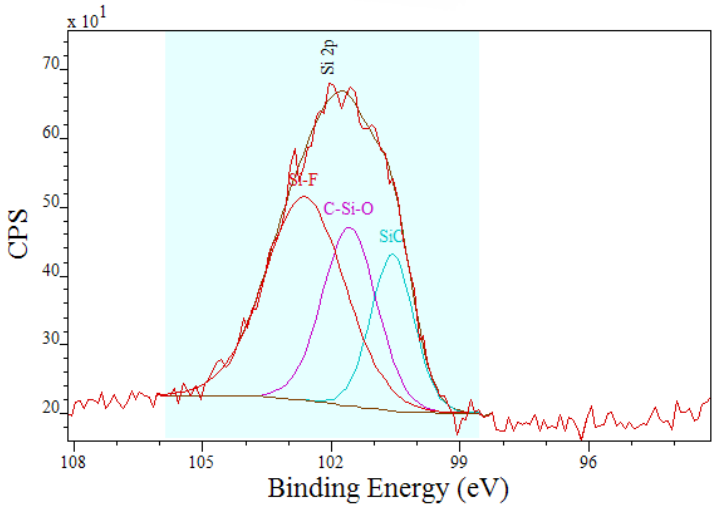

Figure 8-11 High-resolution spectra of the Si 2p peak from the Si,O,F doped plate

Table 8-3 Peak component attributions from the Si 2p peak

Species	% atomic concentration	Peak position (eV)	FWHM
Si-F	**49.60**	**102.6**	**2.7**
Si-O-C	**29.75**	**101.6**	**2.0**
Si-C	**20.65**	**100.6**	**1.4**

XPS data from the counter body are shown in Figure 8-12, this was also obtained to ascertain if a transfer-layer was present on the pin. Trace amounts of S and P were detected on individual spots but were not present consistently.

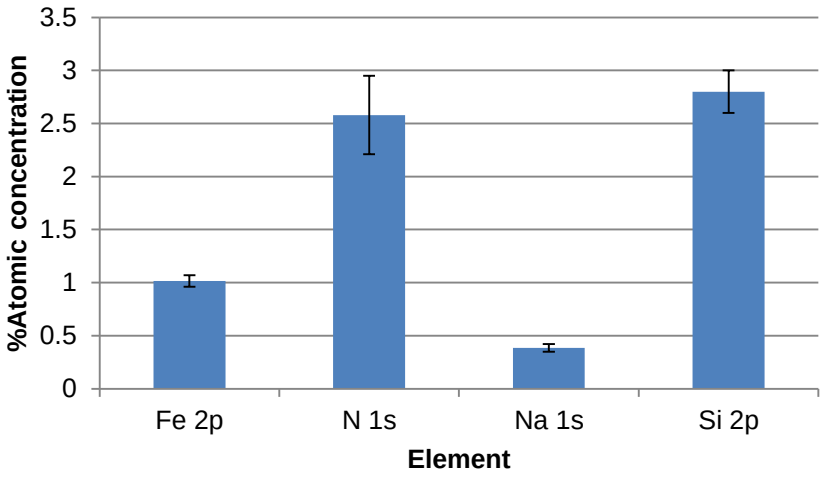

Figure 8-12 XPS analysis results of the cast iron counter body (carbon and oxygen omitted for scaling). Sodium is noted as contamination

The counter body contains large amounts of carbon with a peak value of 284.5 eV, suggesting this is transferred DLC from the plate. Also Si is detected again suggesting the DLC has transferred from the plate. High-resolution scans again were recorded at Si 2p and are given in Figure 8-13.

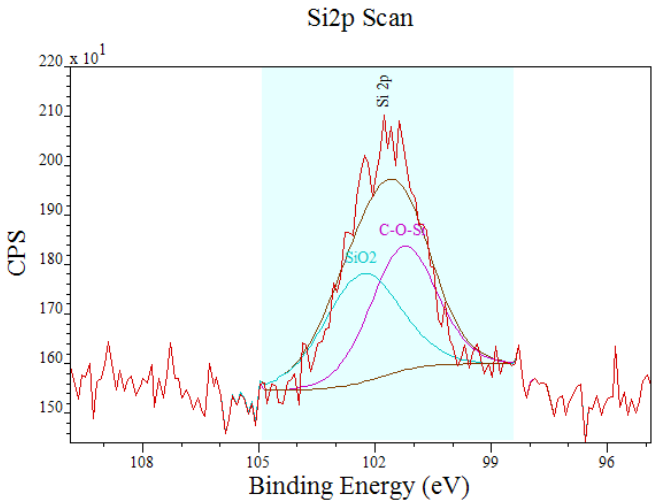

Figure 8-13 High-resolution spectra of the Si 2p peak from the pin mated against the Si,O,F doped plate

The presence of SiOx and Si-O-C are noted following thorough peak component fitting with accurate FWHM values listed in Table 8-4, for expected compounds. No Si-C is detected on the pin.

Table 8-4 Peak attribution of the Si2p peak components

Species	% atomic concentration	Peak position (eV)	FWHM
Si-O-C	**49.95**	**101.3**	**2**
$Si-O_2$	**50.05**	**102.3**	**2.3**

8.4.9. ToF SIMS chemical mapping of Si,O,F DLC:

To further clarify the surface reactions on the modified plate ToF-SIMS results were sought as this method is highly sensitive to the upper-most surface and therefore ideal for characterising nanometre thin films, like the one under investigation. They are given in Figure 8-14.

ToF-SIMS chemical mapping is shown in Figure 8-14. It shows how certain F and Si species are distributed within the DLC. Various forms of both species are present across the plate. Enhanced build-up of a novel SiOF anion fragment on the plate is clear. As this fragment is far richer in the worn area it is demonstrable that this is produced as part of the wear process.

Also, there is a noticeable amount of HS^- in the wear scar; the source of HS^- in this case is the lubricant. The formation of the SiOF- fragment ion appears to represent a protective tribolayer. As the overall wear of the plate decreases and the friction increases it appears that this layer is similar to a ZDDP derived phosphate glassy film, increasing overall friction but lowering wear.

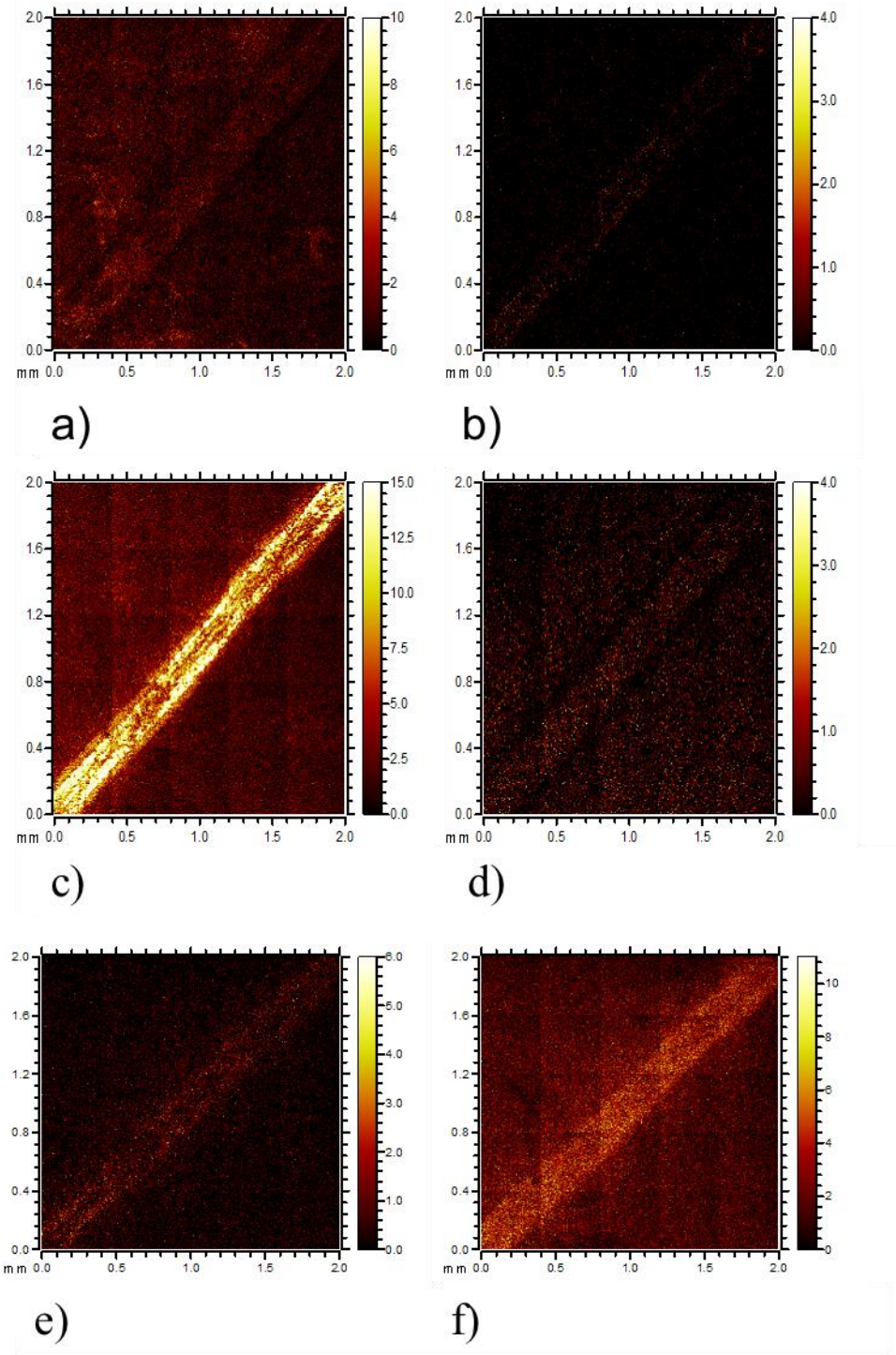

Figure 8-14 ToF-SIMS chemical maps of anions in the wear track and surrounding area. a) C_2H_2F b) SiF c) SiOF d) CF_3 e) S f) HS

8.5. **Summary**

The trend of Si-DLCs to exhibit enhanced oxidative wear is well documented. It would appear, following this initial research, that this trend can be inhibited by inclusion of F to the dopant matrix. This relies upon F being stable toward oxidation and forming strong bonds to Si.

- A novel, tri-doped DLC has been produced that exhibits enhanced wear resistance both when compared with low Si-DLC and with a-C:H DLC films.
- The novel DLC appears to mitigate wear by producing a SiOF containing species in the worn area that is able to limit oxidative wear.
- It can be concluded that inclusion of F with Si impedes the wear of the coating, this is especially relevant to Si-DLCs as a whole, which typically undergo higher wear when compared to a-C:H DLCs.
- The friction performance of the coating in low-additive oil is comparable with the other DLCs tested.
- The mechanical parameters of the coating are also comparable, indicating the enhanced wear resistance is indeed due to the specifically tailored tribochemistry of the coating; as opposed to the hardness of the film.

Chapter 9 Discussion

9.1. Overview of discussion

This discussion chapter is split into seven main themes that have been identified following analysis of the results obtained. The results previously detailed will be compared to key findings with other literature available and both agreement and discord will be examined. The main areas of focus are:

- Differences between the surfaces investigated,
- Carbon hybridization state,
- Friction of the systems examined,
- Wear of the systems,
- Tribochemistry,
- Resolving oxidative wear of Si-DLCs,
- The role of iron.

9.2. Differences between surfaces investigated

As addressed in the literature review in section 2.1.1, Diamond-Like Carbon coatings and steel are distinctly different surfaces. This is due to their different surface energies and surface chemistry, which in turn is largely controlled by the amount of oxygen at the surface. Oxygen is able to make polarised bonds with elements in the surface as well as form hydrogen bonds with species that adsorb onto the surface. These surface differences are also present when examining Si-DLC and a-C:H DLC, but to a lesser extent.

Spectral analysis combined with known atomic compositional data of the low-Si DLC coating enables a large portion of the DLCs native, pre-worn structure to be elucidated. Pre-wear SIMS and XPS data was not sought for the current study on a-C:H DLC as this data would not be particularly useful.

This is because the bulk of the a-C:H DLC is made up of solely C and H; XPS would not yield interesting data in this instance as it cannot detect hydrogen. Again, in depth analysis of the high Si-DLC was not pursued as this coating did not perform as well as the other two and was removed from the testing matrix after initial experiments.

9.2.1. Surface wettability of the coatings

One effect inclusion of Si and O has is via the surface wettability of the coating. The a-C:H coating is more hydrophobic than the low Si-doped coating as shown in Figure 4-4, section 4.2.3. This is because Si and O are able to combine to form polar species within the coating. This allows a greater amount of SiO_x species at the surface, as verified by solid-state NMR and XPS analysis. These species could be considered as analogous to ferrous oxides on a steel surface [28, 29]. This is because Si and Fe have similar electronegativity values, as shown in Table 9-1, which allow polarised bonds to be formed with O. This makes the coating more like a steel surface when compared to the a-C:H coating [46]. In comparison, C is closer in value to O in terms of electronegativity, leading to a less polarised surface. These results are further validated by the practice of coating certain metal surfaces with Si oxides to maximise their surface wettability with water [167]. Increasing Si content of DLCs has previously been shown to increase water wettability of the coating [47].

Table 9-1 Electronegative values of certain elements [46]

Element	Electronegativity value (χ)
Fe	**1.83**
Si	**1.90**
H	**2.20**
C	**2.55**
O	**3.44**

9.2.2. Si within the DLC coating

To fully understand the role Si plays within the DLC matrix NMR analysis was obtained of the bulk coating. NMR characterisation of the chemical states of Si in the film is in line with previous literature characterisations [85]. For the high Si-DLC, Si is bonded to both C and O, thus affecting the sp^3/sp^2 ratio. The precursor for this coating is a siloxane, where the Si-O-Si bond is the backbone of the molecule as shown in Figure 9-1. It seems that a large portion of the siloxane bonding survives, or is recombined and thus maintained during, the PECVD process.

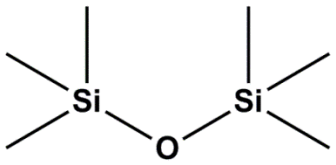

Figure 9-1 Formula of HMDSO

This is verified as the XPS spectra of the low Si-DLC shows a large peak indicative of Si-O-C bonding, which is shown in Figure 4-5. This survival is most probably due to a combination of the very stable Si-O bond strength and also from the molecule being sterically protected from the process by the organic side chains [78, 82, 192].

The large content of oxygen within both the high and low Si films complicates characterisation of the bonding and microstructure within the films. The observed changes in the sp^2 content as per NMR spectra as given in section 4.2.2, could be indicative of additional C-O type compounds as opposed to conjugated C systems which appear at a similar ppm range.

It is evident from XPS and SIMS data as given in section 4.2.1 that at the surface of the low Si-DLC there are a large number of oxide rich Si species. Whereas, further into the coating, these species are less prevalent as shown by XPS when compared to ERDA data shown in Table 3-1.. From these data sets it is clear that oxidation of the surface has occurred. Various types of Si and O containing species have been shown to influence the friction and wear of Si doped DLCs, not only in this work but also previously in the

literature [25, 26, 76-80]. Therefore their prevalence at the surface prior to testing is noteworthy.

This surface enrichment can be explained as an artefact of production, dangling bonds from the synthesis of DLC coatings at the upper most surface react with species present in the air upon release of vacuum [64]. This causes a higher than normal amount of –H and –OH terminated species at the upper-most surface. Dynamic SIMS data is in agreement with XPS results in that the predominant form of Si within the coating is as the siloxane type species, Si-O-C. This is often the case when siloxane precursors are used [78, 87].

9.2.3. Ambient coating oxidation

XPS results of unworn, low Si-DLC compared with the two thermally treated surfaces yields interesting data as given in section 6.6, Figure 6-6. The spectra confirms that the surface Si atoms have a tendency to oxidise when heated in air without the need for tribological influence. Therefore it is reasonable to assume that the Si in the coating will also tend toward oxidation when heated during tribological testing. This surface oxidation will influence the coatings performance in terms of both friction and wear. This oxidation also represents the beginning of the coating degradation as Si-O bonds form at the expense of Si-H and Si-C bonds, sacrificing some of the diamond-like nature of the coating. Some surface oxidation may be beneficial to the coating, formation of surface oxides in metal systems have been reported to enhance surface wear resistance in certain cases [193]. Additionally, the role of oxides and Si-oxygen compounds are widely reported as being useful to reduce friction within specific Si-DLC systems [26]. Oxides and oxygenated species have previously been reported on unworn Si-DLC [78, 86].

9.3. Carbon hybridisation state

Carbon hybridisation state, or the amount of carbon to carbon single, double or triple bonds is known to effect various properties of the film [75]. Donnet [75] shows the effect of carbon hybridisation state on coating microstructure

in Figure 9-2. As shown, increasing sp^3 content is often linked with the 'diamond-like' nature of the film.

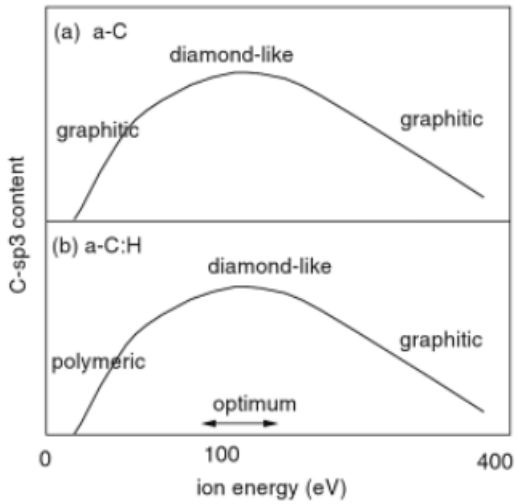

Figure 9-2 sp^3 content as related to diamond-like structure[75]

From the data available from EELS, presented in section 5.2.11 and NMR data given in section 4.2.1; it can be shown that the a-C:H, hydrogenated coating has a large amount of sp^2 hybridisation within the coating. The coating is also mechanically the hardest of the three coatings (22 ± 1.7 GPa). This trend may appear unusual as typically sp^3 type bonding is regarded as superior and more 'diamond-like'.

However, when the coating's chemical composition is compared with the two Si coatings these findings are rationalised by the effect that Si and O inclusion have on the film. When Si and O are included together the chance of an Si,O network increases at the expense of Si-C bonding. A link between decreased hardness and increased Si,O content has been identified previously by some researchers [84, 102]. However, the effect of Si alone (with no O co-dopant) is slightly different, due to the absence of Si-O bonding which can disrupt the films typical order. This is shown in Figure 9-3. It seems there is a complex relationship between Si content and hardness that includes C sp^3 fractions and chemical bonding in the film.

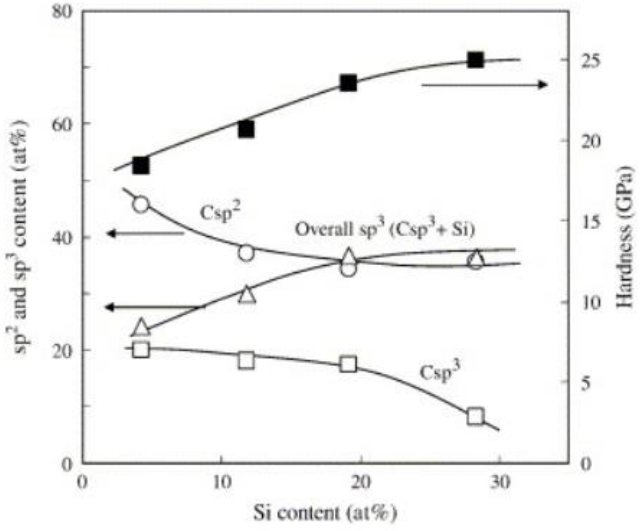

Figure 9-3 Effect of sole Si doping on hardness [85]

The low-Si DLC (with an atomic % Si of 14) tested within this thesis has an unworn sp^2 fraction of ~40% and a hardness value 17.9 GPa. This suggests that for this particular Si-DLC the inclusion of oxygen as a co-dopant does not majorly alter the coatings microstructure in terms of physical properties, in comparison with other solely Si-doped DLCs. In fact it would appear that the inclusion of oxygen has possibly boosted the hardness, when compared to the data shown in Figure 9-3.

9.3.1. Effects of increasing Si doping on the coating's microstructure

When the Si fraction is increased even further, to 21 atomic % (high Si-DLC), the sp^2 fraction increases vastly which was not expected. Typically, inclusion of Si increases the sp^3 fraction. This is due to the preference of Si atoms to not partake in sp^2 bonding with C [81, 162, 163]. The majority of the literature on Si-DLC explains that incorporation of Si increases the fraction of sp^3 bonding in the DLC [81, 82]. However, trends identified in the literature show that in some cases including Si at certain high levels can cause an increase in sp^2 bonding [85, 88, 102]. For the high Si-doped DLC, 80% of the C signal for the sample appears at the 110 to 220 ppm area, associated with

π (or C=C) bonding. This would suggest that at low to medium concentrations of Si in the coating most of the Si is directly bonded to C atoms, enforcing an sp^3 configuration. However, at higher concetrations it seems that Si's role in the coating changes. This trend has been seen before, whereby high levels of Si incorporation equate to higher C=C bonding, typically through a Si-C=C type bonding motif [85].

Also, PECVD parameters like bias can affect sp^2 fractions, Si-DLC films deposited at high values of bias can show an increased sp^2 character [81]. This further underscores the complexity of the PECVD process and underlines the need for each coating to be examined seperately before generalised rules are applied.

9.3.2. sp^2 evolution with time

A change in C hybridisation state is observed at the a-C:H DLC film which progresses with rubbing time. This time dependence could be reliant upon wear processes or perhaps the heating associated with tribotesting. The re-hybridisation seen within the a-C:H coating is extensive, the sp^2 fraction increases from 60% to in excess of 80%. As the increase in sp^2 ratio is not seen with the low Si-DLC coating, which undergoes greater wear, it can be assumed that the sp^2 change is not solely a function of wear. It may be assumed that this process is indicative of release of the compressive stresses associated with DLCs. The large increase of the sp^2 signal for the a-C:H sample indicates that the DLC substructure does now include a larger fraction of sp^2 hybridised Cs than the initial, unworn sample. Interestingly, this fraction of sp^2 carbons is not confined to the upper microstructure, near the contact area, but is present throughout the DLC; demonstrated by the fact that three locations in the coating were analysed.

The low Si-DLC appears to be stable in terms of the coating's C hybridisation ratio as no major change is recorded with tribotesting. This is most likely due to Si's inability to form stable double bonds; thus forcing it to bond in a sp^3 fashion within the coating and securing a network of Cs in this configuration. In addition to this, Si is known to reduce the compressive stresses associated with DLC coatings, as shown in Figure 9-4. This could

potentially remove the bias towards undergoing changes in the micro-structure [81, 102, 194, 195].

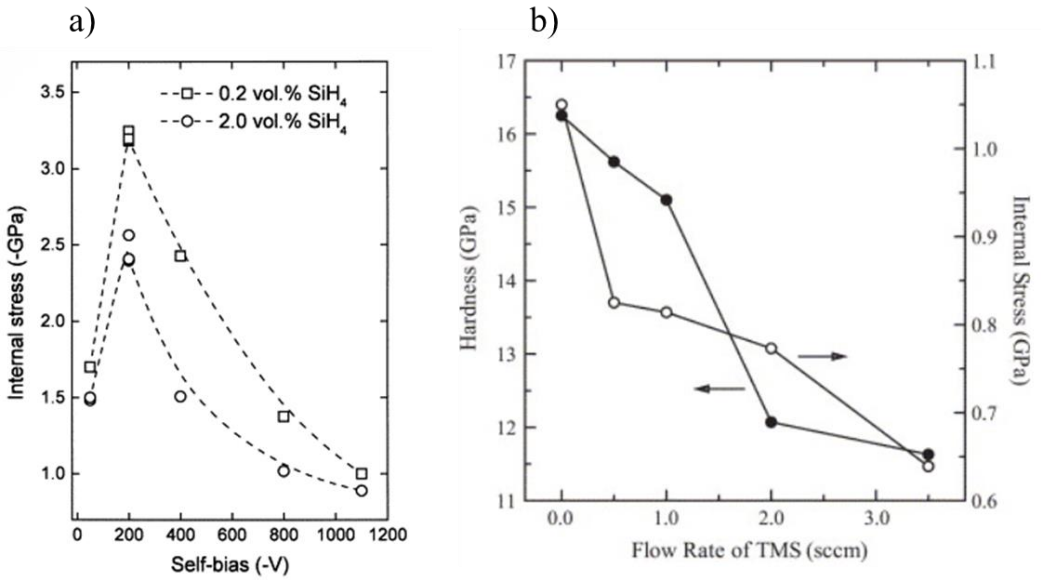

Figure 9-4 Effect of varying Si concentration on internal film stress from a) [81] and b) [85].

Examination of the TEM images of worn and unworn a-C:H DLC is not indicative of formation of a graphitic-type crystalline lattice as shown in Figure 5-19. As such this would suggest that there may be local re-hybridisation of bonding within the coating but this would appear to have no long range order. If elevated levels of sp^2 bonding were confined to the upper surface of the a-C:H DLC this still would not be definitive evidence for graphitisation of the coating. Many C compounds include sp^2 bonding without necessarily being graphitic, of which examples are given Figure 9-5.

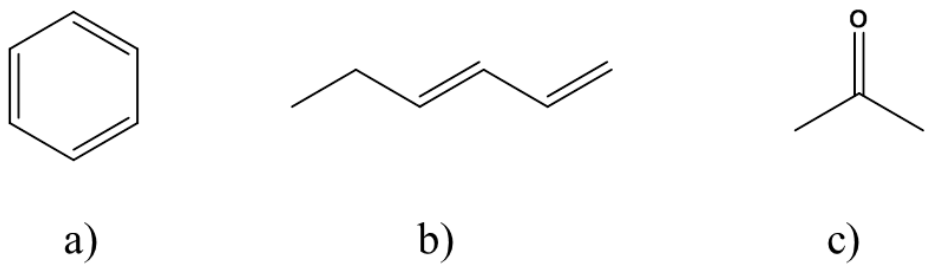

Figure 9-5 Molecules containing sp^2 bonding, as distinct from graphitic sheets. a) benzene b) penta-1,3-diene c) acetone.

Finally, five-membered ring species with pi systems may also be present in the DLCs microstructure. All of these structures could occur within a DLC coating. The prevalence of carbonyl groups at the upper surface of DLCs has been explored in the literature [70]. Formation of any of these compounds could contribute to an upshift in the sp^2 fraction of the film. Aromatic structure like benzene are known to be a stable configuration that C can adopt and have been observed previously within DLC films [196]. If such structures are forming within the DLC it would appear to be beneficial, as proven by the lower wear rate of the a-C:H DLC. This is noteworthy as often high sp^3 or 'diamond-like' DLCs are sought as it is believed they will have enhanced wear resistance. In this case the opposite is true as the low-Si DLC has higher amounts of sp^3 bonding and higher wear rates.

9.4. Friction of the systems examined

9.4.1. Dry friction of low-Si DLC and a-C:H DLC

When in non-lubricated conditions the low Si-DLC shows a far better friction profile than a-C:H DLC. This is shown in the results chapter section 4.2.5, Si-DLC gives a two thirds reduction in friction when compared to a-C:H DLC. This phenomena is widely observed in the literature [26, 77, 79]. The low friction coefficient of Si-DLCs in non-lubricated contacts is usually attributed to the formation of Si-O type species at the contact interface [26, 77-80, 86]. These species are rich in –OH bonds which are also recognised as potentially being able to reduce friction [25, 99]. Although no mechanism for the reduced friction in dry environemtns has been settled on, it would seem that the most likely factors are either: inclusion of additional –OH/polar speicies or production of an easy-shear layer of SiO_x debris. An illustrative schematic of this is shown in Figure 9-6.

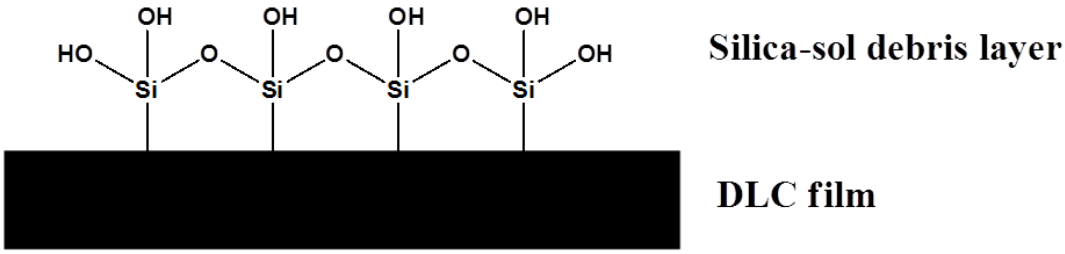

Figure 9-6 Schematic representation of hydroxyl and oxygen rich surface layer of Si-DLC

9.4.2. Lubricated friction

Lubricated friction values of Si-DLC coatings are typically within the ranges shown below in Table 9-2. Allowing for the unique case of Si,O-DLC lubricated by water, which is distinctly different than the systems lubricated by mineral oil; the friction results are typically higher than could be expected from the low friction behaviour as observed in dry sliding.

Table 9-2 Data from the literature of Si and Si,O DLCs friction coefficients

Author	Lubricant	DLC	Coefficient of friction
Yamaguchi [172]	**Commercial ATF (Ca,P, S, containing. No Zn)**	**20 % Si-DLC**	**~ 0.1 – 0.12**
Ban [104]	**Mineral oil (with ZDDP)**	**3 - 36 %Si-DLC**	**~ 0.06 – 0.08**
Lanigan, (section 5.2.1)	**Commercial lubricant (Ca, P, Zn, S containing)**	**14% Si,O-DLC**	**~ 0.09 – 0.1**
Wu [84]	**Water**	**3 – 10 % Si,O-DLC**	**~ 0.06 – 0.09**

A variety of processes occur in lubricated contacts that would explain this loss of enhanced lubricity. These include: general dilution of SiO_x species by the oil, active removal by lubricant additives (dispersants) and formation of a tribofilm that prevents replenishment of SiO_x species. All these factors

therefore allow the friction of all the DLCs tested (both doped and a-C:H) to broadly fall into a similar range when tested in the same oil.

This suggests that the friction in lubricated contacts is actually dictated by the tribofilm or lubricant additives as opposed to the coating. It is likely that both these factors play key roles with regards to the friction. To explore the properties of fully formulated oils more fully, the lubricant package must be examined. Dispersant additives are typically succinimide based and are specifically added to the blend to remove soot and insoluble particles [110]. SiO_x type compounds match this category very well and as such should be actively sequestered from the surface by the lubricant additive, as shown schematically in Figure 9-7.

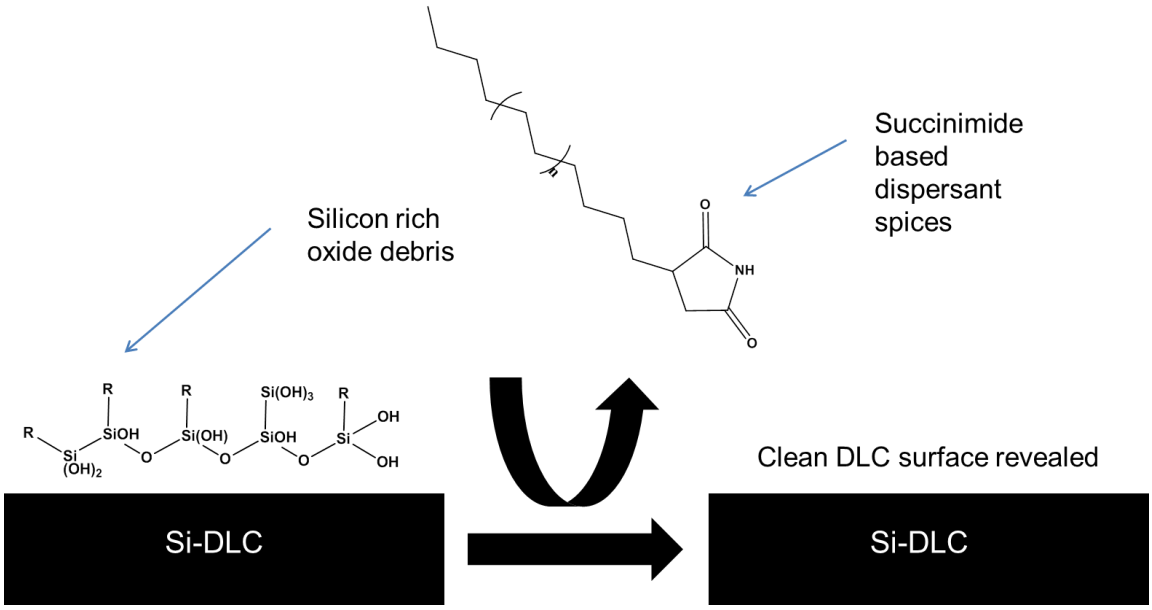

Figure 9-7 Si rich oxide debris being removed by dispersant species

Further to this, fully formulated oils are blended specifically to form protective tribofilms at the contact. These films build upon the native substrate, this effect obscures the substrate as depicted in Figure 9-8. Therefore, any constituent of it that contributes to the friction profile, like SiOx species, would have their effects negated as they are no longer a surface rich speices; being effectively ‘buried’ below the tribofilm. Thick tribofilms that obsure the initial contact surface are well-known and not only limited to

ZDDP films but also occur from reactions of detergent additives [115, 127, 128].

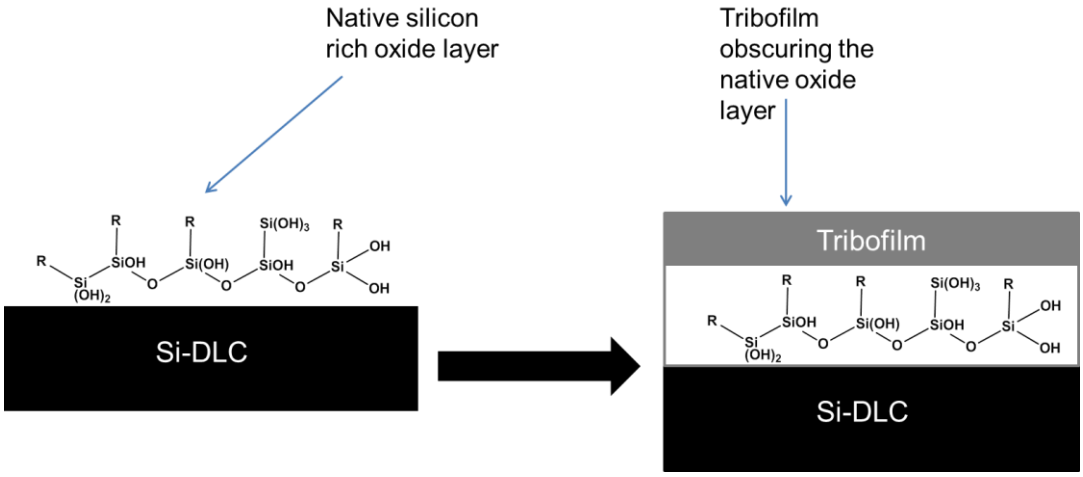

Figure 9-8 Schematic of tribofilm obscuring the native oxide layer

The friction results obtained in the results chapters sections 4.2.6 and 5.2.1 show that in the oils examined, both Si-DLCs exhibit similar friction coefficients to that of a-C:H DLC. In terms of the presence of a tribofilm, XPS and ToF-SIMS data confirms formation of a protective tribofilm on both the low-Si DLC and the a-C:H DLC. The tribofilms are composed of various elements including: Ca, P, Zn and S. Surface analysis results from the DLC suggest that the predominate species by which these elements are included are as Ca phosphate with some pyrophosphates, Zn oxide and some simple sulphides.

Therefore it can be concluded that the formation of the tribofilm inhibits the low friction behaviour that can be observed at dry Si-DLC/steel contacts in a variety of ways. Primarily, mechanically hard tribofilms are known to foster higher coefficients of friction [115, 127, 197]. Further to this, the tribofilm protects the coating from oxidation as apparent from ToF-SIMS mapping of low Si-DLC inside and outside of the worn area. The worn area is richer in the less oxidised form of Si present in the coating. This sharp decline in the rate of oxidation of the Si within the coating therefore equates to a reduction in formation of the Si-O type species. Thus no SiO_x species are formed and

therefore cannot reduce the coefficient of friction. Correspondingly, the friction of the low Si-DLC system rises to a similar level of the a-C:H DLC.

At longer time intervals, the inclusion of the friction modifier species, GMO, does not appear to enhance either DLCs friction performance when compared to the other one, as they show comparable coefficients of friction. This is again accounted for by the formation of a chemically similar tribofilm, the two surfaces have similar tribochemical properties once the films have formed. Therefore GMO will have a similar affinity for the surface, due to the similar surface interactions it will make. It is also possible that GMO is not an effective FM species for this tribocouple, despite showing promise in other DLC/DLC contacts [97, 99, 112].

9.4.3. The dependance of the friction performance of low Si-DLC on oil formulation

As discussed above, oil additives can often dictate the friction regime of certain contacts. This can be achieved by creating a hard, wear resistant layer that increases friction or by the effective use of friction modifier species, like GMO [99, 197]. The friction profiles of the low Si-DLC/steel system when in oil A is compared to oil D in Figure 6-4 . As shown, oil A and oil D give similar coefficients of friction despite being distinctly different oils. The wear profiles however are very different depending on the oil; an overview of wear is explored in more depth in section 9.5. Friction of the system is complicated by these factors:

- The presence of the friction modifier in Oil A
- The possible antagonistic effect on friction of an anti-wear film as produced from Oil A
- The formation of Si-O containing compounds in Oil D (which are inhibited by anti-oxidants in Oil A)
- The presence of a dark transfer layer on the pin that appears to affect friction when tested in Oil D

The absence of a more pronounced difference between the two could be due to the well reported ability of Si-DLC's to self-lubricate when trace water is present, as is inevitable in non-vacuum, laboratory conditions [26]. The presence of both Si and O within the DLC coating allow for formation of, previously discussed, Si-O species and Si-OH species. However, as the friction appears to be the same in oil D as it is for fully formulated oil toward the end of the test duration, this indicates another factor affecting friction reduction for the sample tested in oil D.

Optical examination of the plate and the pins given in Figure 6-5 gives useful information on what happens at the interface tested in oil D. The pin shows a black pad at the point of contact. XPS of this layer identifies the presence of a Si-O type species. This layer is not present on the pin that was tested in fully formulated oil. It would appear that this layer is the reason for reduced friction in oil D and represents a transfer layer from the low Si-DLC that maintains lower friction. Therefore, it would appear that the formation of the transfer film on the counter body for the oil D tested sample does reduce friction and this affect is continued after severe wear of the coating. The transfer layer contains Si-O type moieties as identified by XPS, as explored in section 6.7.2. This species is not observed when the pin tested in formulated oil is examined. Transfer films on self-mated DLC contacts have been shown to positively affect friction by reducing adhesive interactions [198] [199].

Presence of Zn, S and P containing groups on both the DLC and counter body tested in formulated oil confirms the presence of a protective tribofilm. Zn type tribofilms are known to raise friction values; this could explain why the friction is higher than may be expected for a system involving DLC [197].

9.4.4. Friction modifier efficacy

Glycerol mono-oleate, or GMO, was included as the friction modifier in one oil formulation. GMO is known to be an effective friction modifier for certain DLC interfaces [97, 99]. If GMO is an effective friction modifier for the steel/steel system however is not established. GMO is a surface active FM and as such has to adhere directly to either interface through the polar head

group [200, 201]. This allows for the long organic chain to extend outward into the oil and this reduces kinetic friction in the boundary regime by separating the two sliding bodies. This lubrication mechanism is known as the ‘Bowden-Tabor model’ [49, 200]. It could be the case that GMO is actually able to interact in a different, superior way with the ferrous surfaces as explored in Figure 9-9. As GMO has a highly polar head group it is feasible that the increased polarity of the ferrous surfaces could enhance additive adsorption which thus fosters the decrease in friction.

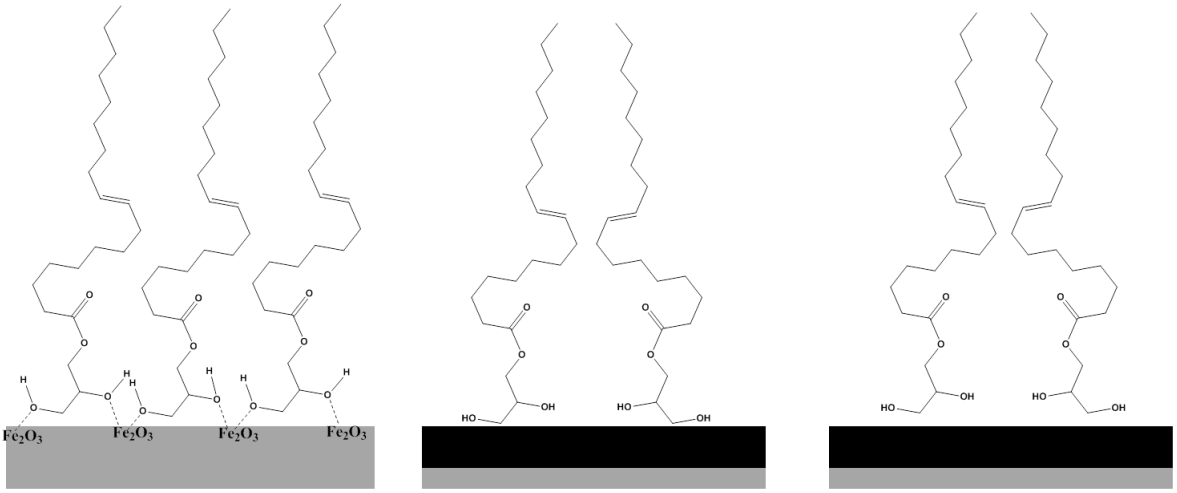

a) Steel surface b) Si-DLC c) a-C:H

Figure 9-9 GMO's potential enhanced surface interaction with a ferrous surface. The iron oxide in a) could co-ordinate with the diol head-group to maximise GMOs adsorption to the surface. This is not possible with the DLC surfaces

Finally, it is also possible that the Fe ion is playing a key role in mediating the friction reduction. Fe ions have been shown to break down esters in tribological contacts, thus creating carboxylates as shown in Figure 9-9 [201].

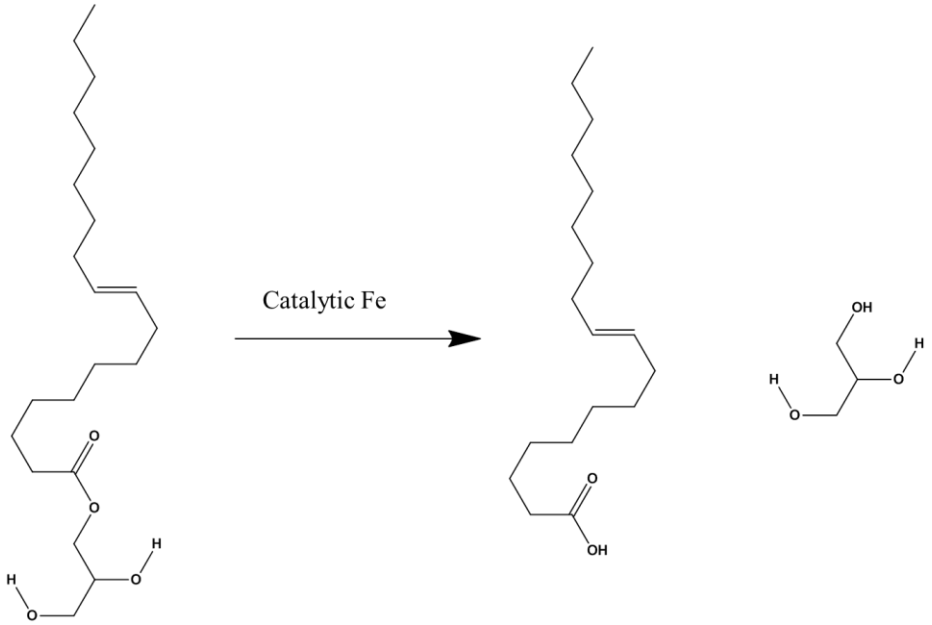

Figure 9-10 Reaction scheme of Lewis acid (Fe ion) catalysed degradation of the ester moiety in GMO

These species have superior adherance to the ferrous bodies when compared to alcohols [201]. This superior adhereance could well result in a superior friction profile. Conversely, it has been shown that GMO interacts with DLC (when at a steel/DLC interface) via the ester group and that this can give very low coefficients of friction [112]. Due to the differences between a steel and a DLC surface it is likely that the mechanism via which GMO is adsobred to the DLC depends on terminal –OH groups. These groups on the DLCs surface would be able to form strong hydrogen bonds with the diol groups.

Friction values for all the DLCs tested were slightly higher than the steel surface in oil A. DLC surfaces when sliding against DLC counter bodies typically show lower friction than this [27, 68, 70]. Oils A and B used in these experiments are designed for optimum use within a ferrous system, as typically found in car engines. As such the lubricant blend has not been tailored toward the different parameters assocaited with a DLC surface. It is highly likely that these friction values could be improved with further modificiation of the lubricant package. Inclusion of the organic friction modifier, GMO, which has been reported to work well with DLCs is a good starting point [99].

9.4.5. Surface active species

GMO is not the only surface active species inlcuded in the lubricant blend. Detergent additives are also known to be surface active and can form tribofilms under certain contiditions [127, 128]. The lubricant package used here has a Ca based detergent included. It would appear that in some cases there is competition between GMO and the detergent for surface space. This competion for surface space has been noted previously with ZDDP and other surface active additives [197, 202]. The low-Si DLC's friction performance is actually slightly improved when GMO is excluded from the lubricant blend as shown in Figure 4-10. It appears there is competiton for surface space between two additives in Oil A with regards to the low-Si DLC surface.The a-C:H DLC shows friction coefficients within error of each other for either oil. This therefore shows no preference for oil in terms of performance.

Detergents interact with polar surfaces as they have charged head groups and long-hydrophobic tails; this makes them very similar to FM species. The detergent in this case is actually more polar than GMO which explains its affinity for the Si-DLC. This effect has been observed before where a Ca based detergent was able to form tribofilms and affect friction on steel and DLC films [128]. The detergent used herein could have the ability to reduce friction however; it would do this in a markedly different way to GMO, through a different bonding mechanism.

XPS analysis confirms the presence of Ca early into the testing for the low Si-DLC when tested in oil B. The Ca cation present is brought to the surface from the detergent species. It is proposed that the difference in the head groups of the friction modifier and detergent species tested herein plays a key role in determining the friction of the system. The differing surface activities causes the inversion of predicted friction data for the Si coating, whereby Oil B shows the best friction profile.

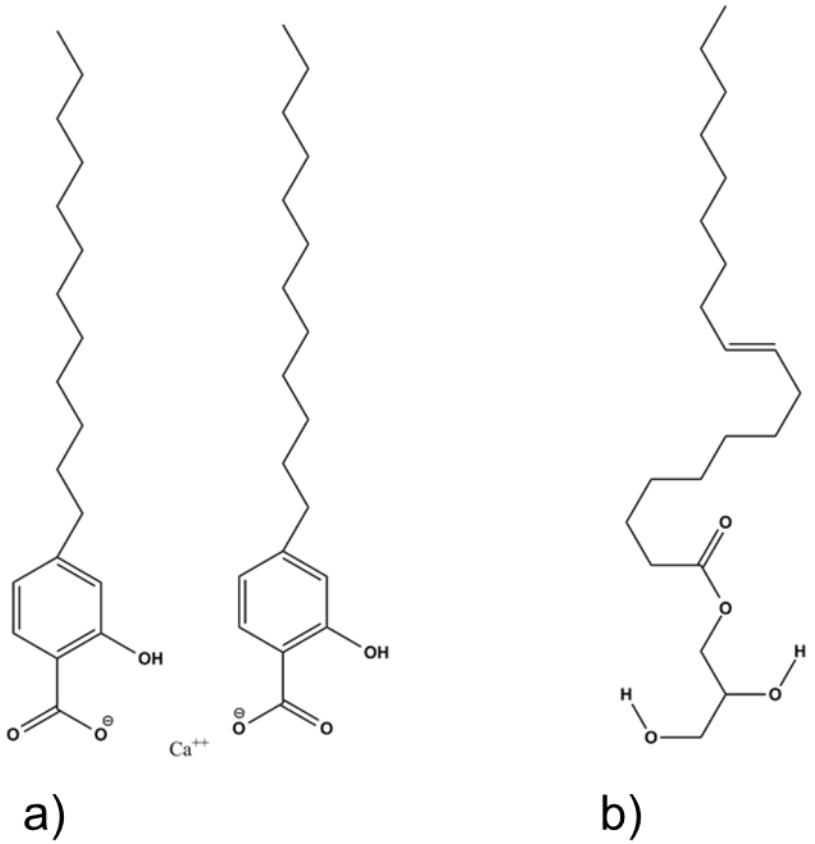

Figure 9-11 Detergent type molecules a) compared with GMO b). The charged carboxylate head groups on the detergent molecule allow it to adhere more strongly to a polar surface (when not in a micelle).

This can be shown from the XPS data which indicates that when Oil A is tested with low Si-DLC there is a greater inclusion of C, but a decrease in Ca. This clearly indicates GMO is competing with the Ca containing detergent molecule for surface space at the interface. This also results in greatly diminished phosphorus and Zn signals for the DLC when tested with FM containing oil.

The mechanism by which this competition occurs would appear to be from GMO physically preventing build-up of a ZDDP type tribofilm at the low Si-DLC surface. GMO takes up surface space at the contact and retards film growth as shown in Figure 9-12.

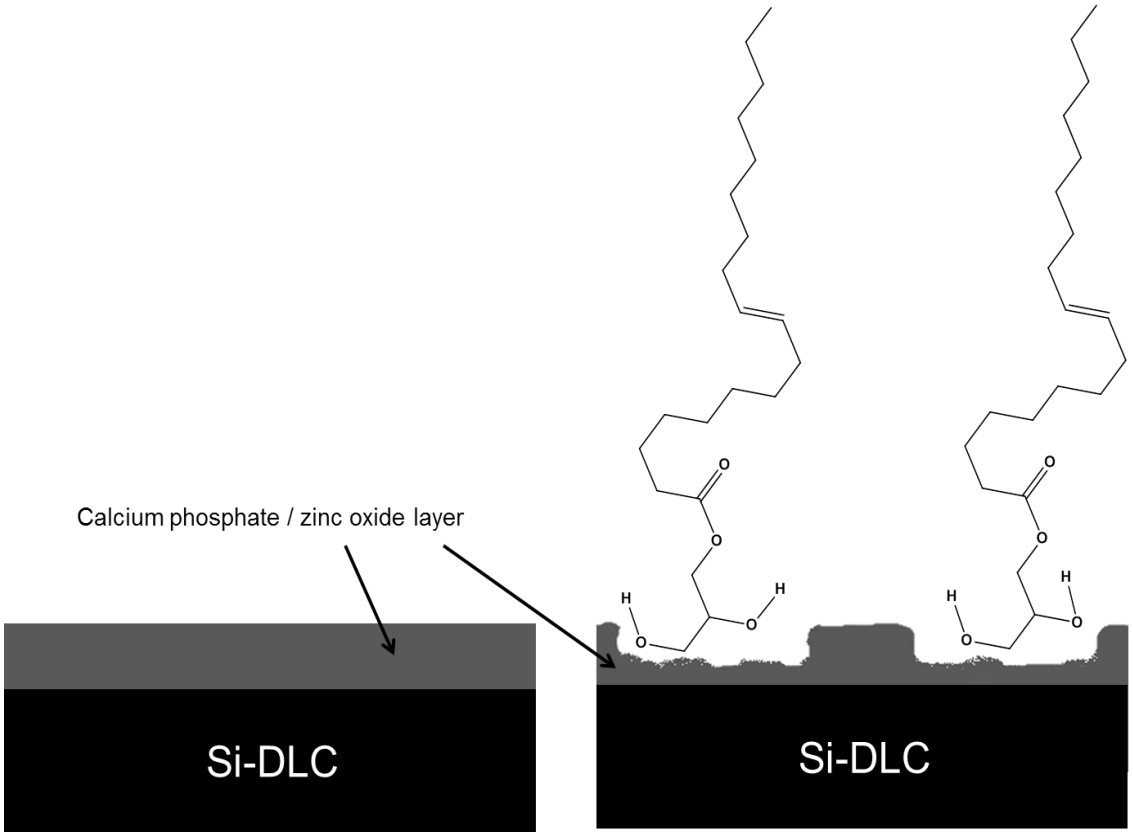

Figure 9-12 Schematic of the interactions GMO has with the tribofilms. GMO occupies sites at the surface, preventing full build-up of an effective tribofilms. Additional inclusion of GMO equates to a loss of Ca, P and Zn.

This type of surface competition has been seen before at steel/steel interfaces with organic friction modifiers [197, 202]. Taylor and Spikes [197] note that regardless of the additive, whether it be a detergent, friction modifier or dispersant; the film thickness when compared with ZDDP alone is always thinner [197]. This is shown in Figure 9-13.

Although this may initially seem like a negative consequence of inclusion of the friction modifier, this could actually be beneficial as it allows greater understanding of what processes take place at the interface. The low Si-DLC clearly has an increased affinity for charged head groups, as found in detergents.

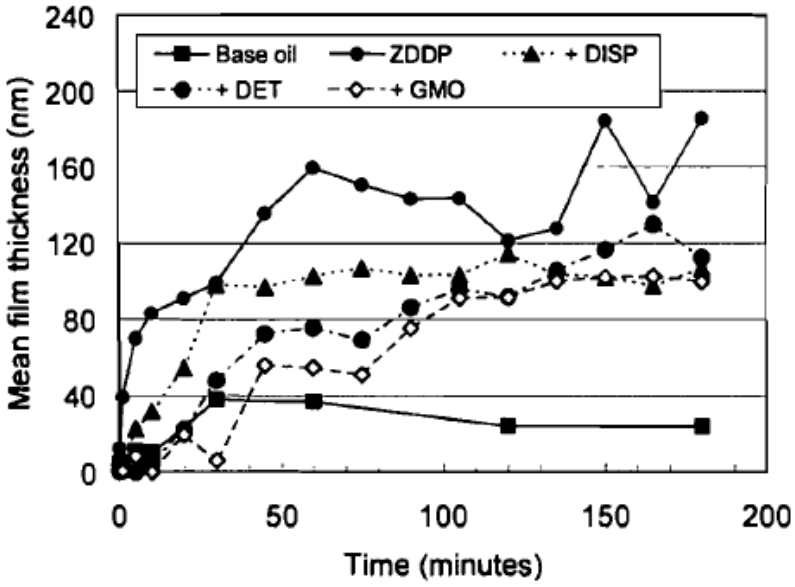

Figure 9-13 Effect of ZDDP film thickness by oil additives [197]

This knowledge could be used to devise new FMs specifically for low Si-doped DLCs. The competition for surface space between surface active species is also not a negative in and of itself. Even if the FM species can out-compete tribofilm forming additives like ZDDP, due to DLCs innate low-wear nature, the friction reduction that could be afforded could well out-weight the penalty of increased wear in some instances.

When comparing the XPS data from the a-C:H and low Si-doped DLCs, the difference in species identified in the worn area is quite noticeable. The a-C:H sample only appears to accrue Ca in the worn area by the two hour interval as illustrated in Figure 9-14.

9.4.6. Self-mated friction

When comparing the friction profiles of the steel/steel tribopair and the low Si-DLC/Si-DLC tribopair the results are notably different. Initially, the friction of the steel/steel system is low but as the experiment approaches the half-way point the friction sharply increases.

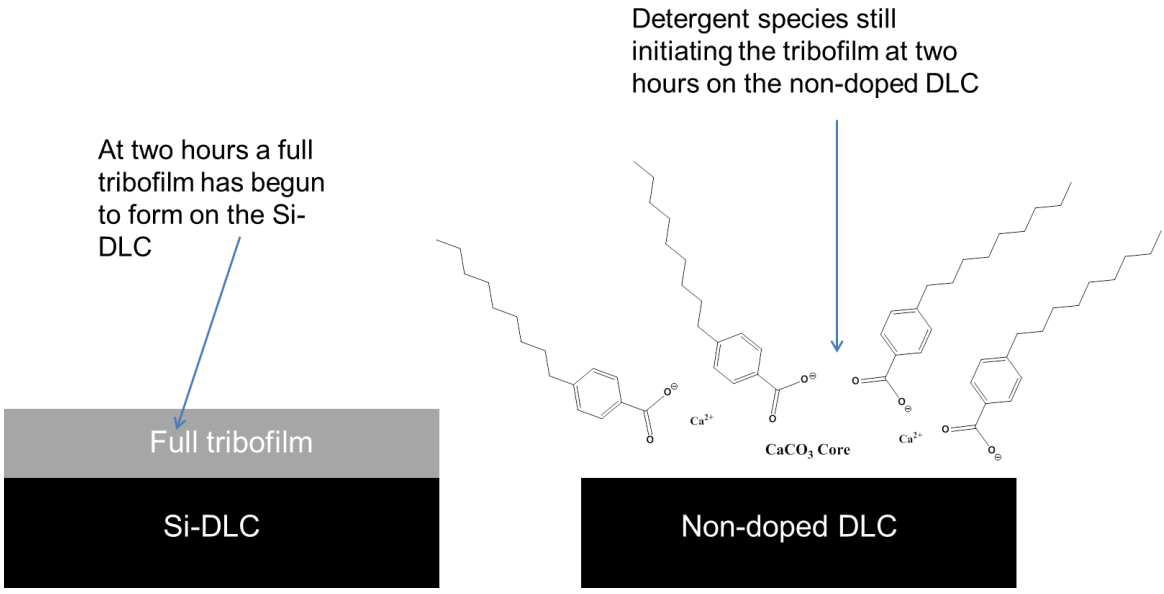

Figure 9-14 Tribofilms at two hours compared. At two hours there is a fuller tribofilm on the Si-doped sample consisting of Ca,P and Zn. Whereas, the a-C:H sample only contains Ca.

Conversely, no change outside of standard deviation in friction coefficient is detected for the low Si-DLC tribopair. This friction behaviour could be the product of various phenomena. However, with the parameters of the experiment known, the most likely explanation is formation of a high-friction tribofilm on both surfaces. XPS analysis demonstrates that this is indeed what is happening at the surface. At all times measured, the low Si-DLC tribopair exhibits a far lower friction value than the steel tribopair. During the running in period the low Si-DLC's friction coefficient is approximately half the value of the steel tribopair, at steady state the low Si-DLC continues to outperform the steel/steel contact.

The friction for the steel/steel system follows predictable trends, lower running in friction prior to full formation of a Ca/ZDDP tribofilm [197]. The lower initial friction is due to the fact that the mechanically harder Ca/ZDDP film has not yet fully formed. Upon its complete formation the friction of the system increases, this is especially noticeable at the steel/steel interface. The friction for the low Si-DLC tribopair shows the expected low friction of a DLC coating [41, 68, 70, 97, 98]. The two surfaces are designed to be low friction when self-mated, prior to tribofilm formation. The main mechanism

for this is that the majority of the sliding surfaces are C-H terminated and these surface sliding against each other do not form many strong interfacial interactions. A key role is also played by –OH terminated surfaces on the DLCs which help facilitate lower friction [68, 70, 99]. The steel/steel tribopair experiences more surface interactions which equates to higher friction, as the surfaces adhere more strongly, due to the metal oxide layer ever-present on steel surfaces.

Steady state friction is constant and higher at the steel/steel interface due to formation of a tenacious tribofilm on the surfaces. Tribofilms in the steel/steel systems are known to be on the order of 50- 100 nm thick and are also known to negatively affect friction [115, 197]. The tribofilm on the low Si-DLC tribopair is far thinner, as observed from the large C and Si signals originating from the DLC still being present in the XPS spectra, suggesting a thickness of less than 10 nm [137]. The difference in tribofilm thickness could be key to the differing friction behaviours.

The key role of Si oxides in reducing friction at Si-DLC/Si-DLC interfaces is well reported within the literature [26, 77, 113]. This beneficial relationship again disappears at the Si-DLC/Si-DLC contact under oil lubrication. Data presented in section 7.2.4 (where surface modified of low Si-DLC is explored) helps to elucidate why this relationship is not maintained in lubricated conditions. Figure 9-15 shows how –OH groups are eliminated from the interface by silinizaton.

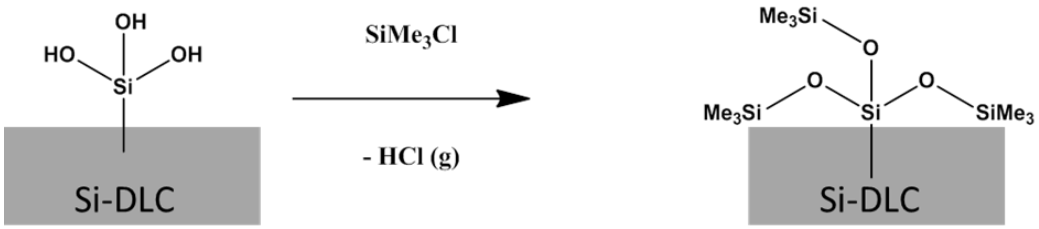

Figure 9-15 'Capping' of free -OH groups on the Si-DLC surface. Me represents the methyl, or CH_3 group.

As there is a relatively small change in the initial friction values, it can be shown that the SiO_x species do not play the dominant role in lubricated

friction of Si-DLCs. If the SiO_x species were playing a dominant role it would be expected that silanization of the surface would alter the friction profile in some way. This is because the SiO_x species are highly polar and incorporate many –OH functionalities onto the low Si-DLCs surface. Surface –OH groups are known to afford reduction in friction at DLC interfaces [98, 99, 111]. Even when the free –OH groups are capped with organic, non-polar, groups the friction values of the system are not drastically altered as shown in Figure 7-9. With the effect of the Si-OH species shielded from the interface they can no longer contribute to the friction profile. However, the friction data remains unchanged even after this modification. This therefore confirms that in a lubricated contact the role of surface oxides on Si-DLC's friction performance is very minor. In other work, salinization of Si-DLCs has been shown to improve friction performance by virtue of increasing hydrophobicity, however these test were conducted without lubricant [95].

9.5. **Wear of the systems**

The process of wear is a complex one that involves many different mechanisms and influential factors. As such, it seemed important to get a good overview of the wear profile of the main system examined by conducting wear tests at different times. This would allow for running-in wear to occur and a tribofilm to be formed. This then can be used to assess if the running-in wear is mitigated by the formation of a tenacious tribofilm later in the testing that drastically reduces wear rates. This data can later be compared to very long duration testing, as conducted in an engine. Despite the experimental conditions being different between the two, it will still give useful data of the lifetime wear performance of the two main DLCs examined.

9.5.1. Wear analysis from short and long duration tests

As expected, both Si-DLCs had far higher wear rates than that of the a-C:H sample at the initial testing interval. This phenomena is consistently observed in the literature [77, 79, 104, 105, 113, 114]. Also observed is that increasing per cent Si atomic concentration of the coating results in

increased wear rates, this behaviour is also widely noted [77, 84, 104]. The role Si and Si oxides play in the enhanced wear of Si-DLCs has been previously detailed [43]. The a-C:H DLC shows no measurable wear in either oil (A or B) at the two hour interval. In part, this is one of the motivations for long duration tribotesting of the DLCs. Also, the ability of the low Si-DLC to form a thick tribofilm warranted further investigation. This thicker film could result in lower wear by the test end when compared to a-C:H DLC. It must be noted that the steel/steel tribopair has the highest wear of all the contacts and that, in all cases; the DLCs outperform steel in terms of wear performance.

Wear profiles of the low Si-DLC and the a-C:H DLC over longer testing in Oil A show some differences. Initially the low Si-DLC has a constant wear rate, between two and five hours as shown on page 98, section 5.2.2. It would appear that this is the time interval during which the tribofilm is forming. After this period, the wear rate drops.

For the a-C:H DLC there is a sharp drop in wear rate between the first instance of measurable wear (seven hours) and the next (fourteen hours). This indicates that the a-C:H DLC is not only inherently more wear resistant than the low Si-DLC, but also that it is able to form an effective tribofilm once wear has occurred. Conversely the low Si-DLC appears to require an ‘activation time’ as shown in Figure 5-4. The wear rate remains steady between the two and seven hour mark, despite the presence of calcium phosphate which is known to reduce wear [176, 177]. After this period the wear rate drops. Time-resolved XPS data explains this trend well. Initially the tribofilms on either DLC are rich in Ca and have less phosphorous, negligible amounts of Zn and no sulphur. It is known that phosphates and polyphosphate glass play a crucial role in wear reduction so it follows that whilst the phosphorous containing layer is still being formed wear is correspondingly higher [115, 176, 177]. Ca based detergents are known to act in an anti-wear fashion at steel/steel interfaces but the wear impeding ability of this type of film does not match ZDDP [127].

It becomes apparent that the manufacturer’s design of each coatings allows for the differing wear profiles, with the low Si-DLC being 1 µm thicker than

the a-C:H sample, this means the greater running-in wear does not jeopardise the coating's overall lifetime with respect to wear. The coatings behave very similarly with regards to species formed in the worn area, the only difference being that the low Si-DLC incorporates more tribologically relevant species (P, Zn) at a faster rate, a feature perhaps due to its enhanced wear.

The type of Ca ZDDP film seen on both coatings is well documented and it appears that, without an abundance of Fe ions as would be present in the traditional steel/steel system Ca plays an even more important role in the oil. Ca replaces Zn in the phosphate glass network [147, 176, 177]. The exchange of Ca and Zn between ZDDP and the detergent molecules that occurs at the interface cannot be instantaneous as it depends on the detergent species encountering the surface and then going on to react with ZDDP. Thus, at the initial stages of the experiment the low Si-DLC undergoes a higher rate of wear while the Ca phosphate/pyrophosphate layer forms. The mechanism of this film formation is explored in more detail below. Mechanically the low Si-DLC coating is not as hard as the a-C:H coating, as well as being more prone to oxidative wear than the a-C:H coating. As such it is less able to resist wear without formation of a tribofilm. Zn type additives are known to have a time-dependence with regards to the build-up of the tribofilm [115, 203]. With the large drop in wear after the seven hour mark for the low Si-DLC it becomes apparent that a similar time-dependant mechanism is operating here.

9.5.2. Fully-fired engine wear test results

The wear relationship elucidated above for the low Si-DLC and the a-C:H DLC appears to be maintained when tested in a fully fired engine for 300 hours. The a-C:H DLC has lower wear than the low Si-DLC coating by the end of the testing. Wear of both DLC-coated mated parts is far lower than the steel/steel tribo-couple. This affirms that both DLCs do indeed reduce wear within a fully-fired engine. The tappet coated in the low Si-DLC is higher than the a-C:H DLC coated tappet by the end of testing. This verifies that incorporation of 14% Si increases overall wear of the coating which is in line with similar findings in the literature and within this project [84]. This then

confirms that Si-DLCs have innately higher wear when compared to a-C:H DLCs, and that this is conserved even in fully-formulated oil in a fired engine.

9.5.3. Coating hardness in the worn area

ZDDP films are known to produce hard films in the worn area that effectively resist wear [115]. Due to this well-known behaviour nanoindentation experiments were conducted on the worn DLCs, the data shows that, despite the formation of a thicker tribofilm in the case of the low Si-DLC; neither of the anti-wear films produced appear to increase measured hardness of the area. Typically, ZDDP films on steel/steel contacts can grow to 100 nanometres in depth and create a hard, physically protective film [115]. It would appear that this is not the mechanism of protection for the DLC films examined herein; as no improvement in surface hardness is observed. Due to the thin nature of the tribofilms formed it is extremely difficult to deconvolute the contribution of the coating from that of the film [204]. However, it appears that the main mechanism of protection from ZDDP in this instance is by the formation of a tenacious, chemically resistant tribofilm; as opposed to a thick, mechanically-hard layer. There are changes associated in the measurements of the a-C:H coating whereby the error appears reduced as time progresses. It is probable that polishing wear has occurred and is the reason for this decrease in error. Polishing a surface is known to improve the accuracy of nanoindentation values, as surface asperities can influence data points for this type of measurement [182].

9.6. Tribochemistry

9.6.1. Tribofilm composition

Time resolved XPS analysis sheds light on the growth of the tribofilm and helps elucidate the structure of the film. Analysis of the surfaces can be combined with knowledge of the lubricant blend and fundamentals of tribology to gain a fuller understanding of what is happening at the interface.

As certain parts of the oil's composition are known, specifically that the phosphorous content is solely accounted for by ZDDP in the oil. This means that the Ca phosphate/pyrophosphate novel species must be formed as a result of the tribo-contact. The phosphorous therefore must be sequestered from the ZDDP and combined with Ca at the surface to create the tribolayer observed, behaviour often seen in steel/steel systems [176, 177, 205]. This leaves Zn and S available to react with any other molecules present, leading to the formation of metal oxides and sulphides.

With the low Si-DLC, high-resolution spectra of the C peak window at the 35 hour point shows evolution of a third peak at a higher eV value. This suggests further build-up of detergent molecules on the upper surface of the tribofilm. This would therefore suggest that at the thirty five hour mark the tribofilm is indeed fully formed as no more $CaCO_3$ from the detergent core goes on to react with ZDDP, but instead forms a deposit on the top of the tribofilm. This behaviour of a tribofilm reaching its maximum thickness and plateauing has been seen before, as noted in the work by Spikes [115] shown below in Figure 9-16. The ability of ZDDP to prevent oxidation is a well-known phenomenon, as given in Figure 9-17. This appears to be key to reduction of wear with the low Si-DLC contact.

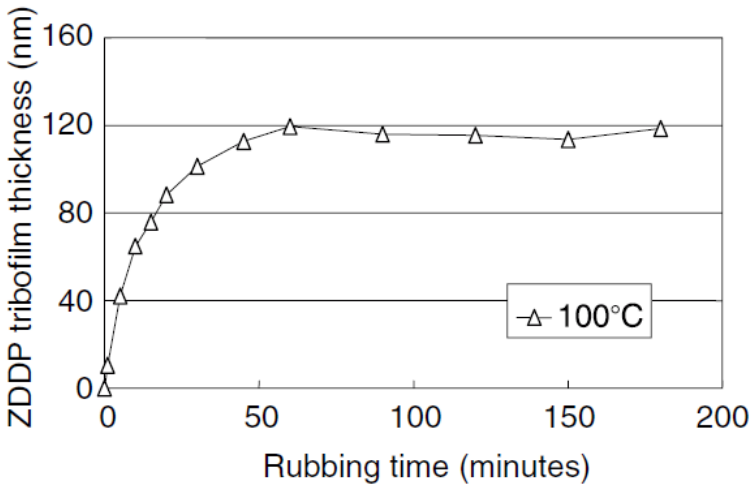

Figure 9-16 ZDDP reaches a maximum thickness after approximately 50 minutes [115]

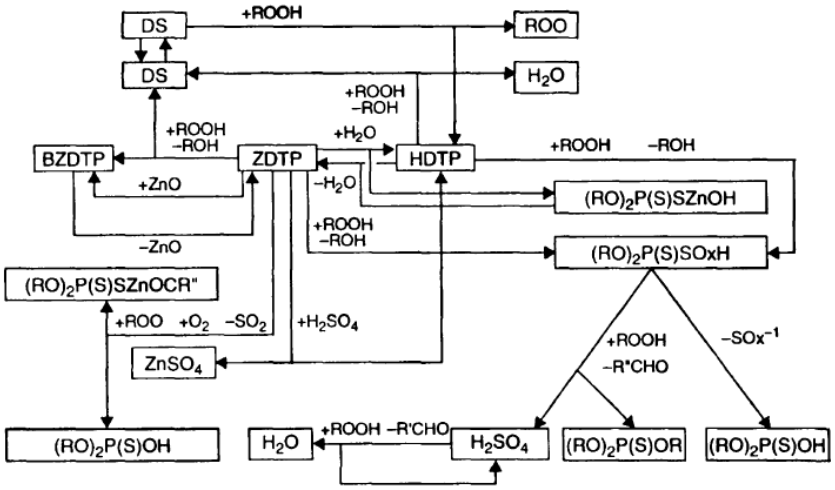

Figure 9-17 Schematic of ZDDPs anti-oxidant reactions [115]

XPS analysis of the steel counter bodies paired with either DLC plate were obtained. Both pins show strong evidence for formation of a Ca phosphate type anti-wear film, as expected in this system [176, 177]. When comparing the pin and the plate some differences are noted. All species that are present are incorporated onto the steel at a larger per cent atomic concentration than on the either DLCs, possibly due to enhanced surface wettability; facilitating a more fully-developed tribofilm. The XPS binding eV for FeS_2 and ZnS have closely matched values of 162.8 and 162.6 eV respectively; as such it is difficult to accurately attribute which metal sulphide is presence on which surface. However, stoichiometry dictates that it is most likely a combination of both the sulphides. This is because in the ZDDP molecule as given in Figure 9-21, contains more than double the atomic concentration of S when compared to Zn.

Differences are to be expected between DLC surfaces and ferrous ones as the presence of Fe should enhance the formation of a ZDDP type film. The film forming behaviour of ZDDP is well known when examining steel surfaces under this type of lubrication [147, 206-208]. The acceleration of tribofilm formation is due to the labile nature of the dithiophosphate ligand which readily undergoes ligand exchange, swapping Zn^{2+} for Fe^{3+} [115, 209]. This new MDDP (M = Fe) complex is less thermally stable and therefore allows faster reactions [115].

It would appear that for both DLCs examined Ca is playing a key role whereby it effectively replaces not only Zn, as seen previously in the literature, but also iron [176, 177]. This then facilitates formation of a tribofilm without the presence of a ferrous body (despite the fact that there is one in this instance). Tribofilms are present on both the DLCs and both of these show time dependencies.

There is little stronger evidence for the formation of a polyphosphate film, as depicted in

Figure 9-18, which are often associated with ZDDP. As the oil package contains both ZDDP and a Ca based detergent it is unlikely that a polyphosphate glass has formed, although it cannot be ruled out. What is most likely when considering the additives used (specifically ZDDP with a source of Ca) is the formation of shorter chain, pyrophosphates, and Ca phosphate [176, 177]. Both of which have been confirmed by XPS and SIMS analysis.

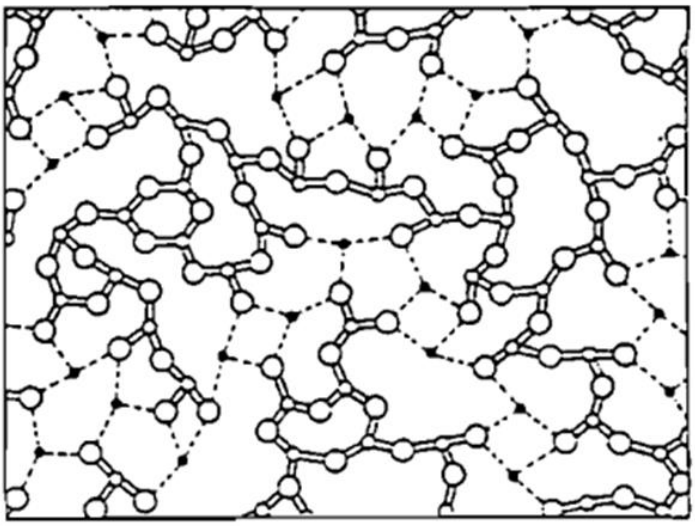

○ oxygen atoms,
○ glass "former" cations (P, S),
● "modifier" cations (Fe, Zn),
solid lines: covalent bonds,
dotted lines: ionic bonds.

Figure 9-18 Schematic of polyphosphate glass from [210]

Glassy phosphate films are some-what hard to accurately characterise as the repeating P-O unit that makes up the backbone of the glass is also present in phosphates and similar moieties that are more likely candidates when examining certain tribolayers [147]. Further to this, as the lubricant package has a Ca based detergent the likelihood of a glassy phosphate film occurring decreases as Ca promotes the formation of the phosphate anion and shorter chain polyphosphates. The $Ca_xPO^y_n$ species are able to afford wear protection to the coating, however literature on the topic indicates that they are not as effective at doing so as the Zn polyphosphate glass [211, 212].

All DLC films represents a hard, physically protective layer. It would seem that a thick, mechanically hard tribofilm is unnecessary for the DLCs tested to effectively resist wear; a conclusion drawn from the lack of any great increase in surface hardness upon tribotesting. Although admittedly, it is difficult to extract nanohardness data from films as thin as the ones examined [204, 213]. The main mechanism of wear, as discussed previously appears to be from atomic-scale chemical processes, namely systematic oxidation of the coatings constituents [36, 37, 214]. This systemic oxidation is somewhat inevitable as thermodynamic driving forces tend to constantly push most carbonaceous systems to form the more stable oxides where possible. Since the role of oxygen in the wear processes of DLCs is a major factor, ZDDP can (and indeed already is) be used as an anti-wear additive for DLC/steel contacts. However, it could be argued that the main mechanism by which ZDDP inhibits wear at the DLC side of the interface is via anti-oxidant activity. This is not to say that there is no scope for further lubricant optimisation. More tailored lubricant additives for DLC's specific wear profile could be developed, perhaps blended to include additional organic anti-oxidants.

9.6.2. Engine test-derived tribofilms

The tendency of Si-DLC films to produce Si rich oxides is well reported, as explored in Table 2-4. This trend is maintained when tested in a fully-fired engine as well. The harsher oxidative conditions of an engine, due to the

presence of oxygen radicals and reactive gases, could explain the higher wear rate the low Si-doped coating has when compared to the a-C:H coating. In comparison the a-C:H coating will undergo oxidation less easily as, thermodynamically; C is less amenable to spontaneous oxidation than Si. The Si-rich oxide species have, in some cases, been accredited with reducing friction [25, 26, 76-80]. To an extent, formation of these could possibly be looked upon as a positive event, if the overall wear was lower.

It is notable that, despite engine testing being carried out for several hundred hours, there are not more elements within the worn area of either DLC as examined by XPS. ToF-SIMS data however expands on this showing a similar tribofilm is present on the tappets as is found from bench testing. Both include elements crucial to wear-reduction: Zn, S and P. Phosphorus is incorporated into the tribofilm as the phosphate group; this is significant as phosphate groups are a key part of the anti-wear film produced by ZDDP in steel systems. A similar chemical make-up to the classical ZDDP-steel film should result in enhanced wear protection [115]. When compiling XPS and SIMS data, it is possible to conclude that a very thin (less than 10 nm) tribofilm is present on both tappets. The film is made of Ca, P, S and Zn with P present as the phosphate in both films. The difficulty of analysing the film with XPS, before and after etching shows that the film is too thin for a strong response from XPS. These type of nanometre thin tribofilms have been found in similar engine tested DLC components [215].

9.6.3. Comparison with bench test results

Despite confounding factors such as different contact pressures (0.1 GPa for steel/DLC pin-on-plate tribometer, 1.5 GPa for DLC/DLC pin-on-disc) the major difference between the tribofilms produced from the engine testing appears to be the intensity and concentration of elements in the film. Bench top tribometers have, herein, given good responses to XPS. This suggests they have thick tribofilms in excess of tens of nanometres [137, 138]. These results are in-line with similar literature findings of engine tested DLC parts, having 2-3 nm thick tribofilms present [215]. The lower response from the engine tested components by XPS suggests a far thinner tribofilm is present. This does not appear to influence the ability of the film to repress wear, as

proven by the complete survival of the a-C:H coating after 300 hours testing. The reason for the thicker films on the tribometer tested samples would appear to be the ideal conditions allowed for with tribometers, specifically the nature of the point contact allowing for continued tribocontact in one well-defined area. This allows for good build-up of species of interest. When compared to the real conditions associated with the engine, far less ideal conditions are encountered as shown by the large worn area of the low Si-doped tappet.

9.6.4. Differences in tribofilms on low Si-DLC *versus* a-C:H DLC

The main difference observed between the two DLCs tribofilms is that the low Si-DLC is able to produce a thicker tribofilm as verified by ToF-SIMS etching and from observing wear scar cross sections using TEM. The most probable explanation of this is that the thickness of these tribofilms is dependent on surface wettability. Steel is known to form thick tribofilms (on the scale of 100 nms) and has a high surface wettability due to the oxide layer on the surface [216]. The low Si-DLC has greater wettability when compared to a-C:H DLC. Enhanced surface wettability would appear to allow for larger build-up of surface active species including detergents and friction modifiers, shown schematically in Figure 9-19.

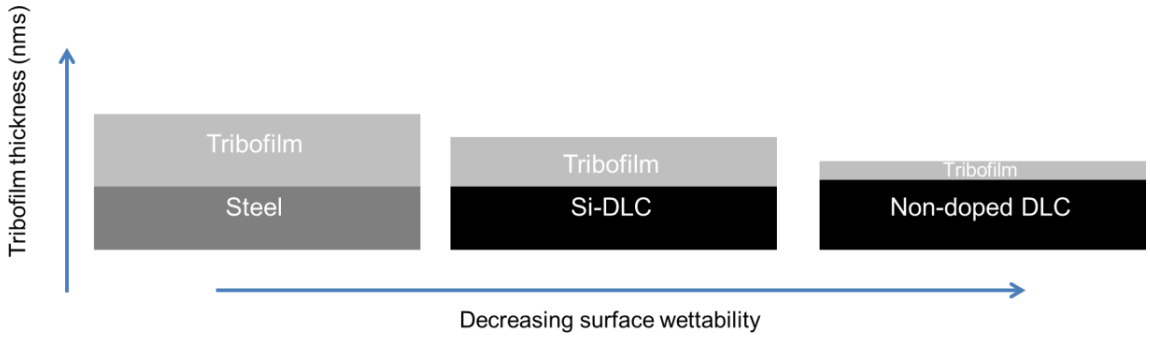

Figure 9-19 Possible relationship between surface wettability and tribofilm thickness

9.6.5. Proposed tribofilm mechanism

It appears that initiation of the two tribofilms is carried out by the over-based detergent species. This conclusion can be drawn from the observation that on the a-C:H coating, at the two hour time interval the tribolayer is made-up almost exclusively of a $CaCO_3$ species. The a-C:H coating appears to have very similar tribochemistry as the Si-DLC, but with a slower onset of formation. As such, it is taken as a model for the initiation of the tribofilm. Knowledge of the lubricant blend helps elucidate the process; detergent species are initially more surface active than ZDDP due to 'forced coalescence'.

This is depicted in Figure 9-20 and helps to explain the film forming mechanism [127]. Further to this, over-based detergents have been shown to produce CaO species at steel/DLC interfaces [128]. CaO is a highly reactive species, and therefore a highly viable candidate as a tribochemical initiator molecule [128]. Combining these factors, the initiation of the tribofilm would seem to begin with detergent micelles encountering the DLC surface and then releasing $CaCO_3$. Over-based Ca detergent micelles encounter the surface and rupture releasing $CaCO_3$. This then allows for formation of a more reactive form of Ca,· the oxide. This process, evolution of CaO from CaO_3 is known as calcination [217]. Simultaneously, a build-up of carbon-rich surfactant molecules that previously encased the carbonate core occurs [128]. The detergent is the prime candidate for the initiation of the tribofilm as surfactant species require no activation period and are effective within a wide temperature range [218]. In addition to this CaO itself, when formed is a very reactive species [219].

A. Step A shows the DLC prior to film formation
B. Step B shows the product of forced coalescence of the detergent micelle onto the DLC surface, with the detergent micelle core being revealed
C. Step C shows the augmentation of the tribofilm with other oil additives

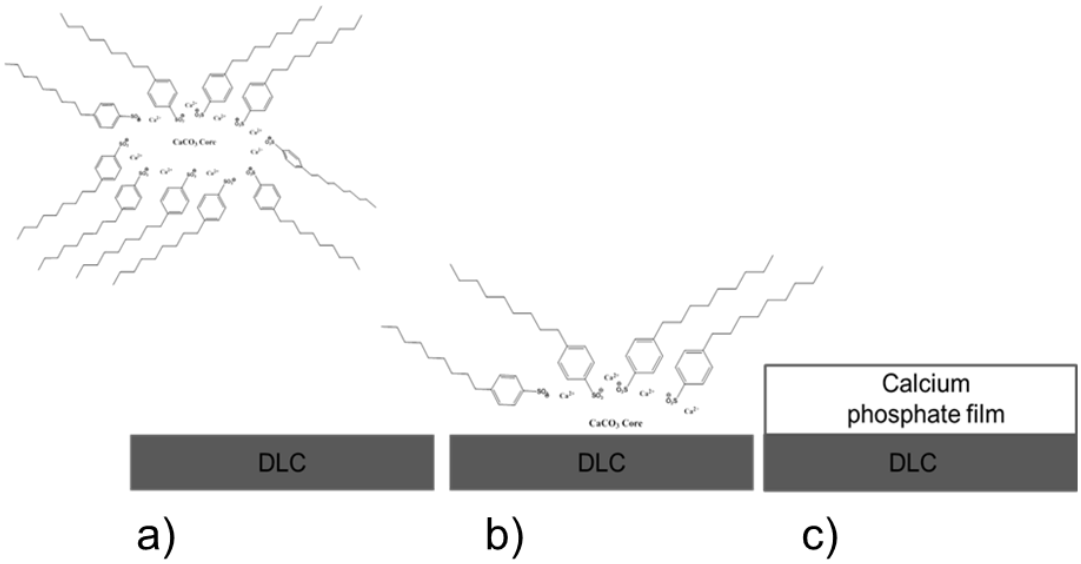

Figure 9-20 Initiation of the tribofilm formation by the detergent in a tri-step process.

ZDDP itself is not a polar molecule (a property that is partially reliant on the organic group chain length). It is soluble in oil without the need for a micelle type solubilising solution. Nor is it immediately surface active. Therefore the conclusion can be made that after film initiation by the detergent species, this allows further chemical reactions with ZDDP.

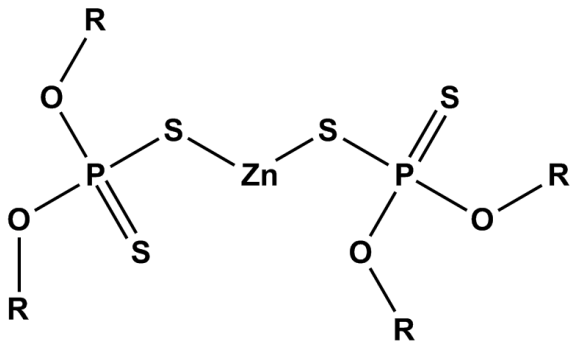

Figure 9-21 Structural formula of ZDDP with R denoting variable organic side chains

The reactive Ca species is then able to initiate formation of the more effective wear-resistant, tenacious tribofilm. A reaction between ZDDP and the Ca species occurs to generate a Ca and PO_3 type tribofilm, this is in line with known behaviour of these systems as well as chemical thermodynamics [177]. These species include the PO^3 anion and similar oxides, evidence also indicates inclusion of pyro-phosphates.

Zn and S species are then activated toward reaction with the surface due to the loss of P from ZDDP. XPS and SIMS are inconclusive about the exact nature of the species produced. It is probable that there is a mix of both ZnS and ZnO. Stoichiometry dictates that ZDDP contains an excess of S to exclude sole formation of the metal sulphide. Therefore some HS^- type species are also expected, this is confirmed by ToF-SIMS.

Toward the end of the experimental duration the atomic concentration of Ca appears to increase sharply. This is indicative of build-up of more detergent molecules on top of the already established tribofilm. High-resolution C peak fitting also supports this with a new peak apparent for the carbonate, as shown in Figure 5-8. This suggests the detergent micelles are still encountering the interface and rupturing but are no longer reacting with ZDDP at this stage.

There are some differences between XPS and ToF-SIMS data as can be expected with any differing analytical techniques. ToF-SIMS is a highly sensitive technique that can detect down to one atomic layer; as such it is more sensitive than XPS and can detect species that XPS would not [137]. This suggests that some species are present in minute amounts within the tribofilms and in some cases can only be detected by ToF-SIMS.

9.7. **Resolving oxidative wear of Si-DLCs**

9.7.1. Mechanism of enhanced wear of Si-DLC

Many authors have noted the tendency of Si-DLCs to wear at a far higher rate than a-C:H DLCs [76, 77, 79, 84, 104, 113, 114]. A novel insight into the wear processes of Si-DLC is explored here. The findings of which were

disseminated in the paper associated with this work, the details of which are given in the preface. Due to the large difference in wear when comparing the low Si-DLC in Oils A and D it is demonstrable that Si, O-DLC shows high dependency on oil formulation. Oil D (the low additive oil) contains no anti-wear or anti-oxidant additives whereas Oil A can be regarded as rich in these compounds. Well-established chemical thermodynamics can help to illustrate the wear process occurring at the DLC interface.

There is a large bond dissociation energy, 798 kJ mol^{-1} associated with the O-Si bond. This is indicative of how strong the bond that forms is and the thermodynamic driving force for its production. When Si is incorporated to the DLC matrix it can only make certain bonds as listed in Table 9-3. These are: Si-H, Si-Si, Si-O and Si-C bonds. The oxidation of C-Si and Si-H bonds are thermodynamically favourable and as such can proceed via oxidation from atmospheric species [83, 220].

Table 9-3 Dissociation energy of key bonds

Bond	Dissociation Energy (kJ/mol) [46]
H-Si	**298**
H-C	**337**
C-O	**377**
C-Si	**435**
O-Si	**798**

Oil additives like ZDDP and similar compounds are able to inhibit oxidation [115]. They do this by themselves being oxidised. It is interesting to note the large build-up of PO_3 and SO_2 in the worn area, indicative of oxidation of sulphur and phosphorous compounds. The area they accrue in corresponds to the worn area on the chemical map where highly oxidised Si species are lacking. Preferential oxidation has taken place, protecting the Si-DLC from further oxidative wear.

As well as these oxidised species the wear scar also contains HS-. This corresponds to sulphur at its lowest oxidation state which is also present

mainly in the worn area. It would seem that certain additives in the oil are accruing in the wear scar. Here they are able to protect the Si-coating from further oxidative wear by themselves being oxidised.

As oil D does not contain the anti-oxidant species required to inhibit oxidation the process is allowed to proceed unfettered. This facilitates chemical break down of the coating and results in the observed higher wear, as demonstrated by chemical mapping that shows formation of SiO_x species in the worn area. This behaviour is very similar to the tribochemistry observed when Si-DLCs undergo dry sliding. Formation of Si oxides are noted [26, 221]. Also, when lubricated by water which is a rich source of O, oxidation of Si is also noted [105].

Chemical deterioration of the coating is facilitated by mechanical wear. The reciprocating pin, cleaves apart bonded elements that make up the DLC coating. As the coating is predominately made up of C-H, C-C, C-Si, Si-H and Si-O bonds this bond breakage, in most cases will leave a reactive C, or C centred dangling bond, or the analogous reactive Si [68, 70].

If the bond cleavage results in a C centred dangling bond being formed, several reactions can then take place, as shown in Figure 9-22. Both the formation of C-H and C-O-(H) bonds are thermodynamically favourable. Hydrogen for abstraction can be provided by anti-oxidants or other sources of H in the system. As such these species can passivate the dangling bonds effectively, thus terminating the radical species.

However, if a Si dangling bond is created it is not thermodynamically favourable for a Si-H bond to form and remain stable. A Si-C bond would not represent the thermodynamic minimum for this system either and is also less likely to form as freely-available sources of reactive C are scarce. Sources of oxygen are abundant in various forms from both oxygen in the air and oxygen containing chemical moieties in the oil.

As such the formation of Si-O bonds are favourable in these conditions and can be seen to form when allowed. The presence of the anti-oxidants and anti-wear additives in oil A can sharply reduce the oxidation of the Si in the coating. This is achieved by out-competing the Si for sources of oxygen.

This results in the formation of a layer of PO_x and SO_x compounds, instead of the more oxidised Si species identified at the upper surface of the DLC.

These compounds then build-up in the worn area forming a protective tribofilm. This film is able to reduce the rate of oxidation of Si within the coating resulting in reduced total wear when compared with Oil D.

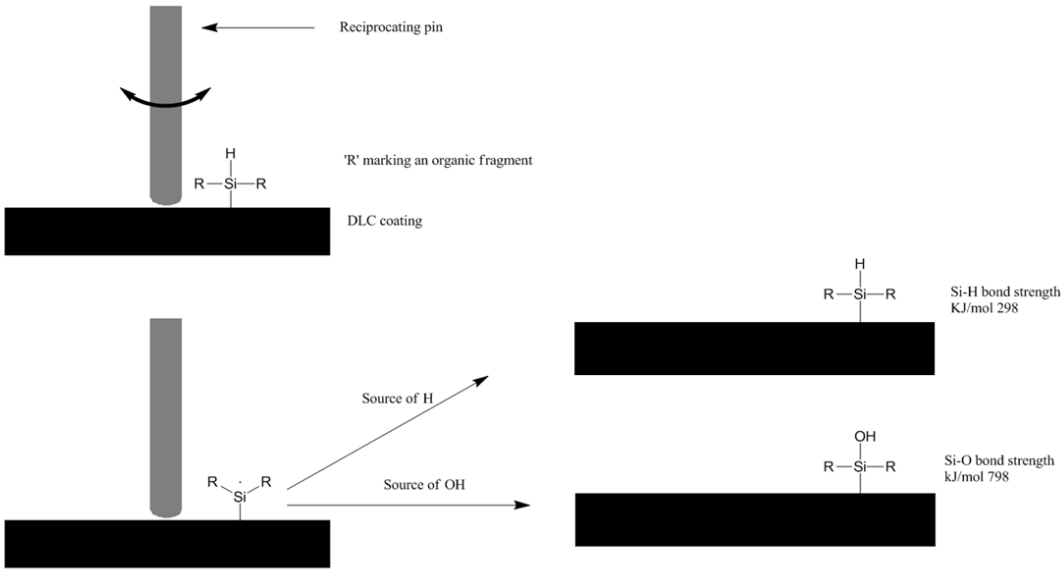

Figure 9-22 Schematic of wear caused by pin contact with DLC

9.7.2. Repressing oxidative wear within Si-doped DLCs

Following directly on from the finding that oxidation plays a major role in the wear of Si-DLCs and often limits its effectiveness, strategies to counter this behaviour were explored. One tribochemically valid and novel approach is detailed again in the paper of which details are in the preface. Inclusion of F as a co-dopant within the Si,O-DLC matrix appears to repress wear of the coating to levels below that of the undoped coating. Chemical tailoring of the DLC was designed to reduce wear at Si. A tribochemical justification of the mechanism by which wear is repressed is explored.

A clear change in both friction and wear behaviour of the DLC is noticed when Si,F and O are simultaneously included as the dopant species. This in

itself is not unusual due to the extent this must affect the microstructure and reactivity of the coating. However, the inversion of the expected wear pattern for Si- and Si,O- DLCs, is notable; it would appear that doping Si,O-DLCs with F is an effective method to protect the coating from aggravated wear rates.

ToF-SIMS also confirms the presence of a SiOF- fragment on the plate which is given in Figure 8-14. Therefore, it can be concluded that the dopants are still present and able to impart their tribological effects on the system. Si on the plate is present in varying forms including a Si-F species. This Si-F species is not maintained when the transferred DLC layer (present on the pin) is analysed. The reduction in wear imparted by tri-doping could be hugely beneficial as Si dopants increase coating adherence to the substrate, alter the sp^2:sp^3 ratio and affect surface wettability [43, 85, 86]. Being able to effectively include all of Si's beneficial properties into the DLC coating without the intrinsic increase in wear would be an excellent prospect for DLCs within many applications. Adding to this, the enhanced wear resistance of the Si,O,F DLC when compared to the a-C:H DLC goes on to further prove that inclusion of this tri-dopant system is indeed an effective wear protection strategy for DLCs.

The bond strengths of some Si compounds are available in Table 9-3**.** The pairing of Si and F represent the strongest bonds Si is able to make. This is because Si is an electropositive element whereas F is the most electronegative element known. Because of this, the two elements form very thermodynamically strong bonds [46, 222, 223].

The combination of both these dopants in a DLC is an exciting prospect as it appears to effectively secure Si from oxidative wear without the need of oil-based anti-oxidant or anti-wear additives. Si,O,F doping improves the overall wear profile of the samples explored by reducing plate wear whilst maintaining low-levels of counter body wear. Literature precedents of higher wear for Si-DLCs can easily be rationalised when the broader picture is observed by inclusion of F. The main mechanism for reduced friction in Si-DLC contacts is identified as being caused by production of SiO_x species. These are often referred to as Si rich oxide debris [26, 43, 77, 105]. This

debris represents oxidative destruction and removal of Si within the coating which in turn amplifies wear of the DLC as a whole.

Typically, Si bonds to O in a silica lattice type arrangement facilitated by oxygen's bivalency, however fluorine is monovalent [224]. This monovalency effectively caps the formation of a Si-O lattice network and retards oxidative wear, as the Si-F bond is stable with regards to oxygen. The lattice network relies on bridging, divalent oxygen atoms. Fluorine atoms cannot facilitate this bridging as they are only able to form one bond.

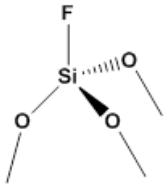

Figure 9-23 F-doped a-SiO_2 glass

Glassy films, specifically phosphate based ones, are known to be very good at reducing wear within boundary lubricated contacts [115, 116]. Si is known to form many glasses based around silica and silicate chemistry. There are many examples of doped silica glasses that exhibit different properties, an example of this is F doped a-SiO_2 [225]. This specific glass exhibits good chemical durability at the cost of mechanical strength [226, 227]. Structurally, the F doped glass is different to other glasses in that the inclusion of F depolymerises the silicate network as shown in Figure 9-23. This occurs via non bridging F which helps to remove strained bonds [225]. Stress within the silicate network is known to play a key role in the degradation of the Si-O-Si chain [25, 228]. It appears that removal of this strain and increasing chemical durability of the F doped silicate glass is what is the cause of repression of wear within the tri doped DLC. Coupled with this is the potential of the SiOF glass species to increase surface wettability and thus adsorption of useful species. The noticeable appreciation of HS- in the worn area would indicate that the worn area is indeed accruing tribologically relevant species, which is evidence for increased surface wettability.

9.8. The role of iron

9.8.1. Thermal- vs. Tribo- films on low Si-DLC films

In order to fully understand both the films formed on the DLC surfaces, comparisons must be made with the corresponding steel tribopair. Therefore, XPS analysis was obtained of the steel/steel tribopair. There is already literature surrounding the characterisation of the tribology associated with steel/steel contacts in fully-formulated lubricants which helps elucidate surface interactions. The most prominent feature of those films is that Ca (derived from the detergent) typically replaces Zn in the film producing shorter chain phosphates and metaphosphates [176, 177, 205]. These films are not quite as effective as the Zn derived polyphosphate glass at repressing wear but are nonetheless effective in this role. Typically Zn is found as the sulphide in these contacts [177].

Thermal films of ZDDP can be derived when lubricants are heated in the presence of a ferrous substrate as shown in Figure 9-24. These typically produce similar films to the tribologically obtained film with: polyphosphates, sulphides, sulphates and varying Zn species [133, 229].

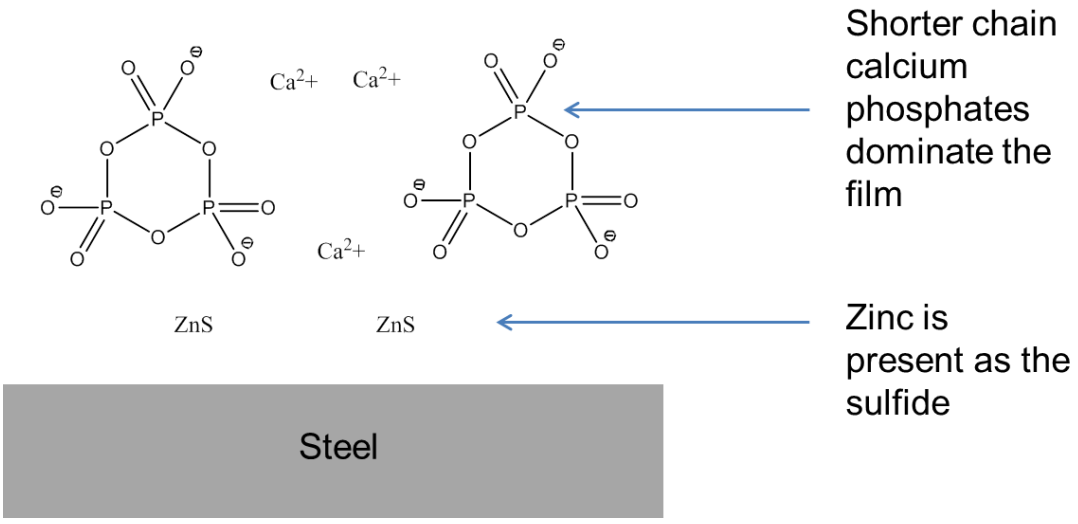

Figure 9-24 Thermal-film as formed on a steel plate

9.8.2. Thermal films on DLC

The thermal film produced on the low Si-DLC showed key differences to those encountered in the literature on steel thermal films. The main changes between the tabulated spectra as given in Table 9-4; up-shift in C 1s position coupled with clear adsorption of Zn species, does indicate presence of a thermal film. This would suggest that a source of C (either DLC or lubricant based) on the surface has been oxidised. This could possibly be as part of a reaction to form $ZnCO_3$, or merely to form additional C-O surface moieties. There are two possible mechanisms by which this Zn film could form. It is notable that there is no Ca signal from the film, tribofilms observed previously at DLC/steel interfaces (as tested under slightly different conditions) appear to nucleate with Ca species that generate the basis of the tribofilm proper. Ca also plays a key role in the tribofilms reported earlier, with Ca contributing the most atomic per cent of elements derived from the oil formulation. In the case of the thermal film it is most likely that, due to lack of reciprocating motion, the detergent micelles are less likely to encounter and flocculate on the surface. This behaviour, dependence of detergent species' film thickness with surface rubbing, has been shown previously at steel contacts. Stable film thicknesses in those cases, being achieved after 30 minutes of rubbing [127]. The dependence of the detergent species film forming abilities upon rubbing is unsurprising. This is because the detergents are formulated into the lubricant as micelles, and the micelles must rupture to release the $CaCO_3$ core within. The micelles themselves are not surface active and are stable in the oil without presence of mechanical agitation, or 'forced coalescence' [127]. This results in greatly reduced Ca adsorption within the thermal film, to the extent where Ca is undetectable by XPS analysis.

A dependence on rubbing or mechanical agitation is not seen for ZDDP, which is known to produce thermal films [133]. ZDDP is known to undergo thermal degradation to form films when in contact with a steel coupon [133, 134]. Decomposition of ZDDP on steel results in several products, these include various organic and simple sulphides as well as insoluble phosphorous/Zn polyphosphates; these species are not the dominant

species found herein [117, 133, 134]. As shown in Table 9-4, the thermal film observed on the low Si-DLC is distinctly different to a steel-ZDDP thermal film, being exclusively composed of Zn species.

Table 9-4 Tribochemistry of thermal films on steel compared with Si-DLC thermal film. Nd = not detected

Element	Low Si-DLC thermal film obtained herein	Steel thermal film [133]	Steel thermal film [229]
P	**Nd**	**Polyphosphates**	**polyphosphates**
S	**Nd**	**Sulphide**	**Sulphide/SO_4**
Zn	**Various Zn oxides/carbonates**	**Zn pyro/polyphosphate**	**ZnS/$ZnSO_4$**

Due to the lack of other elements typically associated with a ZDDP film, it would seem that a catalyst is required to accelerate the formation of the thermal film. With the thermal films generated on steel, this catalyst could indeed be Fe; transition metal ions are well-known for their ability to catalyse various reactions [230]. This is partly due to their ability to switch between oxidation states and provide electrons for reactions; for Fe these states are typically Fe^{2+} and Fe^{3+} [231]. Zn however only has one typically viable oxidation state: Zn^{2+}, this appears to be what prevents it from acting catalytically.

However, as addressed earlier it seems that Ca is also able to accelerate film formation in the DLC system. Ca again only has one viable oxidation state Ca^{2+}, however a route of initiation proposed around calcination does not require variable oxidation states. Of course, for Ca to do this the detergent micelles have to encounter the DLC's surface with sufficient force, as previously discussed. With the thermal film this does not appear to happen.

In terms of a mechanistic explanation of the formation of the Zn species reported; firstly, thermal degradation of ZDDP in the presence of air could yield a source of reactive Zn that is then adsorbed onto the low Si-DLC

surface. This could then react with molecular oxygen as shown schematically in Figure 9-25.

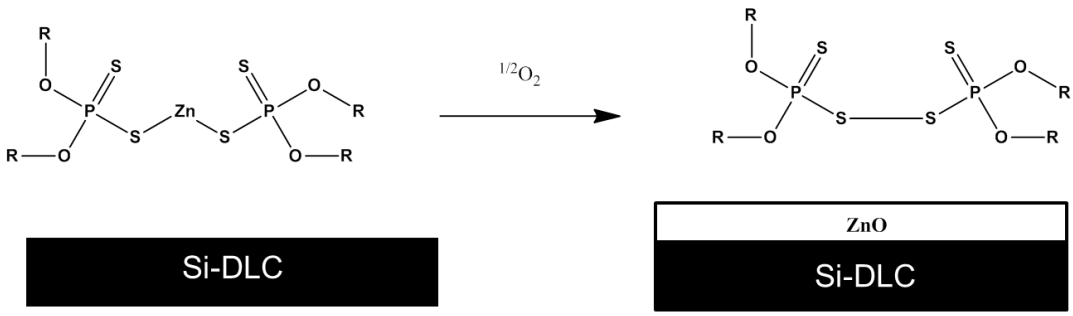

Figure 9-25 Possible route of formation of ZnO on Si-DLC surface

With evidence from the XPS spectra obtained, it is most likely that the other species generated from this reaction with oxygen remain in solution. This then leaves the Zn species as the lone species strongly adsorbed to the DLCs surface.

A second seemingly plausible but unlikely mechanism can be ruled out, which is: in solution ZDDP could undergoes a ligand exchange reaction with Ca from the detergent. This would yield $ZnCO_3$ and a CaDDP species would remain in solution, explaining the lack of Ca, P and S in the spectra. However, the chelating behaviour of dithiophosphate ligands is well known to be preferential for heavy metals, like Zn, over alkali earth metals, like Ca [115, 209]. Therefore, it would seem most probable that the former mechanism is the relevant one in this case and that the film obtained is indeed the product of a thermally generated tribofilm, as opposed to the product of a homogenous ligand-exchange reaction.

9.8.3. Tribofilms on DLCs

As addressed above, the presence of elements including Zn, Ca, P and S is identified on the tribofilms examined. Research in the literature on Si-DLC/steel contacts also finds tribofilms composed of ZnO/ZnS as well as Ca and P [104, 110, 172]. In this instance it would appear that Fe does not play a vital role in tribofilm formation as a multi-component film can be observed.

If Fe perhaps accelerates the formation of the polyphosphate glass cannot be commented on in this instance. This is due to the lubricant blend employed, the combination of detergent and ZDDP typically prevents polyphosphate glass formation under these conditions [177]. Instead, various Ca phosphates are the dominant species with shorter chain polyphosphates present. This behaviour is akin to the steel/steel system [177]. The thermal film produced when the low Si-DLC is heated at 80 ºC for seven hours was solely composed of ZnO and trace N. This is not the same as the tribologically obtained film. This suggests mechanical agitation does influence film formation. Mechanisms for this most likely include the wearing of the DLC coating resulting in the formation of reactive C or Si centre which can then react with any available chemical moiety, as discussed in a previous paper [43]. Also included would be the integral role rubbing plays on the formation of detergent related films on surfaces [197]. Neither of these conditions are met for the thermally derived sample as mechanical wear is required for both. It seems that Ca plays a key role in dictating the tribochemistry of the system. When Ca is not observed in the film, in the case of the thermal film, a greatly altered film is produced. This is in spite of the presence of another metal on the surface, Zn. When the system is exposed to mechanical agitation and therefore the detergent can flocculate, it seems that this helps initiate a tribochemical reaction. As previously discussed, Ca is known to replace Zn in ZDDP films so this is perhaps unsurprising. Again, it seems to be the case that Ca is acting in lieu of Fe in the Si-DLC/Si-DLC contact and creating the reactive, metallic layer required for formation of a more classical Zn/S/P type tribofilm.

Figure 9-20 previously showed the postulated three-stage process of film nucleation. Initially, no film forms as the detergent has not encountered the DLC surface. Upon contact the detergent molecule is burst open, allowing the $CaCO_3$ core to deposit on the surface. Finally this film goes on to react with species in the lubricant to form the tribofilm proper.

It is unclear why the system has a preference for Ca as opposed to Zn with regards to a metallic tribochemical initiator. As addressed before, a possible

explanation is that localised heat spikes reach high enough temperatures to convert $CaCO_3$ into CaO with loss of CO_2.

Compiling the data from XPS analysis as given in Figure 7-7, appears to show that formation of the tribofilm on the plate enables the SiO_x species to be maintained in the film. This could maximize adsorption of ‘useful’ species on the plate, as SiO_x species are highly polar, similar to iron oxides. An increase in SiO_x compounds at the surface should cause a higher surface wettability, as indicated by the low Si-DLC’s greater wettability when compared with a-C:H DLC which was demonstrated in Figure 4-4.

Furthermore, surface wettability of other Si-DLCs, as assessed in the literature (derived from HMDSO), have been shown to increase with heating. This is attributed to incorporation of additional oxygen [47]. Many important lubricant additives are surface active so maximisation of the surface polarity is highly relevant, with the ideal goal of matching a steel surface’s energy profile.

Chapter 10 Overarching conclusions

This thesis examines many aspects of both Si-doped DLC and a-C:H DLC. Various findings have been made and novel research themes established. Some of the most prominent findings include:

1. Inclusion of Si within a DLC matrix can affect both coating wettability and sp^2:sp^3 ratio.

2. Low Si-DLC/steel pairings do offer an advantage in terms of friction when compared to a-C:H/steel contacts, in dry sliding conditions.

3. Si-DLC coatings consistently exhibit higher wear when compared to a-C:H DLC coatings. This is due to fundamental chemical thermodynamics associated with silicon doping. This is particularly true during the running-in phase of wear.

4. Both DLCs form thin, tenacious tribofilms that markedly reduce wear.

5. Increasing Si content correspondingly increases overall wear of the coating.

6. Si-DLCs appear stabilised with respect to their sp^2:sp^3 ratio with regards to any change with wearing. This was not seen with the a-C:H DLC which undergoes a change in the sp^2:sp^3 ratio when tribotested. This change in sp^2 ratio could be caused by alleviation of compressive stress and part of the reason for lower wear within a-C:H DLCs.

7. Si-DLCs appear to form thicker tribofilms than a-C:H DLCs, however this does not necessarily result in lower wear. This effect is attributed to increased surface wettability.

8. Si-DLCs lose their inherent ability to self-lubricate when oil is used at the interface.

9. The inherent tendency of Si-DLC to oxidise can be attenuated with inclusion of F as a co-dopant. Inclusion of the dopant appears to promote formation of a glassy a-SiOF film in the worn area.

10. Si-DLC/Si-DLC contacts can and do form tribofilms without the need for a ferrous body. These films are very similar to those obtained at Si-DLC/steel contacts.

11. The low Si-DLC examined does not form a ZDDP based film analogous to a steel ZDDP thermal film.

10.1. **Optimisation strategies**

In order to maximise Si-DLCs performance several factors could be optimised:

- Additional incorporation of NOCH anti-oxidants in lubricant blends. Ideally these would not require a prolonged activation period (as sometimes seen with ZDDP). This would protect the Si-DLC from oxidative wear.

- Using only the lowest atomic % of Si required in the application so as to minimise tendency to wear via oxidation.

- Employing a gradient whereby Si is only included at the substrate/DLC interface and not the DLC/counter-body interface could effective cap oxidative wear, yet offer the increased adherence associated with Si-DLCs.

In dry-sliding applications that require low friction Si-DLC coatings are recommended. However, in lubricated contacts a-C:H performs better in terms of wear resistance. As the friction coefficients of the two are similar in lubricated contacts, a-C:H DLCs would be preferred here.

10.2. **Future work**

Following on from the research generated within this thesis there are several topics that emerge as candidates for further in-depth study. These split into three main themes.

10.2.1. Further elucidation of tribochemical mechanisms

Building on the surface analysis work conducted in the thesis it would be interesting to further explore tribofilm forming mechanisms. This would allow for possible surface modifications or more effective doping; enabling faster forming, more tenacious tribofilms.

- To validate the theory that over-based calcium carbonate detergent molecules are able to initiate the tribofilm, via formation of CaO, a study could be conducted whereby the gases given off are assessed for carbon dioxide.
- Rate of formation of tribofilms on DLCs should be compared both with the presence of detergent additives and without, to verify their role in the process.
- Filtering of post tribo-tested oil and separation of the particles from this would be valuable future work. If particulate debris was loaded on to a TEM grid, chemical information about the particles, including weather SiOx species are present in the debris could be established. This would be useful information as the role of SiOx species in lubricated contacts is still not fully understood.
- Further work would also include auger electron spectroscopy to compliment the data from XPS. Auger spectroscopy is far more surface sensitive (2 – 10 atomic layers) when compared to XPS. It has the ability to detect species only present at 0.1%, making it ideal for the thin films encountered in this work, specifically those formed on the a-C:H DLC.
- The effect of friction modifier species, like GMO, have on the tribofilm at DLC/steel contacts needs further investigation. It is known that at steel/steel contacts various species can inhibit and modify the

tribofilms structure, whether this remains true with DLCs needs to be established.

10.2.2. Doping of DLCs

As there is clear room to further optimise DLC with regards to doping, especially with Si content, more research could be undertaken here.

- A lower %Si DLC (perhaps 1-2 atomic %) should be compared with a-C:H DLCs in order to see if the positive effects of Si inclusion can be maintained without the need for co-dopants to repress the negative effects associated with Si- DLCs.
- As inclusion of F as a co-dopant with Si appears to mitigate the higher wear often seen with Si-DLCs it would be interesting to test a Si-DLC/steel contact in fully-formulated lubricant with an F-based oil additive. This additive may impart the benefits of an Si,F doped DLC without the need for the PVD modification.

10.2.3. Water based lubricants

As DLCs are innately lower wear when compared with ferrous surfaces this opens up research into water based tribo-systems. As water is a far inferior lubricant in terms of wear protection than a fully-formulated oil, novel additives could be tested at DLC/steel interfaces to assess their compatibility within water lubrication.

- This could extend to a water-based lubricant study of Si-DLC with an inorganic F additive, which may be easier to achieve as an inorganic F salt compound would most likely be more reactive than a C-F type organic species.
- Water based lubricants would be ideal with regards to green goals. Testing a variety of water based additives that are environmentally acceptable with either Si-DLC or a-C:H type DLCs. There are many green additives already in existence that could be tested as a more benign vehicle for P or S incorporation into the tribofilm, such as naturally occurring molecules.

References

1. Dictionary, O.E., *"tribology, n."*. 2014: Oxford University Press.
2. Dowson, D., *History of Tribology*. 2009: John Wiley & Sons Incorporated.
3. Shaffer, S. *Tribology 101 – Introduction to the Basics of Tribology*. [webinar] [cited 2014 09/10/2014]; Available from: http://www.bruker.com/fileadmin/user_upload/8-PDF-Docs/SurfaceAnalysis/TMT/Webinars/Tribology_101_Webinar-1_Intro_and_Basics_29-Jan-2013.pdf.
4. Pitenis, A., D. Dowson, and W. Gregory Sawyer, *Leonardo da Vinci's Friction Experiments: An Old Story Acknowledged and Repeated.* Tribology Letters, 2014. **56**(3): p. 509-515.
5. Dowson, D., *A tribological day.* Proceedings of the Institution of Mechanical Engineers, Part J: Journal of Engineering Tribology, 2009. **223**(3): p. 261-273.
6. Jost, H.P., *Tribology — Origin and future.* Wear, 1990. **136**(1): p. 1-17.
7. Holmberg, K., P. Andersson, and A. Erdemir, *Global energy consumption due to friction in passenger cars.* Tribology International, 2012. **47**(0): p. 221-234.
8. Gov.uk. *Exhaust Air Quality Pollutant Emissions Testing*. [Government webpage] 2013 [cited 2013 17/10]; Available from: http://www.dft.gov.uk/vca/fcb/exhaust-emissions-testing.asp.
9. J.T. Houghton, Y.D., *Climate Change 2001:The Scientific Basis*, in *Cambridge University Press*. 2001.
10. Hansen, J.Q., M. Winther, and S.C. Sorenson, *The influence of driving patterns on petrol passenger car emissions.* Science of The Total Environment, 1995. **169**(1–3): p. 129-139.
11. Kahn, M.E., *New Evidence on Trends in Vehicle Emissions.* The RAND Journal of Economics, 1996. **27**(1): p. 183-196.
12. Schobert, H.H., *Energy and Society: An Introduction*. 2002: Taylor & Francis.
13. Spikes, H., *Low- and zero-sulphated ash, phosphorus and sulphur anti-wear additives for engine oils.* Lubrication Science, 2008. **20**(2): p. 103-136.
14. Myhre, G., F.-M. Bréon, and O. Boucher, *Anthropogenic and Natural Radiative Forcing.* Notes, 2011. **16**.
15. Dictionary, O.E., *"friction, n."*: Oxford University Press.
16. Neale, M.J., *The Tribology Handbook*. 1995: Elsevier Science.
17. Bhushan, B., *Principles and applications of tribology*. 1999: Wiley. 588-589.
18. Skakoon, J.G. *There's the Rub*. [cited 2012 16 July]; Available from: http://images.asme.org/MEMagazine/Articles/2009/January/17076.gif.
19. Priest, M. and C.M. Taylor, *Automobile engine tribology — approaching the surface.* Wear, 2000. **241**(2): p. 193-203.

20. Stachowiak, G.W. and A.W. Batchelor, *Engineering Tribology*. Materials & Mechanical. 2006: Butterworth-Heinemann. 1-832.
21. Truhan, J.J., J. Qu, and P.J. Blau, *The effect of lubricating oil condition on the friction and wear of piston ring and cylinder liner materials in a reciprocating bench test.* Wear, 2005. **259**(7–12): p. 1048-1055.
22. Tamminen, J., C.-E. Sandström, and P. Andersson, *Influence of load on the tribological conditions in piston ring and cylinder liner contacts in a medium-speed diesel engine.* Tribology International, 2006. **39**(12): p. 1643-1652.
23. Stachowiak, G.W., *Wear: materials, mechanisms and practice*. 2005: Wiley.
24. Tung, S.C. and M.L. McMillan, *Automotive tribology overview of current advances and challenges for the future.* Tribology International, 2004. **37**(7): p. 517-536.
25. Sen, F.G., et al., *Low friction and environmentally stable diamond-like carbon (DLC) coatings incorporating silicon, oxygen and fluorine sliding against aluminum.* Surface & Coatings Technology, 2013. **215**: p. 340-349.
26. Oguri, K. (1992) *Two different low friction mechanisms of diamond-like carbon with silicon coatings formed by plasma-assisted chemical vapor deposition.* J. Mater. Res. **7**.
27. Kano, M., et al., *Ultralow friction of DLC in presence of glycerol mono-oleate (GNO).* Tribology Letters, 2005. **18**(2): p. 245-251.
28. Kalin, M., et al., *The Effect of Doping Elements and Oil Additives on the Tribological Performance of Boundary-Lubricated DLC/DLC Contacts.* Tribology Letters, 2004. **17**(4): p. 679-688.
29. Kalin, M. and J. Vižintin, *Differences in the tribological mechanisms when using non-doped, metal-doped (Ti, WC), and non-metal-doped (Si) diamond-like carbon against steel under boundary lubrication, with and without oil additives.* Thin Solid Films, 2006. **515**(4): p. 2734-2747.
30. Dictionary, O.E., *"wear, n."*. 2014: Oxford University Press.
31. Suominen Fuller, M.L., et al., *The use of X-ray absorption spectroscopy for monitoring the thickness of antiwear films from ZDDP.* Tribology Letters, 2000. **8**(4): p. 187-192.
32. Zhang, Z., et al., *Tribofilms generated from ZDDP and DDP on steel surfaces: Part 1, growth, wear and morphology.* Tribology Letters, 2005. **19**(3): p. 211-220.
33. Archard, J.F., *Contact and Rubbing of Flat Surfaces.* Journal of Applied Physics, 1953. **24**(8): p. 981-988.
34. P. Suh, N., *The delamination theory of wear.* Wear, 1973. **25**(1): p. 111-124.
35. Meng, H.C. and K.C. Ludema, *Wear models and predictive equations: their form and content.* Wear, 1995. **181–183, Part 2**(0): p. 443-457.
36. Bhaskaran, H., et al., *Ultralow nanoscale wear through atom-by-atom attrition in silicon-containing diamond-like carbon.* Nat Nano, 2010. **5**(3): p. 181-185.
37. Jacobs, T.B., et al., *On the Application of Transition State Theory to Atomic-Scale Wear.* Tribology Letters, 2010. **39**(3): p. 257-271.

38. Jacobs, T.D.B. and R.W. Carpick, *Nanoscale wear as a stress-assisted chemical reaction.* Nat Nano, 2013. **8**(2): p. 108-112.
39. Dardalis, D. *Rotating Liner Engine A New Approach to Reduce Engine Friction and Increase Fuel Economy in Heavy Duty Engines* [pdf] 2004 [cited 2014; Available from: http://www.rotatingliner.com/RLE-Article-Final-022404.pdf.
40. Robertson, J., *Diamond-like amorphous carbon.* Materials Science and Engineering: R: Reports, 2002. **37**(4–6): p. 129-281.
41. Erdemir, A. and C. Donnet, *Tribology of diamond-like carbon films: recent progress and future prospects.* Journal of Physics D-Applied Physics, 2006. **39**(18): p. R311-R327.
42. Kalin, M., et al., *Metal-doped (Ti, WC) diamond-like-carbon coatings: Reactions with extreme-pressure oil additives under tribological and static conditions.* Thin Solid Films. **518**(15): p. 4336-4344.
43. Lanigan, J., et al., *Tribochemistry of silicon and oxygen doped, hydrogenated Diamond-like Carbon in fully-formulated oil against low additive oil.* Tribology International, (in press) 2014.
44. Grill, A., *Review of the tribology of diamond-like carbon.* Wear, 1993. **168**(1-2): p. 143-153.
45. Podgornik, B., S. Jacobson, and S. Hogmark, *DLC coating of boundary lubricated components—advantages of coating one of the contact surfaces rather than both or none.* Tribology International, 2003. **36**(11): p. 843-849.
46. Speight, J.G., *Lange's Handbook Of Chemistry* MCGRAW-HILL, Editor. 1999.
47. Grischke, M., et al., *Variation of the wettability of DLC-coatings by network modification using silicon and oxygen.* Diamond and Related Materials, 1998. **7**(2–5): p. 454-458.
48. Kalin, M. and M. Polajnar, *The Effect of Wetting and Surface Energy on the Friction and Slip in Oil-Lubricated Contacts.* Tribology Letters, 2013. **52**(2): p. 185-194.
49. Bowden, F.P., J.N. Gregory, and D. Tabor, *Lubrication of metal surfaces by fatty acids* Nature, 1945. **156**(3952): p. 97-101.
50. Kalin, M. and J. Vižintin, *A comparison of the tribological behaviour of steel/steel, steel/DLC and DLC/DLC contacts when lubricated with mineral and biodegradable oils.* Wear, 2006. **261**(1): p. 22-31.
51. De Barros Bouchet, M.I., et al., *Mechanisms of MoS2 formation by MoDTC in presence of ZnDTP: effect of oxidative degradation.* Wear, 2005. **258**(11-12): p. 1643-1650.
52. Archer, N.J., *Chemical vapour deposition.* Physics in Technology, 1979. **10**(4): p. 152.
53. Hainsworth, S.V. and N.J. Uhure, *Diamond like carbon coatings for tribology: production techniques, characterisation methods and applications.* International Materials Reviews, 2007. **52**(3): p. 153-174.
54. Voevodin, A.A. and J.S. Zabinski, *Superhard, functionally gradient, nanolayered and nanocomposite diamond-like carbon coatings for wear protection.* Diamond and Related Materials, 1998. **7**(2–5): p. 463-467.

55. Hauert, R., *An overview on the tribological behavior of diamond-like carbon in technical and medical applications.* Tribology International, 2004. **37**(11–12): p. 991-1003.
56. Wang, R., et al., *Delamination and spalling of diamond-like-carbon tribological surfaces.* Diamond and Related Materials, 2002. **11**(10): p. 1797-1803.
57. Yatsuzuka, M., et al., *Microstructure of interface for high-adhesion DLC film on metal substrates by plasma-based ion implantation.* Vacuum, 2008. **83**(1): p. 190-197.
58. Lung, B.H., M.J. Chiang, and M.H. Hon, *Effect of gradient a-SiCx interlayer on adhesion of DLC films.* Materials Chemistry and Physics, 2001. **72**(2): p. 163-166.
59. Schwarz, C., et al., *Investigation on wear and adhesion of graded Si/SiC/DLC coatings deposited by plasma-enhanced-CVD.* Diamond and Related Materials, 2008. **17**(7–10): p. 1685-1688.
60. Bonetti, L.F., et al., *Adhesion studies of diamond-like carbon films deposited on Ti6Al4V substrate with a silicon interlayer.* Thin Solid Films, 2006. **515**(1): p. 375-379.
61. Sheeja, D., et al., *Tribological properties and adhesive strength of DLC coatings prepared under different substrate bias voltages.* Wear, 2001. **249**(5–6): p. 433-439.
62. Wei, C. and J.-Y. Yen, *Effect of film thickness and interlayer on the adhesion strength of diamond like carbon films on different substrates.* Diamond and Related Materials, 2007. **16**(4–7): p. 1325-1330.
63. Yamauchi, Y., *Surface Modification of DLC Thin Films with Plasma Processing.*
64. Yamauchi, Y., et al., *Effect of annealing on diamond-like carbon characteristics by electron spin resonance spectral analysis.* Thin Solid Films, 2011. **519**(20): p. 6693-6697.
65. Yamauchi, Y., et al., *Chemical diagnosis of DLC by ESR spectral analysis.* Thin Solid Films, 2010. **518**(13): p. 3492-3496.
66. Biegelsen, D.K. and M. Stutzmann, *Hyperfine studies of dangling bonds in amorphous silicon.* Physical Review B, 1986. **33**(5): p. 3006-3011.
67. Tsu, R., et al., *Passivation of dangling bonds in amorphous Si and Ge by gas adsorption.* Physical Review B, 1987. **35**(5): p. 2385-2390.
68. Erdemir, A., *Genesis of superlow friction and wear in diamondlike carbon films.* Tribology International, 2004. **37**(11-12): p. 1005-1012.
69. Erdemir, A., *The role of hydrogen in tribological properties of diamond-like carbon films.* Surface and Coatings Technology, 2001. **146-147**(0): p. 292-297.
70. Konicek, A.R., et al., *Origin of Ultralow Friction and Wear in Ultrananocrystalline Diamond.* Physical Review Letters, 2008. **100**(23): p. 235502.
71. Braun, A., et al., *Advantages of soft X-ray absorption over TEM-EELS for solid carbon studies—a comparative study on diesel soot with EELS and NEXAFS.* Carbon, 2005. **43**(1): p. 117-124.
72. Kasai, P.H., *Carbon Overcoat: Structure and Bonding of Z-DOL.* Tribology Letters, 2002. **13**(3): p. 155-166.

73. Donnet, C. and A. Erdemir, *Tribology of Diamond-like Carbon Films: Fundamentals and Applications*. 2007: Springer.
74. Colaco, R. and et al., *Micro-to-nano triboactivity of hydrogenated DLC films.* Journal of Physics D: Applied Physics, 2009. **42**(8): p. 085307.
75. Donnet, C., *Tribology of diamond-like carbon films: fundamentals and applications*. 2008, Springer Science.
76. Gilmore, R. and R. Hauert, *Control of the tribological moisture sensitivity of diamond-like carbon films by alloying with F, Ti or Si.* Thin Solid Films, 2001. **398–399**(0): p. 199-204.
77. Kim, M.-G., K.-R. Lee, and K.Y. Eun, *Tribological behavior of silicon-incorporated diamond-like carbon films.* Surface and Coatings Technology, 1999. **112**(1–3): p. 204-209.
78. Moolsradoo, N., *Thermal Stability and Tribological Performance of DLC-Si-O Films.* Advances in Materials Science and Engineering, 2011. **2011**.
79. Pham, D.-C., et al., *Tribochemical interactions of Si-doped DLC film against steel in sliding contact.* Journal of Mechanical Science and Technology, 2007. **21**(7): p. 1083-1089.
80. Tanaka, A., M. Suzuki, and T. Ohana, *Friction and Wear of Various DLC Films in Water and Air Environments.* Tribology Letters, 2004. **17**(4): p. 917-924.
81. Damasceno, J.C., et al., *Deposition of Si-DLC films with high hardness, low stress and high deposition rates.* Surface and Coatings Technology, 2000. **133–134**(0): p. 247-252.
82. Papakonstantinou, P., et al., *The effects of Si incorporation on the electrochemical and nanomechanical properties of DLC thin films.* Diamond and Related Materials, 2002. **11**(3–6): p. 1074-1080.
83. Koda, S., *Kinetic aspects of oxidation and combustion of silane and related compounds.* Progress in Energy and Combustion Science, 1992. **18**(6): p. 513-528.
84. Wu, X., et al., *Characteristics and tribological properties in water of Si-DLC coatings.* Diamond and Related Materials, 2008. **17**(1): p. 7-12.
85. Iseki, T., et al., *Structural analysis of Si-containing diamond-like carbon.* Diamond and Related Materials. **15**(4-8): p. 1004-1010.
86. Kato, N., H. Mori, and N. Takahashi, *Spectroscopic ellipsometry of silicon-containing diamond-like carbon (DLC-Si) films*, in *Physica Status Solidi C - Current Topics in Solid State Physics, Vol 5, No 5*, H. Arwin, U. Beck, and M. Schubert, Editors. 2008, Wiley-V C H Verlag Gmbh: Weinheim. p. 1117-1120.
87. Veres, M., et al., *Characterisation of a-C:H and oxygen-containing Si:C:H films by Raman spectroscopy and XPS.* Diamond and Related Materials. **14**(3-7): p. 1051-1056.
88. Varma, A., V. Palshin, and E.I. Meletis, *Structure–property relationship of Si-DLC films.* Surface and Coatings Technology, 2001. **148**(2-3): p. 305-314.
89. Butter, R.S., et al., *Production and wetting properties of fluorinated diamond-like carbon coatings.* Thin Solid Films, 1997. **311**(1–2): p. 107-113.
90. Howard, J.A.K., et al., *How good is fluorine as a hydrogen bond acceptor?* Tetrahedron, 1996. **52**(38): p. 12613-12622.

91. Miyake, S., et al., *Improvement of boundary lubrication properties of diamond-like carbon (DLC) films due to metal addition.* Tribology International, 2004. **37**(9): p. 751-761.
92. Ji, L., et al., *Microstructure and mechanical properties of Mo/DLC nanocomposite films.* Diamond and Related Materials, 2008. **17**(11): p. 1949-1954.
93. Fu, R.K.Y., et al., *Thermal stability of metal-doped diamond-like carbon fabricated by dual plasma deposition.* Diamond and Related Materials, 2005. **14**(9): p. 1489-1493.
94. Yang, L., et al., *Friction reduction mechanisms in boundary lubricated W-doped DLC coatings.* Tribology International, 2014. **70**(0): p. 26-33.
95. Choi, J., et al., *Self-assembled monolayer on diamond-like carbon surface: formation and friction measurements.* Tribology International, 2003. **36**(4–6): p. 285-290.
96. Tan, M., et al., *Solvent effect on the formation of self-assembled monolayer on DLC surface between n-hexane and Vertrel XF.* Applied Surface Science, 2008. **254**(20): p. 6332-6336.
97. Matta, C., et al., *Tribochemistry of tetrahedral hydrogen-free amorphous carbon coatings in the presence of OH-containing lubricants.* Lubrication Science, 2008. **20**(2): p. 137-149.
98. Matta, C., et al., *Superlubricity and tribochemistry of polyhydric alcohols.* Physical Review B, 2008. **78**(8).
99. Kano, M., et al., *Ultralow friction of DLC in presence of glycerol mono-oleate (GMO).* Tribology Letters, 2005. **18**(2): p. 245-251.
100. de Barros'Bouchet, M.I., et al., *Boundary lubrication mechanisms of carbon coatings by MoDTC and ZDDP additives.* Tribology International, 2005. **38**(3): p. 257-264.
101. Miyake, S., et al., *Boundary Lubrication Characteristic of Metal-Containing Diamond-Like Carbon (DLC) Films with Poly Alpha Olefin (PAO) Lubricant.* Tribology Online, 2008. **3**(5): p. 310-315.
102. Ikeyama, M., et al., *Effects of Si content in DLC films on their friction and wear properties.* Surface and Coatings Technology, 2005. **191**(1): p. 38-42.
103. Vengudusamy, B., A. Grafl, and K. Preinfalk, *Influence of Silicon on the Wear Properties of Amorphous Carbon Under Dry and Lubricated Conditions.* Tribology Letters, 2014. **53**(3): p. 569-583.
104. Ban, M., et al., *Tribological characteristics of Si-containing diamond-like carbon films under oil-lubrication.* Wear, 2002. **253**(3-4): p. 331-338.
105. Wu, X., et al., *Tribochemical reaction of Si-DLC coating in water studied by stable isotopic tracer.* Diamond and Related Materials, 2008. **17**(2): p. 147-153.
106. Donnet, C., et al., *The role of hydrogen on the friction mechanism of diamond-like carbon films.* Tribology Letters, 2001. **9**(3): p. 137-142.
107. Kalin, M., et al., *The lubrication of DLC coatings with mineral and biodegradable oils having different polar and saturation characteristics.* Surface and Coatings Technology, 2006. **200**(14-15): p. 4515-4522.
108. Israelachvili, J.N., D.J. Mitchell, and B.W. Ninham, *Theory of self-assembly of hydrocarbon amphiphiles into micelles and bilayers.*

Journal of the Chemical Society, Faraday Transactions 2: Molecular and Chemical Physics, 1976. **72**(0): p. 1525-1568.
109. Lu, W. and D.D.L. Chung, *Effect of Rust on the Wettability of Steel by Water.* Cement and Concrete Research, 1998. **28**(4): p. 477-480.
110. Ando, J., et al., *Tribological properties of Si-containing diamond-like carbon film under ATF lubricated condition.* Wear, 2009. **266**(1-2): p. 239-247.
111. Topolovec-Miklozic, K., F. Lockwood, and H. Spikes, *Behaviour of boundary lubricating additives on DLC coatings.* Wear, 2008. **265**(11-12): p. 1893-1901.
112. Minami, I., et al., *Investigation of tribo-chemistry by means of stable isotopic tracers, part 2: Lubrication mechanism of friction modifiers on diamond-like carbon.* Tribology Transactions, 2007. **50**(4): p. 477-487.
113. Gilmore, R. and R. Hauert, *Comparative study of the tribological moisture sensitivity of Si-free and Si-containing diamond-like carbon films.* Surface and Coatings Technology, 2000. **133–134**(0): p. 437-442.
114. Lubwama, M., et al., *Characteristics and tribological performance of DLC and Si-DLC films deposited on nitrile rubber.* Surface and Coatings Technology, 2012. **206**(22): p. 4585-4593.
115. Spikes, H., *The History and Mechanisms of ZDDP.* Tribology Letters, 2004. **17**(3): p. 469-489.
116. Willermet, P.A., et al., *Mechanism of formation of antiwear films from zinc dialkyldithiophosphates.* Tribology International, 1995. **28**(3): p. 177-187.
117. Fuller, M.L.S., et al., *Solution decomposition of zinc dialkyl dithiophosphate and its effect on antiwear and thermal film formation studied by X-ray absorption spectroscopy.* Tribology International, 1998. **31**(10): p. 627-644.
118. Nicholls, M.A., et al., *Review of the lubrication of metallic surfaces by zinc dialkyl-dithiophosphates.* Tribology International, 2005. **38**(1): p. 15-39.
119. Haque, T., et al., *Effect of oil additives on the durability of hydrogenated DLC coating under boundary lubrication conditions.* Wear, 2009. **266**(1-2): p. 147-157.
120. Costa, R.P.d.C., et al., *Enhanced DLC wear performance by the presence of lubricant additives.* Materials Research, 2011. **14**: p. 222-226.
121. Farr, J.P.G., *Molybdenum disulphide in lubrication. A review.* Wear, 1975. **35**(1): p. 1-22.
122. Grossiord, C., et al., *MoS2 single sheet lubrication by molybdenum dithiocarbamate.* Tribology International, 1998. **31**(12): p. 737-743.
123. Bartz, W.J., *Solid lubricant additives—effect of concentration and other additives on anti-wear performance.* Wear, 1971. **17**(5–6): p. 421-432.
124. Morina, A., et al., *ZDDP and MoDTC interactions in boundary lubrication—The effect of temperature and ZDDP/MoDTC ratio.* Tribology International, 2006. **39**(12): p. 1545-1557.
125. Rounds, F.G., *Soots from used diesel engine oils-their effects on wear as measured in 4-ball wear tests*. 1981, SAE Technical Paper.

126. Shinyoshi, T., Y. Fuwa, and Y. Ozaki, *Wear analysis of DLC coating in oil containing Mo-DTC*. 2007, SAE Technical Paper.
127. Topolovec-Miklozic, K., T.R. Forbus, and H. Spikes, *Film Forming and Friction Properties of Overbased Calcium Sulphonate Detergents.* Tribology Letters, 2008. **29**(1): p. 33-44.
128. Kubo, T., et al., *Boundary film formation from overbased calcium sulfonate additives during running-in process of steel-DLC contact.* Wear, 2008. **265**(3-4): p. 461-467.
129. LCC, C.O.C. *Dispersants*. [cited 2014; Available from: https://www.oronite.com/products/dispersants.asp.
130. Chevron. *Dispersants*. 2014 [cited 2014; Available from: https://www.oronite.com/products/dispersants.asp.
131. Rudnick, L.R., *Lubricant Additives: Chemistry and Applications, Second Edition*. 2009: Taylor & Francis.
132. Forbes, E.S., *Antiwear and extreme pressure additives for lubricants.* Tribology, 1970. **3**(3): p. 145-152.
133. Bancroft, G.M., et al., *Mechanisms of tribochemical film formation: stabilityof tribo- and thermally-generated ZDDP films.* Tribology Letters, 1997. **3**(1): p. 47-51.
134. Fuller, M., et al., *Chemical characterization of tribochemical and thermal films generated from neutral and basic ZDDPs using X-ray absorption spectroscopy.* Tribology International, 1997. **30**(4): p. 305-315.
135. Perez Delgado, Y., et al., *Impact of wire-EDM on dry sliding friction and wear of WC-based and ZrO2-based composites.* Wear, 2011. **271**(9–10): p. 1951-1961.
136. Childs, T.H.C. and F. Sabbagh, *Boundary-lubricated wear of cast irons to simulate automotive piston ring wear rates.* Wear, 1989. **134**(1): p. 81-97.
137. Hofmann, S., *Practical surface analysis: state of the art and recent developments in AES, XPS, ISS and SIMS.* Surface and Interface Analysis, 1986. **9**(1): p. 3-20.
138. Liu, H. and T.J. Webster, *Nanomedicine for implants: A review of studies and necessary experimental tools.* Biomaterials, 2007. **28**(2): p. 354-369.
139. Wu, W.-J. and M.-H. Hon, *Thermal stability of diamond-like carbon films with added silicon.* Surface and Coatings Technology, 1999. **111**(2–3): p. 134-140.
140. Briggs, G.B.D., *High Resolution XPS of Organic Polymers*. 1992, Chichester: Wiley.
141. Briggs, D., *Surface analysis of Polymers by XPS and static SIMS*. 1998, Cambridge: OUP.
142. Yan, X.B., et al., *Characterization of hydrogenated diamond-like carbon films electrochemically deposited on a silicon substrate.* Journal of Physics D-Applied Physics, 2004. **37**(17): p. 2416-2424.
143. Moulder, J., W. Stickle, and P. Sobol, *Handbook of X Ray Photoelectron Spectroscopy (P/N 624755)*. 1992: Perkin-Elmer, Physical Electronics Division.
144. Alexander, M.R., et al., *A study of HMDSO/O2 plasma deposits using a high-sensitivity and -energy resolution XPS instrument: curve fitting*

of the Si 2p core level. Applied Surface Science, 1999. **137**(1–4): p. 179-183.
145. Miller, D.J., M.C. Biesinger, and N.S. McIntyre, *Interactions of CO2 and CO at fractional atmosphere pressures with iron and iron oxide surfaces: one possible mechanism for surface contamination?* Surface and Interface Analysis, 2002. **33**(4): p. 299-305.
146. Alexander V. Naumkin, A.K.-V., Stephen W. Gaarenstroom, and Cedric J. Powell. *NIST X-ray Photoelectron Spectroscopy Database* NIST Standard Reference Database 20, Version 4.1 [Web database] 2000 15/9/2012 [cited 2013 2013]; Available from: http://srdata.nist.gov/xps/.
147. Chusuei, C.C., et al., *Calcium phosphate phase identification using XPS and time-of-flight cluster SIMS.* Analytical chemistry, 1999. **71**(1): p. 149-153.
148. Zemlyanov, D., *Electron spectroscopy: A new window opens.* Nat Nano, 2011. **6**(10): p. 612-613.
149. Vickerman, J.C., J.C.V.D. Briggs, and D. Briggs, *TOF-SIMS: Materials Analysis by Mass Spectrometry*. 2013: IM Publications.
150. Deval, J., et al., *Reconfigurable hydrophobic/hydrophilic surfaces in microelectromechanical systems (MEMS).* Journal of Micromechanics and Microengineering, 2004. **14**(1): p. 91.
151. Choong, W.K., S.U.o.N.Y.a.B. Chemical, and B. Engineering, *The Determination of Contact Angle of Water on Graphite Surface: Using Grand Canonical Transition Matrix Monte Carlo*. 2007: State University of New York at Buffalo.
152. Yuan, Y. and T.R. Lee, *Contact Angle and Wetting Properties*, in *Surface Science Techniques*, G. Bracco and B. Holst, Editors. 2013, Springer Berlin Heidelberg. p. 3-34.
153. Bryant, M., et al., *Characterisation of the surface topography, tomography and chemistry of fretting corrosion product found on retrieved polished femoral stems.* Journal of the Mechanical Behavior of Biomedical Materials, 2014. **32**(0): p. 321-334.
154. Daniels, H., et al., *Investigating carbonization and graphitization using electron energy loss spectroscopy (EELS) in the transmission electron microscope (TEM).* Philosophical Magazine, 2007. **87**(27): p. 4073-4092.
155. Ponsonnet, L., et al., *EELS analysis of hydrogenated diamond-like carbon films.* Thin Solid Films, 1998. **319**(1-2): p. 97-100.
156. Oliver, W.C. and G.M. Pharr, *An improved technique for determining hardness and elastic modulus using load and displacement sensing indentation experiments.* Journal of Materials Research, 1992. **7**(06): p. 1564-1583.
157. Oliver, W.C. and G.M. Pharr, *Measurement of hardness and elastic modulus by instrumented indentation: Advances in understanding and refinements to methodology.* Journal of Materials Research, 2004. **19**(01): p. 3-20.
158. Albertazzi, A., et al., *Applications of a White Light Interferometer for Wear Measurement of Cylinders*, in *Interferometry XIV: Applications*, E.L. Novak, W. Osten, and C. Gorecki, Editors. 2008, Spie-Int Soc Optical Engineering: Bellingham.

159. Harasaki, A. and J.C. Wyant, *Fringe modulation skewing effect in white-light vertical scanning interferometry.* Applied Optics, 2000. **39**(13): p. 2101-2106.
160. O'Donnell, K.A., *Effects of finite stylus width in surface contact profilometry.* Applied Optics, 1993. **32**(25): p. 4922-4928.
161. Poon, C.Y. and B. Bhushan, *Comparison of surface roughness measurements by stylus profiler, AFM and non-contact optical profiler.* Wear, 1995. **190**(1): p. 76-88.
162. West, R., M.J. Fink, and J. MICHL, *Tetramesityldisilene, a Stable Compound Containing a Silicon-Silicon Double Bond.* Science, 1981. **214**(4527): p. 1343-1344.
163. Wang, Y., et al., *A Stable Silicon(0) Compound with a Si=Si Double Bond.* Science, 2008. **321**(5892): p. 1069-1071.
164. Vij, D.R., *Handbook of Applied Solid State Spectroscopy*. 2007: Springer.
165. Edgar, M., *Physical methods and techniques NMR spectroscopy.* Annual Reports Section "B" (Organic Chemistry), 2012. **108**(0): p. 292-315.
166. Chan, J.C.C. and S.E. Afonin, *Solid State NMR*. 2011: Springer.
167. Mittal, K.L., *Contact Angle, Wettability and Adhesion*. 2003: Taylor & Francis.
168. Takabayashi, S., et al., *X-ray photoelectron analysis of surface functional groups on diamond-like carbon films by gas-phase chemical derivatization method.* Surface and Interface Analysis, 2010. **42**(2): p. 77-87.
169. Paik, N., *Raman and XPS studies of DLC films prepared by a magnetron sputter-type negative ion source.* Surface and Coatings Technology, 2005. **200**(7): p. 2170-2174.
170. Ronkainen, H., et al., *Differentiating the tribological performance of hydrogenated and hydrogen-free DLC coatings.* Wear, 2001. **249**(3–4): p. 260-266.
171. Li, H., et al., *Friction behaviors of hydrogenated diamond-like carbon film in different environment sliding against steel ball.* Applied Surface Science, 2005. **249**(1–4): p. 257-265.
172. Yamaguchi, T., et al., *Sliding velocity dependency of the friction coefficient of Si-containing diamond-like carbon film under oil lubricated condition.* Tribology International, 2011. **44**(11): p. 1296-1303.
173. Ronkainen, H., S. Varjus, and K. Holmberg, *Friction and wear properties in dry, water- and oil-lubricated DLC against alumina and DLC against steel contacts.* Wear, 1998. **222**(2): p. 120-128.
174. Haque, T., A. Morina, and A. Neville, *Effect of Friction Modifiers and Antiwear Additives on the Tribological Performance of a Hydrogenated DLC Coating.* Journal of Tribology, 2010. **132**(3): p. 032101.
175. Kosarieh, S., et al., *Tribological performance and tribochemical processes in a DLC/steel system when lubricated in a fully formulated oil and base oil.* Surface & Coatings Technology, 2013. **217**: p. 1-12.
176. Wan, Y., et al., *Effects of detergent on the chemistry of tribofilms from ZDDP: studied by X-ray absorption spectroscopy and XPS*, in

Tribology Series, M.P.G.D. D. Dowson and A.A. Lubrecht, Editors. 2002, Elsevier. p. 155-166.
177. Pereira, G., et al., *Chemical and mechanical analysis of tribofilms from fully formulated oils Part 1 – Films on 52100 steel.* Tribology - Materials, Surfaces & Interfaces, 2007. **1**(1): p. 48-61.
178. Liu, E. and S.D. Kouame, *An XPS Study on the Composition of Zinc Dialkyl Dithiophosphate Tribofilms and Their Effect on Camshaft Lobe Wear.* Tribology Transactions, 2013. **57**(1): p. 18-27.
179. Fourches, N., G. Turban, and B. Grolleau, *Study of DLC/silicon interfaces by XPS and in-situ ellipsometry.* Applied Surface Science, 1993. **68**(1): p. 149-160.
180. Bancroft, G.M., et al., *Toward a comprehensive understanding of solid-state core-level XPS linewidths: Experimental and theoretical studies on the Si 2p and O 1s linewidths in silicates.* Physical Review B, 2009. **80**(7).
181. Scientific, T.F. *XPS Analysis of Stainless Steel Surfaces - Application Note: 52108*. [pdf] 2011 [cited 2014; Available from: www.revbase.com/tt/sl.ashx?z=73090c66&dataid=265909&ft=1.
182. Jiang, W.-G., J.-J. Su, and X.-Q. Feng, *Effect of surface roughness on nanoindentation test of thin films.* Engineering Fracture Mechanics, 2008. **75**(17): p. 4965-4972.
183. Colby, R., et al., *Cross-sectional transmission electron microscopy of thin graphite films grown by chemical vapor deposition.* Diamond and Related Materials, 2010. **19**(2): p. 143-146.
184. Equey, S.b., et al., *Reactions of zinc-free anti-wear additives in DLC/DLC and steel/steel contacts.* Tribology International, 2008. **41**(11): p. 1090-1096.
185. Curran, H.J., et al., *A Comprehensive Modeling Study of n-Heptane Oxidation.* Combustion and Flame, 1998. **114**(1–2): p. 149-177.
186. ACEA. *ACEA - European Automobile Manufacturers' Association*. 2013 [cited 2013 19/11/2013]; Available from: http://www.acea.be/images/uploads/files/2012_ACEA_Oil_Sequences.pdf%20as%2029th%20May%202013.
187. Cumpson, P.J., et al., *Depth profiling organic/inorganic interfaces by argon gas cluster ion beams: sputter yield data for biomaterials, in-vitro diagnostic and implant applications.* Surface and Interface Analysis, 2013. **45**(13): p. 1859-1868.
188. Wagner, M.S., et al., *Limits of detection for time of flight secondary ion mass spectrometry (ToF-SIMS) and X-ray photoelectron spectroscopy (XPS): detection of low amounts of adsorbed protein.* Journal of Biomaterials Science, Polymer Edition, 2002. **13**(4): p. 407-428.
189. Barr, T.L. and S. Seal, *Nature of the use of adventitious carbon as a binding energy standard.* Journal of Vacuum Science & Technology A, 1995. **13**(3): p. 1239-1246.
190. Marciano, F.R., et al., *Improvement of DLC electrochemical corrosion resistance by addiction of fluorine.* Diamond and Related Materials, 2010. **19**(5–6): p. 537-540.
191. Yao, Z.Q., et al., *Structural, mechanical and hydrophobic properties of fluorine-doped diamond-like carbon films synthesized by plasma*

immersion ion implantation and deposition (PIII-D). Applied Surface Science, 2004. **230**(1-4): p. 172-178.
192. Meškinis, Š. and A. Tamulevičienė, *Structure, Properties and Applications of Diamond Like Nanocomposite (SiOx Containing DLC) Films: A Review.* Materials Science, 2011. **17**(4): p. 358-370.
193. Rainforth, W.M., et al., *High resolution observations of friction-induced oxide and its interaction with the worn surface.* Tribology International, 2002. **35**(11): p. 731-748.
194. Ohana, T., et al., *Tribological properties and characterization of DLC films deposited by pulsed bias CVD.* Diamond and Related Materials, 2004. **13**(4–8): p. 1500-1504.
195. Lee, K.-R., et al., *Structural dependence of mechanical properties of Si incorporated diamond-like carbon films deposited by RF plasma-assisted chemical vapour deposition.* Thin Solid Films, 1997. **308–309**(0): p. 263-267.
196. Tamor, M.A., et al., *Pendant benzene in hydrogenated Diamond-Like Carbon* Applied Physics Letters, 1989. **55**(14): p. 1388-1390.
197. Taylor, L.J. and H.A. Spikes, *Friction-Enhancing Properties of ZDDP Antiwear Additive: Part I—Friction and Morphology of ZDDP Reaction Films.* Tribology Transactions, 2003. **46**(3): p. 303-309.
198. Schall, J.D., G. Gao, and J.A. Harrison, *Effects of Adhesion and Transfer Film Formation on the Tribology of Self-Mated DLC Contacts†.* The Journal of Physical Chemistry C, 2009. **114**(12): p. 5321-5330.
199. Wu, W.J., T.M. Pai, and M.H. Hon, *Wear behavior of silicon-containing diamond-like carbon coatings.* Diamond and Related Materials, 1998. **7**(10): p. 1478-1484.
200. Ruths, M., et al., *Exploring the "friction modifier" phenomenon: nanorheology of n-alkane chains with polar terminus dissolved in n-alkane solvent.* Tribology Letters, 1999. **6**(3-4): p. 207-214.
201. Murase, A. and T. Ohmori, *ToF-SIMS analysis of model compounds of friction modifier adsorbed onto friction surfaces of ferrous materials.* Surface and Interface Analysis, 2001. **31**(3): p. 191-199.
202. Ratoi, M., et al., *The impact of organic friction modifiers on engine oil tribofilms.* RSC Advances, 2014. **4**(9): p. 4278-4285.
203. Vengudusamy, B., et al., *Tribological properties of tribofilms formed from ZDDP in DLC/DLC and DLC/steel contacts.* Tribology International. **44**(2): p. 165-174.
204. Liskiewicz, T.W., et al., *Short note on improved integration of mechanical testing in predictive wear models.* Surface and Coatings Technology, 2013. **237**(0): p. 212-218.
205. Kasrai, M., et al., *X-Ray Absorption Study of the Effect of Calcium Sulfonate on Antiwear Film Formation Generated From Neutral and Basic ZDDPs: Part 1—Phosphorus Species.* Tribology Transactions, 2003. **46**(4): p. 534-542.
206. Pereira, G., et al., *Chemical characterization and nanomechanical properties of antiwear films fabricated from ZDDP on a near hypereutectic Al–Si alloy.* Tribology Letters, 2005. **18**(4): p. 411-427.
207. Pereira, G., et al., *A multi-technique characterization of ZDDP antiwear films formed on Al (Si) alloy (A383) under various conditions.* Tribology Letters, 2007. **26**(2): p. 103-117.

208. Brow, R.K., et al., *The short-range structure of zinc polyphosphate glass.* Journal of Non-Crystalline Solids, 1995. **191**(1–2): p. 45-55.
209. Roundhill, D.M., *Extraction of metals from soils and waters*. 2001: Springer.
210. Belin, M., J.M. Martin, and J.L. Mansot, *Role of Iron in the Amorphization Process in Friction-Induced Phosphate Glasses.* Tribology Transactions, 1989. **32**(3): p. 410-413.
211. Cizaire, L., et al., *Chemical analysis of overbased calcium sulfonate detergents by coupling XPS, ToF-SIMS, XANES, and EFTEM.* Colloids and Surfaces A: Physicochemical and Engineering Aspects, 2004. **238**(1–3): p. 151-158.
212. Willermet, P.A., et al., *The composition of lubricant-derived surface layers formed in a lubricated cam/tappet contact II. Effects of adding overbased detergent and dispersant to a simple ZDTP solution.* Tribology International, 1995. **28**(3): p. 163-175.
213. Bhushan, B. and X. L, *Nanomechanical characterisation of solid surfaces and thin films.* International Materials Reviews, 2003. **48**(3): p. 125-164.
214. Gotsmann, B. and M.A. Lantz, *Atomistic Wear in a Single Asperity Sliding Contact.* Physical Review Letters, 2008. **101**(12): p. 125501.
215. Mutafov, P., et al., *DLC-W coatings tested in combustion engine — Frictional and wear analysis.* Surface and Coatings Technology, (0).
216. Trevoy, D.J. and H. Johnson, *The Water Wettability of Metal Surfaces.* The Journal of Physical Chemistry, 1958. **62**(7): p. 833-837.
217. McKetta, J.J., *Encyclopedia of Chemical Processing and Design: Volume 6 - Calcination Equipment to Catalysis*. 1978: Taylor & Francis.
218. Vipper, A.B., et al., *Tribological performance and mechanism of action of overbased detergents.* Lubrication Science, 1997. **9**(2): p. 207-217.
219. Schächter, Y. and H. Pines, *Calcium-oxide-catalyzed reactions of hydrocarbons and of alcohols.* Journal of Catalysis, 1968. **11**(2): p. 147-158.
220. Fritzsche, H. and C.C. Tsai, *Porosity and oxidation of amorphous silicon films prepared by evaporation, sputtering and plasma-deposition.* Solar Energy Materials, 1979. **1**(5–6): p. 471-479.
221. Yang, S.H., et al., *Effect of environment on the tribological behavior of Si-incorporated diamond-like carbon films.* Wear, 2002. **252**(1–2): p. 70-79.
222. Rock, P.A., *Chemical Thermodynamics*. 1983, University Science Books.
223. Timms, P.L., et al., *Silicon-Fluorine Chemistry. I. Silicon Difluoride and the Perfluorosilanes.* Journal of the American Chemical Society, 1965. **87**(13): p. 2824-2828.
224. Hench, L.L. and J.K. West, *The sol-gel process.* Chemical Reviews, 1990. **90**(1): p. 33-72.
225. Youngman, R.E. and S. Sen, *The nature of fluorine in amorphous silica.* Journal of Non-Crystalline Solids, 2004. **337**(2): p. 182-186.
226. Martin, J.W., *Concise Encyclopedia of the Structure of Materials*. 2006: Elsevier Science.

227. Committee, E.D.F.A.S.D.R., *Microelectronics Failure Analysis: Desk Reference*. 2004: ASM International.
228. Michalske, T.A. and S.W. Freiman, *A molecular interpretation of stress corrosion in silica.* Nature, 1982. **295**(5849): p. 511-512.
229. Li, Y.-R., et al., *Studies on ZDDP Thermal Film Formation by XANES Spectroscopy, Atomic Force Microscopy, FIB/SEM and 31P NMR.* Tribology Letters, 2008. **29**(1): p. 11-22.
230. Jana, R., T.P. Pathak, and M.S. Sigman, *Advances in Transition Metal (Pd,Ni,Fe)-Catalyzed Cross-Coupling Reactions Using Alkyl-organometallics as Reaction Partners.* Chemical Reviews, 2011. **111**(3): p. 1417-1492.
231. Kung, H.H., *Transition Metal Oxides: Surface Chemistry and Catalysis*. 1989: Elsevier Science.